

ABSTRACT

SUN, WUJIN. DNA Nanoclew-Mediated Drug Delivery.
(Under the direction of Dr. Zhen Gu).

The characteristic microenvironments of diseased areas, such as acidity and overexpressed enzymes, constitute both challenges and opportunities for targeted delivery of therapeutics. Advances in material chemistry have expanded the tool box available to design physiological signal-responsive drug delivery systems through customizing the size, shape, charge, and surface ligands of drug delivery carriers. DNA is a natural carrier to store and transmit genetic information. However, the polymeric nature of DNA also makes it a versatile material that could be programmed to load a large variety of therapeutic molecules through interactions like intercalation, conjugation, hybridization or adsorption. The degradability of DNA *in vivo* also makes it a promising material that could be readily cleared from the biological system.

Here, we have adopted a facile DNA synthesis technique termed rolling-circle amplification to prepare programmable single stranded DNA that could self-assemble into compact nanoparticles termed DNA nanoclew (NC). We explored the DNA NC as a platform nanocarrier for the delivery of various types of therapeutics, including an anticancer chemotherapeutic drug, cancer cell apoptosis inducing cytokine and genome editing ribonucleoprotein. To deliver the chemotherapeutic doxorubicin, the drug was intercalated into the DNA NC. DNase that could cleave the DNA NC for drug release was encapsulated in a cationic and acid degradable nanocapsule, which was assembled onto the DNA NC through electrostatic interaction. The nanoassembly could efficiently release the loaded drug

in response to tumor associated acidity. To deliver the genome editing tool CRISPR-Cas9 into the nuclei of targeted cells, the DNA NC was programmed to be complementary to the guiding RNA of the ribonucleoprotein and a cationic polymer shell was coated for facilitated endosome escape. Balancing the interaction between DNA NC and the ribonucleoprotein dramatically boosted the genome editing efficacy. To deliver the cytokine tumor necrosis factor (TNF)-related apoptosis-inducing ligand (TRAIL) to the plasma membrane of cancer cells. The TRAIL was loaded into two complementary DNA NC and the contact of the two DNA NC was controlled through a liposome shell that could be degraded by the tumor associated PLA2. Release of the TRAIL loaded DNA NCs from the liposomes led to the shape transformation of the carrier from nanoparticle to microfibers, inhibiting cellular uptake of TRAIL and enhancing its apoptosis signaling on plasma membrane.

© Copyright 2017 Wujin Sun

All Rights Reserved

DNA Nanoclew-Mediated Drug Delivery

by
Wujin Sun

A dissertation submitted to the Graduate Faculty of
North Carolina State University
in partial fulfillment of the
requirements for the degree of
Doctor of Philosophy

Biomedical Engineering

Raleigh, North Carolina

2017

APPROVED BY:

Dr. Zhen Gu
Committee Chair

Dr. Chase Beisel

Dr. Frances Ligler

Dr. Matthew Fisher

Dr. Ke Cheng

BIOGRAPHY

Wujin Sun was born in Jiangyan, Jiangsu, China. He received his B.S. degree in Bioengineering in 2010, followed by a M.S. degree in Biochemical Engineering from Nanjing Tech University. He then joined Prof. Zhen Gu's laboratory in the Joint Department of Biomedical Engineering at the University of North Carolina at Chapel Hill and North Carolina University for his Ph.D. training since 2013. His research is focused on the development of smart drug delivery systems, incorporating polymer, lipid and DNA based nanostructures, for the delivery of small molecules, proteins and nucleic acids.

ACKNOWLEDGMENTS

Firstly, I would like to acknowledge my advisor, Prof. Zhen Gu, for his mentorship and constant support. Prof. Gu introduced me to a wonderful interdisciplinary field where material engineering and biotechnology are integrated to generate innovative solutions for existing challenges. His passion for innovation and attention for details inspired me a lot. I would like to thank Prof. Chase Beisel for introducing me to the cutting-edge technology of CRISPR-Cas. I would also like to thank Prof. Frances Ligler, Prof. Ke Cheng and Prof. Matthew Fisher for being my committee members and providing valuable insights of my research.

I am also grateful to past and current members of the Gu Lab: Dr. Ran Mo, Dr. Tianyue Jiang, Dr. Wanyi Tai, Dr. Jin Di, Dr. Dennis Pacardo, Dr. Hongliang Xin, Dr. Xiuli Hu, Dr. Yue Lu, Dr. Jinqiang Wang, Dr. Chao Wang, Dr. Zhaowei Chen, Dr. Edikan Archibong, Dr. Junjie Yan, Dr. Xudong Zhang, Mr. Quanyin Hu, Mr. Jicheng Yu, Ms. Yanqi Ye, Ms. Yuqi Zhang...for their help and support during my research.

Lastly, I would like to thank my family, especially my parents and my wife Wenyan Ji. Their encouragement and unlimited support have been a major impetus for me.

Chapter 1 of this dissertation is a version of “Wujin Sun, Quanyin Hu, Wenyan Ji, Grace Wright, Zhen Gu. Leveraging Physiology for Precision Drug Delivery, *Physiological Reviews*, 97: 289 2017”. Chapter 2 is a version of “Wujin Sun, Zhen Gu, Engineering DNA scaffolds for delivery of anticancer therapeutics, *Biomaterials Science*, 3: 1018, 2015”.

Chapter 3 is a version of “Wujin Sun, Tianyue Jiang, Yue Lu, Margaret Reiff, Ran Mo, Zhen Gu, Cocoon-Like Self-Degradable DNA Nanoclew for Anticancer Drug Delivery, *Journal of the American Chemical Society*, 136: 14722, 2014”. Chapter 4 is a version of “Wujin Sun, Wenyan Ji, Jordan Hall, Quanyin Hu, Chao Wang, Chase Beisel, Zhen Gu, Self-Assembled DNA Nanoclews for the Efficient Delivery of CRISPR–Cas9 for Genome Editing, *Angewandte Chemie International Edition*, 54: 1, 2015”. Chapter 5 is a version of “Wujin Sun, Wenyan Ji, Quanyin Hu, Jicheng Yu, Chao Wang, Chenggen Qian, Gabrielle Hochu, Zhen Gu, Transformable DNA nanocarriers for plasma membrane targeted delivery of cytokine, *Biomaterials*, 96: 1, 2016”.

Work in this dissertation was supported by the grants from NC TraCS, NIH’s Clinical and Translational Science Awards (CTSA, NIH grant 1UL1TR001111) at UNC-CH, Sloan Fellowship Award from the Alfred P. Sloan Foundation, and the start-up package from the Joint BME Department of UNC-CH and NCSU to Z.G.

TABLE OF CONTENTS

LIST OF TABLES	x
LIST OF FIGURES	xi
CHAPTER 1 INTRODUCTION.....	1
1. Motivation and Objective	1
2. Overview of drug delivery systems	2
2.1. Why deliver?	2
2.2. What to deliver?	8
2.3. How to deliver?	10
3. Physiological barriers and designing criteria for drug delivery systems	12
3.1. Extracellular barriers	13
3.2. Intracellular barriers	21
3.3. Designing criteria of nanocarriers for drug delivery	28
4. Smart drug delivery systems mediated by physiological signals.....	35
4.1. Nanomedicine responsive to physiological triggers	39
4.2. Programmed multi-stimuli-responsive delivery systems	57
5. Clinical impact of drug delivery system	64
6. Summary	70
7. Dissertation Scope and Organization	70
CHAPTER 2 ENGINEERING DNA SCAFFOLDS FOR DELIVERY OF	
ANTICANCER THERAPEUTICS.....	72
1. Introduction	72

2. Various DNA scaffolds for different anticancer drug delivery	75
2.1. Small-Molecule Drugs	75
2.2. Nucleic Acids	78
2.3. Proteins.....	83
3. DNA scaffolds-based stimuli-responsive drug delivery	84
4. Conclusion and outlook.....	85
CHAPTER 3 COCOON-LIKE SELF-DEGRADABLE DNA-NANOCLEW FOR ANTICANCER DRUG DELIVERY	88
1. Introduction	88
2. Materials and Methods	90
2.1. Materials.....	90
2.2. Preparation and Characterization of DNA nanoclew (NCl).	92
2.3. Preparation and characterization of DNase I nanocapsule (NCa).....	93
2.4. DOX loading and release.	95
2.5. Assembly and characterization of NCl/NCa.....	96
2.6. Conjugation of NCl with folic acid.....	97
2.7. Cell culture.....	97
2.8. Determination of endocytosis pathways.	98
2.9. Intracellular distribution.....	98
2.10. <i>In vitro</i> cytotoxicity assay.....	99
3. Results and Discussion	100
3.1. Preparation of acid degradable nanococoon	100
3.2. Uptake and intracellular distribution of the nanococoon	105

3.3. <i>In vitro</i> anticancer efficacy.....	107
4. Summary	111
 CHAPTER 4 EFFICIENT DELIVERY OF CRISPR-CAS9 FOR GENOME EDITING	
VIA SELF-ASSEMBLED DNA NANOCLEWS	112
1. Introduction	112
2. Materials and Methods	114
2.1. Materials.....	114
2.2. Clone, expression and purification of Cas9 protein.	115
2.3. Transcription and purification of single-guide RNA (gRNA).	116
2.4. Plasmid DNA cleavage assay to detect Cas9 activity.	117
2.5. Preparation and characterization of DNA NC.	117
2.6. Assembly and characterization of Cas9/sgRNA/NC/PEI.	118
2.7. Cell culture and EGFP gene disruption assay.	119
2.8. SURVEYOR assay to detect genomic modifications.	120
2.9. DNA sequencing to detect genomic mutations.	120
2.10. Determination of endocytosis pathways.	121
2.11. Intracellular distribution of Cas9.	121
2.12. <i>In vitro</i> cytotoxicity.....	122
2.13. <i>In vivo</i> EGFP disruption.....	122
2.14. Statistics.	123
3. Results and Discussion	123
3.1. Preparation of Cas9 protein and sgRNA.	123
3.2. Characterization of the nanoassembly.	125

3.3. Uptake and intracellular trafficking of delivered Cas9/sgRNA.....	129
3.4. Gene editing in the U2OS-EGFP reporter cell line.....	132
3.5 Gene editing in U2OS-EGFP xenograft tumor model.....	136
4. Summary	138
 CHAPTER 5 TRANSFORMABLE DNA NANOCARRIERS FOR PLASMA	
MEMBRANE TARGETED DELIVERY OF CYTOKINE	139
1. Introduction	139
2. Materials and Methods	141
2.1. Materials.....	141
2.2. Preparation of TRAIL	143
2.3. Preparation of Ni ²⁺ modified DNA NC.....	143
2.4. Characterization of DNA NCs loaded with TRAIL.....	144
2.5. Encapsulation of DNA NC into liposome and PLA2 triggered release.....	146
2.6. Cell culture.....	146
2.7. Cellular distribution and endocytosis pathway of delivered TRAIL	147
2.8. Cell apoptosis assay	148
2.9. <i>In vitro</i> cytotoxicity.....	149
2.10. Statistics	149
3. Results and Discussion	149
3.1. Preparation and characterization of Ni ²⁺ modified DNA NC	149
3.2. Loading TRAIL onto DNA NC	150
3.3. Encapsulation of TRAIL-NC in POPC liposome and PLA2 triggered release	152
3.4. Cell membrane targeted delivery of TRAIL	154

3.5. <i>In vitro</i> cytotoxicity.....	157
4. Conclusion	160
CHAPTER 6 SUMMARY AND OUTLOOK	161
REFERENCES.....	167

LIST OF TABLES

Table 1-1. Summary of exemplary physiological stimuli-responsive formulations discussed in this review.....	35
Table 1-2. Representative Clinical Translations of Precision Nanomedicine Delivering Anticancer Therapeutics.	65
Table 3-1. Sequences of DNA oligos.....	93
Table 3-2. Sizes and zeta potentials of different particles.....	103
Table 4-1. Sequences of DNA oligos.....	124
Table 5-1. Sequences of DNA oligos.....	145

LIST OF FIGURES

Figure 1-1. Typical routes of drug administration that include ocular, sublingual, buccal, oral, intravenous, intramuscular, subcutaneous, transdermal, nasal, pulmonary, vaginal and rectal routes. Different drug delivery systems were developed to overcome various physiological barriers associated with the routes. The physiochemical properties and therapeutic targets of the drugs determined the choices of drug administration routes. 3

Figure 1-2. Physiological barriers for nanocarrier based drug delivery system. Nanocarriers enter the systemic circulation by intravenous injection and undergo opsonization by interacting with serum proteins. The opsonization facilitates nanoparticle clearance by reticuloendothelial system, leading to non-specific accumulation of nanocarriers in organs like liver and spleen. In the blood flow, fluid dynamics of the nanocarrier influences their margination towards vascular walls. The low permeability of vascular endothelium poses another significant hurdle for nanocarriers, especially the tight junctions associate with blood-brain barrier. After extravasation into tumor microenvironment, the nanocarrier needs to diffuse through the dense extracellular matrix against high interstitial pressure to reach the tumor cells. For drugs that work in intracellular compartments, the nanocarrier needs to be internalized through endocytosis and escape the endosome to reach other organelles. Even after entering in the cells, the cell membrane associated multidrug resistant pumps could also pump out the delivered chemotherapeutics..... 13

Figure 1-3. Parameters for nanoformulation design. Properties of the nanocarrier could be tailored modularly from the perspective of size, material composition, shape, surface

chemistry and targeting ligand conjugation to overcome the sequential physiological barriers for precise drug delivery. 31

Figure 1-4. Mechanisms of stimuli-responsive nanocarrier for drug delivery. The drugs could be released from the nanocarrier upon physiological signal triggered a) degradation, b) swell or shrink, c) dissociation, d) uncapping the pores of mesoporous silica nanoparticles. d)

Nanocarrier activation for cell penetration with exposed moieties. 40

Figure 1-5. Harnessing physiological traits of tumor for precise drug delivery. The nanocarrier could reach the tumor either by actively binding to tumor specific receptors or passively through the EPR effect. Physiological signals in the extracellular space, such as pH gradient, enzyme, ROS and hypoxic environment could be utilized to trigger the release of drugs targeting extracellular objectives or activate the nanocarrier for further intracellular penetration. Intracellular environment, such as acidity, enzymes, ROS, reducing potential, ATP gradient, could be used to trigger intracellular nanoparticle transport or drug release. . 43

Figure 2-1. Example DNA nanoscaffolds for anticancer drug delivery. (a) DNA nanostructures assembled from multiple “DNA tiles”.^[285, 545] (b) DNA nanocarriers based on “DNA origami”.^[343, 529] (c) DNA nanoassemblies based on rolling circle amplification.^[98, 546]

(d) Hybrid drug delivery carriers with DNA scaffold as functional moiety.^[390, 470]

Reproduced with permission..... 74

Figure 2-2. Intracellular delivery of DOX using a DNA nanococoon synthesized by rolling circle amplification. (a) Main components of the DNA nanococoon and mechanism for intracellular delivery of DOX. (b) Hydrodynamic size of DNA nanococoon and TEM image

of DNA nanoclew complexed with gold nanoparticle stained DNaseI nanocapsule. Scale bar is 100 nm (c) Confocal laser scanning microscopy images of DNA nanococoon mediated DOX delivery in MCF-7 cells. Red for DOX, green for endolysosome and blue for nucleus. Scale bar is 10 μ m. Reproduced with permission from ref. [98]...... 77

Figure 2-3. Delivery of siRNA using a DNA tetrahedron assembled from DNA tiles. (a) Schematic for the DNA tetrahedron formation. (b) Structure of the DNA tetrahedron with ligands. (c) Pharmacokinetic profile of the siRNA loaded DNA tetrahedron in mice bearing KB tumor and distribution of the nanoparticle in major organs after 12 h of injection. (d) Representative fluorescent image of dose-dependent accumulation of the DNA nanoparticle in KB tumors. Reproduced with permission from ref. [285]...... 80

Figure 2-4. ATP responsive delivery of DOX using polymeric nanoparticles functionalized by an ATP-binding DNA scaffold. (a) Schematic of the ATP responsive drug delivery system. (b) DOX release from the DNA-aptamer duplex as response to different nucleotides. (c) Representative image of MDA-MB-231 tumor bearing mice treated with different formulations. Reproduced with permission from ref. [456]. 86

Figure 3-1. a) Main components of the cocoon-like self-degradable DNA clew, consisting of DOX/FA-NCI/NCa, and acid triggered DOX release. b) Schematic illustration of efficient delivery of DOX by DOX/FA-NCI/NCa to nuclei for cancer therapy. I. Internalization in endosomes; II. pH-triggered degradation of NCI for DOX release; III. Accumulation of DOX in cell nuclei..... 90

Figure 3-2. Synthesis of NCl by rolling circle amplification. I). With a cyclized ssDNA a template and a DNA oligo as primer, long chain single stranded DNA containing repeated sequence of the template was synthesized. II). The synthesized RCA product self-assembled into nanoclew-like structure by intra-molecular hybridization..... 91

Figure 3-3. a) Cyclization of the ssDNA template. Lane 1, DNA ladder; Lane d2, 5' phosphorylated ssDNA template; Lane 3, cyclized ssDNA template; Lane 4, circular ssDNA template treated with Exo I. b). 0.8 % agarose gel analysis of the RCA product. c). Stability of NCl. Lane 1, non-treated NCl; Lane 2, NCl treated with DMEM containing 10 % FBS for 24 h; Lane 3, NCl treated with DMEM containing 10% FBS for 48 h. 101

Figure 3-4. a) Hydrodynamic size of NCl by dynamic light scattering (DLS). Inset: AFM image of NCl. Scale bar is 500 nm. b) Hydrodynamic size of NCa. Inset: TEM image of NCa. Scale bar is 10 nm. c) CD spectra of native DNase I and NCa. d) DNA-degrading activities of NCa and cNCa at pH 7.4 and pH 5.4. Bars represent mean \pm SD (n = 3). 102

Figure 3-5. The fluorescence spectra of DOX solution (10 μ M) with increasing concentrations of NCl (0.15 - 2.4 μ g/mL). 102

Figure 3-6. DOX entrapment efficiency and loading capacity by NCl. The DOX entrapment efficiency is the ratio of (added DOX - DOX washout out in supernatant)/added DOX. Drug loading capacity is the weight ratio of loaded DOX/(loaded DOX + NCl). Bars represent mean \pm SD (n = 3)..... 103

Figure 3-7. a-c) TEM image of DNase I (a), NCa (b) and NCa after incubation at pH 5.4 for 2 h (c). Scale bar is 10 nm. d-f) Hydrodynamic size of native DNase I (d), NCa (e) and NCa after incubation at pH 5.4 for 2 h (f)..... 104

Figure 3-8. CLSM images of NCI/NCa assembly. NCI was loaded with DOX (DOX/NCI) and NCa was conjugated with AF488-NHS for imaging (AF488-NCa). Scale bar is 50 μm 105

Figure 3-9. a). Hydrodynamic size of NCI/NCa. Inset: TEM image of NCI/Au-NCa. Scale bar is 100 nm. The arrows indicate Au-NCa adsorbed on NCI surface. b) DOX released from DOX/NCI/NCa and DOX/NCI/cNCa at pH 7.4 and pH 5.4. Bars represent mean \pm SD (n = 3). c) AFM images of NCI/NCa after incubation at pH 7.4 and pH 5.4 for 2 h. Scale bar is 500 nm. 106

Figure 3-10. a) Relative uptake efficiency of DOX/FA-NCI/NCa by MCF-7 cells. *P < 0.05, **P < 0.01 compared with control. Bars represent mean \pm SD (n = 3). b) CLSM images of MCF-7 cells after incubation with DOX/FA-NCI/NCa for different time. Late endosome and lysosomes were stained by LysoTracker green. Red: DOX; green: endo-lysosome; blue: Hoechst 33342; yellow: colocalization of red and green pixels; magenta: colocalization of red and blue pixels. Scale bars are 10 μm . c) In vitro cytotoxicity of DOX/NCI, DOX/NCI/NCa and DOX/FA-NCI/NCa against MCF-7 cells for 24 h. *P < 0.05. Bars represent mean \pm SD (n = 6). d) In vitro cytotoxicity of the blank FA-NCI, NCa and FA-NCI/NCa against MCF-7 cells for 24 h. Bars represent mean \pm SD (n = 6)..... 108

Figure 3-11. CLSM images of MCF-7 cells after incubation with DOX/FA-NCI/NCa for different time. The late endosome and lysosomes are stained with LysoTracker (green), while the nuclei were stained with Hoechst. Scale bars are 10 μm 109

Figure 3-12. CLSM images of MCF-7 cells after incubation with DOX/FA-NCI/AF488-NCa for different time. The nuclei were stained with Hoechst. Scale bars are 10 μm 110

Figure 3-13. In vitro cytotoxicity of DOX/NCI/cNCa and DOX/NCI/NCa against MCF-7 cells for 24 h. *P < 0.05. Bars represent mean \pm SD (n = 6). 110

Figure 4-1. Schematic design of the DNA NC mediated CRISPR-Cas9 delivery system. (a) Preparation of Cas9/sgRNA/NC/PEI. I: The NC was synthesized by RCA and loaded with the Cas9/sgRNA complex through Watson-Crick base pairing; II: PEI was coated onto Cas9/sgRNA/NC for enhanced endosome escape. (b) Delivery of Cas9/sgRNA by the DNA NC based carrier to the nucleus of the cell for genome editing. I: Bind to cell membrane; II: Endocytosis; III: Endosome escape; IV; Transport into the nucleus; V: Search for target DNA locus in the chromosome and introduce double strand breaks for genome editing. ... 114

Figure 4-2. SDS-PAGE (12%) of purified Cas9. The purified Cas9 showed molecular weight of ~160 KDa. 124

Figure 4-3. a) Agarose gel electrophoresis (0.8%) of purified sgRNA (lane 1) and cgRNA (lane 2). b) Cas9 activity assay using linearized plasmid pCAG-EGFP (5556 bp) as substrate. Only Cas9 complexed with sgRNA can digest the plasmid DNA..... 127

Figure 4-4. Particle characterization of Cas9/sgRNA/NC-12/PEI. (a) Monitoring zeta potential of the Cas9/sgRNA/NC-12/PEI assembly process. Bars represent mean \pm SD (n = 3). (b) Hydrodynamic size distribution of Cas9/sgRNA/NC-12/PEI. (c) AFM image and d) TEM image of Cas9/sgRNA/NC-12/PEI with scale bars of 400 nm and 100 nm, respectively. 127

Figure 4-5. Optimization of PEI concentration for coating Cas9/sgRNA/NC-12 by measuring the zeta potential..... 128

Figure 4-6. Hydrodynamic size distributions and AFM images of NC-12, Cas9/sgRNA/NC-12 and Cas9/sgRNA/NC-12/PEI. Scale bar 400 nm..... 128

Figure 4-7. CLSM images of Cas9/sgRNA/NC-12/PEI assembly. Red for Cas9 stained with AF647, blue for NC-12 stained with Hoechst 33342 and green for PEI labeled with FITC. Scale bar is 20 μ m..... 129

Figure 4-8. a) CLSM images of U2OS.EGFP cells incubated with Cas9/sgRNA/NC-12/PEI for 1 h, 2 h, 4 h and 6 h (Cas9 and sgRNA concentrations at 100 nM). Green for EGFP, red for Cas9 stained with AF647 and blue for nuclei stained with Hoechst 33342. Scale bar is 10 μ m. b) Relative Cas9/sgRNA/NC-12/PEI uptake by U2OS.EGFP cells in the presence of different endocytosis inhibitors (Cas9 and sgRNA concentrations at 100 nM). ** $P < 0.01$ as compared to the control group. Bars represent mean \pm SD (n = 3). c) In vitro cell viability of U2OS.EGFP cells treated with Cas9/sgRNA/NC-12/PEI and Cas9/sgRNA/PEI by flow cytometry. The cells were stained with TO-PRO-3 live/dead stain after the treatment and analyzed by flow cytometry. Bars represent mean \pm SD (n = 3)..... 130

Figure 4-9. Confocal laser scanning microscopy images of U2OS.EGFP cells incubated with Cas9/sgRNA/NC-12/PEI for 1 h, 2 h, 4 h and 6 h (Cas9 and sgRNA concentrations at 100 nM)..... 131

Figure 4-10. Genome editing by Cas9/sgRNA delivered by DNA NC (8 µg/mL) coated with PEI (10 µg/mL). a) Fluorescent microscope images and flow cytometry analysis of U2OS.EGFP cells treated with Cas9/sgRNA/PEI and Cas9/sgRNA/NC-12/PEI (Cas9 and sgRNA concentrations at 100 nM). Green represents EGFP and blue represents nuclei stained with Hoechst 33342. Scale bar is 100 µm. b) T7EI assay of U2OS.EGFP cells treated with Cas9/gRNA/NC-12/PEI and Cas9/gRNA/PEI. c) EGFP disruption assay of Cas9/gRNA delivered by different DNA NCs. Percentages of EGFP negative cells after treating with Cas9/sgRNA/NC-23/PEI, Cas9/sgRNA/NC-12/PEI, Cas9/sgRNA/NC-0/PEI and Cas9/sgRNA/PEI at different Cas9/sgRNA molar ratios were profiled. Bars represent mean ± SD (n = 3). 134

Figure 4-11. Flow cytometry analysis of U2OS.EGFP cells treated with formulations containing cgRNA, which did not show any EGFP disruption efficacy. 135

Figure 4-12. DNA sequencing of Cas9/sgRNA targeted genomic locus in U2OS.EGFP cells. Target sequence complementary to the sgRNA is underlined and PAM sequence is shown in bold. Mutations were detected in 7 out of 20 sequenced clones. Number of insertion/deletion as compared to the wild type sequence is shown on the right. 135

Figure 4-13. a) Agarose gel electrophoresis (0.8%) of synthesized NC-23, NC-12 and NC-0 in lane 1, 2 and 3, respectively. b) Analysis of NC stability after incubating with
xviii

Cas9/sgRNA for 24 h. Lane 1, 3, 5 were for untreated NC-23, NC-12 and NC-0 and lane 2, 4, 6 showed Cas9/sgRNA treated NC-23, NC-12 and NC-0, respectively..... 136

Figure 4-14. In vivo delivery of Cas9/sgRNA into U2OS.EGFP xenograft tumors in nude mice. Tumor sections were collected 10 days after intratumoral injection of Cas9/sgRNA/NC-12/PEI. The EGFP was stained by FITC conjugated GFP antibody and nuclei were stained with Hoechst 33342. Scale bar is 50 μm 137

Figure 4-15. Tissue section of tumor treated with Cas9/cgRNA/NC-12/PEI. The EGFP was stained by FITC conjugated GFP antibody and nuclei were stained with Hoechst 33342. The Scale bar is 50 μm 137

Figure 5-1. Schematic of phospholipase activated membrane targeted cytokine delivery system. (a) Preparation of TRAIL-NC-L. The DNA NC was first prepared by RCA and then (I) modified with Ni^{2+} . After (II) loading TRAIL through Ni^{2+} -His tag affinity, (III) the TRAIL-NC was encapsulated into a POPC liposome that could be degraded by PLA2. (b) Main components of TRAIL-NC-L and mechanism of PLA2 triggered morphological transformation of the DNA NCs. (IV) Highly expressed PLA2 in the tumor microenvironment degrades the liposome shell to release TRAIL-NC. (V) Complementary DNA NCs hybridize into microscopic fibers. (c) Effect of the morphological change on TRAIL localization. (VI) TRAIL loaded spherical nanoparticle are efficiently internalized. (VII) Hybridized DNA fibers are highly impermeable to cell membrane, facilitating the interaction of TRAIL and death receptors. 142

Figure 5-2. (a) Hydrodynamic size distributions and TEM images of the synthesized DNA NCs. scale bars 200 nm (b) TEM image of Ncf/NCr mix, scale bar 200 nm. (c) AFM imaging of Ncf, NCr, and Ncf/NCr mix. Scale bar represents 500 nm. (d) Representative element mapping of Ni²⁺ modified DNA NC. Shown here is Ni²⁺ modified Ncf, scale bar represents 100 nm. 151

Figure 5-3. (a) SDS-PAGE of purified TRAIL. (b) Hydrodynamic size distributions and TEM imaging of TRAIL loaded DNA NCs. TRAIL-Ncf and TRAIL-NCr showed similar size distribution with a mean diameter of ~104 nm. TRAIL was stained with AuNP. Scale bars represent 100 nm. (c) CLSM characterization of the colocalization of TRAIL and DNA in TRAIL-Ncf and TRAIL-NCr. Red fluorescence indicated AF 647 labeled TRAIL; blue fluorescence showed Hoechst 33342 stained DNA NCs. Scale bar represents 10 μ m..... 153

Figure 5-4. (a) Hydrodynamic size distribution of POPC liposome encapsulating TRAIL-Ncf. (b) Agarose gel electrophoresis analysis of encapsulating DNA NC into POPC liposome. Lane L showed DNA ladder, Lane 1: Unpurified TRAIL-Ncf-L, Lane 2: Unpurified TRAIL-Ncf-L treated with 1% Triton X-100. Encapsulation efficiency was estimated from the band intensity by Image J, where the encapsulated amount is the difference between Lane 2 and Lane 1. (c) Release of TRAIL-NC from POPC liposome. Lane L showed DNA ladder; Lane 1 and 4, purified POPC liposome encapsulating TRAIL-Ncf and TRAIL-NCr; Lane 2 and 5, TRAIL-Ncf-L and TRAIL-NCr-L treated with PLA2; Lane 3 and 6, TRAIL-Ncf-L and TRAIL-NCr-L treated with 1% Triton X-100 as 100% release. (d) Representative TEM image of POPC liposome encapsulating TRAIL-NC. Shown

is TRAIL-NCf-L. (e) TEM image of TRAIL-NCf-L after PLA2 treatment. (f) TEM image of TRAIL-NCf-L/TRAIL-NCr-L after PLA2 treatment. Scale bars all indicate 200 nm..... 154

Figure 5-5. (a) CLSM analysis of subcellular localization of delivered TRAIL. COLO 205 cells were incubated with TRAIL-NCf-L and TRAIL-NCr-L separately or simultaneously after PLA2 pretreatment. TRAIL was labeled with AF 647 and membrane of COLO 205 cells was stained with AF488-WGA. White arrows indicate TRAIL on cell membrane and blue arrows indicate internalized TRAIL. Scale bars indicate 20 μ m. (b) Quantitative analysis of the amount of TRAIL internalized by COLO 205 cells or bound on cell membrane. (c) Endocytosis pathway analysis of TRAIL delivered by TRAIL-NCf-L and TRAIL-NCr-L. Data was presented as mean \pm SD (n = 3). ** P <0.01..... 157

Figure 5-6. (a) APO-BrdU TUNEL assay of COLO 205 apoptosis induced by different TRAIL delivery formulations after PLA2 pretreatment. Scale bar indicates 200 μ m. (b) Annexin V-FITC/PI staining based flow cytometry analysis of COLO 205 apoptosis after treating with different TRAIL delivery formulations for 12 h. I, control cell untreated with any formulation; II, TRAIL-L after PLA2 pretreatment; III, TRAIL-NCf-L after PLA2 pretreatment; IV, TRAIL-NCr-L after PLA2 pretreatment; V, TRAIL-NCf-L/TRAIL-NCr-L after PLA2 pretreatment; VI, TRAIL-NCf-L/TRAIL-NCr-L without PLA2 pretreatment. (c) In vitro cytotoxicity of TRAIL-L, TRAIL-NCf-L, TRAIL-NCr-L and TRAIL-NCf-L/TRAIL-NCr-L after PLA2 pretreatment. Colo 205 cells were treated with different formulations for 24 h. (d) In vitro cytotoxicity of carriers without loaded TRAIL after PLA2 pretreatment. Data were presented as mean \pm SD (n=6). * P <0.05, ** P <0.01..... 159

CHAPTER 1 INTRODUCTION

1. Motivation and Objective

Physiological barriers dwindle the convenience and efficacy of drug administration, demanding the development of drug delivery systems (DDSs) [1-6]. DDSs, including devices and formulations [7-10], were designed to meet the physiological traits of diseases for improved pharmacokinetic and pharmacodynamic properties of drugs [11-14]. In the meantime, extensive research efforts in DDSs generated a large collection of publications covering multiple disciplines [15-23].

DDSs have evolved during the last six decades and could be briefly classified into three generations [24, 25]. Early systems (since ~1950s) were designed as oral formulations [26] or transdermal patches for delayed drug release [27]. Basic principles for drug release were established, such as diffusion, dissolution, osmosis, or ion exchange during this period [28]. The second generation controlled release (since 1980s) mainly refers to the efforts to keep a constant drug concentration in the blood [29]. Few second generation DDSs entered the market [30], but the development of bio-responsive polymers during this period paved the way for more controllable DDSs [31]. The emerging third generation of DDSs based on nanomaterials (since ~2010) was proposed with modular and tunable physiochemical properties [32] to facilitate the prospect of “precision medicine” [33-35], where personalized genomics data would be taken into account for customized drug administration and optimized pharmacokinetics [36-39].

In this review, we will start with a big picture of the drug delivery field concerning the basic rationale for why, what and how drugs are delivered for improved therapeutic efficacies. Then we will focus on the latest drug delivery platform - nanocarriers - with cancer as a model disease to describe the physiological barriers and corresponding strategies for targeted drug delivery. Recent strategies for devising “smart” nanomedicine will also be discussed with the aim of harnessing physiological cues for controlling the targeting and release behaviors of the nanocarriers, such as activated cellular uptake or stimuli-responsive drug release. Lessons learned from FDA-approved nano-formulations or formulations undergoing clinical trials will also be discussed.

2. Overview of drug delivery systems

2.1. Why deliver?

It is well accepted that pharmaceutical agents administered via different routes (Figure 1-1), especially through systemic administration, often leads to adverse side effects even though pharmaceutically beneficial effects could be achieved. To address this dilemma, DDSs, developed in the form of either formulations or devices [40] work as media between the drugs and the patients. These forms enhance the therapeutic efficacy and safety of the drugs by improving their absorption, distribution, metabolism and excretion (ADME) profiles [41, 42]. An ideal DDS should be able to shield the therapeutics from unwanted physical or physiochemical damages and deliver the right amount of drugs to the right

location to act within the body during the right period of time [43]. Decades of development enabled DDSs with a wide array of beneficial properties to improve the pharmacokinetic and pharmacodynamic profiles of drugs [44], uncovering a wealth of opportunities for bringing Ehrlich's concept of “magic bullet” to life [45].

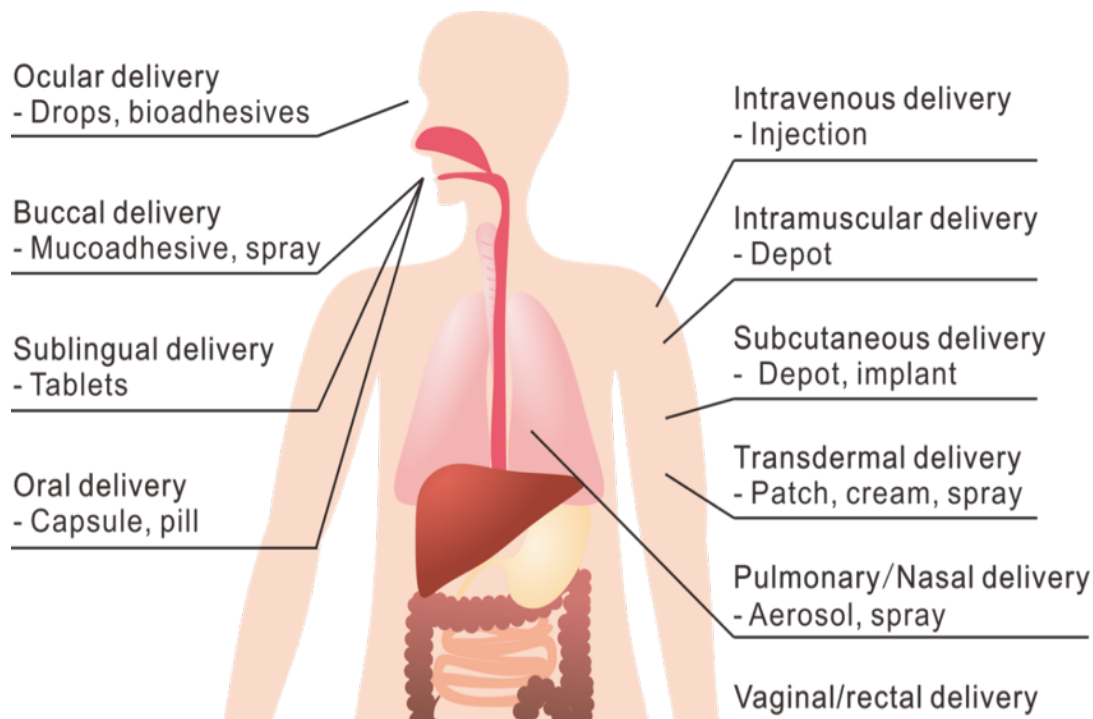


Figure 1-1. Typical routes of drug administration that include ocular, sublingual, buccal, oral, intravenous, intramuscular, subcutaneous, transdermal, nasal, pulmonary, vaginal and rectal routes. Different drug delivery systems were developed to overcome various physiological barriers associated with the routes. The physiochemical properties and therapeutic targets of the drugs determined the choices of drug administration routes.

2.1.1. Absorption

DDSs can help enhance the absorption of drugs, promoting their transportation from the site of administration into blood circulation by 1) improving the solubility of poorly

dissolvable drugs or 2) changing the route of drug administration [46, 47]. Therapeutic efficacies of hydrophobic drugs are often hampered by their low water solubility, which could be mitigated by loading the drugs into amphiphilic material based formulations [48, 49] or milling the therapeutic compounds into nanocrystalline particles [50-52]. For example, the surfactant based self-emulsifying DDSs could keep hydrophobic drugs in fine emulsions, making them easier to be absorbed from the gut when administered orally [53]. Additionally, the oligosaccharide cyclodextrin (CD), characterized by its hydrophobic internal cavity and hydrophilic external surface, is a popular excipient for improving the solubility of therapeutics, such as the hydrophobic anticancer drugs camptothecin (CPT) [54] and SN-38 [55], by forming host-guest inclusion complexes [56]. With the assistance of some non-ionic or ionic stabilizers, NanoCrystal® Technology applied high shearing forces to mill micron sized drug crystals into stably dispersed nanoparticles [50], where the subcellular size of nanoparticles enabled them to penetrate the capillary walls. The NanoCrystal® Technology has brought about numerous clinically approved formulations, including the immunosuppressant drug Rapamune® and the antiemetic drug Emend® [42]. In contrast to changing the physiochemical properties of the drugs, switching the drug administration route is a straightforward method for enhancing drug absorption. For the non-invasive drug administration routes, such as oral administration [57], absorption of most drugs is mainly a process of passive diffusion across the gastrointestinal (GI) tract, where the concentration gradient of the drug is the main driving force for diffusion, leading to limited absorption rate. In addition, the existence of some efflux mechanisms, such as the p-glycoprotein that can

excrete drug from vascular circulation into the intestinal lumen, further limits the absorption of orally administered drugs. Furthermore, metabolism of the administered drugs in the GI tract or the liver before they reach the blood circulation, known as the first pass metabolism, could also reduce the bioavailability of the drugs. To bypass these limitations, parenteral administration routes were explored with numerous types of DDSs being developed. Accurate dosing and rapid absorption by intravenous (IV) or intramuscular (IM) injections are widely used for administering drugs. However, the associated pain of these methods elicited people's interest in less invasive surrogates. For examples, microneedle arrays have emerged as a great alternative due to its low cost and simplicity for drug administration [58, 59]. Recently, a smart insulin patch made of painless microneedle arrays containing glucose sensitive vesicles was demonstrated for convenient treatment of type-1 diabetes, which held great promise to relieve diabetic patients from the pain of injecting insulin [60].

2.1.2. Distribution

DDSs can help control the spatial-temporal distribution of delivered drugs [61]. The control of spatial drug distribution, which generally refers to the process involving transporting drugs from blood circulation into the tissues, aims to direct drugs specifically into the site of action; while the temporal control is meant to regulate the timing of drug release or pro-drug activation. DDSs, especially nanocarriers, could be functionalized with specific targeting agents to bind to different types of diseased tissues [62, 63]. For example, monoclonal antibody HER2 can target anticancer drugs toward HER2 positive breast tumors, enhancing the therapeutic efficacies by the order of 100 – 10000 times [64]; Peptides

targeting adipocytes is capable of guiding nanoparticles containing small interfering RNA (siRNA) into fat-storing tissues for treating obesity [65]; Monosaccharides and their derivatives like galactose and N-acetylgalactosamine are able to target transcription factor or siRNA into the hepatocytes [66-68]; To control the timing of drug release or activation, DDSs incorporating stimuli-responsive moieties were designed [69] for different types physiological factors, such as glucose levels [70-72], pH gradient [73-76], redox gradients [77-80], overexpressed enzymes [81, 82], and ATP gradients [83].

2.1.3. Metabolism and excretion

DDSs can alter the metabolism and clearance of delivered drugs through 1) altering the routes through which drugs are transported within the body; 2) shielding the therapeutic agents from adverse physiochemical environments; 3) delaying drug release and 4) bypassing the active drug efflux transporters [84, 85]. The liver and kidney are the major sites for drug clearance. Drugs administered into the body generally undergo metabolic changes, especially in the liver, which is known as “biotransformation” [86]. Different types of hepatic enzymes, mainly oxidases and transferases, transform drugs into more clearable derivatives significantly affecting their half-life, clear rate and bioavailability. Drugs absorbed by the GI tract will go through the liver via the portal vein before reaching systemic circulation, a circumstance known as the “first-pass effect” that influences the bioavailability or activity of many orally administered drugs [87]. Turning to other parenteral drug administration routes, such as transdermal [88], buccal [89], nasal [90], rectal [91] or vaginal [92], could directly bypass the portal venous system. Alternatively, formulations could also help drugs to

circumvent hepatic metabolism. For example, the lipid-based nano-formulations could be engineered to make use of the lymphatic system for distribution even after oral administration [93]. When drugs enter the blood by different delivery methods, multiple clearance mechanisms exist for eliminating drugs from circulation, such as digestive enzymes, the mono-nuclear phagocytic system (MPS) and renal clearance [94, 95]. Drug delivery formulations encapsulating drugs in a closed compartment could prevent them from enzymatic attacks in numerous types of physiological environments. For example, an in-situ polymerized nanogel coating on bio-molecular therapeutics could shield proteins from protease digestion [96, 97], protect DNA from DNase [98] or miRNA from RNase [99] degradation. PEGylation, a technique of covalently conjugating poly(ethylene glycol) (PEG) onto therapeutic agents or DDSs, has become a widely adopted strategy for improving the stealth of drugs or DDSs [100]. The highly hydrophilic PEG absorbs a large extent of water that can function as a natural barrier to isolate the loaded cargoes from enzymatic degradations, preventing the therapeutic agents from being sequestered into MPS and reducing glomerular filtration by increasing the hydrodynamic size of the formulations.

Compared with adjusting the interaction between drugs and the physiological environments [101], sustained drug release systems provide an effective way for controlling drug clearance [102-104]. Implantable depots capable of continuously releasing drugs for days or even months are convenient systems for delivering fragile drugs, which generally undergo rapid metabolism or clearance, with improved patient compliance [105, 106]. After repeated treatment by the same therapeutic agents, in particular with chemotherapeutics,

cancer cells would become resistant to that drug or its homologues by overexpressing active efflux transporters of the ATP binding cassette (ABC) containing the protein family [107]. Nanoparticle based DDSs can bypass these transmembrane multidrug resistance (MDR) transporters by targeting other receptors on cancer cell membranes [108, 109]; co-delivering an inhibitor of the transporters or incorporating stimuli-responsive drug release could also significantly block the MDR [110].

2.2. What to deliver?

Tailoring a carrier for a drug requires investigation of the chemical composition and target site of the drug [111]. Drugs having the same molecular composition and functioning against physiologically proximal targets generally face the same barriers for delivery [112], thus can be delivered by analogous strategies. Deliverable therapeutics includes small molecule drugs, proteins, nucleic acids and therapeutic cells. Small molecule therapeutics are classic drugs that make up the majority of drugs on the market [113]. They are frequently developed as regulators, mainly inhibitors, of target proteins or other bio-molecules [114, 115]. Compared with biologics, small molecule drugs can reach targeted sites relatively easily and penetrate through cell membrane effectively. Even though small molecule therapeutics remain the primary type of available drugs, in recent years a considerable increase of FDA approved biologics, mainly protein therapeutics, from 27% in 2014 in contrast to 7% in 2013 [116]. Proteins participate in all life activities, including transporting biomolecules or transducing signals within and between cells, driving biochemical reactions

and supporting cellular or tissue scaffolds [117]. Unlike small molecule drugs that are limited to simple functionalities, protein therapeutics perform more diverse yet specific activities that could be typically classified into 1) replacing or replenishing deficient proteins; 2) targeting specific molecules and 3) vaccination [118]. Proteins are usually impermeable to the cell membrane as a result of their relatively large size and electrostatic charges, making extracellular targets more accessible to protein therapeutics. Recently, encouraged by the advances in the intracellular protein delivery systems [43], proteins functioning in intracellular compartments hold great potential for healthcare applications. Nucleic acids represent a broad class of therapeutic molecules with applications in immunotherapy and gene therapy. Pathogen derived nucleic acids, such as the CpG motif targeting Toll Like Receptor 9 (TLR9) in the endosome to stimulate immune cells or viral genomic fragments capable of vaccinating the recipient [119] are efficient alternatives to protein based immune therapeutics. Gene therapies based on the delivery of nucleic acids are regarded as promising individualized treatments towards various types of life-threatening genetic disorder associated diseases such as cancer, AIDS, diabetes or other hereditary diseases [120, 121]. A diverse array of therapeutically active nucleic acids, including antisense nucleotides [122], small interfering RNA (siRNA) [123, 124], microRNA (miRNA) [125, 126], plasmids [127], mRNA [128, 129] or genome editing tools [130, 131] have been discovered. Nucleic acid based gene therapies must be delivered intracellularly, making the development of efficient vehicles to deliver these drugs extremely important in order to take advantage of nucleic acid therapeutics [132-134]. In addition to delivering chemically definable molecules, entire cells

can also serve as therapeutics either in the context of the natural antigens on the cell membrane or from the perspective of living cells as a functional entity. The antigenicity of exogenous cells could be used to train human immune systems by mimicking natural infections. There has been a long history of using inactivated or suppressed pathogens as vaccines against epidemic diseases [135-137]. Recent development of cell based vaccines [138] or chimeric antigen receptor modified T-cell therapies [139] even cast light on treatment of endogenously originated disease, including cancer. Living cell based therapies focused on replenishing functional cells to diseased organs, working in an organ replacement manner [140].

2.3. How to deliver?

To meet the physiological requirement of various drug targets, numerous types of DDSs were developed ranging from macro-, to micro- and to nanoscale. Macroscale DDSs, which generally refers to drug delivery devices with at least one dimension greater than 1 mm in size [141, 142]. Macroscale devices were developed in varying forms, such as wearable devices [143, 144], mucoadhesives [145] and long-term drug releasing implants [146, 147]. From the perspective of material, polymers are preferred for preparing physiologically compatible DDSs [102, 148-150]. Representative polymers for these devices include natural polymers like dextran, alginate, chitosan, gelatin or synthetic polymers such as poly(lactic-co-glycolic acid) (PLGA) or poly(β -aminoester) [70]. Drugs could be loaded into either a “reservoir”, where the drugs are enclosed by a polymeric membrane; or a

“matrix”, where the drugs are embedded in polymeric networks [151]. Release of the drugs could be through diffusion, where the steric hindrance from the polymer scaffold dominates; competitive dissociation, where the drug exhibits specific affinity towards the polymeric carrier; or degradation, where the polymer scaffold could be eroded via dissolution, hydrolysis or enzymatic digestion [152]. Sensitivity to environmental signals could also be incorporated into polymeric systems for smart drug delivery [153]. DDSs in the micro-scale are generally referred as microparticles that are injected locally in the tissue. Microparticles with large diameter ($> 1 \mu\text{m}$) would get stuck in the capillary bed or get caught by Kupffer cells in the liver, making them unsuitable for systemic injection [154]. When administered locally, the steric hindrance from the extracellular matrix will limit the movement of microparticles and hold the microparticles in the site of injection. This feature leads to widespread applications of microparticles as drug depots [155].

Unlike microparticles, the nanoscopic size (generally less than 200 nm) enables the nanocarriers to filter through the fenestrations of liver blood vessels as well as penetrate into tumor tissue by EPR effect [156-158]. Of note, EPR effect is not a unique phenomenon limited to solid tumors, but a more prevalent character exhibited by many types of diseases, for example, fungal infections, heart failure, hepatitis A, sclerosis, renal associated diseases [159-162]. The size of the nanocarriers needs to be meticulously controlled since larger nanocarriers ($> 500 \text{ nm}$) are susceptible to macrophage uptake while smaller nanocarriers ($< 8 \text{ nm}$) are easily cleared out via renal excretion pathway. Nanocarriers have become a widely investigated DDS with cancer as the most researched target [163]. Various types of material

have been demonstrated to construct the nanocarriers [164], such as the polymer based nanogels, micelles, polymersomes and dendrimers [165, 166]; the lipid based solid lipid nanocarriers, liposomes [167], or lipid-like lipidoids [168] ; the inorganic nanocarriers, including gold nanoparticles [169, 170], carbon nanotubes, graphene [171], nanodiamonds [172], magnetic particles [173] and liquid metal nanoparticles [174]; the macomolecular assembly based DNA [175-177] and protein nanocarriers [178].

3. Physiological barriers and designing criteria for drug delivery systems

The ability to direct therapeutic levels of drugs to the desired site is a prerequisite to achieve efficacious outcomes in treating a variety of diseases. Cancer is the best representative of these diseases, where sufficient accumulation of potent anticancer drugs is the goal for applying nanocarriers. However, physiology poses different barriers to impede nanocarriers from realizing this distant goal [179]. For a better concept on how to design cancer-targeting nanocarriers, the sequential barriers from extracellular space to intracellular compartments (Figure 1-2) after intravenously administering the nanocarriers will be introduced. Corresponding strategies to overcome these barriers will also be discussed.

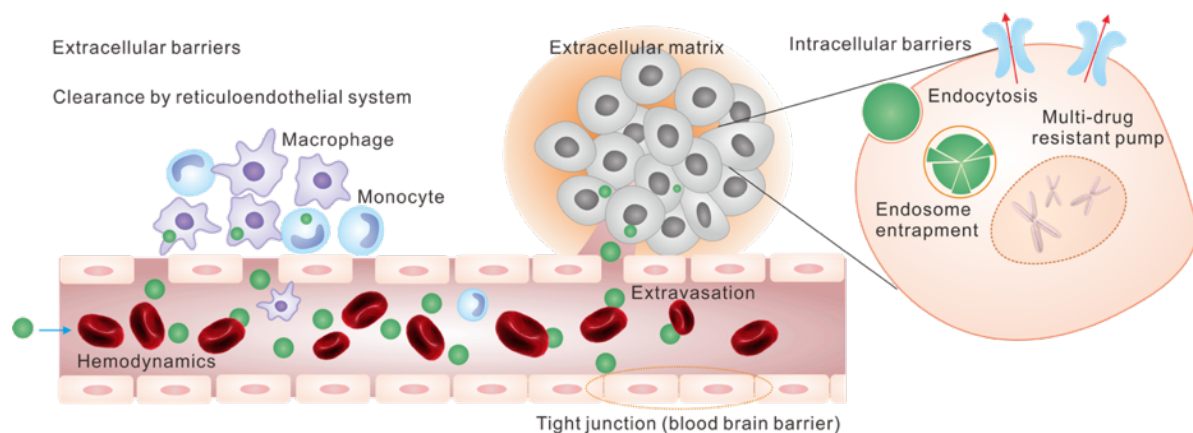


Figure 1-2. Physiological barriers for nanocarrier based drug delivery system. Nanocarriers enter the systemic circulation by intravenous injection and undergo opsonization by interacting with serum proteins. The opsonization facilitates nanoparticle clearance by reticuloendothelial system, leading to non-specific accumulation of nanocarriers in organs like liver and spleen. In the blood flow, fluid dynamics of the nanocarrier influences their margination towards vascular walls. The low permeability of vascular endothelium poses another significant hurdle for nanocarriers, especially the tight junctions associate with blood-brain barrier. After extravasation into tumor microenvironment, the nanocarrier needs to diffuse through the dense extracellular matrix against high interstitial pressure to reach the tumor cells. For drugs that work in intracellular compartments, the nanocarrier needs to be internalized through endocytosis and escape the endosome to reach other organelles. Even after entering in the cells, the cell membrane associated multidrug resistant pumps could also pump out the delivered chemotherapeutics.

3.1. Extracellular barriers

3.1.1. Nanoparticle-immune system interaction

When the nanocarriers are injected into blood circulation, rapid adsorption of serum protein onto the nanocarrier occurs. Numerous types of protein, such as fibrinogen, globulin, and albumin, will form a corona around the nanocarriers, a process termed as opsonization. This nanoparticle-protein complex is very susceptible for uptake by circulating or residential phagocytes [180, 181]. The opsonization-internalization mediated nanocarrier clearance

works as the first and major barrier in the blood, causing ~ 50% loss of the administered dose hours after injection [182]. In addition, the opsonization causes collateral damage to the targeting ligands modified on nanocarriers by shielding them from interacting with the targeted receptors [183]. Opsonization is affected by surface properties of the nanoparticles such as particle size, surface charge, shape, hydrophobicity and biological functionalities [44, 184]. Generally cationic nanoparticles are more susceptible to MPS clearance than neutral or negatively charged ones [185]. By far, the most well-established strategy for evading opsonization and MPS is to coat or graft the surface of the nanocarrier with PEG, a process termed as PEGylation [186]. As for the mechanism for PEGylation, it is generally thought that the highly hydrophilic PEG could efficiently capture water molecules and form a hydrating layer on the nanocarriers, hindering serum proteins from adsorption. Instead of ascribing the “stealth effect” to protein repellence, a recent report by Wurm and coworkers highlighted the role of changed composition of remained protein corona [187]. The accumulation of a lipoprotein (clusterin) rather than coagulation related proteins was shown to be sufficient for reducing nonspecific uptake. Huang et al. pioneered the PEGylation approach for cloaking nanoparticles with PEG and enhancing their circulation time [188]. Conformations of the PEG on the nanocarrier surface are significantly affected by PEG density, from the mushroom conformation (low PEG density) to transition state (intermediate density), and to the brush mode (high density) [189]. Grafting sufficient density of PEG chains, preferably high density PEG, to cover the surface of the nanocarrier is key for enabling full protection of the nanoparticle and preventing opsonization [190]. In addition to

the classic PEGylation, polymeric PEG substitutes or new “stealth” strategies based on biomimetic components were also demonstrated by different research groups. Zwitterionic polymers pioneered by Jiang and coworkers could induce hydration electrostatically and resist protein adsorption effectively, leading to ultralow fouling on nanocarriers or implantable devices [191, 192]. Zhang, Gu and their coworkers recently demonstrated a strategy harnessing the natural long-circulating capability of human platelets for evading opsonization [193-195]. Polymeric nanoparticles cloaked by platelet membranes exhibited reduced macrophage recognition than the uncoated nanoparticle [196]. Using a more direct approach, Discher and coworkers use a peptide derived from CD47 on the cell membrane as a “marker of self” [197]. Modifying nanocarriers with the “self” peptide significantly inhibited phagocytosis and prolonged the circulation time.

While it is necessary for cancer cell-targeted nanoparticles to avoid immune system surveillance, efficient interactions with immune cells, such as binding or internalization, are desirable for cancer immune therapy [198, 199]. The basic rationale behind cancer immune therapy is to mobilize the immune cells to raid cancer cells, an elegant strategy that has made revolutionary progress towards eradicating existing cancer cells and preventing future recurrence [200]. The expression of tumor associated antigens (TAAs), including neoantigens, proteins expressed from mutated genes, or proteins with altered modification patterns, could tell cancer cells apart from normal cells [201]. Nanoparticles deliver TAAs to professional antigen-presenting cells (APCs), like dendritic cells, leading to the presentation of TAA-derived fragments to T-lymphocytes and activating TAA-specific cytotoxic T-cells

[202]. Additionally, adjuvants capable of magnifying the responses of APCs or T-cell, such as toll-like receptor agonists, could be incorporated into the nanocarriers [203]. Small nanoparticles (ideally 10 – 40 nm) generally exhibit more efficient infiltration into the immune organs and generate stronger interaction with dendritic cells [204]. In this way, nanomedicine serves as “cancer vaccine”. Besides delivering TAAs, blocking the inhibitors of T-cell activation, such as TGF β , CTLA4 and PD-L1, also emerged as an effective approach for cancer immune therapy [205-207]. Monoclonal antibodies towards checkpoint inhibitors, including Ipilimumab (target CTLA4), Nivolumab and Pembrolizumab (target PD-1), were approved by FDA and the PD-1 antibodies were further designated as “breakthrough therapy”.

3.1.2. Hemodynamics

In cases where nanocarriers escape MPS internalization, the nanocarriers need to interact with vascular endothelial walls, especially at the tumor site, to extravasate into the tumor tissue. In this process, fluid dynamics of the nanocarriers in blood vessels plays an important role for the contact [208]. Movements of nanocarriers after administration could be classified as circulation, margination, adhesion and internalization by endothelial cells [209]. Among these movements, margination of nanocarriers towards blood vessel walls is an important contributing factor for promoting the particle-endothelial cell interaction. Generally, red blood cells tend to flow in the center of the blood vessel, forcing platelets to accumulate near the blood vessel walls [210]. As for nanocarriers, their distribution would be significantly affected by their size and geometry [40]. For the typical spherical nanocarriers,

such as small liposomes with a size of 10-100 nm, a small fraction of the administered nanocarriers could marginate to blood vessel walls during circulation [211]. Anderson and coworkers demonstrated a synthetic lipid based nanoformulation that could complex small RNA therapeutics into multi-lamellar liposome-like structure with sizes ranging from 35 nm to 60 nm. The nanocarrier efficiently avoided the capture by immune cells or hepatocytes and shuttled the RNA cargo into endothelial cell as well as solid tumors in the lung [209, 212]. Aside from size, this margination could be enhanced by tuning the geometries of the nanocarriers. For example, discoidal or ellipsoidal nanocarriers could tumble and roll during circulation, the nanoparticles could oscillate between opposite sides of the blood vessel walls, increasing the chance of contacting endothelial cells [213]. It has been reported that the aspect ratio of these particles correlate with their drifting velocities toward the vessel walls, affecting their adhesion and accumulation at tumor sites [214]. In a recent report, drug conjugated poly(L-glutamic acid) released in situ from a micro-size vascular depot could self-assemble into nanoparticles [215]. This dynamic strategy improved vascular dynamics of the nanopartilce and enhanced its tumor tropism.

3.1.3. Abnormal vasculature: EPR effect and interstitial fluid pressure

While the sealing of endothelial cells by tight junction proteins formed the blood-brain barrier (BBB) [216], the aggressive angiogenesis of the tumor generates tortuous blood vessels with leaky “gaps” [217, 218]. Nanocarriers could extravasate into the tumor microenvironment through the leaky vasculature and remain there due to reduced lymphatic drainage [219]. In addition to the traditional concept of “static gaps”, recent studies further

support the EPR effect with “dynamic vents” that formed spontaneously along the tumor vessels, allowing the extravasation of nanoparticles (70 nm) into the interstitial space [220]. EPR effect has become the number one principle for designing nanocarriers in drug delivery as it is highly strong in cancers. Numerous nanocarrier based anticancer DDSs based on the EPR effect have been approved for clinical use, such as the liposome nanocarrier encapsulating doxorubicin (Doxil) or the paclitaxel-albumin stabilized nanocarrier [221, 222]. However, challenges remain for harnessing the EPR effect for anticancer therapy. A tumor is not a homogeneous tissue, both tumors in clinical circumstances and in animal models are highly diverse [223]. Vascular densities vary with the stages of the cancer as well as the types of the tumors [224, 225]. Tumors with a high-density vasculature, such as renal cell carcinoma or hepatocellular carcinoma, tend to have a high EPR effect; while those with a low-density vasculature, such as prostate or pancreatic cancers, tend to exhibit low EPR effect [226]. To conquer the heterogeneity of the EPR effect, methods for increasing blood pressure with angiotensin II [156] or vascular normalization [227] were demonstrated. Rather than increasing vascular pressure, a strategy for improving vascular permeability with transforming growth factor- β (TGF- β) inhibitor was also proposed by Kataoka and coworkers [228]. The uneven vasculature of tumors brings about the EPR effect as a powerful tool for cancer targeted drug delivery. However, the same mechanism could also cause the extravasation of an excessive volume of fluid into the tumor microenvironment, increasing interstitial fluid pressure (IFP) and viscosity [229]. Other tumor-associated factors could contribute to the IFP such as the poor lymphatic drainage [230], steric stress from the

aggressively proliferating cancer cells, considerable fibrosis, and a compact extracellular matrix. The interstitial blood flow is the major force for distributing nanoparticles in the tumors. However, the elevated IFP poses a barrier for the extravasation and diffusion of nanoparticles to different regions of the tumor, especially to the tumor parenchyma, leading to reduced yet heterogeneous drug delivery and compromising therapeutic efficacies [231]. To overcome the IFP barrier, strategies targeting the IFP inducing factors were demonstrated, such as reducing angiogenesis by blocking VEGF [232, 233] and reducing collagen density in the extracellular matrix [234]. Overall, the EPR effect and IFP constitute contradictory forces in the process of nanoparticle extravasation into tumor, a balance of these two forces needs to be taken into consideration for devising effective solid tumor targeting nanocarriers [235].

3.1.4. Extracellular matrix

Nanocarriers that successfully overcome the barrier of vascular endothelial membrane will reach the tumor microenvironment and meet the next obstacle, namely the extracellular matrix (ECM) [236]. The ECM is a complex non-cellular network composed of various types of networked macromolecules, including polysaccharides proteoglycans, proteins, and glycoproteins [237]. The ECM interacts with the tumor cells in a reciprocal way, where the ECM offers a framework affecting tumor morphology and development, the cells are continuously constructing or re-arranging the ECM [238-240]. The physical rigidity of the ECM poses significant steric hindrance for nanoparticle diffusion, trapping the nanoparticles or inducing premature drug release before reaching the tumor [241]. The ECM could be

structurally divided into two parts: the basement membrane and the interstitial matrix. The basement membrane is constructed by stroma, epithelial and endothelial cells together to function as a scaffold for the mural and endothelial cells, while the interstitial matrix is primarily built by the stroma cells [242]. The basement membrane is a continuous and compact sheet-like structure mainly composed of type IV collagen, fibronectin, laminins with entactin and nidogen as linkers [243]. Ratios of the constituents vary between different tumors or different sections of the same tumor, contributing to the heterogeneity of tumors. The porous basement membrane does not elevate IFP and the nanocarriers penetrate the basement membrane through passive diffusion. Penetration efficacies of the administered nanocarriers were mainly affected by the collagen fiber densities and pore sizes [244-246]. To overcome the barrier of the basement membrane, a transient window of basement membrane remodeling could be harnessed. The window is created by angiogenesis, which demands the degradation of type IV collagen by matrix metalloproteases (MMP2 or MMP9) [247, 248]. Slightly different from the basement membrane, the interstitial matrix is charged and highly hydrophilic with primary constituents including proteoglycans, fibrillar collagens, fibronectin and tenascin C [249, 250]. Thick aligned type I collagen fiber is the main composition of the collagen. Combined with the restricted volume of interstitial space, the interstitial matrix is denser than the basement membrane [251]. The accumulated tension leads to increased IFP, making it more difficult for nanocarriers to diffuse through. To overcome this barrier, several strategies have been demonstrated. For example, degrading the matrix with co-administered collagenase or hyaluronidase [252-255], dilating the matrix

pores by hypertonic solution [256], or decreasing the crosslinking of collagen fibers [257], could all significantly enhance the diffusion of nanocarriers.

3.2. Intracellular barriers

While a small fraction of anticancer therapeutics target specific receptors on cancer cell membranes, such as antibodies and cytokines [258, 259], most drugs need to be delivered to intracellular targets to exert effect [260]. Therefore, following extravasation into the tumor site, it is desirable that the nanocarriers are capable of shuttling the cargoes into an intracellular compartment. To reach the targeted subcellular compartment, more barriers arise from the subcellular structures of the cells [261].

3.2.1. Internalization

Small molecular therapeutics, especially those with high hydrophobicity, are capable of passively diffusing through the lipid bilayer plasma membrane [262]. However, for protein or nucleic acid based therapeutics, nanocarriers are generally needed for transportation into the cells [43, 263]. Numerous internalization pathways exist and the entry is affected by various properties of the nanocarrier, such as particle size, surface charge, physiochemical composition and the modification with targeting ligands [264]. For nanocarriers that are not modified with any specific targeting ligand, the uptake is mainly through endocytosis [265], where vesicles emerge from plasma membrane to encapsulate and internalize the nanoparticles together with extracellular fluids. Size plays a major role in demining the endocytosis pathway. Large particles (up to 1 μm) usually enter the cells by

macropinocytosis and the clathrin-dependent pathway generally takes up nanoparticles smaller than 120 nm [266, 267]. Smaller nanoparticles could be internalized through the caveolae-dependent pathway (50 nm to 100 nm) or the clathrin and caveolae independent pathway (< 50 nm) [268]. The size cut-off is indefinite and surface chemistries significantly affect internalization pathways. Also, the internalization pathways are not exclusive, therefore a specific type of nanocarrier could be internalized through a combination of several pathways [269]. Besides size, extensive research efforts have been devoted to optimize geometrical properties of nanocarriers for enhanced cellular uptake [270] [271, 272]. Due to the negative charge of phospholipids, positively charged nanocarriers generally show stronger interaction with plasma membranes, leading to increased internalization [273]. In addition to tuning the physical properties of nanocarriers to increase endocytosis, specific receptors overexpressed on cancer cell membranes could also be exploited for facilitated and selective internalization. For example, epidermal growth factor receptor (EGFR) [274], folate receptor [275], transferrin receptor [276], lectins [277] and low-density lipoprotein receptor [278] are well-characterized receptors to induce efficient cellular uptake. Different types of targeting ligands, including small molecules [279], antibody [280], peptide [281] and aptamers [282] can be easily functionalized onto the surface of the nanocarriers [283, 284]. For example, the folate receptor is a commonly overexpressed receptor by many types of cancers. Modifying high concentrations of the small molecule ligand folic acid onto a DNA nanocarrier was demonstrated to facilitate the intracellular delivery of siRNA [285].

3.2.2. Endosome/lysosome escape

After internalization of the nanoparticles through plasma membrane invagination, as in the case of the classic clathrin-mediated endocytosis, the nanocarriers are generally trapped inside the vesicles that help them enter the cells – known as endosomes [286-288]. As the endosome matures, it tends to traffic toward and fuses with the lysosome, where the acidic and enzyme rich environment would lead to the degradation of the nanocarrier as well as the cargoes [289]. Meanwhile, the trafficking of nanocarriers from late endosome to extracellular space through recycling pathways, as in the case for cationic lipid nanocarriers, further limit the cytosolic availability of delivered drugs [288]. The endo-lysosome entrapment poses the most critical barrier for the intracellular drug delivery, especially for macromolecular therapeutics. To overcome this barrier, various endosome escape agents derived from viral or bacterial invasion machineries were utilized for nanoparticle escape from the endosome membrane [290-292]. The methods for endosome escape could be further classified into different mechanism, such as proton-sponge effect [293], nanoparticle-endosome membrane fusion [294, 295] and photochemical disruption [296]. Acidification of the endosome played an important role for cellular uptake of nanoparticles [287, 288], towards which the proton-sponge effect is a widely adopted approach that is generally integrated with polyamine-based polymers with a pKa rang of 5-7 [297]. These polymers are able to buffer the acidification of the endosome, increasing the influx of ions into endosomal compartments and causing rupture of the endosome membranes. The most representative example of this type of polymer is Polyethylenimine (PEI), a potent transfection reagent for

genetic engineering of various types of cell lines [298]. For the membrane fusion based mechanisms, fusogenic lipids or peptides are usually incorporated into the nanocarriers. The popular fusogenic lipid 1,2-Dioleoyl-sn-glycero-3-phosphoethanolamine (DOPE) is an acid-responsive lipid that undergoes a phase transition from bi-layered to hexagonal conformation for fusing with endosome membrane [299]. Besides phase transition, ionizable lipid with optimal pKa around 6.2 to 6.5 was proposed to be effective in promoting membrane fusion [286, 287]. Endosome acidification would trigger the formation of ion pairs between the lipid and endosome membrane, promoting lipid exchange and drug release into the cytosol. It has been recognized that the pKa and hydrophobicity of the lipids are crucial properties for preparing efficient intracellular DDSs [300, 301], and the balance between pKa and hydrophobicity has become a guideline for synthetic lipid and polymeric carriers [302-304]. Fusogenic peptides inspired from the viral capsids, such as KALA or H5WYG, also exhibit structural changes in the acidic environment of the endosome [305]. The negatively charged or neutral peptides will transform from random coils into rigid and hydrophobic helices to insert into the membrane of the endosomes. Another applicable approach for inducing endosome escape in a spatial-temporally controlled manner involves photosensitizer-mediated photochemical therapy [306]. Small molecular or polymeric photosensitizers could generate ROS when excited by externally applied photons, leading to drastic destruction of the endosome [307]. However, this method is complicated by damage to the delivered cargoes.

In addition to the various methods for disrupting the endosome membrane, an emerging facile strategy is to bypass the endo-lysosome. Different endocytic pathways lead to distinct intracellular fate of nanoparticles, endosomes generated by the caveolae-mediated endocytosis tend to fuse with caveosomes and bypass the lysosome fusion [308]. A representative nanoparticulate system is the spherical nucleic acids, which use highly organized nucleic acid oligos to coat the surface of gold nanoparticles covalently [309]. Instead of being internalized through the classic clathrin-mediated endocytosis, this nanoparticle binds the class A scavenger receptor on cell membrane and get endocytosed through caveolae and lipid raft-mediated pathway, arriving at early endosome [310]. Then, through a not yet well-characterized mechanism, possibly associated with the sorting of nanoparticles towards Golgi apparatus or endoplasmic reticulum [311], this nanoparticle could be trafficked to the cytosol without the assistance of endosome escaping agents.

Of note, in spite of all the difficulties of getting nanoparticles out of endosome entrapment, the endosome is not merely a trap. If the timing of endosome escape could be fine-controlled, endosomes could offer a fast ride along the cytoskeleton to move the nanoparticles closer to the interior of the cells [312]. Even though most endosome vesicles end up fusing with lysosomes, endosomes are capable of shuttling the cargo to different subcellular organelles, such as the Golgi apparatus, the mitochondria and the endoplasmic reticulum [313, 314]. This feature would be very useful for nuclei targeted gene delivery, since the endosome assisted migration towards the nuclei would be more efficient than passively diffusing the nucleic acid through the cytoplasm [315].

3.2.3. Nuclear import

The nucleus stores genetic information of the cells, where many therapeutic targets are located [316]. In a non-dividing cell, the nucleus is wrapped in a double-layered lipid envelope, where the pores on the membrane regulate the traffic in and out of the nucleus. Generally, molecules smaller than 5 nm (approximately the size of a 40 KDa protein) could diffuse through the pores passively; while larger ones (up to 39 nm in diameter) need to be transported actively by the importing machineries [317, 318]. The low efficiency of nucleus entry from the cytosol becomes a bottleneck for nucleus targeted gene therapies [319]. To overcome this barrier, nuclear localization sequences (NLS) are often fused with targeted proteins [320]; attached to desired plasmids [321] or nanoparticles [322] for facilitating nucleus transport. The NLS interacts with the nuclear pore associated proteins, including importin α and β , and form a protein complex that could be pulled into the nucleus by the nuclear pore complex [323, 324]. The most popular NLS was derived from the large T antigen protein of SV40 virus and it is capable of enhancing nuclear transport efficiency of plasmid by 10 to 1000-fold [325]. Other available NLS include peptides derived from importin β [326] or the N-terminus of yeast transcription factor GAL4 [327]. An alternative strategy to NLS for nuclear-targeted plasmid delivery borrows the transportation of endogenous transcription factors [328]. By coding a sequence that could bind constitutively expressed transcription factors such as NF- κ B into the plasmids, transcription factor facilitated nuclear transport could be achieved [329]. A general sequence, designated as “nuclear targeting sequence”, that can bind various types of transcription factors was derived

from SV40 enhancer, which could serve as a universal strategy for facilitated nuclear delivery [330]. Furthermore, due to the characteristic expression of transcription factors in different cell lines [331], selective nuclear transport in desired cells could also be achieved by coding the selected transcription binding sequence.

3.2.4. Drug efflux pumps

After overcoming the multiple barriers, the administered drugs finally reach the desired intracellular loci of the targeted cell. The delivery task may still fail, especially for chemotherapeutics, due to the potential drug resistance of the cells. Drug resistance develops either intrinsically before administering the therapeutics or externally after extended exposure to chemotherapeutics [332]. The chemotherapeutic resistance stems from complex mechanisms that involve defects in the apoptosis machineries, induction of alternative DNA repair pathways, structural changes of the drug targets, and elevated expression of drug efflux pumps [333]. Among the different mechanisms, the drug efflux pump is the most significant barrier that could pump out not only the administered drugs but also a wide range of therapeutics with structural similarities, leading to multidrug resistance (MDR) [334-336]. The MDR could remarkably reduce intracellular drug concentrations and compromise the therapeutic efficacies. Classic MDR pumps are comprised of proteins from the superfamily of proteins containing ATP-binding cassette (ABC) [337]. Representative pump proteins include the P-glycoprotein, where the P stands for permeability [338]; the breast cancer resistance protein (BCRP) [339] and the multidrug resistance-associated protein (MRP) [340]. The P-glycoprotein mainly pumps cationic and lipophilic drugs, the BCRP mainly

transport anions, and the MRP binds substances somewhere in between [341]. To overcome the MDR, viable strategies involve optimizing the nanocarrier compositions or co-delivering different agents for bypassing MDR pump recognition, inhibiting transporter activity or its expression [12]. For example, nanocarriers based on the amphiphilic copolymer Pluronic could abrogate MDR through several well-studied mechanisms: the polymer could be incorporated into cell membranes and alter its viscosity; it could lower the activity of the MDR pumps by reducing intracellular ATP level; it could enhance apoptosis signaling by triggering the release of cytochrome C as well as ROS; and it could also avoid intracellular vesicle entrapment of the nanoparticles [342]. Many other nanomaterials that could avoid the MDR were also demonstrated, such as DNA origami [343], guanidinium modified polyphosphoester [344]. For co-delivering MDR regulating therapeutics, small molecular MDR modulators, such as the P-glycoproteins inhibitors verapamil [345] and tariquidar [346] or the BCRP inhibitor CG918 [347], could significantly reduce the transportation as revealed from the 10 to 100- fold decrease in IC₅₀ values. Similarly, co-encapsulating siRNA to target the MDR transporter could also help reduce the MDR [348].

3.3. Designing criteria of nanocarriers for drug delivery

The journey of the nanocarriers from the syringe to the targeted site is full of barriers, leaving only a small fraction of those “lucky” nanocarriers reaching the destination. Advances in material science have enabled researchers with the ability to precisely manipulate the properties of nanocarriers in terms of their material composition, size, shape

and surface properties (Figure 1-3) [349-351]. To provide a straightforward concept of how to prepare efficient nanocarriers, we have summarized the preferred values for these parameters as below:

3.3.1. Size: To prepare nano-particulate carriers for drug delivery, size is the parameter of top priority that needs to be controlled within the optimal range. To obviate the complication of shape, we will use spherical nanocarrier as a model to discuss the size preferences of nanocarriers for anticancer therapies. Nanocarriers that are too small (< 10 nm) are easily cleared from the circulation through glomerular filtration [352], while nanocarriers that are too large ($> 2 \mu\text{m}$) tend to clog the blood vessel due to the limited diameter of the capillaries ($\sim 5 \mu\text{m}$) [353]. For tumor-targeted nanocarriers, the size should be tailored to fit the EPR effect, which limits the particle size within 500 nm [354] and preferentially greater than 200 nm [355]. Nanocarriers larger than 200 nm also risk clearance by other organs, such as liver, spleen, or lung, reducing their circulation half-time. In addition to tumor accumulation, the ability to penetrate dense solid tumors makes nanocarriers within sub-100 nm range more efficient carriers. A systemic investigation of mono-dispersed silica based nanocarriers with three different sizes (20 nm, 50 nm and 200 nm) showed that nanocarriers of 50 nm diameter showed the highest tumor accumulation and penetration efficacies, more efficient than nanocarriers near the lower and higher size limits [356]. Overall, nanocarriers within the size range of 10 to 200 nm, preferentially smaller than 100 nm [357], are typically suitable for tumor targeted drug delivery.

3.3.2. Shape: Emerging studies on the effect of nanocarrier shapes revealed that the shape could significantly affect the delivery efficacy from multiple aspects of the delivery process, including circulation, extravasation and internalization by targeted cells [358-360]. Currently, nanospheres, nanodiscs, nanorods and nanocylinders are among the most investigated geometries. From the perspective of circulation, nanocarriers with a cylindrical [361] or disc-like [362] structure showed distinct hemodynamic patterns versus spherical ones, circulation half-time could be enhanced either by orienting the nanocarrier to follow blood flow or by tumbling in the blood vessels. In addition, the shape of the nanocarriers affects macrophage recognition [363], further affecting the bio-distribution patterns. For targeted internalization by cancer cells, nanocarriers with a bacteria-like rod shape, such as gold nanorods [364] and silicon nanorods, generally demonstrate higher intracellular uptake efficiencies than their spherical counterparts possibly due to the evolved machineries in mammalian cells against bacteria. Particularly, non-spherical nanocarriers have shown the potential to exhibit better drug delivery efficacies than spherical nanocarriers, which makes shape an applicable parameter for nanocarrier optimization. To fully utilize the benefits of shapes for optimized drug delivery, emerging strategies that use morphologically transformable nanocarriers were demonstrated [365, 366]. For example, a nanocarrier capable of transforming from nanodisks to nanospheres upon environmental triggers, including pH, or chemicals, could take advantage of the elliptical disc shape to avoid macrophages and utilize the spherical shape for internalization [367].

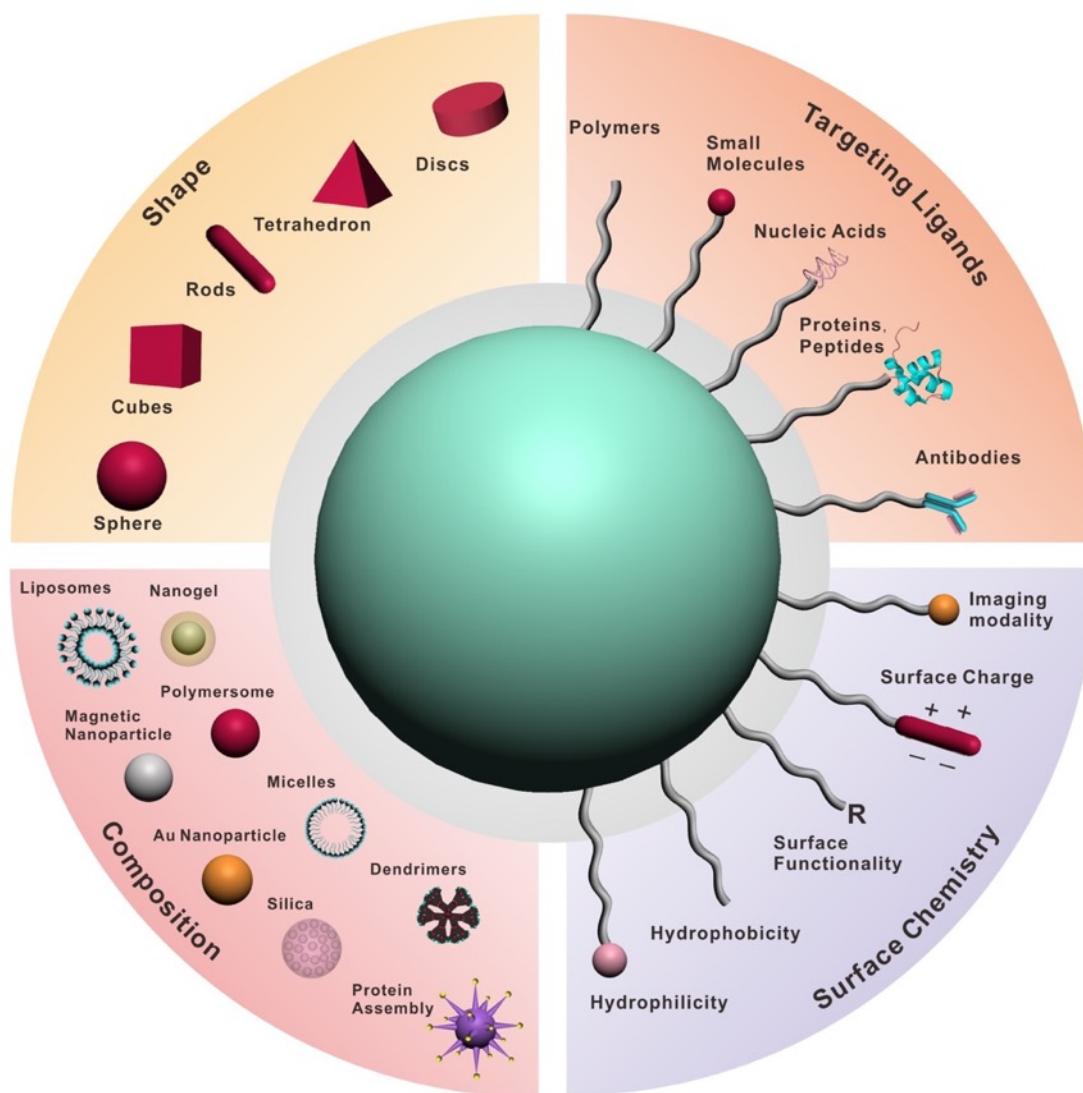


Figure 1-3. Parameters for nanoformulation design. Properties of the nanocarrier could be tailored modularly from the perspective of size, material composition, shape, surface chemistry and targeting ligand conjugation to overcome the sequential physiological barriers for precise drug delivery.

3.3.3. Surface Charge: Due to the negative charge of cell membranes [368], positively charged nanocarriers typically exhibit superior *in vitro* internalization efficacy versus

negatively charged or neutral ones [369, 370]. This phenomenon holds for numerous types of cell lines, including macrophages or cancer cells [371]. Generally, positively charged nanocarriers were endocytosed through the clathrin-dependent pathway while negatively charged nanoparticles tend to be internalized through the caveolae-mediated pathway [308, 372]. However, for *in vivo* administration, the positive charge on nanocarriers could easily attract serum proteins, which are mostly negatively charged, to form protein corona, increasing the risk of being cleared out by immune cells. In addition, the high positive charge also risks disrupting platelets and causing hemolysis [373, 374]. In view of this, negatively charged or neutral nanocarriers are better choices for long circulation. To balance the need of long circulation and enhanced cellular uptake, a popular strategy called “charge-reversal” was incorporated into many nano-particulate systems [375]. For this strategy, the nanocarriers were tailored to maintain a neutral or slightly negative charge while in circulation but shift to a positive charge when reaching the tumor microenvironment. Generally, the acidic extra-tumoral microenvironment is used as a trigger to cause the shedding of the negatively charged shells from the positively charged cores [376]; or switching the charge of a synthetic peptide, where the isoelectric point could be tuned [377].

3.3.4. Surface composition: Since the surface of nanocarriers is the frontier part that contacts the cells, interaction from the surface components with cells would affect the fate of the delivery process. For example, cellular internalization could be significantly affected by the hydrophobicity or hydrophilicity of the surface and hydrophobic nanocarriers could be easily internalized [378]. In this case, the classic PEGylation strategy dramatically increases

the hydrophilicity of the surfaces and elongates their circulation time. Complementary strategies to the PEGylation strategy to further reduce the chance of being cleared out by the complement system have been suggested to modify surface of the nanocarriers with self-markers, such as factor H or CD 47 [379] or use naturally derived cell membranes [193, 194]. Besides avoiding macrophage recognition, the existence or absence of targeting ligands on nanocarrier surfaces could influence their adhesion and entry into targeted cancer cells. The overexpressed receptors on tumors as well as vascular proximal endothelial cells make targeting ligands a favorable component for targeted delivery with improved precision [380]. Even though, it is necessary to keep in mind that healthy cells also share the receptors of the tumor cells but at a lower expression level [381, 382]. Significant damage by the targeting ligand still exists.

3.3.5. Elasticity and degradation: Elasticity of the nanocarriers is another parameter that could be tuned to optimize the delivery efficacy [383, 384]. It has been demonstrated that the energy cost of wrapping up a nanoparticle by the cell membranes decreases as a function of increasing stiffness [385], making rigid nanoparticles easier for cellular uptake. However, rigid nanocarriers are easily cleared out when administered *in vivo*. In comparison, elastic nanocarriers exhibit better circulation performances in a way similar to red blood cells (RBC) [386], where the elastic RBC could be easily deformed to squeeze through blood vessels even narrower than their diameter. So, enhancing the elasticity of the nanocarriers is a straightforward option for improving the circulation of the nanoparticles. Biodegradability is another important consideration for designing nanocarriers from the perspective of drug

release efficacy as well as biocompatibility. When degradation or dissociation of the nanocarrier is needed to release the encapsulated drug, methods to maintain the drug in the carrier during circulation but release it after arriving at its destination become important for efficient drug delivery [387]. In this case, functional moieties that could be degraded by specific signals in the tumor microenvironment could be incorporated into the nanocarriers to control the drug release [388]. For the issue of biocompatibility, it is preferable to use nanomaterial that could be degraded into non-toxic products. However, for non-degradable nanocarriers, such as metallic based nanocarriers, it is desirable that the nanocarriers could be cleared out of the body after finishing the mission of delivery [389]. As an example to address the issue, Chan and coworkers have demonstrated a strategy of combining biodegradable DNA into metallic nanocarriers, making the nano-assembly dissociable into smaller nanocarriers for clearance [390].

Designing nanocarriers for efficient drug delivery is a comprehensive task that needs to take the considerations of multiple criteria associated with physiology into a single formulation. In the next section, we will discuss some exemplary strategies for preparing “smart” formulations that can leverage the physiological signals in the diseased tissue for controlled release of therapeutics.

4. Smart drug delivery systems mediated by physiological signals

To achieve nanocarrier-mediated drug delivery with higher spatial-temporal precision, bio-inspired strategies that endow the delivery vehicles with the capability of interacting with physiological environment and determining when and where to release the payload are gaining increased interest (Table 1-1). To design these “smart” formulations, stimuli-responsive moieties that translate physiological signals at tumor microenvironment into behaviors of the nanocarriers, such as swelling, degradation, morphological change and charge reversal have been developed (Figure 1-4). Nanomedicine responsive to physiological stimuli, including acidic pH, overexpressed enzymes, redox gradient, or elevated metabolite concentrations, holds great promise for improved anticancer efficacy (Figure 1-5). They could exhibit better pharmacokinetic profiles with reduced concern of premature drug leakage during circulation and improved tumor targeting efficacies, where a higher percentage of the administered drug would be accumulated in the targeted cells.

Table 1-1. Summary of exemplary physiological stimuli-responsive formulations discussed in this review.

Stimuli	Nanoplatform	Responsive moiety/ responsive type	Drugs	Target Type	Ref.
Acidic environment	polyelectrolyte/DN	peptide/charge reversal for internalization	Plasmid for gene therapy/phototherapy	non-small cell lung carcinoma	[394]
	peptide-nucleic acid conjugate	peptide/conformational change for direct membrane penetration	Anti-microRNA-155	lymphoma	[126]

Table 1-1 continued

	siRNA- conjugated amino-dextrans	Acetal linkage/ endosomal cleavage for drug release	siRNA	-	[396]
	DNA-alkyl conjugate	Acetal linkage/targeting ligand shedding for endosome escape	Transcription factor Nrf2	hepatocytes	[66]
	RBC membrane coated polymeric nanoparticle	Glycerol dimethacrylate/endosomal degradation for drug release	DOX/TRAIL	Primary and circulating tumor	[194]
	Polymer-Liquid metal conjugate	Liquid metal/fusion and degradation for ligand/drug release	DOX	HeLa	[174]
Enzyme activity	Peptide-dendrimer conjugate	Peptide/MMP cleave for internalization	Plasmid encoding siRNA/DOX	U-87 malignant glioma	[403]
	PEG-drug conjugate	Peptide/MMP cleavage mediated PEG shedding for internalization	PTX	non-small cell lung cancer	[404]
	Capped MSN	Peptide/MMP cleavage for drug release	Cisplatin	lung cancer	[405]
	Modified graphene oxide	Peptide/furin cleavage for sequential drug release and internalization	DOX/TRAIL	Lung cancer A549	[408]
	Gel coated liposome	hyaluronic acid/HAase mediated drug release and internalization	DOX/TRAIL	Breast cancerMDA-MB-231	[409]
	Peptide modified liposome	Peptide/legumain cleavage activated internalization	DOX	Breast and lung cancer	[411]
	Polymeric nanogel	Peptide/furin cleavage for drug release	caspase-3	Hela	[412]
	Polymer/DNA complex	Peptide/kinase mediated charge reversal for drug release	plasmid	B16 melanoma	[413]
	Quinone modified liposome	Trimethyl quinone/ quinone reductase cleavage for drug release	calcein	-	[414]
Reducing gradient	Capped MSN	Disulfide/GSH cleavage for drug release	DOX	Hela	[422]
	PEG-dendrimer	PEG shedding for internalization	DOX/siRNA	B-cell lymphoma 2	[423]

Table 1-1 continued

	Polymer nucleic acid conjugate	Disulfide/drug release	siRNA	HeLa	[424]
	Polymeric nanogel	Disulfide/nanoparticle degradation for drug release	P53	Breast cancer	[426]
	Polymer/DNA complex	Disulfide, Diselenide/drug release	DNA	HepG2	[427]
	Pillararene assembly	Ferrocenium/polarity change for assembly disruption	DOX/siRNA	HeLa	[428]
ROS	Polymer/nucleic acid complex	Thioketal/drug release	siRNA	intestinal inflammation	[437]
	liposome	Aryl boronic ester/protein activation	RNAse A	-	[439]
	Peptide-drug conjugate	boronic acid/activated internalization	Imaging agent	leukemia	[446]
	Polymer conjugated nanocrystal	Thioesters/polarity change for assembly disruption	PTX	-	[442]
	Ferrocenium modified polymeric assembly	Ferrocenium/polarity change for assembly disruption	pyrene	-	[444]
Hypoxic condition	Polymer/nucleic acid complex	Azobenzene/PEG shedding for internalization	siRNA	HeLa	[453]
	Modified dextran nanoparticle	2-nitroimidazoles/polarity change for drug release	DOX	squamous carcinoma	[454]
ATP gradient	HA nanogel coated DNA duplex	ATP aptamer/drug release	DOX	Breast cancer	[456]
	Graphene oxide aggregate	ATP aptamer/aggregate disassembly for drug release	DOX	HeLa	[459]
	Capped MSN	Zn ²⁺ -dipicolylamine/drug release	DOX, CPT	HeLa	[460]
	Polymer/nucleic acid assembly	phenylboronic acid/drug release	siRNA	-	[461]

Table 1-1 continued

	Protein assembly	ATP consuming protein/conformational change for assembly disruption	Imaging agent	HeLa	[462]
Synergistic multi- stimuli	Polymeric micelle	Ketal+disulfide/pH and acid responsive micelle degradation	DOX	HeLa	[464]
	Polymer-drug conjugate	aromatic ester + aliphatic ester/redox and esterase facilitated drug release	Aspirin, cisplatin	prostate and cisplatin resistant ovarian cancer	[465]
	Polymer nanoparticle	thioetal + chitosan/ROS and acid triggered conformational change for drug release	curcumin	ankle inflammation	[466]
	Polymer-drug conjugate based micelle	Thioester + phenol ester/ROS and redox responsive drug release	SN38	Breast cancer	[467]
Sequential stimuli	Capped MSN	Peptide + disulfide/MMP and redox sequentially activated internalization and drug release	DOX	squamous cell carcinoma and human colon cancer	[468]
	Polymeric nanoparticle	Calcium phosphate + HA/pH and HAase triggered sequential release of siRNA and DOX	siRNA/DOX	ovarian cancer	[469]
	liposome	Fusogenic lipid + ATP aptamer/ pH and ATP sequentially triggered endosome escape and drug release	DOX	Breast cancer	[470]
	DNA nanoparticle	Glycerol dimethacrylate + DNA/ pH and DNase sequentially triggered drug release	DOX	ovarian cancer	[98]
	Polymeric nanoparticle	HA + human serum albumin + glycerol dimethacrylate/ HAase,	TRAIL/cilengitide	Breast cancer	[471]

Table 1-1 continued

Polymeric micelle	Glucose oxidase + 2-nitroimidazoles/glucose and hypoxia sequentially triggered drug release	insulin	diabetes	[60]
-------------------	---	---------	----------	------

4.1. Nanomedicine responsive to physiological triggers

4.1.1. Acidic environment

Local decrease of pH in different tissues (such as the GI tract and vagina), subcellular compartments (such as the endosome and lysosome), or disease-associated conditions (such as infection, inflammation and tumor microenvironment) provides a reliable signal to trigger the drug release from the DDSs. For tumors, the abnormal metabolic activities, like the elevated rate of glycolysis, together with poor lymphatic drainage lead to the accumulation of lactic acid. Tumor-targeted nanocarriers will experience subtle pH changes when they extravasate from the blood circulation (pH 7.4) to the extracellular space of tumors (pH 6-7.2) [391]. Nanocarriers internalized into intracellular space will undergo a further decrease of pH in endosomes (pH 5.0 - 6.0) and lysosomes (pH 4.0 -5.0) [392]. To harness the pH gradient, numerous pH-responsive formulations have been developed based on two mechanisms: 1) incorporating protonatable polymers (such as polyacids, polybases, or polyamino acids) that could allow solubility or conformational changes upon acid stimulation; 2) utilizing acid labile moieties (like bicarbonate salts), or acid-cleavable bonds (such as hydrazine, acetal and ester) to enable disruption of the nanocarrier in acidic environments [75].

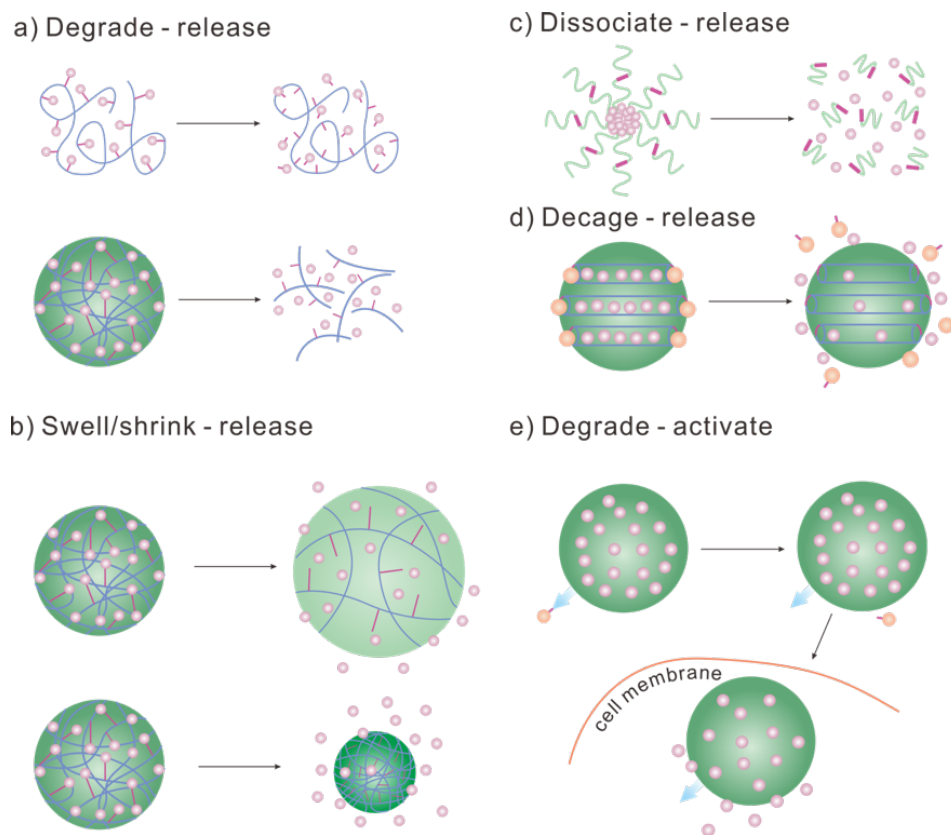


Figure 1-4. Mechanisms of stimuli-responsive nanocarrier for drug delivery. The drugs could be released from the nanocarrier upon physiological signal triggered a) degradation, b) swell or shrink, c) dissociation, d) uncapping the pores of mesoporous silica nanoparticles. d) Nanocarrier activation for cell penetration with exposed moieties.

The subtle pH difference between blood circulation and extracellular space of tumors is often utilized as a cue to activate the nanocarriers for better tumor penetration or cancer cell internalization, such as shedding the stealth coating, exposing the cell penetrating peptide, or converting the surface charge. For example, Hammond and coworkers demonstrated a sheddable layer coated nanocarrier prepared by a layer-by-layer deposition technique for acidity-triggered internalization *in vivo* [393]. A stealth layer composed of PEG

was coated onto the positively charged inner layer consisting of PLL through the modified linkers: iminobiotin and neutravidin. The iminobiotin-neutravidin bond is stable at alkaline conditions (pH 8-12) but it is easily dissociated at acid pH (4-6). Cloaking the positive charge of PLL by PEG could reduce the incidence of non-specific uptake during circulation. However, when accumulated in the tumors, interaction between the iminobiotin and neutravidin is compromised upon exposure to the acidic tumor microenvironment, exposing the positively charged PLL layer for facilitated cellular uptake. By incorporating amino acids, including glutamic acid (Glu) and histidine (His), into the polymer backbone composed of PEG, Kempson and coworkers prepared the polymer poly(PEG-His-Glu) with tunable pH induced charge reversal properties for enhanced anticancer gene delivery [394]. Charge behavior of the nano-formulation is dictated by the interaction between the three polyelectrolytes: the negatively charged DNA, positively charged PEI, and the charge reversible poly(PEG-His-Glu). The researchers tuned the ratio of the three components and demonstrated that the protonation of amino acids at acid environment (pH 6.8) could reverse the charge of the nanocarrier from negative (pH 7.4) to positive, facilitating intracellular uptake. An acid-dependent uptake profile was observed for the charge reversible nanocarrier, while the “always positively charged” control without the poly(PEG-His-Glu) did not show any difference with varying pH. The charge reversal enabled systemic administration of the nanocarriers and a single injection induced the therapeutic level expression of the anticancer protein in the tumor. Besides activating the electrostatic interactions between nanocarriers and cell membranes, acidity-triggered conformational change of peptide was also proven to

be an efficient way of tumor-targeted delivery. Slack and coworkers have demonstrated the application of a peptide that could fold into a rigid α -helix in an acidic environment, named the pH low insertion peptide (pHLIP), for targeted delivery of anti-microRNA [126]. During circulation, the random morphology of the peptide made it impermeable to the cell membrane, reducing non-specific internalization and achieving passive accumulation in tumors. The acidic extracellular space of the tumors induced the folding of pHLIP, which was later inserted into the cancer cell membranes and translocated into the cytosol via an endocytosis-independent way. By appending a neutrally charged peptide nucleic acid (PNA), which was designed to absorb the oncogenic microRNA-155 in cancer cells, the researchers showed that the pHLIP could shuttle the PNA cargo into the cytosol of cancer cells *in vivo* with high tumor specificity.

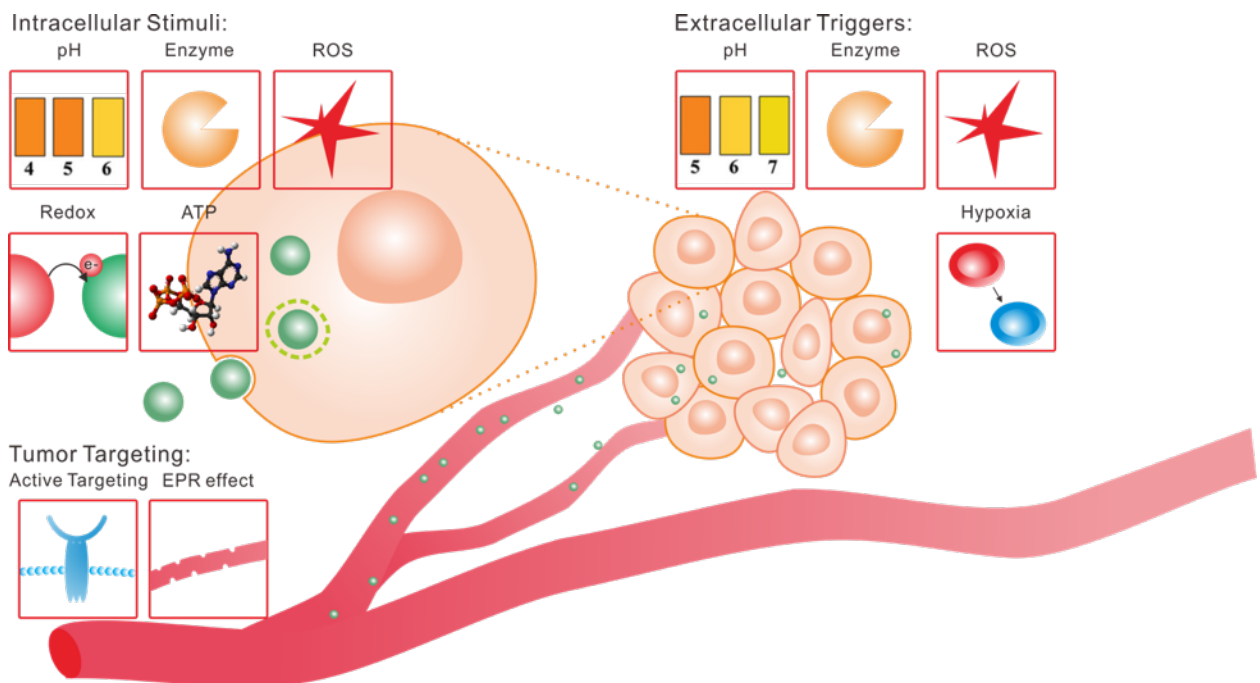


Figure 1-5. Harnessing physiological traits of tumor for precise drug delivery. The nanocarrier could reach the tumor either by actively binding to tumor specific receptors or passively through the EPR effect. Physiological signals in the extracellular space, such as pH gradient, enzyme, ROS and hypoxic environment could be utilized to trigger the release of drugs targeting extracellular objectives or activate the nanocarrier for further intracellular penetration. Intracellular environment, such as acidity, enzymes, ROS, reducing potential, ATP gradient, could be used to trigger intracellular nanoparticle transport or drug release.

In addition to the extracellular acidity activated cellular uptake, the stronger acidity of intracellular vesicles is generally utilized to activate intracellular trafficking or degrade the nanocarriers for drug release. Davis and coworkers demonstrated a nano-formulation with an intracellularly sheddable targeting ligand to overcome the BBB [395]. The receptor-mediated transcytosis was harnessed for traversing the BBB and the protein transferrin was modified as targeting ligand onto 80-nm gold nanocarriers via an acid degradable linker. Binding to the transferrin receptor on the blood side initiated the transcytosis, where the acidification in the vesicles cleaves the acid labile linker and release the gold nanocarriers to the brain side. Furthermore, it was shown that formulations with the acid cleavable linker showed much higher transcytosis efficacies than the non-cleavable counterparts. Fréchet and coworkers designed acetal linked amino-dextran for efficient and acid-cleavable delivery of siRNA [396], the acetal linker between siRNA and the modified polysaccharide allowed fast release of the siRNA cargo upon endosomal acid degradation. In another intracellular acidity trigger trafficking system, Murthy and coworkers devised a DNA based nanocarrier that could shed the modified targeting ligands after being internalized into endosomes and expose the membrane disruption moieties for endosome escape [66]. Compared with the acidity-

assisted intracellular trafficking, endo-lysosomal acidity triggered drug release has been explored more prevalently. Unlike conventional nanocarrier degradation through the cleavage of labile linkers, a novel strategy utilizing the acid response of liquid metal was demonstrated recently as a viable approach for mediating acid triggered drug release as well as clearing metallic nanocarriers from the body [174]. In this system, Lu et al. applied a eutectic metal alloy (gallium and indium) that behaves like liquid with low-viscosity at room temperature to prepare nanocarriers. The liquid metal was sonicated into nanocarriers and stabilized with thiolated ligands, such as thiolated (2-hydroxypropyl)- β -cyclodextrin for drug loading and thiolated hyaluronic acid for tumor targeting. The ligand modified liquid metal nanocarrier could target the cancer cells after systemic administration and enter the cells through macropinocytosis. The endosomal acidity will then induce the fusion of the liquid metal, shedding the modified ligands as well as the drug contained in the ligand. The released model drug DOX then diffused into the nucleus of the tumor cells and caused massive remission as evidence from their histological analysis. Unlike the Hg, this liquid metal is highly biocompatible. Toxicological analysis of the empty nanocarriers in mice models did not reveal any detectable damage to platelets or tissues (such as liver or kidney) over the period of 3 months. Furthermore, corrosive products of the liquid metal also helped reverse drug resistance of cancer cells.

4.1.2. Enzyme activity

Pathological conditions, such as inflammation or cancer, are often associated with elevated expression of certain hydrolytic enzymes (including protease, phospholipase or

glycosidase) when compared with normal states [397-399]. Enzymes secreted into the extracellular matrix of tumors, such as matrix metalloproteinase (MMP), phospholipase, hyaluronidase and gelatinase, generally contribute to the aggressiveness of cancers. They are among the most intensively investigated triggers for tumor-targeted drug delivery, such as activating cellular internalization moieties or trigger drug release extracellularly. Similarly, characteristic intracellular enzymes of cancer cells, such as furin, kinase, esterase and cathepsine [400, 401] were also demonstrated as possible cues. Substrates that could be specifically cleaved by these enzymes were incorporated into the nanocarriers as the enzyme specific sensor and actuators.

For nanocarriers that utilize extracellular enzymes for activation or release, MMP is the most popular target. Tsien and coworkers demonstrated an exemplary MMP activated cell-penetrating peptide for tumor selective delivery of imaging agents [402]. This activated peptide is constructed by fusing polyarginine (a positively peptide that mediates robust cellular internalization) with a polyanionic domain to neutralize the positive charges via a MMP2/9 cleavable linker. Using a peptide-dye conjugate, it was demonstrated that the polyanionic moiety inhibited the electrostatic interactions between the polyarginine moiety and cell membrane, reducing cellular uptake during circulation until it was cleaved off by the MMP-2/9. *In vivo* studies showed that the MMP activatable peptide could enhance tumor specific accumulation of the imaging agent by ~3-fold. Jiang and coworkers further extended this MMP activated peptide to modify anticancer-drug delivery nanocarriers [403]. In this system, dendrigraft poly-L-lysine nanocarrier was modified with the peptide and the larger

volume of nanocarriers enabled the co-delivery of two types of anticancer drugs simultaneously: a plasmid encoding siRNA (targeting vascular endothelial growth factor (VEGF)) for inhibiting angiogenesis and small molecule drug DOX for cancer cell killing. MMP activated internalization of the nanoparticle enhanced the specificity of tumor-targeted delivery of the gene and chemotherapies when compared with nanocarriers coated with non-responsive peptides. This led to significant reduction in blood vessel formation and increase in cancer cell apoptosis using a xenograft glioma model in mice. Torchilin and coworkers devised a MMP-2 triggered PEG-sheddable micelle for delivering the hydrophobic drug paclitaxel (PTX) [404]. The hydrophobic PTX, hydrophilic PEG was linked through a MMP-2 cleavable peptide to prepare the amphiphilic building block of the micelle (PEG2000-peptide-PTX). A TAT peptide was conjugated to a shorter PEG chain and another hydrophobic moiety phosphoethanolamine to form another cell penetrating building block (TAT-PEG1000-PE), which could be buried under the PEG2000-peptide-PTX during circulation. Cleavage of the peptide in tumor microenvironment shed the PEG2000 shell and exposed the buried TAT peptide for enhanced cellular uptake. Besides controlled cellular internalization, Meiners and coworkers also demonstrated the application of MMP degradable peptide for controlled drug release from nanocarriers using MSN as a model [405].

Besides MMP, other tumor-associated enzymes were also explored for controlled anticancer drug delivery. Furin is an important convertase that processes substrate proteins for secretion; it is distributed both on the cell membrane and in the intracellular compartment

(mainly Golgi network) [406, 407]. Jiang et al. incorporated the peptide substrate of furin into a graphene based nanocarrier, where the drug release and nanoparticle internalization are controlled by the overexpressed furin on cancer cell membrane [408]. In this system, the model cytokine TRAIL was conjugated to a furin sensitive peptide, which was further conjugated to the graphene oxide sheet via a PEG linker, and the DOX was loaded into the graphene oxide sheet through π - π stacking. When the nanoparticle arrives at the tumor microenvironment through the EPR effect, cell membrane associated furin will cleave the peptide linker, releasing TRAIL into extracellular space. Then the remaining part of the nanocarrier will be internalized into the endosomal compartment for DOX delivery. It was demonstrated that the furin cleavable nanocarrier showed significantly higher anticancer efficacy than non-degradable counterparts. Jiang et al. also demonstrated a strategy utilizing the overexpressed hyaluronidase in extracellular environment for the sequential delivery [409]. In this system, a core-shell structured nanocarriers with a liposome as DOX loading core and hyaluronic acid (HA) gel as TRAIL loading shell was prepared. Hyaluronidase degradation of the HA shell released TRAIL in extracellular environment and it also exposed the cell penetrating peptide on the liposome surface for facilitated internalization. Besides long-established enzymes, new enzymes correlated to tumor progression are also under investigation. For example, legumain is a protease overexpressed by tumor associated macrophages (TAM) and it can be trafficked from cytosol to membrane under hypoxia or starvation [410]. To utilize this signal, Xiang and coworkers conjugated the tri-peptide substrate of legumain (AAN) onto the side chain of the TAT peptide and then appended

drug-containing liposomes with the altered version of TAT peptide [411]. The AAN modification reduced TAT-mediated cellular internalization by 72.65% percent, which could be reversibly recovered by legumain cleavage.

Intracellularly overexpressed enzymes are also attractive triggers for controlling intracellular behaviors of the nanocarriers. Biswas et al. utilized furin in the intracellular compartment for releasing protein therapeutics from the polymeric nanogel [412]. In this acrylamide based nanogel, positively charged monomer was incorporated for enhanced cellular uptake and the peptide sensitive to furin was incorporated into the crosslinkers to make this protein encapsulated nanogel degradable in the presence of furin. Katayama and coworkers utilized intracellular protein kinase to trigger the release of DNA plasmid from DNA/polycationic peptide complexes [413]. Cationic polypeptide that could be specifically phosphorylated by protein kinase C α was screened from a large library and polymerized with acrylamide radically. The polycationic polymer complexed with negative charged DNA and transported it inside cells, where phosphorylation by the protein kinase will convert the charge of the peptides to negative, releasing the DNA cargo intracellularly. The specific activity of tumor associated protein kinase C α made this system a tumor selective DNA delivery carrier. McCarley and coworkers demonstrated a quinone modified liposome and utilized quinone reductase as a stimulus for drug release [414]. Trimethyl quinone modified to the N-terminus of the constituent lipid was cleavable upon the reductase activation, releasing the liposome content. In addition, Amorós and coworkers demonstrate the application of various types of intracellular enzymes, such as caspase-3 [415], β -D-

galactosidase [416], cathepsin B [417] to control the capping of mesoporous nanoparticles, realizing enzyme controlled intracellular drug release.

4.1.3. Reducing gradient

The reducing gradient between the intracellular compartment and the extracellular environment is a robust physiological stimulus that attracted great interest for controlled drug delivery. Intracellular concentrations of the glutathione tri-peptide (GSH) is approximately 2-10 mM, which is maintained in reducing the state by other reducing factors (such as nicotinamide adenine dinucleotide phosphate hydrogen (NADPH), nicotinamide adenine dinucleotide (NADH), or thioredoxinred) [418]. In sharp contrast, extracellular GSH level is 2-20 μ M [419]. Furthermore, the GSH level is at least 4-fold higher in tumor when compared with normal tissues [420, 421], making the reduction gradient based nanocarriers more tumor selective.

Nanocarriers are often incorporated with GSH sensitive bond, typically the disulfide bond, for intracellular activation or degradation. The disulfide bond is stable in the mildly oxidative extracellular space, but after crossing the plasma membrane it will be converted into thiol or undergo thiol-disulfide exchange by interaction with reducing agents. Luo et al. demonstrated the application of disulfide bond to control an α -cyclodextrin and folic acid based capping in MSN nanocarriers [422]. Tang and coworkers used the disulfide bond to link low-generation polyamidoamine (PAMAM) dendrimers with branched PEG shells for enhanced gene and chemotherapeutic delivery [423]. Intracellular degradation of the disulfide bond exposed the siRNA and DOX co-loaded PAMAM dendrimer for passive drug

release. DeSimone and coworkers devised a siRNA pro-drug by covalently conjugating siRNA onto a hydrogel nanocarrier via a disulfide linker [424]. The nanocarrier was prepared by the particle replication in nonwetting templates (PRINT) method to enable either entrapment or conjugation of the siRNA. The covalent conjugation reduced the risk of burst release compared to the gel entrapment based loading method. The disulfide linker allowed selective release of siRNA inside targeted cells, while the control conjugate with a non-cleavable linker failed to release the drug. Using a disulfide containing crosslinker, Zhao et al. prepared a GSH degradable nanogel for intracellular delivery of various types of anticancer proteins, such as caspase-3 [425], apoptin [388], or p53 [426]. Cellular entry could be mediated either by a positively charged monomeric component [388, 425] or by a cancer specific targeting ligands to target the overexpressed luteinizing hormone releasing hormone (LHRH) receptors [426]. After internalization, then the polymeric shell will shed off intracellularly to release the encapsulated payload for inducing apoptosis.

In addition to the classic disulfide bond, other redox-responsive mechanisms were also explored. Selenium is element that belongs to the same family as sulfur; the higher electron number in selenium makes it a better electron donor than acceptor. He et al. applied the diselenide bond, which is more difficult to be reduced than thiol bond, for constructing a reducing gradient dependent stepwise unpacking system [427]. In the nanosystem, low molecular weight PEI was polymerized through diselenide bond and complexed the DNA cargo through electrostatic interaction. Upon this complex, another layer of disulfide bond modified HA was adsorbed. It was demonstrated that 5 μ M GSH was sufficient to degrade

the disulfide bond based shell (mimicking reducing potential the nanoparticle encountered just after cellular uptake); while 5 mM was needed to disassociate the diselenide bond based core (mimicking the reducing potential of the cytosol). In another study, the charge and hydrophilicity change of ferrocenium cation upon GSH reduction was incorporated into an amphiphilic building block for preparing redox-responsive nanoassembly [428]. The hydrophobic pillararene based building block was sandwiched by two ferrocenium cations, making the conjugate amphiphilic. The cationic amphiphile allowed efficient loading of siRNA through electrostatic interaction during the sonication-mediated assembly process and it also contributed to efficient cellular uptake. After cellular internalization, reduction of ferrocenium to ferrocene in the cytoplasm shifted the polarity of the building block from amphiphilic to hydrophobic, destabilizing the assembly and releasing the siRNA. When co-delivering siRNA and DOX, it was demonstrated that the nanosystem could efficiently inhibit drug resistance and increase the cytotoxicity of chemotherapeutics.

4.1.4. ROS

Intracellular metabolism of oxygen generates ROS, such as singlet oxygen (1O_2), anion radical (O_2^-), hydroxyl radical ($\cdot OH$), and hydrogen peroxide (H_2O_2) [429]. Aggressive metabolism and damaged ROS scavengers (such as antioxidant enzymes) lead to detrimental accumulation of ROS inside cancer cells [430]. The level of ROS in tumor cells could reach 10 to 100-fold that of normal cells, which in return further contributes to DNA damage or mutation, exacerbating tumor malignancy [431]. ROS accumulation is a common feature shared by various types of diseases, such as inflammation [432], neurodegenerative

disease [433], diabetes [434, 435], cardiovascular disease [436]. To harness the ROS as a physiological cue for controlled drug delivery, nanocarriers were prepared by incorporating labile bonds that could be cleaved (such as thioketal [437, 438], aryl boronic acid [439, 440], or proline [441]) or undergo polarity change (such as thiolester [442], or propylene sulfide[443], ferrocene[444]) upon oxidation.

Murthy and coworkers utilized the thioketal based polymer poly-(1,4-phenyleneacetone dimethylene thioketal) for oral delivery of the siRNA [437]. The polymer is resistant to acid, alkaline or proteolytic degradation but sensitive to ROS triggered cleavage, enabling site-specific delivery of nanoparticle to ROS generating inflamed or cancerous intestines. Xu and coworkers demonstrated a ROS triggered protein deprotection method for spatial-temporal control of protein activities after delivery [439]. The key lysine residue of the model anticancer protein RNase A was caged by a 4-nitrophenyl 4-(4,4,5,5-tetramethyl-1,3,2-dioxaborolan-2-yl) benzyl carbonate through a ROS labile boronic acid linker. In this proof-of-principle study, cationic lipid was used for intracellular delivery of the modified RNase A for protein-modification based therapy [445]. It was shown that only the aryl boronic acid linked cage could be cleaved off after exposure to H₂O₂ while a non-degradable control failed to reactivate the RNase A. The ROS labile boronic acid linker has also been incorporated into an activatable CPP for *in vivo* agent delivery [446]. Similar to the MMP activatable CPP [402], the positively charged CCP (Arg9) was caged by an anionic moiety (Glu9) through the ROS sensitive 4-boronic mandelic acid linker. Exposure to H₂O₂ led to fragmentation of the peptide, activating intracellular penetration.

Using a ROS-mediated polymer polarity change strategy, Leroux and coworkers coated an ROS sensitive polymeric shell for controlling the aggregation of nanocrystal [442]. Tuning the affinity between the thioester based amphiphilic polymer and the hydrophobic PTX nanocrystals generated stable core-shell nanocarriers in non-oxidative condition. ROS converts the hydrophobic thioesters to hydrophilic sulfoxide or sulfone, destabilizing the shell for PTX release. Staff et al. utilized the polarity change of ferrocenium/ferrocene upon oxidation for controlling drug release [444]. Polymer containing the ferrocenium was formulated into a nanocapsule that held a drug loaded liquid core. Oxidation of the polymer changed local polarity of the nanocapsule, releasing the loaded drug.

4.1.5. Hypoxic condition

Hypoxia is a hallmark of primary tumors [447], where the disorganized tumor vasculature caused limited oxygen diffusion to regions far away from the capillaries ($> 200 \mu\text{m}$) [448]. This hypoxic environment posed a survival pressure to select phenotypic or genetic mutations that favor hypoxia, generating more chemo-resistant, death-resistant, invasive, and metastatic cancer cell variants. The major role of hypoxia in tumor progression and drug-resistance made hypoxia an attractive target for cancer therapy. Huge amounts of efforts have been devoted to target the hypoxic area, such as developing hypoxia activated chemotherapeutics [449], engineering anaerobic bacteria to express tumor suppressing protein [450]. Due to the severe hypoxia in tumor but not normal tissues, there is an emerging trend for harnessing hypoxia for designing tumor targeted nanocarriers for theranostics [451, 452].

To utilize the hypoxia as a cue, hypoxia labile bonds were generally incorporated into polymeric nanoparticles. Torchilin and coworkers used azobenzene as a hypoxia cleavable linker to prepare a PEG sheddable nanocarrier for hypoxia targeted delivery of siRNA [453]. Building block consisted of PEG, azobenzene, PEI and the lipid DOPE was prepared to form micelles, where the siRNA payload was complex into the nanocarrier through electrostatic interaction. When the siRNA loaded micelle diffuses to the hypoxic tumor region, the PEG shell will be cleaved off and expose the cationic PEI layer for cancer cell uptake. Thambi *et al.* incorporated the hypoxia sensitive group 2-nitroimidazoles (NI) into the side chain of the hydrophilic polymer Carboxymethyl dextran [454]. Due to the hydrophobicity of NI, the amphiphilic polymer could self-assemble into nanocarriers and load a hydrophobic drug inside. When the nanocarrier was exposed to hydrophobic environment, the NI group reduced to a hydrophilic derivative, destabilizing the self-assembly for drug release. It was demonstrated that the hypoxia-responsive nanoparticle showed hypoxic cancer cell/tumor selectivity both *in vitro* and *in vivo*. In spite of the progresses made in harnessing hypoxia for triggering nanocarrier activation or drug release, diffusing the nanocarriers to tumor regions distant from the blood vessels could be very challenging.

4.1.6. ATP gradient

The progressive proliferation of tumors leads to the up-regulation of various types of metabolites. As the “molecular unit of currency”, ATP plays a central role in metabolic energy transfer. There is a sharp ATP concentration difference between extracellular ($< 5 \mu\text{M}$) and intracellular environments (1 - 10 mM). Increased intracellular ATP has been observed

for cancerous tissues [455]. Thus, ATP has emerged as a new physiological trigger, recently investigated for controlled intracellular drug delivery.

To construct ATP-responsive nanosystem, the ATP binding aptamer (a short single stranded DNA) is the most widely used ATP sensitive moiety [83]. Mo *et al.* applied the ATP aptamer as the ATP sensor as well as drug release actuator for DOX delivery [456]. In this formulation, the ATP aptamer with its complementary strand was hybridized into a DNA duplex, which provides a “GC” pair for loading the DOX. The DOX loaded DNA duplex was condensed with a positively charge peptide protamine and then coated with a polymer shell composed of HA. Systemic administration of the nanoparticle led to targeted accumulation in the tumor tissue, where the HA shell got degraded by the HAase rich tumor environment and shuttle the DOX loaded DNA duplex intracellularly. When exposed to the high ATP level of the intracellular compartment, ATP competitively binds the ATP aptamer and dissociates the DNA duplex for DOX release. Compared with a nonresponsive DNA core, the ATP aptamer based nanocarrier showed significantly enhanced tumor growth inhibition. The relatively short length of the ATP aptamer made it easy to be adapted to different types of nanosystems [457, 458]. [459].

In addition to the classic ATP aptamer, other ATP binding molecules were also explored for constructing ATP-responsive DDSs. Lee and coworkers utilized the strong affinity between ATP and Zn^{2+} -dipicolylamine to prepare an ATP-responsive theranostic system [460]. In this three-layered nanocarrier, an upconversion nanoparticle core was coated with MSN, where the pores of MSN could be used to load anticancer drugs (DOX or CPT)

capable of absorbing fluorescence emission from the core. The MSN was further modified with Zn^{2+} -dipicolylamine, upon which a layer of polypeptide containing aspartate was coating for capping the pore. Exposing the nanocarrier to intracellular level of ATP will dissociate the polypeptide coating due to the competitive binding between ATP and Zn^{2+} -dipicolylamine, releasing the loaded drug and recovering the fluorescence of the upconversion nanocarrier core. Inspired by the application of phenylboronic acid in RNA chromatography, Naito *et al.* exploited the reversible interaction between phenylboronic acid and the ribose ring present in nucleic acids for ATP-responsive siRNA delivery [461]. In this PEG-polylysine based polyion complex, phenylboronic acid was conjugated to the cationic polylysine segment. SiRNA was loaded into the nanocomplex through both polylysine-mediated electrostatic interaction and phenylboronic acid generated reversible covalent bonds. ATP sensitivity could be controlled by tuning the ratio between phenylboronic acid and siRNA.

In spite of efforts devoted to designing ATP-responsive nanosystems, these strategies all face the common challenge of ATP resolution. The ATP aptamer is adenosine specific, making ATP and ADP equivalent triggers. ATP binding polymers are based on phosphate (Zn^{2+} -dipicolylamine) or ribose (phenylboronic acid) competition, making any phosphate or ribose containing molecules viable alternatives to ATP. Currently, the chemical moiety with the highest ATP fidelity involves the use of proteins that utilize ATP as substrate. Aida and coworkers harnessed the specific ATP consuming capability of a protein chaperon GroEL for designing ATP-responsive DDSs [462]. Naturally, GroEL grabs incorrectly folded proteins

into its cavity for refolding and then release it through conformational changes powered by ATP hydrolysis. In the engineered version of GroEL, GroEL monomer was polymerized into a tube through a Mg^{2+} coordination based mechanism. Payload could be conjugated to a guest “wrong folded” protein for loading into the cavity of GroEL. Further modification of the protein assembly with boronic acid derivative made the nanosystem permeable to the cell membrane, where intracellular ATP triggered conformational change of the monomers for nanotube disassembly and drug release.

4.2. Programmed multi-stimuli-responsive delivery systems

To further enhance treatment precision and efficacy, two or multiple physiological trigger-relevant designs can be integrated into the formulations to achieve programmed performance. Nanocarrier activation or drug release could be controlled by physiological triggers in boolean logic ways (AND, OR). The triggers could either work synergistically (where any one of the cues could activate drug activation/release alone, but combined cues will lead to more effective drug release) or sequentially (where the multiple trigger function in tandem and all the triggers are essential) [463].

4.2.1. Synergistic stimuli-responsive systems

Synergistic stimuli-responsive nanocarriers have been extensively explored to incorporate a combination of distinct physiological triggers (such as pH/redox, redox/enzyme, pH/ROS, oxidation/reduction) for controlled drug delivery. The “either trigger A or trigger B” logic could help achieve a more specific drug targeting (where the target region

is characterized by both A and B) or overcoming the heterogeneity of tumors (where A and B are distributed in different regions of the same tumor).

The synergistic effect of pH and redox on drug release has been broadly studied for facilitated drug release. Lu *et al.* incorporated the pH sensitive ketal group and the GSH cleavable disulfide bond into a PEG and polyserine based graft co-polymer [464]. The polymer with a disulfide linked PEG backbone (hydrophilic) and ketal modified polyserine pendants (hydrophobic) self-assemble into core-shell nanoparticle that encapsulated the hydrophobic drug DOX in the core. It was demonstrated that the dual-responsive nanocarrier could be disrupted after exposure to GSH (10 mM) and acid condition (pH 5.0) either separately or in combination. The delivered DOX could be observed in the nucleus of targeted cells after incubation for 4 h, inducing high levels of apoptosis. Dhar and coworkers demonstrated a redox/esterase dual-responsive nanocarrier for simultaneous delivery of two drugs [465]. Aspirin and cisplatin were co-delivered in the same nanocarrier for their anti-inflammatory and anticancer effects, an efficient combination therapy against prostate cancer resistant to castration. In this nano-formulation, aspirin and cisplatin were conjugated to second-generation dendrons through aromatic ester and aliphatic ester bonds respectively. Then the dendrons were linked to a PLA backbone for incorporation into a PLGA-PEG based self-assembly. Facilitated release of aspirin was observed in the presence of esterase while cisplatin was released much faster by sodium ascorbate-mediated reduction. The co-delivery system enabled stringent control of drug dosages and exhibited improved anticancer efficacy in cisplatin resistant cancer cell lines. Analysis of the empty carrier showed high

biocompatibility with low cytotoxicity or immunogenicity using a model RAW 264.7 cell line. Pu *et al.* demonstrated a ROS/pH-responsive nanosystem for targeted delivery of a model anti-inflammatory drug curcumin [466]. This nanocarrier is mainly composed of *N*-palmitoyl and Cy3 modified chitosan and a thioketal based polymer. Protonation of amine groups in chitosan would affect their charge-mediated repulsion and cause conformational change. ROS would shift the polarity of the polymer from hydrophobic to hydrophilic, destabilizing its association with the nanocarrier. The hydrophobic curcumin assembled into the hydrophobic core of the nano-assembly. The nanocarrier exhibited high stability in physiological pH and efficiently accumulated at inflamed tissue. Rapidly cellular internalization was observed within 15 min reaching targeted tissue. ROS scavenging effects occurred either extracellularly or intracellularly to exert therapeutic effects.

In addition to responding to two orthogonal stimuli, Wang *et al.* demonstrated a nanocapsule that could be degraded by two opposite stimuli: GSH and ROS [467]. In this system, the labile phenol ester of the model anticancer drug SN38 was found sensitive to hydrophilic neighboring group mediated electron withdrawing as well as GSH-mediated thiolysis, both of these conditions could trigger the degradation of the phenol ester bond and release the drug. The hydrophilicity based electron withdrawing was further controlled by a hydrophobic thioester that could be oxidized by ROS to become hydrophilic. The amphiphilic building block constitutes of the hydrophilic PEG and the hydrophobic SN38 self-assembled into a nanocapsule. Exposure to either ROS or GSH could cleave off SN38 and disrupt the nanoassembly. The GSH/ROS dual responsive system holds the promise to

overcome the heterogeneous oxidative states at different regions or stages of a tumor.

4.2.2. Sequential stimuli-responsive systems

Sequentially triggered DDSs were typically designed for enhancing subcellular specificity. The “trigger A then trigger B” strategy encodes the stimuli-responsive components in different layers of a nanosystem and then exhibits a stepwise activation along the pathway to destination. Trigger A is often an endogenous physiological stimulus, but trigger B could be either from the physiological environment or from pre-designed components in the nanocarriers.

Zhang and coworkers devised an enveloped MSN to harness extracellular MMP and intracellular GSH in tandem for programmed nanoparticle internalization and drug release [468]. A disulfide bond was used to anchor MSN surfaces with β -CD, upon which adamantane linked with a multifunctional peptide was docked. The peptide is composed of a RGD targeting ligand, MMP sensitive region, and anionic poly(aspartic acid). DOX was loaded into MSN pores as a model drug. After systemic administration, the anionic poly(aspartic acid) augments the circulation efficacy of the nanoparticle by avoid unspecific uptake. MMP in extracellular environment then cleave the poly(aspartic acid) shell and expose the RGD peptide for inducing cancer cell specific uptake. The β -CD will be removed by intracellular GSH to liberate the loaded DOX. Choi *et al.* devised a pH/HAase co-responsive carrier for stepwise degradation of a core-shell structured nanocarrier for siRNA and DOX delivery [469]. For the core, HA modified with the hydrophobic 5β -cholic acid self-assembled into nanoparticles, entrapping the DOX inside. To load the anionic siRNA

onto the anionic HA nanoparticle, Zn²⁺-dipicolylamine based RNA receptor was conjugated to the HA core for binding siRNA through ZN(II)-phosphate interaction. To reduce the perturbation of siRNA loading by physiological phosphates, a layer of calcium phosphate based shell was further coated. After systemic administration, the calcium phosphate shell would be dissolved by extra-tumoral pH and partially expose the HA core for CD-44-mediated targeting and internalization. Further removal of the calcium phosphate shell occurred in the endosome-lysosome, releasing the siRNA together with phosphate and calcium ion for proton-sponge-mediated endosome escape. The encapsulated DOX would then be released after HAase degradation of the HA core.

In contrast to using sequential endogenous triggers, incorporating autonomous responsive components into the nanocarrier enables the design of more sophisticated systems for executing predesigned sequential reactions. The artificially created/potentiated second trigger could complement the absence or low intensity of the second signal for more robust nanocarrier activation or drug release.

Mo *et al.* demonstrated a pH/ATP sequential responsive system for DOX delivery, where endogenous endolysosomal pH was the first trigger. The second ATP trigger and ATP-responsive moieties were all incorporated in the nanosystem that was programmed to take effect after pH activation [470]. This two liposome based ATP delivery and ATP-responsive release system was designed for supplementing external ATP for triggering drug release intracellularly. In one liposome modified with pH-responsive fusogenic peptide, the DOX loaded ATP aptamer duplex was encapsulated, while another unmodified liposome was

designed for delivering ATP. After co-administering the two liposomes, they accumulated at the tumor by the EPR effect. Internalization of the liposome in acidic endolysosome activates the fusogenic peptide for liposome and endosome membrane fusion, exposing the ATP aptamer to ATP for triggering DOX release. In the study by Sun *et al.*, a pH/DNase based sequential stimuli-responsive system was demonstrated [98]. The endogenous pH was used to activate the second trigger DNase for nanocarrier degradation and intracellular drug release. In this strategy, a DNA based nanocarrier was prepared by rolling circle amplification for loading DOX through DNA intercalation. The DNase trigger was locked by an acid-degradable nanocapsule. The positively charged nanocapsule was adsorbed onto the DNA nanoparticle through electrostatic interaction to form stable nano-assemblies. Internalization of the nanoassembly by cancer cells led to acid trigger shedding the polymeric capsule, leading to DNase activation in the endosome. The liberated DNase then chop up the DNA carrier and release the loaded DOX.

Hu *et al.* demonstrated a bio-mimetic core-shell nanoparticulate system, in which an acid-degradable polymeric nanocarrier was used as the core for loading the small molecule drug DOX and a membrane derived from platelets for anchoring an anticancer protein TRAIL [194]. The “self marker” rich membrane could reduce immunogenicity and prolong circulation time of the nanocarriers. The P-selectin on the coated platelet membrane could also enhance the cancer targeting efficacies by binding to the overexpressed CD44 on solid tumors or circulating tumor cells, augmenting the interaction between the loaded TRAIL and tumor cells. Surface interaction between the core-shell nanocarrier and cancer cells facilitated

internalization of the nanocarrier, transporting the nanocarrier to the endosome. The polymeric core will undergo gradual degradation in the acidic endosome due to the incorporation of an acid-labile cross-linker, glycerol dimethacrylate, in the polymeric network. The degradation expedited the release of DOX into the endosomal compartment, which further diffused into the nucleus to exert a synergistic anticancer effect with the membrane targeted TRAIL protein. In another study, a HAase/transglutaminase/pH triple stimuli-responsive system was conceived for co-delivering the TRAIL protein and an antiangiogenic peptide (cilengitide) into the extracellular environment of tumors [471]. Endogenous HAase and pH triggers and an exogenous transglutaminase [472] cue provided by the carrier were harnessed to construct a drug containing depot *in vivo* for sustained release. In this core-shell nanocarrier, the transglutaminase was encapsulated into nanogels composed of HA and the HA nanogel constitutes the outer layer of the formulation. The drugs TRAIL and cilengitide were encapsulated into a polymeric gel based core, which was crosslinked by an acid sensitive crosslinker. The core particle was further modified with human serum albumin (HSA) for enhanced stability. Meanwhile, the HSA also provides acryl and amine groups for controlling the aggregation of core. Once administered systemically, the nanoformulation will accumulate in tumor microenvironment, where the rich HAase will liberate transglutaminase from the HA nanogel. The transglutaminase then catalyzed the crosslinking of the HSA on the surface of the core-nanocarrier, aggregating the nano-cores into micro-scaled particles. The micro-aggregation inhibited size dependent endocytosis and nanocarriers and remained in the extracellular environment, where the mildly acidic

condition triggered gradual degradation of the TRAIL/cilengitide containing particle for release.

Besides pH or HAase initiated sequential reactions, endogenous metabolites are also investigated for initiating sequential autonomous responses. Yu *et al.* designed a multifunctional micelle containing enzymes to convert glucose signal to regional hypoxia, which later triggered the innate reduction of the hypoxia sensitive moieties in the nanocarrier for disassembly and drug release [60]. Ye et al. harnessed the natural response of pancreatic cells to glucose for controlled insulin secretion [473]. Pingarroń and coworkers demonstrated a Janus nanoparticle that converts glucose or ethyl butyrate into acidic signals through pre-immobilized enzymes. Then the acidity would automatically trigger drug release from another part of the nanosystem, pH-responsive MSN, for drug release [474].

5. Clinical impact of drug delivery system

The confluence of emerging development of materials and biomedical science provides tremendous translational opportunities of innovative DDSs. Whereas the number of commercialized products is still small, compared to the traditional medications. The total number of nano-formulations that are clinically approved or under clinical trials is on the order of ~250 [475]. From the perspective of the nanoparticulate platform, nanomedicine under clinical investigation could be classified into liposomes, protein bound nanoparticles, antibody-drug conjugates [476], polymer-drug conjugates [477], polymeric micelles, and inorganic nanocarriers. Typical issues involving manufacturing scale, homogeneity and

reproducibility need to be addressed for enhancing success rate in translation [478]. Here, we summarized the clinical translation of nanomedicine for anticancer therapies and highlight recent progresses of stimuli-responsive nano-formulations (Table 1-2).

Table 1-2. Representative Clinical Translations of Precision Nanomedicine Delivering Anticancer Therapeutics.

Name	Formulation	Drug	Status ¹	Indications
Doxil	Liposome	Doxorubicin	First approved in 1995	Ovarian cancer, AIDS-related Kaposi's Sarcoma, Multiple Myeloma
Marqibo	Liposome	Vincristine	Approved in 2012	Acute Lymphoblastic Leukemia
Onivyde	Liposome	Irinotecan	Approved in 2015	Metastatic Adenocarcinoma
Promitil	Liposome	Mitomycin-C	Phase I (NCT01705002)	Metastatic Colorectal Cancer (mCRC)
IHL-305	Liposome	Irinotecan	Phase I (NCT02631733)	Solid Tumors
DCR-MYC	Liposome	siRNA	Phase I (NCT02110563)	Multiple Myeloma, Non-Hodgkins Lymphoma, Pancreatic Neuroendocrine Tumors
Anti-EGFR Immunoliposomes	Liposome	Anti-EGFR + Doxorubicin	Phase I (NCT01702129)	Solid Tumors
TKM 080301	Liposome	siRNA	Phase II (NCT01262235)	Neuroendocrine Tumors, Adrenocortical Carcinoma
MM-302	Liposome	Doxorubicin	Phase II/III (NCT02213744)	Breast Cancer

Table 1-2 continued

Thermodox	Liposome	Doxorubicin	Phase III (NCT00617981)	Hepatocellular Carcinoma
CPX-351	Liposome	Daunorubicin + Cytarabine	Phase III (NCT01696084)	High Risk Acute Myeloid Leukemia
MM-398	Liposome	Irinotecan	Phase III (NCT01494506)	Metastatic Pancreatic Cancer
Abraxane	Protein Bound nanoparticle	paclitaxel	First approved in 2005	Metastatic breast cancer, Locally advanced or metastatic non-small cell lung cancer, Metastatic adenocarcinoma of the pancreas
Ontak	Fusion protein	diphtheria toxin	Approved in 1999	Cutaneous T-Cell Lymphoma
Kadcyla	Antibody-Drug Conjugate	Emtansine	Approved in 2013	HER2-positive, metastatic breast cancer
Brentuximab vedotin²	Antibody-Drug Conjugate	monomethyl auristan E	Approved in 2011	Hodgkin lymphoma and systemic anaplastic large cell lymphoma
Albumin-Bound Rapamycin	Protein Bound nanoparticle	Rapamycin	Phase II (NCT02646319)	Advanced Cancer With mTOR Mutations
CRLX-101	Polymeric Conjugated	Camptothecin	Phase I/II (NCT02769962)	Small Cell Lung Carcinoma, Non-Small-Cell Lung
Eligard	Polymeric nanoparticle	Leuprolide	Approved in 2002	Prostate Cancer
Oncospar	Polymeric Conjugate	Asparaginase	Approved in 1994	Acute lymphoblastic leukemia
NC-4016	Polymeric Micelle	DACH-platin	Phase I (NCT01999491)	Advanced Cancers, Lymphoma
NC-6004	Polymeric Micelle	Cisplatin	Phase I/II (NCT00910741)	Locally Advanced and Metastatic Pancreatic Cancer

Table 1-2 continued

NK-012	Polymeric Micelle	SN-38 (Irinotecan Metabolite)	Phase II (NCT00951054)	Triple Negative Breast Cancer
PK1²	Polymer-drug conjugate	doxorubicin	Phase II (NCT00003165)	Breast cancer
Genexol-PM	Polymeric Micelle	Paclitaxel	Phase III (NCT00876486)	Breast Cancer
Paclical	Polymeric Micelle	Paclitaxel	Phase III (NCT00989131)	Epithelial Ovarian Cancer; Primary Peritoneal Cancer; Fallopian Tube Cancer
Xyotax²	Polymeric Conjugate	Paclitaxel	Phase III (NCT00108745)	Ovarian Carcinoma, Peritoneal Cancer,
CYT-6091	Gold nanoparticle	TNF α	Phase I (NCT00356980)	Adult Solid Tumor

¹ClinicalTrials.gov identifier is given for ongoing trials.

²Drug release that could be triggered by physiological signals.

Doxil[®], DOX loaded liposome, was the first approved nanomedicine for cancer treatment in 1995. Dramatic increase in DOX delivery efficiency was observed (4 -16 fold) using the liposome carrier rather than free DOX [479]. Decades of development generated dozens more liposome based formulations for delivering small molecule drugs (daunorubicin, cytarabine, vincristine, etc.); or macromolecular therapeutics (vaccines, nucleic acids) [480, 481]. Liposome has become a canonical DDS with typical merits for a robust DDS: 1) stable loading and protection of either hydrophilic drugs (in the aqueous core) or hydrophobic drugs (in the lipid bilayer); 2) long circulation, especially after PEG

modification; 3) efficient EPR effect and improved distribution.

Protein nanoparticle based nano-medicine has been demonstrated as a robust platform for drug delivery. Abraxane, nanoparticle albumin bound (Nab) paclitaxel, was approved in 2005 for treating a variety of cancers, including breast, pancreatic, lung, ovarian, gastrointestinal, head neck carcinomas [482, 483]. Albumin is an abundant protein with a hydrodynamic size of 3.5 nm, it tends to bind hydrophobic agents reversibly within plasma. The protein nanoparticle was used to replace the toxic solvent Cremophor and solve the low solubility of paclitaxel. The 130 nm Abraxane nanoparticles dissociate into smaller paclitaxel-albumin complexes (8 nm) upon administration and enter the cells through an albumin-mediated internalization. Success of Abraxane also inspired clinical translation of other chemotherapeutics suffering from poor solubility, such as rapamycin [484]. In addition to protein bound nanoparticles, protein conjugates and fusion proteins were also successfully translated [485, 486]. Trastuzumab emtansine, HER2 antibody conjugated with emtansine *via* a stable linker, was approved in 2013 for treating breast cancer [487]. This nano-formulation significantly improved the survival rate of HER2 positive breast cancer patients. Ontak, a fusion protein of interleukin-2 and diphtheria toxin, was approved in 1999 for targeting cutaneous T-Cell lymphoma [486].

Many polymeric based nano-formulations, including polymer-drug conjugate [488] and micelles, are marketed or in the pipeline for translation. Genexol-PM, a paclitaxel loaded polymeric micelles [489], have been commercialized in many countries, such as South Korea, for treating breast or lung cancer. It is currently under the 505(b)(2) regulatory

pathway for accelerated US FDA approval with Abraxane as a reference. The amphiphilic property of micelles make them suitable for delivering either hydrophilic or hydrophobic therapeutics, generating various micelle-based formulations under clinical investigation [490-495].

Inorganic nanocarriers based on different metals have made their way for clinical imaging [496, 497], cancer thermal therapy [498, 499], or therapeutic delivery. CYT-6091, a gold nanoparticle bound with both TNF α and PEG, has finished phase I clinical trials in patients with advanced stage cancer [500]. Improved safety profiles were observed by the gold nanoparticle based nanomedicine versus free TNF α .

Several successful translations of physiological stimuli-responsive nanomedicine have been demonstrated. Brentuximab vedotin, a CD30 antibody conjugated with monomethyl auristatin E through a cathepsin degradable linker [501], was approved in 2011 for treating refractory Hodgkin lymphoma and systemic anaplastic large cell lymphoma. The CD30 antibody reduced undesired internalization by normal cells and the degradable linker could facilitate drug release inside the tumor microenvironment. The poly(L-glutamic acid) based nanoparticle with paclitaxel conjugated to the side chain was demonstrated to enhance the solubility of paclitaxel for *in vivo* administration [502, 503]. Endosomal enzymes could trigger the degradation of the carrier for drug release. Meanwhile, the degraded glutamate could further enhance paclitaxel tolerance, enabling higher dosage. The poly(L-glutamic acid)-paclitaxel formulation with the trade name Xyotax is currently undergoing phase III clinical trials. Similarly, PK1, a polymer conjugated DOX formulation releasing DOX in

response to endosomal pH or enzymes, is also undergoing clinical investigation [504, 505].

6. Summary

In summary, nanocarriers have contributed to the promising future of “precision medicine” by improving the ADME profiles of various drugs. Increased understanding of the physiology-material interaction has engendered rational guidelines for designing nano-formulations to overcome extracellular and intracellular barriers. Further “evolution” of nanomedicine has shown emerging “intelligence” to sense the physiological environment and act accordingly.

7. Dissertation Scope and Organization

The aim of this dissertation is to develop a DNA based nanostructure as a platform for the delivery of different therapeutics. We will start with an overview of the designing principles for targeted nanomedicine (Chapter 1), discussing the physiological barriers and strategies to overcome these barriers. Then we will specifically focus on the application of DNA as a nanomaterial for the delivery of therapeutics, a summary of recent progresses in the field of DNA nanostructure based nanomedicine will be presented (Chapter 2). In the main part of the dissertation we will demonstrate the application of rolling circle amplification for the preparation of versatile drug delivery systems. Three different types of therapeutic molecules were delivered by the DNA nanoclew, including a chemotherapeutic

anticancer drug (Chapter 3), a ribonucleoprotein complex for the editing of genomic sequence (Chapter 4), and a cytokine that induce apoptosis signaling in cancer cells (Chapter 5).

Chapter 3 reports the preparation of a cocoon-like assembly composed of the DNA NC and an encapsulated DNase. An acid responsive moiety was incorporated into the design to enable acid responsive drug release from the nanocarrier. Chapter 4 reports harnessing the interaction between the DNA NC and the RNA guided cargo for efficient intracellular delivery. Chapter 5 reports a dual nanoparticle delivery strategy that could be activated by tumor-associated phospholipase to achieve shape transformation of the DNA NC. The transformation in morphology of the DNA NC into linear fiber will reduce the cellular uptake of the nanoparticles, making the carrier suitable for plasma membrane targeted delivery of therapeutics.

CHAPTER 2 ENGINEERING DNA SCAFFOLDS FOR DELIVERY OF ANTICANCER THERAPEUTICS

1. Introduction

As an important tool in pharmaceuticals, versatile drug delivery systems have been developed to shield the drugs from detrimental physiological environments as well as reduce their side effects by enhancing their targeting efficiency.^[62, 506] With these carriers, numerous therapeutic cargos, such as small molecules drugs, nucleic acids, peptides and proteins were successfully delivered to their intracellular or extracellular destinations.^[507] Despite the extensively efforts of exploring different materials for anti-cancer drug delivery, only a few formulations based on liposome, polymer and protein carriers were approved by FDA.^[508, 509] To develop a reliable drug delivery system, the designing criteria often incorporate uniform structure, high stability, biocompatibility, targeting abilities, transduction abilities and stimuli-responsiveness.^[43]

DNA is a polymer chosen by nature to store and transmit genetic information. The intrinsic programmability renders DNA a promising material in designing uniform nanostructures for drug delivery.^[510-514] In addition, the prevalent existence of DNase in tissues endows DNA with superb biodegradability,^[515] which could even be incorporated into metallic drug delivery carriers for improved biocompatibility.^[390] Although transfection reagents, such as positively charged polymers or lipids,^[134] were generally used for transgenic studies due to the cell membrane impermeability of free DNA, DNA

nanostructure can readily enter the cell membrane via endocytosis in an agent-free way.^[516, 517] Furthermore, DNA aptamers,^[518] which are single stranded DNAs with antibody-like binding affinity to their target molecule, can interact with environmental signals, such as ATP and pH,^[456, 519, 520] or cellular signal, such as extracellular receptors and intracellular mRNA,^[521, 522] have greatly expanded the toolbox for building DNA-based drug delivery carriers.

Besides hybrid drug delivery carriers that incorporate DNA as a functional moiety, pristine DNA assemblies have been extensively studied over the last three decades since the first demonstration of assembling an immobile nucleic acid junction based on simple Watson-Crick base pairing by Seeman et al. in the 1980s.^[523, 524] Various DNA nanostructures were assembled, such as cubes,^[525] networks,^[526] arrays and arbitrary shapes on a DNA canvas,^[527, 528] from customized DNA tiles with “sticky ends”. In contrast with the “bottom-up” approach of assembling a complex DNA structure from numerous tiles, an alternative “top-down” approach, “DNA origami”, was developed by Rothemund et al. in 2006 by folding a long single stranded DNA with numerous “DNA staples” into arbitrary shapes.^[511] Since then, larger and more complex DNA nanostructures, such as logic-gated robot and a DNA box with controlled lid,^[529, 530] were developed. Thanks to the development of user-friendly software for predicting the structures of DNA assembly, customizing DNA nanostructures has become a routine work.^[531-534] More recently, rolling circle amplification (RCA),^[535-537] a polymerase chain reaction based method to amplify periodically repeated

single strand DNA from a circular single strand template, has also attracted considerable attention in assembling DNA nanostructures, such as sponges and tubes.^[98, 538-542]

The intrinsic multivalency makes DNA a superb carrier for easy drug loading and functionalization,^[543, 544] which can be achieved through covalent conjugation, intermolecular hybridization or intra-molecular intercalation.^[513] In this mini-review, recent advances using DNA scaffolds for anticancer drug delivery were summarized (Figure 2-1) and the challenges for future developments were discussed.

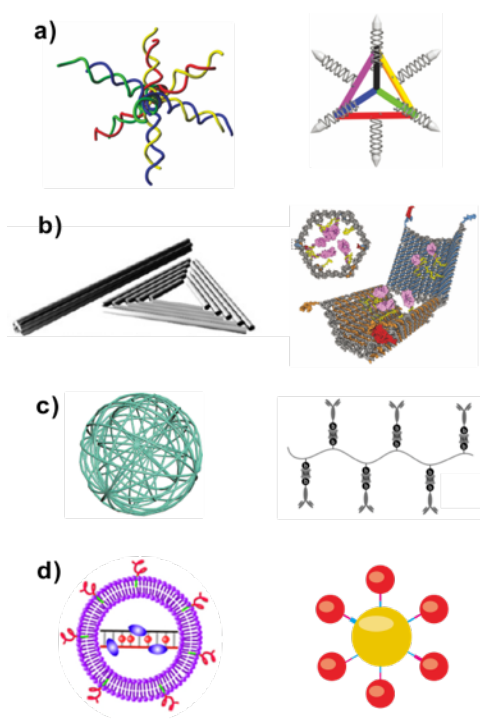


Figure 2-1. Example DNA nanoscaffolds for anticancer drug delivery. (a) DNA nanostructures assembled from multiple “DNA tiles”^[285, 545] (b) DNA nanocarriers based on “DNA origami”^[343, 529] (c) DNA nanoassemblies based on rolling circle amplification.^[98, 546] (d) Hybrid drug delivery carriers with DNA scaffold as functional moiety.^[390, 470] Reproduced with permission.

2. Various DNA scaffolds for different anticancer drug delivery

2.1. Small-Molecule Drugs

Doxorubicin (DOX) is an anthracycline antibiotic that works by intercalating into double stranded DNA, especially at the GC rich regions.^[470] However, free DOX suffers from poor solubility, low selectivity and adverse side effects. The interaction between DOX and DNA makes DNA nanostructure a natural carrier for DOX and DNA nanostructures assembled via different methods were explored for intracellular delivery of DOX. Chang et al. developed a 3-D DNA polyhedra by assembling 5-star and 6-star “DNA tiles” and they were among the first to demonstrate that structured DNA particles were readily uptaken by the cells.^[517] By utilizing the DNA origami method, Jiang et al. folded the long viral single stranded DNA M13mp18 into triangular and tubular structures with hundreds of short DNA staples.^[343] Using regular breast cancer cell line MCF7 and its DOX resistant subline, they demonstrated that the DNA origami carrier could circumvent drug resistance and kill DOX-resistant MCF7 cells. In addition, using a DNA origami based nanotube for DOX delivery, Zhao et al. tuned the intra-molecular twist of the nanostructure and found that higher twist of the structure lead to higher DOX loading capacity and lower intracellular elimination rates.^[547] *In vivo* DOX delivery studies in nude mice xenografted with MDA-MB-231 tumors using a triangular DNA origami showed excellent passive targeting to the tumor tissue without observable systemic side effects.^[548]

Instead of using “DNA tiles” or “DNA origami”, our group recently developed a “DNA nanococoon” for controlled DOX delivery using RCA (Figure 2-2).^[98] After cyclizing a linear ssDNA (~75 bp) into a circular template, long chain ssDNA products with repeated sequences complementary to the DNA template were obtained by RCA. Multiple GC pairs were encoded into the template for enhanced DOX loading and a palindromic sequence was also incorporated to promote the self-assembly of the ssDNA product into a nanoclew-like structure (NCl). After incubating the DOX with NCl, a high DOX loading capacity (66.7%) was achieved using the NCl as carrier. In order to control the DOX release profile from DOX/NCl, DNase I was chosen as a trigger to promote the degradation of NCl. Instead of using free DNase I, an acid degradable polymeric shell was coated onto DNase I to cage the activity of DNase. Also, the positive charge of the polymeric shell converted the zeta potential of DNase I from negative to positive, making it possible to assemble the DNase nanocapsule (NCa) with NCl into a stable complex. The NCl/NCa complex showed increased size (~180 nm) as compared with NCl alone (~150 nm). To further enhance the targeting ability of DOX loaded NCl/NCa, folic acid (FA) was conjugate to a short ssDNA oligo with sequence complementary to NCl. The overall DOX/NCl-FA/NCa complex showed a pH responsive DOX release profile and a very fast intracellular delivery of DOX into the nucleus of MCF7 cell line could be remarkably observed even within 0.5 h after treatment.

In addition to DOX, other small molecules with anticancer effects, such as photosensitizer that can convert light energy into reactive oxygen species, can also be

delivered intracellularly using DNA scaffolds. Unlike the preference for Watson-Crick pairing based GC pairs by DOX, photosensitizer TMPyP4 can intercalate into a special DNA

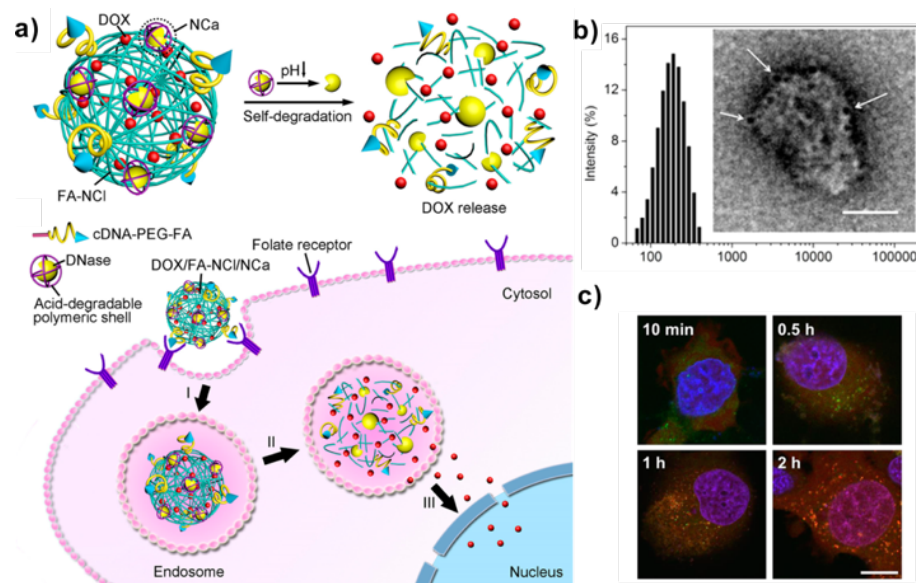


Figure 2-2. Intracellular delivery of DOX using a DNA nanococoon synthesized by rolling circle amplification. (a) Main components of the DNA nanococoon and mechanism for intracellular delivery of DOX. (b) Hydrodynamic size of DNA nanococoon and TEM image of DNA nanococoon complexed with gold nanoparticle stained DNaseI nanocapsule. Scale bar is 100 nm (c) Confocal laser scanning microscopy images of DNA nanococoon mediated DOX delivery in MCF-7 cells. Red for DOX, green for endolysosome and blue for nucleus. Scale bar is 10 μ m. Reproduced with permission from ref. [98].

assembly – G quadruplex,^[549, 550] which was built from stacks of G-quartet arising from the cyclic hydrogen-bonding between four guanines in physiological buffer conditions.^[551] To demonstrate the delivery of photosensitizer TMPyP4 into CEM and Ramos cells, Wang et al. conjugated a DNA aptamer with targeting abilities with a G-quadruplex and the toxicity of TMPyP4 to target cells were doubled using the aptamer-G-quadruplex as a carrier.^[549]

2.2. Nucleic Acids

Besides small molecule drugs, nucleic acids, such as cytosine-phosphate-guanine (CpG),^[552] small interfering RNA (siRNA)^[553] and antisense nucleotides, can also work as anticancer therapeutics by interacting with their cellular targets.

2.2.1 SiRNA

SiRNA is a major player in the process of RNA interference inside eukaryotic cells. The long chain double stranded RNA is first processed by the enzyme Dicer into short siRNA (~22 bp), which can be subsequently recruited into a protein complex RISC (RNA-induced silencing complex). The RISC then cleaves the sense strand of siRNA and uses the remaining antisense strand to find and degrade the target mRNA.^[553] The prospects that synthetic siRNA can nearly silence any gene in the tissue lead to considerable efforts for its therapeutic applications. Lee et al. used a DNA tetrahedral nanoassembly for siRNA delivery by taking advantage of its homogeneous size and controllable ligand orientation (Figure 2-3).^[285] The tetrahedron was assembled from 6 DNA oligos with sticky ends and obtained a final length of 10 nm along each edge. The siRNA was pre-modified with 2'-OMe for enhanced stability and reduced immunogenicity before incorporating into the DNA tetrahedral using its 3' sticky overhangs. Reporter proteins, such as luciferase and green fluorescent protein (GFP), were chosen as targets. *In vitro* study about the effect of targeting ligands on gene silencing efficiency revealed that a minimum of 3 folic acid targeting ligands were needed for GFP silencing. *In vivo* study in nude mice model xenografted with KB tumors capable of expressing firefly luciferase showed ~60% reduction in bioluminescence

by tail-vein as well as intratumour injections. A tumor-specific accumulation of the tetrahedral nanoparticle was also observed after systemic injection and no significant immune response was detected. To simplify the process of loading siRNA into carriers, Hammond and coworkers adopt an approach similar to RCA that transcribed a long single strand RNA containing periodic repeats of siRNA from a circular DNA template by RNA polymerase.^[538] Hairpin structures were programmed into the template to maintain the double strand structure of siRNA as well as to induce the assembly of the product into a sponge like structure. The RNA microsponge worked as a structural scaffold as well as a pro-drug that could be processed into functional siRNA intracellularly. With the help of polyethylenimine (PEI) as condensing as well as endosome escape agent, expression of firefly luciferase was inhibited by 57.6% in T22-Luc cells.

2.2.2 Antisense nucleotides

Similar to siRNA, antisense nucleotide can also block the expression of a target gene. Instead of using a RISC mediated mRNA degradation mechanism, antisense nucleotides can sequence-specifically bind to its target mRNA and recruit RNase H to degrade the RNA strand from the DNA/RNA complex.^[554] Other mechanisms involved in antisense nucleotide regulation might be its ability to arrest transcription and alter mRNA splicing patterns.^[555] Due to the similar gene regulation mechanisms of siRNA and antisense nucleotides, carriers developed for siRNA delivery could also be applied for delivering antisense nucleotides.

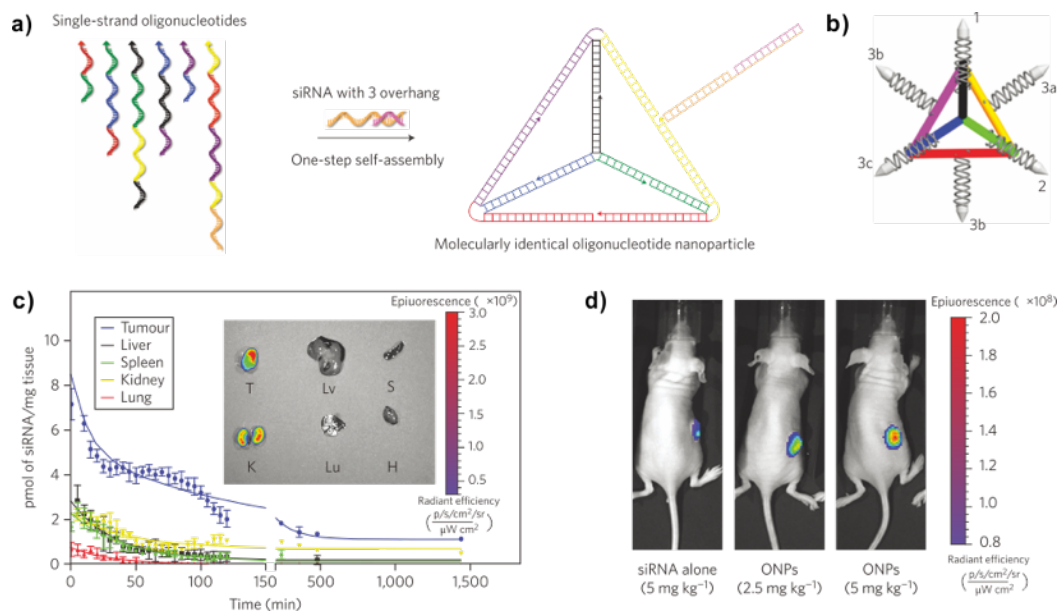


Figure 2-3. Delivery of siRNA using a DNA tetrahedron assembled from DNA tiles. (a) Schematic for the DNA tetrahedron formation. (b) Structure of the DNA tetrahedron with ligands. (c) Pharmacokinetic profile of the siRNA loaded DNA tetrahedron in mice bearing KB tumor and distribution of the nanoparticle in major organs after 12 h of injection. (d) Representative fluorescent image of dose-dependent accumulation of the DNA nanoparticle in KB tumors. Reproduced with permission from ref. [285].

Keum et al. applied the DNA tetrahedron assembly for displaying antisense nucleotides.^[556] Five out of the six edges of the tetrahedron were designed as dsDNA while the left one was designed as ssDNA for antisense nucleotide binding. The antisense nucleotide was designed as a floating loop to maximize its interaction with cytosolic mRNA. The displayed antisense nucleotide showed enhanced uptake efficiency than linear DNA and exhibited efficient gene silencing capabilities *in vitro*. In another report, Roh et al. adopted the RCA approach to generate a long chain ssDNA encoding periodic antisense nucleotides, which could self-assemble into a DNA sponge for intracellular delivery.^[539] Charged

polymers were coated onto the DNA in a layer-by-layer (LBL) method to condense to size of the microsphere from $\sim 1.8 \mu\text{m}$ to $\sim 200 \text{ nm}$. The microsphere has a very high antisense nucleotide loading capacity and the LBL condensed microsphere achieved ~ 50 fold higher luciferase knockdown efficiency than the same amount of free antisense nucleotide delivered by lipofectamine in a SKOV3-LUC/SKOV3 cell line. The formulation also showed superb stability and *in vivo* biodistribution in nude mice model via tail vein injection that primarily accumulated in tumor and kidney.

2.2.3 CpG

The pathogen derived CpG motifs contained an unmethylated cytosine while the CG dinucleotide in mammalian cells often contained methylated cytosine at its C5 position.^[552] Toll-like receptor 9 (TLR9) in the endosome of immune cells, such as dendritic cells and macrophages, can recognize the CpG motif as a “danger signal” and activate the innate immune systems, generating cytokines, chemokines or antibodies.^[552] The immunostimulatory capability makes CpG an effective therapeutic agent against cancer.^[557]

Takakura and coworkers used three or more ssDNA oligos with CpG motif encoded to assemble various polypod-like structures containing different numbers of pod for CpG delivery.^[545, 558] The assemblies showed an average size of 10 nm and the assemblies with six or more pods induced efficient secretion of tumor necrosis factor- α (TNF- α) and interleukin-6 (IL-6) from macrophage-like RAW264.7 cells.^[545] The DNA polypod mediated CpG delivery can also be applied to other cell lines, such as splenic macrophages, murine and bone marrow-derived dendritic cells as well as human peripheral blood mononuclear but not

for macrophages lacking TLR9.^[545] Although CpG uptake in RAW264.7 cells was enhanced with increasing pod numbers, the structural integrity of the assemblies was diminished. To obtain a rigid and stable DNA carrier for CpG delivery, Li et al. assembled a cage-like tetrahedral DNA nanoassembly from four predesigned DNA oligos. The tetrahedral structure was resistant to nuclease degradation and remained stable inside RAW254.7 cells, which was observed from the colocalization of two fluorescent dyes labeled on different vertexes on the tetrahedral after 8 hours.^[543] Using the “DNA origami” method, Schüller et al. folded a 8634-bp ssDNA scaffold with 227 staples into a hollow DNA tube (~80 nm in length and ~20 nm in diameter) with 62 binding sites for CpG oligo anchoring.^[559] A degradation-resistant phosphorothioate backbone was incorporated into the CpG oligo for enhanced stability and this CpG decorated DNA nanotube achieved higher immunostimulation as well as lower cytotoxicity in isolated spleen cells compared with lipofectamine mediated CpG delivery. To simplify the DNA origami folding process, which usually required hundreds of specifically designed staples, Ouyang et al. replaced the commonly used bacteriophage genome with a long ssDNA scaffold prepared by RCA.^[560] Due to the periodic nature of RCA products, only several staples were need to fold the RCA product into a DNA nanoribbon with tunable width and length by controlling the RCA template sequence as well the RCA reaction time. By artificially programing a region of the RCA template for anchoring CpG containing nucleotide, one CpG could be incorporated into each periodic unit of the RCA product and this strategy successfully delivered CpG into RAW 264.7 cells and induced the secretion of TNF- α .

2.3. Proteins

Proteins with anticancer activities, such as antibodies, cytokines, transcription factors and enzymes, were discovered capable of activating the apoptosis pathways or blocking growth signals in cancer cells.^[506, 561] In addition to directly interacting with cancer cells, proteins can also function as antigens to activate leukocytes, such as T cells, after being phagocytized and presented by antigen presenting cells.^[562] The highly specific set of activities makes protein a very diverse and promising class of anticancer therapeutics.

To design a virus-like vaccine for cancer, Liu et al. used the DNA tetrahedron structure to deliver a model antigen, streptavidin, into immune cells together with a CpG motif as antigen adjuvant.^[563] Localization of the antigen inside the lysosome of RAW 264.7 was observed after 2 h of incubation due to the DNA tetrahedron assisted uptake of the antigen. The DNA tetrahedron delivered vaccine induced much higher anti-streptavidin antibody production in BALB/c mice than free streptavidin and CpG over a period of 70 days and the safety of the DNA tetrahedron carrier was confirmed by the absence of any anti-dsDNA antibody. Using a “DNA origami” approach, Douglas et al. assembled a barrel-like DNA robot (35nm×35nm×45nm) with the ability to sense cell surface signals to control its configuration for drug delivery.^[529] The nanobarrel was locked with DNA aptamers, which can be opened by the specific antigen keys presented on cell surfaces. Antibody cargoes were loaded by conjugating to ssDNAs complementary to anchors inside the barrel. The nanorobot successfully delivered CD33 and CDw238 Fab’ fragment antibodies to natural killer leukemia cell and arrested its growth and it also delivered CD3e Fab’ and flagellin Fab’

antibodies to T cells for T cell activation. Besides the “DNA tile” and “DNA origami” based structures, RCA based nanoassembly was also utilized for delivering anti-CD20 clusters to CD20 positive Ramos cells.^[546]

3. DNA scaffolds-based stimuli-responsive drug delivery

Designing hybrid carriers by incorporating nanomaterials, such as polymeric gel,^[456] liposome^[470] and silica^[564] with DNA aptamers is an efficient strategy in developing smart carriers with the ability to release the anticancer therapeutics in response to distinct environmental triggers.^[282]

Using an ATP-binding aptamer, our group devised DNA functionalized polymeric drug delivery carriers, which can utilize the ATP concentration difference between intracellular and extracellular environments for controlled drug delivery.^[456, 459, 470] The ATP-binding aptamer is hybridized with its complementary DNA, which forms a stable double stranded DNA encoding a GC-pair for DOX loading (Figure 2-4).^[456] The high level of intracellular ATP competitively binds the ATP aptamer and dissociated the double stranded DNA into single strands, leading to the release of DOX. The DNA scaffold was condensed with a positively charged protein to form a positively charged core, which was further coated by a layer of negatively charged polymeric hyaluronic acid (HA). In addition to forming a protective shell for the DNA scaffold, the HA also works as a targeting ligand to receptors like CD44 and RHAMM on the surface of several cancer cells. The hyaluronidase rich in

tumor microenvironment can degrade the HA shell and facilitate the intracellular delivery of the DNA scaffold. *In vitro* DOX release study showed an ATP-specific response compared with other types of nucleotides. Intravenous injection of the nanogel into MDA-MD-231 tumour-bearing mice showed longer circulation time of DOX and a 4.19-fold higher DOX accumulation the tumor than DOX solution. Besides utilizing the intracellular ATP level, extrinsic ATP delivered by a liposomal carrier can also be used to trigger DOX release from a hybrid carrier composed of the ATP responsive DNA scaffold and a fusogenic liposome.^[470]

4. Conclusion and outlook

Integrating with the novel “self-assembly” technology as well as interaction between DNA and target drugs, many drug delivery carriers have been recently developed with promising biocompatibility, drug loading capacity and uptake efficiency. The degradability of DNA can be harnessed to improve the biocompatibility of other non-degradable systems. As demonstrated by Chan and coworkers,^[390] DNA scaffolds were utilized to assemble small gold nanoparticles with size of 3 nm, 5 nm and 13 nm into larger colloid structures for enhanced tumor accumulation, which could also be degraded into individual components for facilitated elimination from the body. DNA is a highly programmable molecule characterized by its polyvalency. Instead of delivering one single kind of drug, DNA nanostructures could be programed for co-delivering different drugs or synchronizing the activities of different

proteins. For example, Liu et al. demonstrated the use of a branched DNA nanostructure in assembling three enzymes with complementary activities into a single nanocomplex, leading to greatly enhanced catalytic efficiencies.^[565] To further enhance the efficacy of DNA drug carriers, elements capable of sensing the environmental signal should be incorporated to build smart drug delivery carriers. As demonstrated by the DNA robot for cell specific antibody delivery,^[529] DNA devices capable of sensing inputs from the cell or environment and perform logic calculations for controlled drug release provides a guideline for developing the next-generation drug delivery systems.

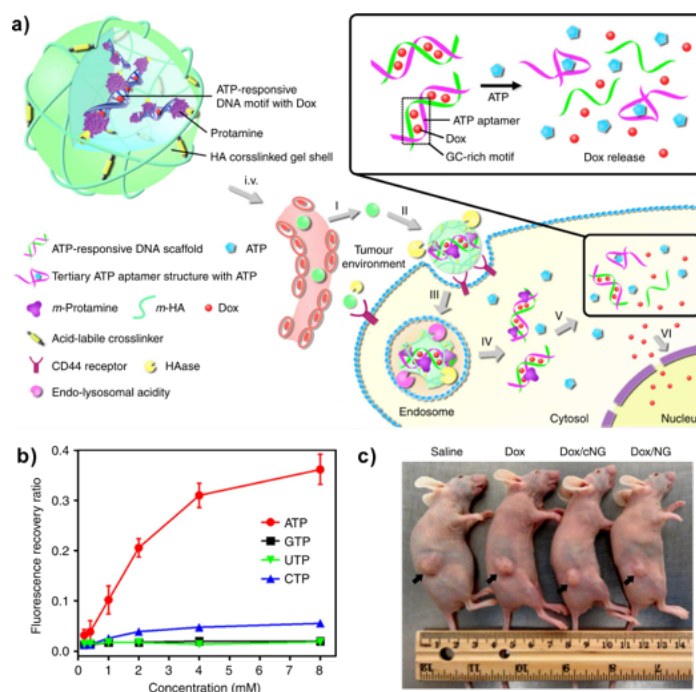


Figure 2-4. ATP responsive delivery of DOX using polymeric nanoparticles functionalized by an ATP-binding DNA scaffold. (a) Schematic of the ATP responsive drug delivery system. (b) DOX release from the DNA-aptamer duplex as response to different nucleotides. (c) Representative image of MDA-MB-231 tumor bearing mice treated with different formulations. Reproduced with permission from ref. [456].

Despite these advantages, as a new arrival to the drug delivery field, DNA nanostructures need to be further investigated for meeting the criteria of clinical potency. Complex interactions between DNA scaffold and living cells, such as DNA degradation^[515] and immunogenicity^[566], posed huge challenges to DNA nanomedicine applications. Although chemical modifications improved DNA stability, specificity of DNA target recognition could be compromised occasionally.^[567] The fact that numerous DNA therapeutics, including ssDNA oligos and dsDNA plasmids,^[566, 568] were developed for immunotherapy highlighted the immunogenic nature of DNA, which often raises a concern. In addition, even though the development of commercial DNA synthesis made customized DNA oligo readily available,^[569] using DNA as a generic material instead of genetic materials is still limited to small scales. Besides improving chemical DNA synthesis techniques for reduced cost, utilizing the DNA synthesis capability of cells could be a natural solution to address this concern.^[570]

CHAPTER 3 COCOON-LIKE SELF-DEGRADABLE DNA-NANOCLEW FOR ANTICANCER DRUG DELIVERY

1. Introduction

Self-assembled DNA nanostructures have been developed with precisely controlled size and architecture.^[285, 529, 530, 540, 542, 546, 571, 572] Upon DNA's intrinsic biocompatibility and degradability, DNA nanostructures hold tremendous promise for drug delivery. Numerous cargos including small-molecule drugs,^[547, 573] small interfering RNA (siRNA),^[285, 538] immuno-stimulatory oligonucleotide CpG,^[543, 559] photosensitizer^[549] and protein^[529] were successfully delivered intracellularly by DNA nanocarriers. Moreover, DNA-based carriers can be readily functionalized either by hybridizing a targeting moiety onto the nanostructure^[285] or programming a targeting aptamer into the DNA chain^[529, 530] for targeted drug delivery. Despite these, strategies utilizing DNA scaffolds for on-demand drug delivery in a stimuli-responsive fashion,^[574, 575] instead of passive release,^[62, 163, 576] still remain elusive. We have recently reported an adenosine triphosphate (ATP)-responsive formulation incorporating short DNA strands (with ATP's aptamer) loaded with DOX, an anticancer drug.^[456, 470] The enhanced drug release inside cancer cells, triggered by a high ATP level was validated. However, this design is limited by a complicated formulation process and relatively low drug loading capacity.

We herein describe a bio-inspired drug delivery carrier by integrating a cocoon-like DNA nano-composite with “caged worm”-deoxyribonuclease (DNase) to achieve self-

degradation for promoting drug release inside cells (Figure 3-1). The DNA structure is based on a “nanoclew” (designated as NCl in this Chapter), “weaved” by the rolling circle amplification (RCA, Figure 3-2), the product of which is often applied in biodetection.^[537] Multiple GC-pair sequences were integrated in the NCl for enhancing loading capacity of DOX.^[456, 470] To facilitate self-assembly, a palindromic sequence is incorporated into the template. To enable degradation of NCl, DNase I is encapsulated into a single-protein based nanocapsule (designated as NCa) with a positively charged thin polymeric shell, cross-linked by acid-degradable linkers using interfacial polymerization (Figure 3-1a).^[96, 577] Furthermore, to achieve a tumor-targeting delivery of DOX folic acid (FA) is conjugated to an NCl complementary DNA (cDNA) oligo followed by hybridization into the DNA NCl. The positively charged NCa can be embedded into the NCl via electrostatic interaction to form the DOX-loaded self-degradable DNA scaffold (designated as DOX/FA-NCl/NCa).

The polymeric capsule cages the activity of DNase I under the physiological pH, which retains DOX in the NCl. When DOX/FA-NCl/NCa is internalized by the cancer cells and enters the acidic endo-lysosome, the polymeric shell of NCa degrades and sheds from DNase I. This results in the immediate rejuvenation of DNase I, thereby rapidly degrading NCl and subsequently releasing the encapsulated DOX for enhanced anticancer efficacy (Figure 3-1b). This formulation represents a novel stimuli-responsive drug delivery system, the trigger of which is pre-loaded with the delivery vehicle and can be activated by cellular environment.

2. Materials and Methods

2.1. Materials.

All chemicals were purchased from Sigma-Aldrich unless otherwise specified, and were used as received. DOX was purchased from BIOTANG Inc. (Lexington, MA,

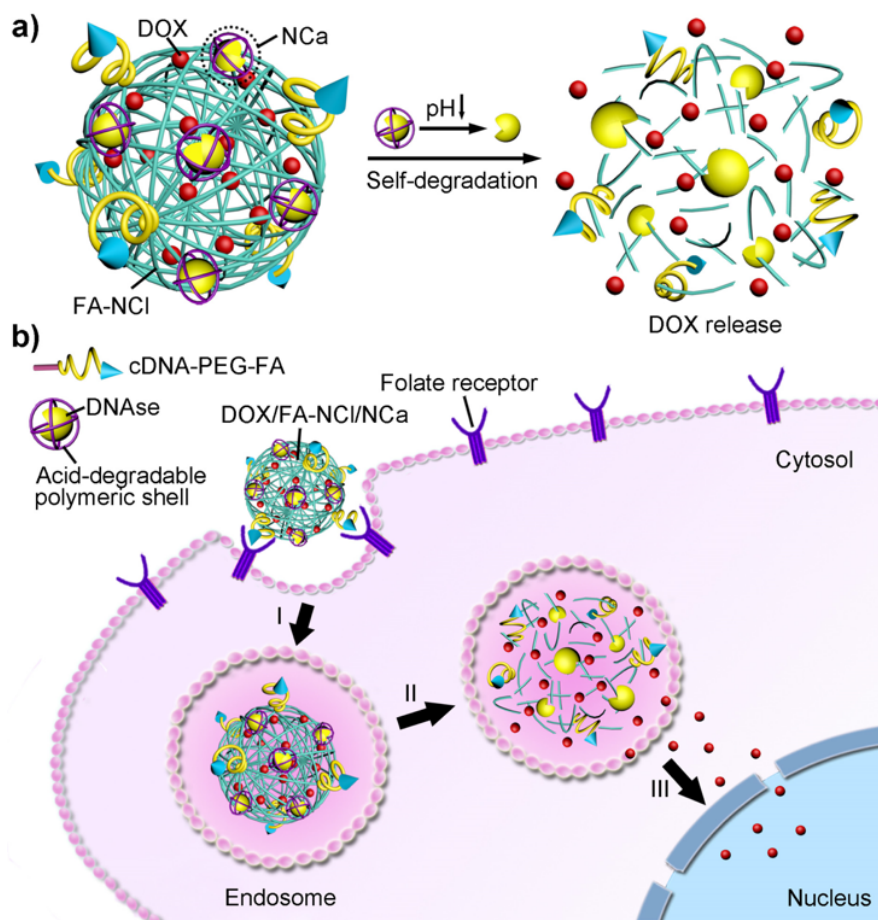


Figure 3-1. a) Main components of the cocoon-like self-degradable DNA clew, consisting of DOX/FA-NCI/NCa, and acid triggered DOX release. b) Schematic illustration of efficient delivery of DOX by DOX/FA-NCI/NCa to nuclei for cancer therapy. I. Internalization in endosomes; II. pH-triggered degradation of NCI for DOX release; III. Accumulation of DOX in cell nuclei.



Figure 3-2. Synthesis of NCl by rolling circle amplification. I). With a cyclized ssDNA a template and a DNA oligo as primer, long chain single stranded DNA containing repeated sequence of the template was synthesized. II). The synthesized RCA product self-assembled into nanoclews-like structure by intra-molecular hybridization.

USA). DNA oligos were purchased from Integrated DNA Technologies Inc. (Coralville, IA, USA). Bovine pancreas DNase I lyophilized powder was purchased from Roche Applied Science (Mannheim, Germany). CircLigase II ssDNA Ligase was purchased from Epicenter (Madison, WI, USA). Bst 2.0 DNA polymerase was purchased from New England BioLabs Inc. (Ipswich, MA, USA). DNA ladder, dNTP, and Exonuclease I were purchased from ThermoFisher Scientific, Inc. (Pittsburgh, PA, USA). Alexa Fluor® 488 N-hydroxysuccinimidyl ester was purchased from Life Technologies (Grand Island, NY, USA). Folic acid-polyethylene glycol 2000-N-hydroxysuccinimidyl ester (FA-PEG-NHS) was purchased from Nanocs Inc. (New York, NY, USA). Glycerol dimethacrylate was purchased from Tokyo Chemical Industry Co., Ltd. (Tokyo, Japan). GelRed was purchased from Biotium Inc. (Hayward, CA, USA). Mono-sulfo-N-hydroxy-succinimido Au-nanoparticles was purchased from NanoProbe (Yaphank, NY, USA).

2.2. Preparation and Characterization of DNA NCI.

Rolling circle amplification (RCA) was used to prepare the NCI. A 5'-phosphorylated ssDNA template (Table 3-1) was cyclized into a circular ssDNA template with CircLigase II ssDNA ligase according to manufacture's instructions. Briefly, 10 pmol ssDNA template was added into a 20 μ L of reaction mixture containing 2.5 mM $MnCl_2$, 1 M betaine and 5 U/ μ L CircLigase II ssDNA ligase. After incubation at 60 $^{\circ}C$ for 1 h, the cyclized template was treated with exonuclease I (1 U/ μ L) at 37 $^{\circ}C$ for 45 min and followed by heat inactivation at 80 $^{\circ}C$ for 15 min. The resultant cyclized ssDNA template was hybridized with 0.5 μ M primer in a 1 \times isothermal amplification buffer (20 mM Tris-HCl pH 8.8, 10 mM $(NH_4)_2SO_4$, 50 mM KCl, 2 mM $MgSO_4$, 0.1% Tween 20) containing 0.2 mM dNTP at 95 $^{\circ}C$ for 5 min. After cooling the template-primer hybridized solution to room temperature, Bst 2.0 DNA polymerase was added to a final concentration of 0.2 U/ μ L and the RCA was performed at 60 $^{\circ}C$ for 17 h followed by heat inactivation at 80 $^{\circ}C$ for 20 min. The obtained NCI was dialyzed against TE buffer (10 mM Tris pH 8.0, 1 mM EDTA) at room temperature in a dialysis unit (20 K MWCO) (Slide-A-Lyzer, Thermo Scientific) for 48 h. Sizes of the template and product were estimated by agarose gel electrophoresis using 0.8% (w/v) agarose gel. After staining with GelRed, the agarose gel was imaged under UV irradiation. DNA concentration of NCI was measured with Nanodrop 2000C spectrometer (Thermo Scientific). Particle size and zeta potential were measured by a Zetasizer (Nano ZS, Malvern). Stability of the RCA product was tested by incubating it in DMEM media containing 10 % fetus bovine serum (FBS) at 37 $^{\circ}C$ for 48 h. For atomic force microscope,

NCl was dropped onto a silicon wafer (Ted Pella), dried and analyzed with Nanoscope (Veeco, Santa Barbara, CA) using tapping mode in ambient air.

Table 3-1. Sequences of DNA oligos.

	Sequences (5'-3')
	Phosphate-
Template (flexible arm, palindromic sequence FA-oligo hybridization site)	GTAAATATTATTTCGACGGGCCTGCTCGAGC TCGAGCTTGCATCGTGCAGCCGAAGCTTG CACGCGTGCTATTAAT
Primer	GCACGCGTGCAAGC
cDNA oligo	GCTTGCACGCGTGC-NH ₂

The 5' and 3' ends of the ssDNA template were mainly composed of A and T to enhance flexibility for ligation. GC/CG pairs were designed into the drug loading sites to increase DOX loading capacity. The palindromic sequence was incorporated to help assemble the ssDNA product into a clew.[648]

2.3. Preparation and characterization of DNase I nanocapsule (NCa).

DNase I was encapsulated in a single protein nanocapsule cross-linked by pH responsive cross-linker.[96] DNase I lyophilized powder was dissolved in 5 mM bicarbonate buffer (pH 8.3) to 1 mg/mL with a PDI of 0.38 ± 0.03 as determined by Zetasizer (Nano ZS,

Malvern). 200 mg/mL acrylamide (AAm) was added to 1 mL of DNase I solution while stirring at 4 °C. After 10 min, the positively charged monomer *N*-(3-aminopropyl) methacrylamide (APMAAm) was added while stirring. Then the pH responsive cross-linker glycerol dimethacrylate (GDA) was added together with 30 µL ammonium persulfate (100 mg/mL in deoxygenated and deionized water) and 3 µL *N,N,N',N'*-tetramethylethylenediamine to initiate the polymerization. The molar ratio of AAm/APMAAm/GDA was 10/1/0.13. The polymerization was allowed to proceed for 60 min and then buffer changed with phosphate-buffered saline (pH 7.4) to remove excess monomers and initiators in a ultracentrifuge unit (MWCO 30 KDa, Millipore). Protein content in the NCa was determined by bicinchoninic acid (BCA) colorimetric protein assay (Thermo Scientific) with bovine serum albumin (BSA) as the standard. Far-UV circular dichroism (CD) spectra of native DNase I and NCa was performed at 20 °C in 0.1 M phosphate buffer (pH 7.4) with protein concentration of 0.2 mg/mL (JASCO J-815 Circular Dichroism Spectrometer). Size and zeta potential of native DNase I and NCa were determined by a Zetasizer (Nano ZS, Malvern). For the non-degradable NCa, a non-degradable cross-linker methylenebisacrylamide was used instead of GDA while other conditions remained the same. For TEM imaging, the samples were dropped on a TEM copper grid (300 mesh) (Ted Pella) and stained with 2% (w/v) uranyl acetate (dissolved in 50% ethanol). The samples were observed by TEM (JEM-2000FX, Hitachi) at 100 kV. DNase I activity was assayed with DNA sodium salt from salmon (0.2 mg/mL) as the

substrate at 37 °C in 200 mM phosphate buffer containing 2.5 mM MgCl₂ and 0.5 mM CaCl₂. A₂₆₀ increases over time were recorded by Nanodrop 2000C (Thermo Scientific).

2.4. DOX loading and release.

The capability of NCl to load DOX was tested by measuring its ability to quench the fluorescence of DOX. NCl of different final concentrations (0.15 - 2.4 µg/mL) was added to 10 µM DOX solution and the fluorescence of DOX/NCl was scanned (excitation 480 nm, emission 520-800 nm) in a microplate reader (Infinite M200 PRO, Tecan). To test the DOX loading efficiency of NCl, 10 µg/mL NCl was incubated with different concentrations of DOX (5-160 µM, DOX/NCl mass ratio of 0.3 - 9.3) at room temperature for 1h. The mixture was then centrifuged at 14000 ×g for 10 min and DOX concentration in the supernatant was analyzed by reading DOX fluorescence (excitation 480 nm, emission 596 nm). Entrapped DOX is calculate as DOX added in the beginning - DOX in the supernatant after centrifugation, DOX entrapment efficiency is calculated as mass of DOX entrapped/mass of DOX added. DOX loading capacity of the DNA carrier is calculated as mass of DOX entrapped/(mass of DOX entrapped + mass of carrier). DOX release profile from NCl was monitored by measuring DOX fluorescence recovery from DOX/NCl/NCa or DOX/NCl/cNca, which was incubated in 0.2 M phosphate buffer (pH 7.4, 5.4) containing 2.5 mM MgCl₂ and 0.5 mM CaCl₂ at 37 °C for 260 min. Samples were taken and centrifuged at 14000 ×g for 10 min and DOX released was quantified by measuring DOX fluorescence.

2.5. Assembly and characterization of NCl/NCa.

10 $\mu\text{g/mL}$ NCl was mixed with 40 $\mu\text{g/mL}$ NCa before each use. Size and zeta potential of NCl/NCa was measured by a Zetasizer (Nano ZS, Malvern). To visualize the assembly by confocal laser scanning microscope (CLSM), DNase I was conjugated with Alexa Fluor® 488 N-hydroxysuccinimidyl ester (AF488-NHS) to obtain AF488 decorated DNase I (AF488-DNase I). 1 mg DNase I was dissolved in 1 mL 0.1 M bicarbonate buffer (pH 8.3), equimolar amount of AF488-NHS (dissolved in anhydrous DMSO) was added into DNase I solution while stirring. The reaction was kept at room temperature for 1h and excessive AF488-NHS was removed by ultracentrifugation (30 K MWCO, Millipore). AF488-DNase I was encapsulated in acid degradable protein capsule by the same method as described above to obtain AF488-NCa. NCl was visualized by the fluorescence of the loaded DOX. The DOX/NCl/AF488-NCa was immobilized in 1% agarose gel and observed with CLSM (LSM 710, Zeiss). To visualize NCl/NCa by TEM, gold nanoparticle (AuNP) was conjugated onto DNase I for imaging. Mono-sulfo-*N*-hydroxy-succinimido AuNP was reacted with native DNase I at molar ratio of 4/1 in PBS buffer (pH 7.4) for 1h. Excessive AuNP was removed by gel filtration using Superdex-75. Concentrations of the AuNP and DNase I was determined by UV/vis spectra based on the molar extinction coefficients (AuNP, $155,000 \text{ M}^{-1}\text{cm}^{-1}$ at 420 nm, DNase I, $36750 \text{ M}^{-1}\text{cm}^{-1}$ at 280 nm). The resulted Au-DNase I had a molar ratio of AuNP/DNase I of 0.91 and it was encapsulated in the nanocapsule (Au-NCa) by the same method as native DNase I. The obtained Au-NCa was mixed with NCl and dropped onto a TEM grid followed by rinsing with deionized water.

Silver enhancement was applied for better TEM imaging by floating the grid on fresh silver enhancement reagent (Nanoprobe) for 1 min. Then the grid was rinsed with deionized water and stained with 1% sodium phosphotungstate at pH 7.0. Uniformed 3-4 nm silver coated AuNP form by this process. PH triggered NCl/NCa degradation was visualized by AFM with NCl/NCa samples incubated at pH 7.4 and pH 5.4 phosphate buffer for 2 h before imaging.

2.6. Conjugation of NCl with folic acid.

The complementary DNA (cDNA) oligo (Table 3-1) for folic acid conjugation was modified with NH_2 at 3' end. After dissolving the oligo in 0.1 M bicarbonate buffer (pH 8.3), folic acid-polyethylene glycol 2000-N-hydroxysuccinimidyl ester (FA-PEG-NHS, dissolved in DMSO) was added while stirring with molar ratio of FA-PEG-NHS/oligo at 2/1. The reaction was protected from light and allowed to proceed at room temperature over night. The conjugation product (cDNA-PEG-FA) was dialyzed against deionized water in a dialysis unit (MWCO 3.5K, Millipore) for 48 h. The obtained cDNA-PEG-FA was hybridized with the NCl at 95 °C for 5 min and then cooled to room temperature. Molar ratio of the repeating unit in NCl to cDNA-PEG-FA was 100:1. Size and zeta potential of FA-NCl was measured by a Zetasizer (Nano ZS, Malvern).

2.7. Cell culture.

Human breast cancer cell line MCF-7 from American Type Culture Collection (Manassas, VA) was cultured in Dulbecco's Modified Eagle's Medium supplemented with

10 % (v/v) FBS, penicillin (100 U/mL) and streptomycin (100 µg/mL) in a 37 °C incubator (Thermal Scientific) under 5% CO₂ and 90% humidity. The cells were regularly sub-cultured with trypsin-EDTA (0.25%, w/w) and cell density was determined with hemocytometer before each experiment.

2.8. Determination of endocytosis pathways.

MCF-7 cells were seeded in 6-well plates (1×10^4 cells per well) and culture for 48 h. Afterwards, the cells were pre-incubated with several inhibitors specific for different endocytosis pathways [chlorpromazine (CPZ, 10 µM) for clathrin-mediated endocytosis; nystatin (NYS, 25 µg/mL) for caveolin-mediated endocytosis; amiloride (AMI, 1 mM) for macropinocytosis; methyl-β-cyclodextrin (MCD, 3 mM) for lipid raft] for 1 h at 37 °C, respectively. Then the cells were incubated with DOX/FA-NCI/NCa at DOX concentration of 2 µM or FA-NCI/AF488-NCa of the same concentration in the presence of the inhibitors for another 2 h. After washing the cells by 4 °C PBS twice, the cells were lysed with Pierce IP lysis buffer (Thermo Scientific) and centrifuged. Fluorescence of DOX and AF488 and protein concentration in the supernatant were measured, respectively, by a microplate reader (Infinite M200 PRO, Tecan).

2.9. Intracellular distribution.

MCF-7 cells (1×10^5 cells per dish) were seeded in confocal dishes and cultured for 24 h. To image nucleus targeting by DOX, the cells were incubated with DOX/FA-NCI/NCa at

DOX concentration of 2 μ M for 10 min, 0.5 h, 1 h, 2 h and 4 h. Afterwards, the cells were washed with 4 °C PBS twice and stained by LysoTracker green (50 nM) (Life Technologies) at 37 °C for 30 min. Then the cells were washed with 4 °C PBS twice and stained with Hoechst 33342 (1 μ g/mL) for 10 min. After washing 4 °C PBS twice again the cells were immediately observed on CLSM (LSM 710, Zeiss). On the other hand, to image the co-localization of NCl and NCa, the cells were incubated with DOX/FA-NCl/AF488-NCa at DOX concentration of 2 μ M for 10 min, 0.5 h and 1 h. The cells were then washed with 4 °C PBS twice and stained with Hoechst 33342 (1 μ g/mL) for 10 min. After washing 4 °C PBS twice again the cells were immediately observed on CLSM.

2.10. *In vitro* cytotoxicity assay.

MCF-7 cells were seeded in 96-well plate (1×10^4 cells per well). After culturing for 24 h, the cells were exposed to DOX/FA-NCl/NCa at different DOX concentrations in FBS free medium for additional 24 h. Afterwards, 20 μ L per well of MTT solution (5 mg/mL) was added and incubate for another 4 h. After removing the culture media, the cells were mixed with 150 μ L of DMSO. The absorbance was measured at a test wavelength of 570 nm with a reference wavelength of 630 nm by a microplate reader (Infinite M200 PRO, Tecan).

3. Results and Discussion

3.1. Preparation of acid degradable nanococoon

To validate our assumption, we first synthesized the DNA NCI by RCA (sequence shown in Table 3-1). Cyclization of the ssDNA template was confirmed by its resistance to Exonuclease I and RCA products with various molecular weights were amplified from the circular ssDNA template (Figure 3-3). NCI presented a high stability after incubating with the culture media containing fetal bovine serum (FBS) (10%, v:v) for up to 48 h (Figure 3-3c). The synthesized ssDNA self-assembled into 3-D clew like structure with an average particle size of 150 nm (Figure 3-4a). Intercalation of DOX into NCI was monitored via the fluorescence intensity of DOX solution, which was significantly declined when NCI was added, due to self-quenching[456, 470] of DOX once interacting with NCI (Figure 3-5). The loading amount of DOX was assessed (Figure 3-6). At the mass ratio of 2.3, NCI showed a maximum DOX-loading capacity of 66.7%. 86.5% of the added DOX was entrapped into the obtained NCI.

Both native DNase I and the obtained NCI had negatively charged surfaces (Table 3-2). To integrate them together, DNase I was encapsulated in a positively charged polymeric single protein nanogel using the in situ free-radical polymerization,[577] which encapsulated DNase I into a capsule with the zeta potential converted from -9 mV to +3 mV. Mono-dispersive NCa was obtained with an average size of 8.0 nm, which showed an increased particle size compared to 4.2 nm of the native DNase I (Figure 3-4b). Encapsulating DNase

I in the capsule showed no impact on its secondary structure (Figure 3-4c) and the acid-responsive degradation[578-580] of NCa was observed (Figure 3-7). Glycerol dimethacrylate (GDA), the pH-responsive cross-linker in NCa is stable at physiological pH but degradable at a lower pH,[96] Degradation of NCa was observed after incubation at pH 5.4 for 2 h. The particle size of NCa remarkably decreased at pH 5.4 compared with that at pH 7.4.

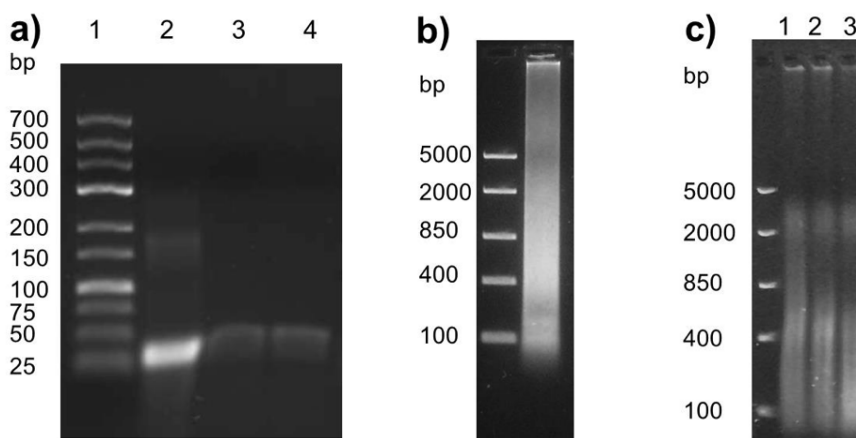


Figure 3-3. a) Cyclization of the ssDNA template. Lane 1, DNA ladder; Lane d2, 5' phosphorylated ssDNA template; Lane 3, cyclized ssDNA template; Lane 4, circular ssDNA template treated with Exo I. b). 0.8 % agarose gel analysis of the RCA product. c). Stability of NCI. Lane 1, non-treated NCI; Lane 2, NCI treated with DMEM containing 10 % FBS for 24 h; Lane 3, NCI treated with DMEM containing 10% FBS for 48 h.

To further substantiate the pH-responsive DNA-degrading capability of NCa, a non-degradable DNase I capsule (cNCa) was taken as a control with a non-degradable cross-linker, methylenebisacrylamide to replace GDA during preparation. The pH responsiveness of NCa was further confirmed by testing the enzymatic activity of DNase I (Figure 3-4d). Due to the non-degradable property of cNCa, the polymeric shell of cNCa impeded the

DNase I activity at both pH 7.4 and pH 5.4. However, NCa showed significantly higher DNase I activity at pH 5.4 than that at pH 7.4.

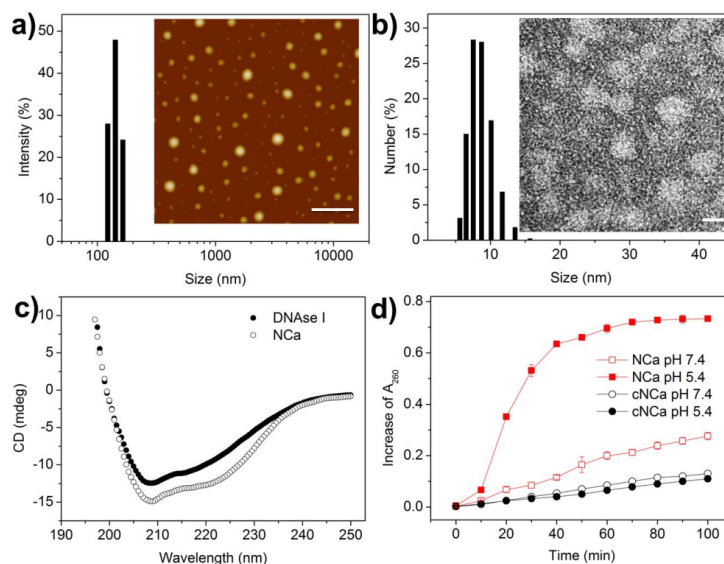


Figure 3-4. a) Hydrodynamic size of NCI by dynamic light scattering (DLS). Inset: AFM image of NCI. Scale bar is 500 nm. b) Hydrodynamic size of NCa. Inset: TEM image of NCa. Scale bar is 10 nm. c) CD spectra of native DNase I and NCa. d) DNA-degrading activities of NCa and cNca at pH 7.4 and pH 5.4. Bars represent mean \pm SD ($n = 3$).

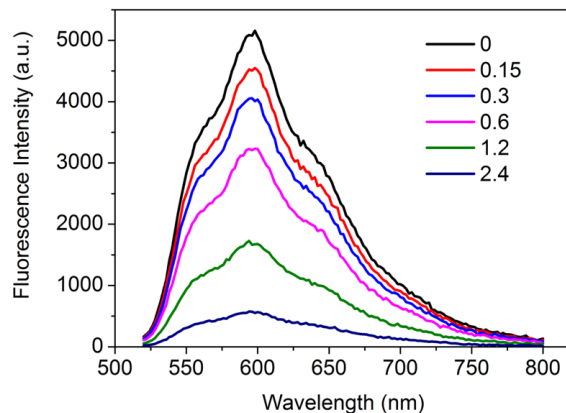


Figure 3-5. The fluorescence spectra of DOX solution (10 μ M) with increasing concentrations of NCI (0.15 - 2.4 μ g/mL).

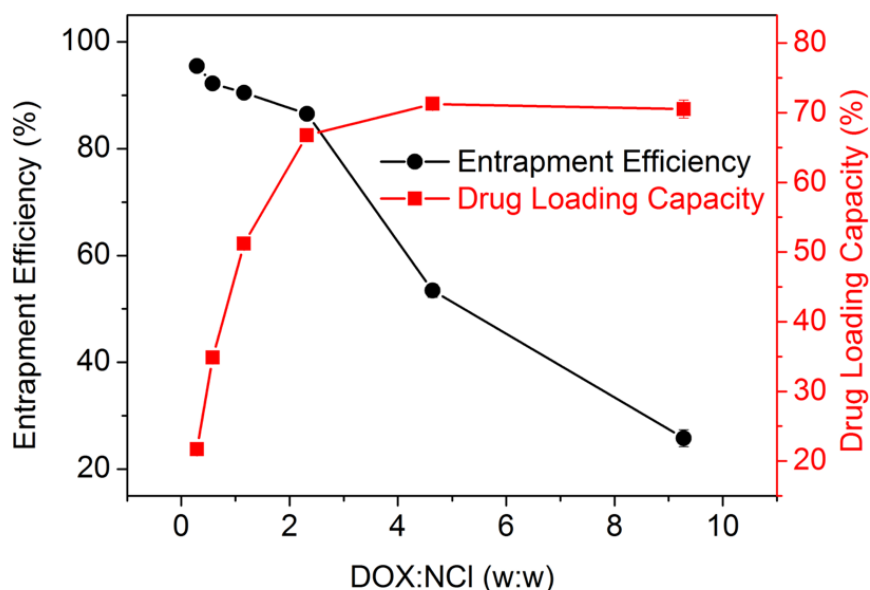


Figure 3-6. DOX entrapment efficiency and loading capacity by NCl. The DOX entrapment efficiency is the ratio of (added DOX - DOX washout out in supernatant)/added DOX. Drug loading capacity is the weight ratio of loaded DOX/(loaded DOX + NCl). Bars represent mean \pm SD (n = 3).

Table 3-2. Sizes and zeta potentials of different particles.

Particle	Size (Diameter, nm)	Zeta potential at pH 7.4 (mV)
DNAseI	4.2 \pm 0.2	-9 \pm 0.5
NCl	150 \pm 15	-22 \pm 2
FA-NCl	155 \pm 18	-21 \pm 3.1
NCa	8 \pm 1	+3 \pm 0.2
cNCl	10 \pm 1.1	+10 \pm 0.5
NCl/NCa	180 \pm 16	+8 \pm 0.4
Au-NCa	12 \pm 1.2	+4 \pm 0.4
DOX/NCl	172 \pm 13	- 34.7 \pm 3.6
DOX/NCl/NCa	211 \pm 18	+ 7.4 \pm 1
DOX/FA-NCl/NCa	221 \pm 19	+ 6.8 \pm 1.2

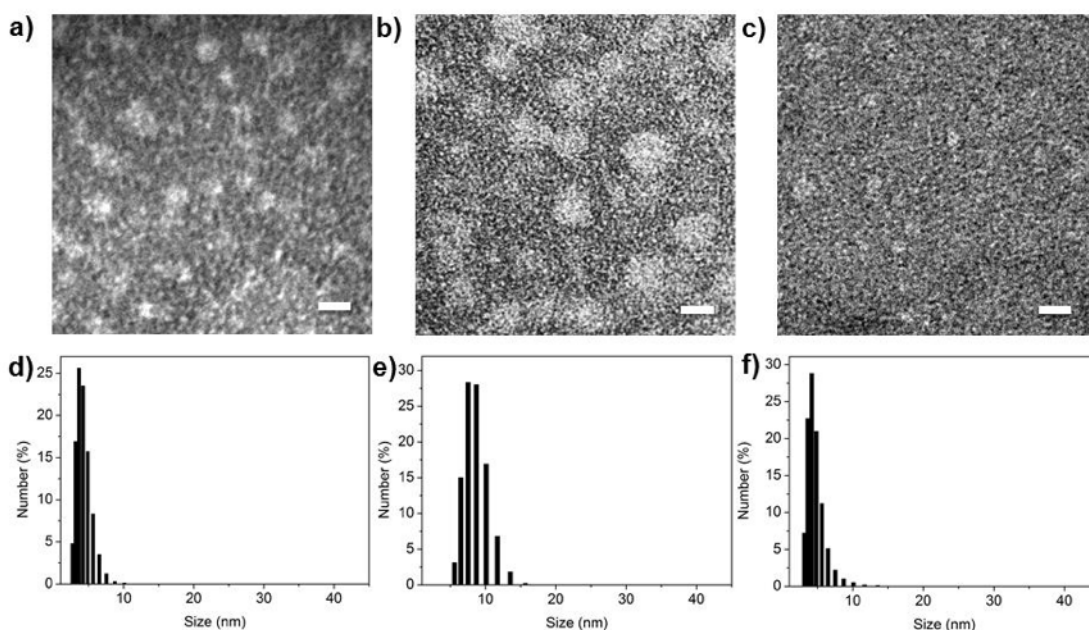


Figure 3-7. a-c) TEM image of DNase I (a), NCa (b) and NCa after incubation at pH 5.4 for 2 h (c). Scale bar is 10 nm. d-f) Hydrodynamic size of native DNase I (d), NCa (e) and NCa after incubation at pH 5.4 for 2 h (f).

Next, we mixed the negatively charged NCl with positively charged NCa to form homogeneous NCl/NCa complex ($PDI = 0.24 \pm 0.02$). The NCl/NCa assembly was observed by the co-localization of the fluorescence signals of DOX (red) in DOX/NCl and Alexa Fluor 488 (AF488 green) in AF488 modified NCa (Figure 3-8). The NCl/NCa assembly increased the average hydrodynamic size of NCl from 150 nm to 180 nm, and the zeta potential of NCl was converted from negative to positive (Figure 3-9a, Table 3-2). Furthermore, the TEM image clearly showed that the gold (Au) nanoparticle-labeled NCa[96, 565] (Au-NCa, Table 3-2) were well decorated into NCl (Figure 3-9a).

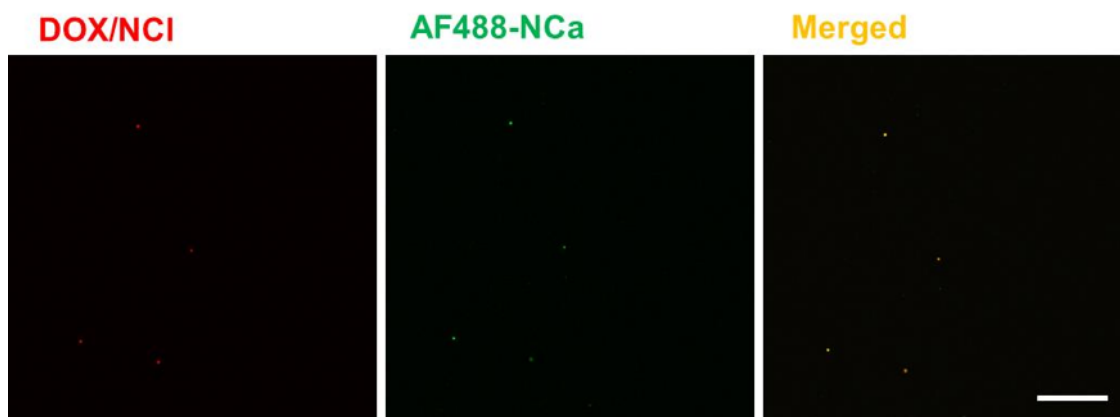


Figure 3-8. CLSM images of NCI/NCa assembly. NCI was loaded with DOX (DOX/NCI) and NCa was conjugated with AF488-NHS for imaging (AF488-NCa). Scale bar is 50 μm .

The release profiles of DOX from DOX/NCI/NCa at different pH values were determined[456] (Figure 3-9b) and pH reduction resulted in a promoted release of DOX. At pH 5.4, the cumulative release rate of DOX within 260 min was 3.7-fold of that at pH 7.4. While there was no apparent difference in the release of DOX from DOX/NCI/cNCa at pH 5.4 and 7.4. Similarly, The NCI/NCa complex remained stable at pH 7.4 within 2 h, while a high degradation efficiency of NCI/NCa was observed at pH 5.4 (Figure 3-9c).

3.2. Uptake and intracellular distribution of the nanococoon

To enhance tumor-targeting efficacy of DOX/NCI/NCa, a ligand containing FA (cDNA-PEG-FA) was hybridized into NC and the hybridization of cDNA-PEG-FA to NCI had no significant change in the particle size and zeta potential of NCI (Table 3-2). The endocytosis pathway of DOX/FA-NCI/NCa was determined by incubating the human breast

cancer (MCF-7) cells overexpressing FR[581] with different inhibitors for specific pathways (Figure 3-10a). Compared with other inhibitors, both chlorpromazine (CPZ) and amiloride (AMI), displayed pronounced effects in inhibiting the internalization of DOX/FA-NCI/NCa. It was suggested that DOX/FA-NCI/NCa was internalized by the cells and localized in the acidic endosomes.

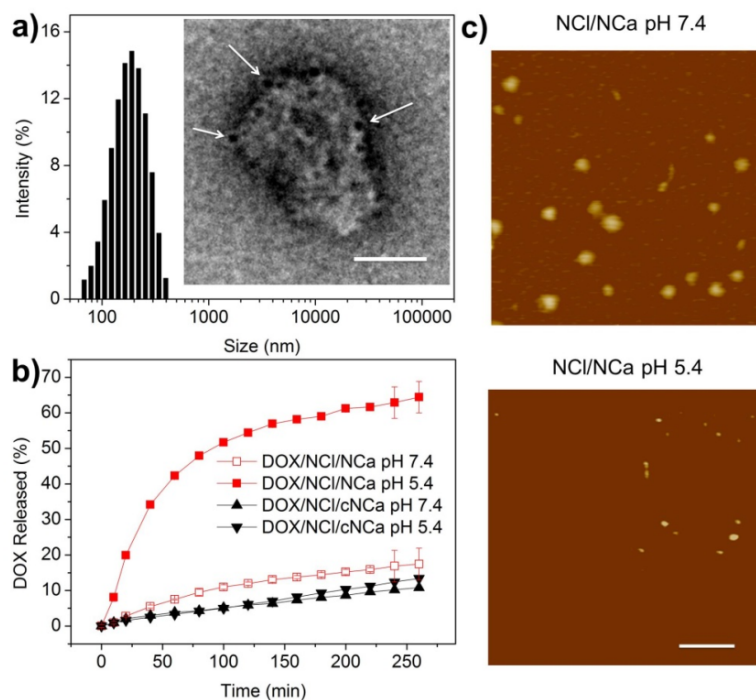


Figure 3-9. a). Hydrodynamic size of NCI/NCa. Inset: TEM image of NCI/Au-NCa. Scale bar is 100 nm. The arrows indicate Au-NCa adsorbed on NCI surface. b) DOX released from DOX/NCI/NCa and DOX/NCI/cNCa at pH 7.4 and pH 5.4. Bars represent mean \pm SD (n = 3). c) AFM images of NCI/NCa after incubation at pH 7.4 and pH 5.4 for 2 h. Scale bar is 500 nm.

Intracellular distribution of DOX/FA-NCI/NCa was then detected (Figure 3-10b, S3-11). The internalization and nucleus targeting of DOX/FA-NCI/NCa in MCF-7 cells was

extremely fast even within the first 10 min to 0.5 h, during which period obvious endo-lysosomal entrapment of DOX and nucleus-targeting of DOX could be observed. Co-localization of DOX/FA-NCl with NCa in MCF-7 cells was also observed (Figure 3-12). In the first 10 min, DOX/FA-NCl/AF488-NCa was internalized together. The fluorescence signals of DOX and AF488 showed a high co-localization. After 0.5 h, a large amount of DOX was released from the DOX/FA-NCl/AF488-NCa into the cytosol and specifically accumulated into the nucleus. Such rapid cytosolic distribution and nucleus-targeting effects of DOX delivered by DOX/FA-NCl/NCa were attributed to the efficient degradation of DOX/FA-NCl by NCa to promote the release of DOX.

3.3. *In vitro* anticancer efficacy

The *in vitro* cytotoxicity of DOX/NCl, DOX/NCl/NCa and DOX/FA-NCl/NCa against MCF-7 cells were estimated (Figure 3-10c). DOX/NCl/NCa showed a remarkably higher cytotoxicity toward MCF-7 cells than DOX/NCl. The half-maximal inhibitory concentration (IC₅₀) of DOX/NCl/NCa was calculated to be 1.2 μ M, noticeably lower than 2.3 μ M of DOX/NCl. It verified that the NCa-mediated DOX release increased the toxicity of DOX delivered by NCl. This was further validated by the significantly higher cytotoxicity toward MCF-7 treated with DOX/NCl/NCa than that associated with DOX/NCl/cNCa (Figure 3-13). Additionally, the conjugation of FA onto the NCl surface enhanced the therapeutic efficacy of DOX (Figure 3-10c). DOX/FA-NCl/NCa had the lowest IC₅₀ of 0.9 μ M compared with both DOX/NCl/NCa and DOX/NCl. The blank FA-NCl without DOX

showed negligible toxicity at any tested concentrations (Figure 3-10d). Of note, although DNase I, the component of the carrier in this research, has been used as an anticancer agent in some other studies,[582] the cytotoxicity of NCa towards MCF-7 at the selected concentration in this study was compromised compared to released DOX (Figure 3-10d).

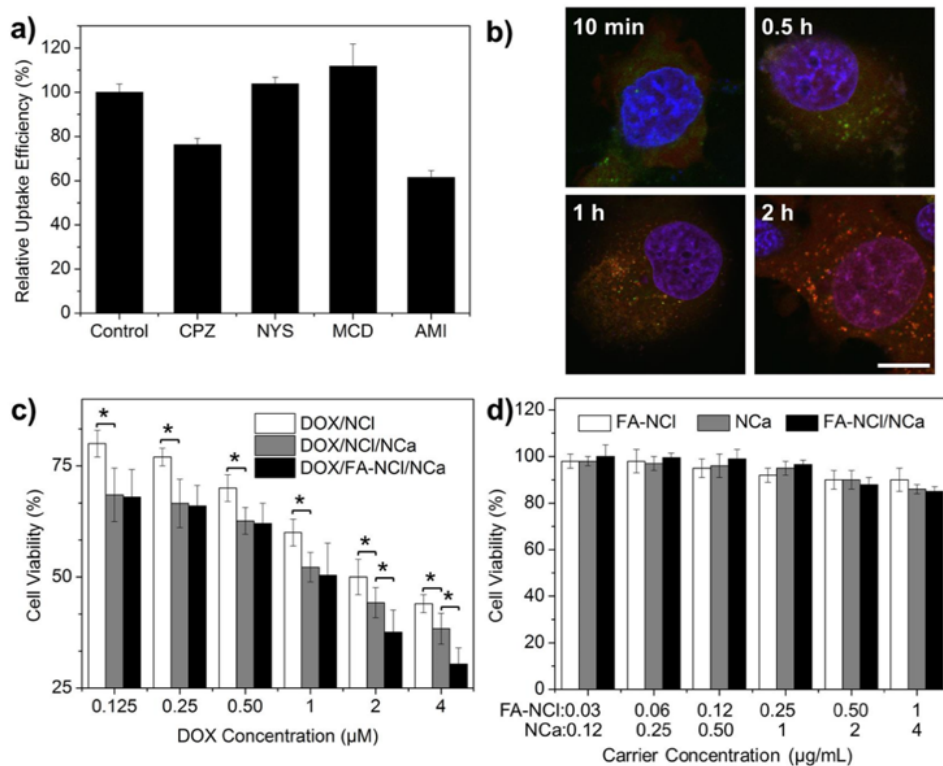


Figure 3-10. a) Relative uptake efficiency of DOX/FA-NCI/NCa by MCF-7 cells. *P < 0.05, **P < 0.01 compared with control. Bars represent mean ± SD (n = 3). b) CLSM images of MCF-7 cells after incubation with DOX/FA-NCI/NCa for different time. Late endosome and lysosomes were stained by LysoTracker green. Red: DOX; green: endo-lysosome; blue: Hoechst 33342; yellow: colocalization of red and green pixels; magenta: colocalization of red and blue pixels. Scale bars are 10 µm. c) *In vitro* cytotoxicity of DOX/NCI, DOX/NCI/NCa and DOX/FA-NCI/NCa against MCF-7 cells for 24 h. *P < 0.05. Bars represent mean ± SD (n = 6). d) *In vitro* cytotoxicity of the blank FA-NCI, NCa and FA-NCI/NCa against MCF-7 cells for 24 h. Bars represent mean ± SD (n = 6).

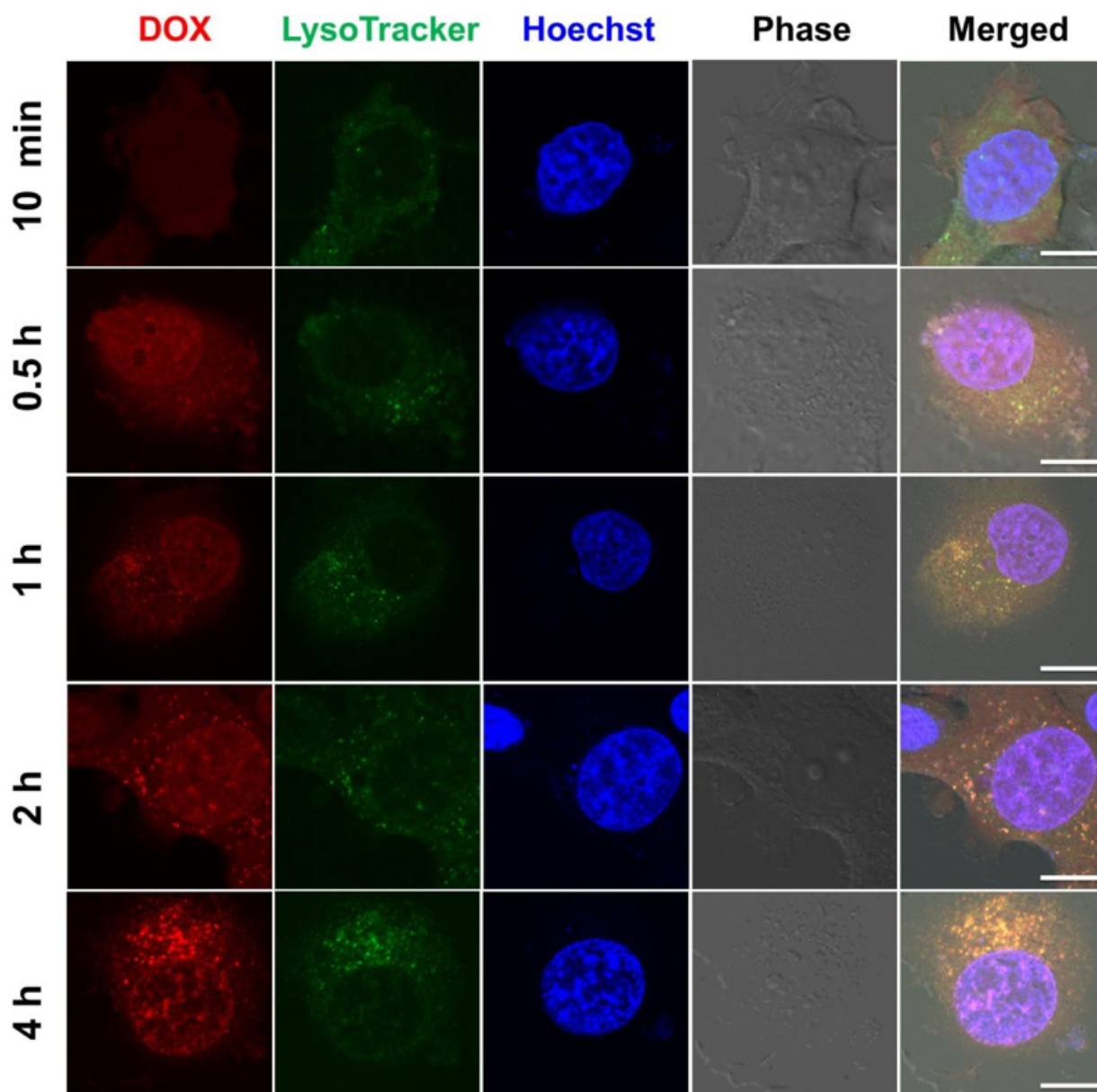


Figure S3-11. CLSM images of MCF-7 cells after incubation with DOX/FA-NCI/NCa for different time. The late endosome and lysosomes are stained with LysoTracker (green), while the nuclei were stained with Hoechst. Scale bars are 10 μ m.

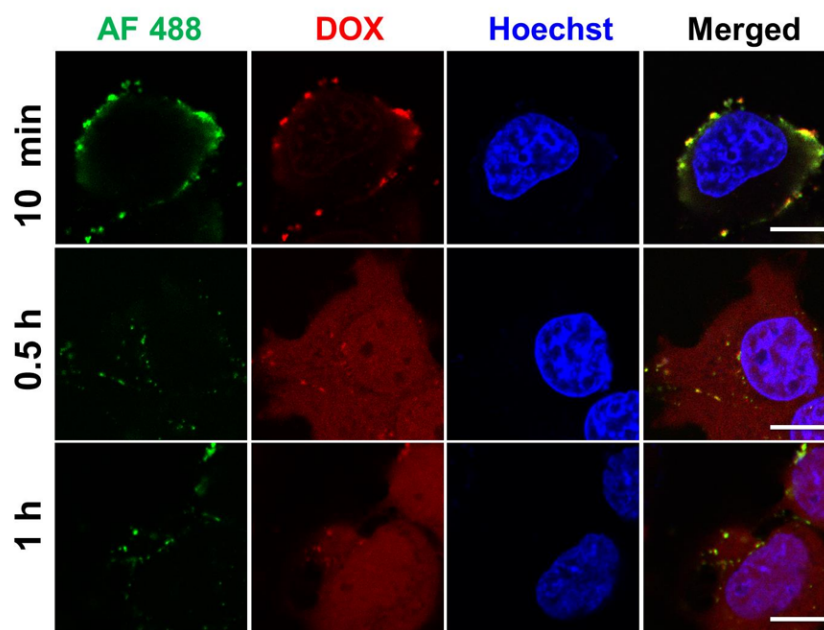


Figure S3-12. CLSM images of MCF-7 cells after incubation with DOX/FA-NCl/AF488-NCa for different time. The nuclei were stained with Hoechst. Scale bars are 10 μm.

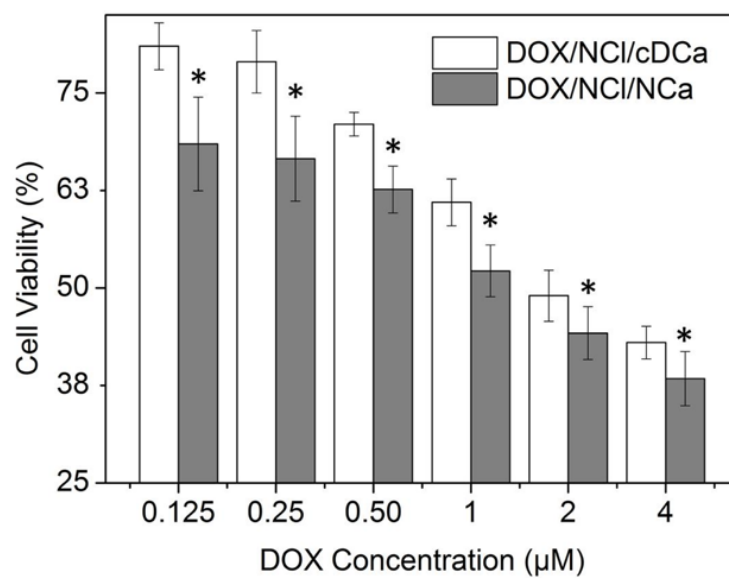


Figure 3-13. *In vitro* cytotoxicity of DOX/NCl/cNca and DOX/NCl/NCa against MCF-7 cells for 24 h. * $P < 0.05$. Bars represent mean \pm SD (n = 6).

4. Summary

In summary, we have developed a bio-inspired self-degradable drug delivery system consisting of a weaved DNA “nanoclew” as a “cocoon matrix” and a “caged” DNase I nanogel as “hibernating worms”. The “worms” can be readily activated to degrade their cocoon to release encapsulated drugs in the endo-lysosomal compartments. We will further evaluate *in vivo* anticancer efficacy and biocompatibility of this delivery system. Our unique strategy provides insights for designing new prodrugs and can be further extended to engineer other programmed drug delivery systems.

CHAPTER 4 EFFICIENT DELIVERY OF CRISPR-CAS9 FOR GENOME EDITING VIA SELF-ASSEMBLED DNA NANOCLEWS

1. Introduction

CRISPR-Cas9 has rapidly transitioned from an RNA-directed defense system in prokaryotes to a facile genome-editing technology.[583] The editing merely requires the Cas9 nuclease and an engineered single-guide RNA (sgRNA): the 20-nucleotide guide portion of the sgRNA recognizes complementary DNA sequences flanked by a protospacer-adjacent motif (PAM), and Cas9 cleaves the recognized DNA.[584] The double-stranded break is then repaired through non-homologous end joining (NHEJ) or homology-directed repair (HDR), allowing defined alterations to the targeted region.[585, 586]

As CRISPR-Cas9 systems undergo further development toward human therapeutics, delivery poses the major challenge. Cas9 and the sgRNA have been overwhelmingly encoded within the DNA of plasmids or viral vectors.[587, 588] However, this DNA can randomly integrate into the genome, potentially giving rise to cancer or other genetic diseases.[589] Furthermore, the template-driven nature of gene expression limits control over the total amount of Cas9 protein and sgRNAs, where excess dosing has been attributed to off-target cleavage.[590, 591] One alternative is to deliver the Cas9/sgRNA ribonucleoprotein complex,[592, 593] which enables greater control over its intracellular concentration and limits the timeframe in which editing can occur. However, delivering protein and RNA remains a central challenge in drug delivery.[43] Most protein therapeutics, such as

enzymes,[594] antibodies[595] or transcription factors,[596] suffer from low stability and poor cell membrane permeability as a result of their fragile tertiary structures and large molecular sizes.[43] The strong negative charges of RNA therapeutics, including siRNA or miRNA, blocks them from diffusing across cell membrane and their susceptibility to endonuclease often requires chemical modification to prevent degradation.[134] Thus, devising an appropriate carrier to shield the protein and RNA from detrimental physiological environment and escort them simultaneously to cell nucleus is highly desirable.

Herein, we report a novel delivery vehicle for CRISPR-Cas9 based on biologically inspired yarn-like DNA nanoclew (NC) (Figure 4-1). The DNA NCs are synthesized by rolling circle amplification (RCA)[537, 538, 597-600] with palindromic sequences encoded to drive the self-assembly of nanoparticles. We previously demonstrated that the DNA NC could encapsulate the chemotherapeutic agent DOX and drive its release based on environmental conditions.[98] Here, we hypothesized that the DNA NC can load and deliver the Cas9 protein together with an sgRNA for genome editing. Inspired by the ability of single stranded DNA (ssDNA) to base pair with the guide portion of the Cas9-bound sgRNA,[601] we designed the DNA NC to be partially complementary to the sgRNA. Following loading of the DNA NC with the Cas9/sgRNA complex, we applied a coating of the cationic polymer polyethylenimine (PEI) to help induce endosomal escape.[602] The Cas9/sgRNA complex delivered to the cytoplasm could then be transported into the nucleus via nuclear-localization-signal peptides fused to Cas9. We expected that the resulting delivery vehicle

could form uniform particles and drive the formation of targeted insertions or deletions (indels) without measurable impact on cell viability.

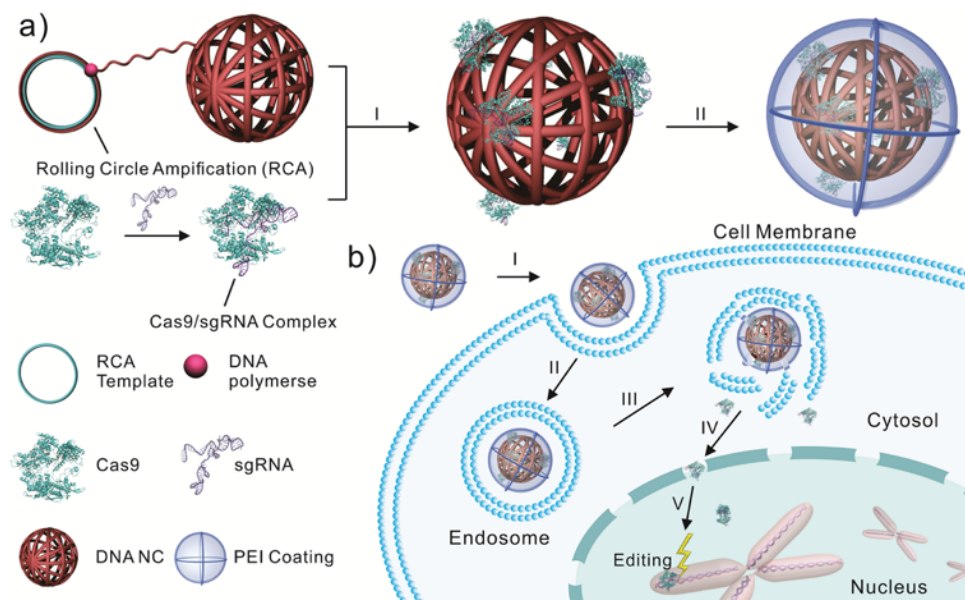


Figure 4-1. Schematic design of the DNA NC mediated CRISPR-Cas9 delivery system. (a) Preparation of Cas9/sgRNA/NC/PEI. I: The NC was synthesized by RCA and loaded with the Cas9/sgRNA complex through Watson-Crick base pairing; II: PEI was coated onto Cas9/sgRNA/NC for enhanced endosome escape. (b) Delivery of Cas9/sgRNA by the DNA NC based carrier to the nucleus of the cell for genome editing. I: Bind to cell membrane; II: Endocytosis; III: Endosome escape; IV; Transport into the nucleus; V: Search for target DNA locus in the chromosome and introduce double strand breaks for genome editing.

2. Materials and Methods

2.1. Materials

All Chemicals were purchased from Sigma-Aldrich (St. Louis, MO, USA) unless otherwise specified and were used as received. DNA oligonucleotides were purchased from

Integrated DNA Technologies Inc. (Coralville, IA, USA). AmpliScribe™ T7-Flash™ Transcription Kit and CircLigase II ssDNA Ligase was purchased from Epicenter (Madison, WI, USA). Bst 2.0 DNA polymerase and PvuI were purchased from New England BioLabs Inc. (Ipswich, MA, USA). Plasmids pCAG-T3-hCAS-pA encoding the Cas9 protein (Addgene No. 48625) and pCAG-GFP encoding EGFP (Addgene No. 11150) were purchased from Addgene (Cambridge, MA, USA). Linear polyethyleneimine (PEI) “max” (M.W. 40,000) was purchased from Polysciences Inc. (Warrington, PA, USA).

2.2. Clone, expression and purification of Cas9 protein.

The human codon optimized *S. pyogenes* Cas9 gene with two nuclear localization sequences (NLS) at the N- and C- termini (Addgene 48625) was amplified and sub-cloned into pET-28a vector (Novagen) with primers Cas9-F/Cas9-R (Table S4-1), adding a N-terminal His₆-tag to the expressed Cas9. *E. coli* Rosetta (DE3) pLysS cells was transformed with pET28a-Cas9 and cultured for Cas9 expression. Briefly, a fresh *E. coli* colony was inoculated into 5 mL LB medium (supplemented with 10 μg/mL kanamycin and 34 μg/mL chloromycetin) and cultured at 37 °C overnight. The cell culture was then diluted with fresh LB medium by 100-fold and continued to culture for another 2-3 h until the OD₆₀₀ reached 0.6-0.8. 0.5 mM isopropyl β -D-1-thiogalactopy- ranoside (IPTG) was added to induce Cas9 expression at 20 °C for 8 h. The cells were then collected by centrifugation (4000 ×g, 15 min), suspended in Buffer A (20 mM Tris-HCl pH 8.0, 0.5 M NaCl, 10 mM imidazole and 1 mM PMSF) and lysed by sonication. Cell debris was removed by centrifugation (20000×g,

115

20 min) and the clear lysate was added to a column containing 1 mL Ni-NTA resin (Qiagen). After washing the column with Buffer B (20 mM Tris-HCl pH 8.0, 0.5 M NaCl and 60 mM imidazole), Cas9 was eluted with Buffer C (20 mM Tris-HCl pH 8.0, 0.5 M NaCl and 500 mM imidazole) and dialyzed against Buffer D (20 mM HEPES pH 7.4, 150 mM KCl, 1 mM DTT and 10% glycerol) at 4 °C overnight. The purified Cas9 was quantified by Bradford assay (Bio-Rad) and analyzed by SDS-PAGE.

2.3. Transcription and purification of single-guide RNA (gRNA).

The sgRNA was transcribed *in vitro* with AmpliScribe™ T7-Flash™ Transcription Kit (Epicentre) according to manufacturer's instructions. Transcription templates encoding a T7 promoter followed by the sgRNA were synthesized by IDT with the sgRNA containing a 20 bp EGFP targeting sequence and a control guiding RNA (cgRNA) that does not target EGFP or any genes in human genome (Table 4-1). The transcribed RNA was extracted by phenol:chloroform:IAA (Ambion) with Phase Lock Gel (5 Prime) to separate the RNA containing water phase. After removing unincorporated nucleotide with illustra Microspin G-50 columns (GE Healthcare), the RNA was ethanol precipitated and re-suspended in DEPC treated water. Purified RNA was analyzed by agarose gel electrophoresis and quantified with Nanodrop 2000c (Thermo Scientific).

2.4. Plasmid DNA cleavage assay to detect Cas9 activity.

Plasmid pCAG-GFP containing the EGFP gene (Addgene 11150) was linearized with PvuI (NEB), purified by GeneJET Gel Extraction Kit (Thermal Scientific) and used as the substrate for Cas9 activity assay. In a reaction volume of 20 μ l containing NEBuffer 3 and linearized plasmid (300 ng), purified Cas9 (50 nM) and sgRNA (50 nM) were added. After digestion for 1 h at 37 °C, the DNA was analyzed by 0.8% agarose gel electrophoresis.

2.5. Preparation and characterization of DNA NC.

The DNA NCs were prepared by RCA using cyclized single stranded DNA (ssDNA) templates. 5' phosphorylated linear ssDNA templates (Table 4-1) were cyclized by CircLigase II ssDNA ligase (Epicentre) following manufacture's instructions. Unligated ssDNA chains were removed with 1U Exo I (NEB) at 37°C for 45 min followed by heat inactivation at 80°C for 15 min. The cyclized ssDNA template (10 pmol) was added into 1 mL 1 \times isothermal amplification buffer (NEB) together with 0.5 μ M primer and 200 μ M dNTP and heated to 95°C for 5 min. After hybridizing the template and primer by cooling the mixture to room temperature, Bst 2.0 DNA polymerase (0.2 U/ μ L) was added to initiate the RCA. The RCA was performed at 65°C overnight and the denatured polymerase after the reaction was removed by centrifugation at 14,000 \times g for 2 min. The supernatant was recovered and dialyzed against DI water using a Slide-A-Lyzer (20K MWCO, Thermo Scientific) for 48 h. The synthesized DNA NCs were analyzed by 0.8% agarose gel

electrophoresis and .Nanodrop 2000C (Thermal Scientific) was applied to measure the concentration and purity of the DNA NC. NC with high purity ($A_{260}/A_{280} > 1.8$) was used for further studies. To evaluate the stability of NC, 300 ng NC was incubated with Cas9 (50 nM) and gRNA (50 nM) in NEBuffer 3 at 37°C for 24 h and then analyzed using 0.8% agarose gel electrophoresis. Zeta potential and particle size of NC were measured with a Zetasizer (Malvern). To image the NC by atomic force microscopy (AFM), the NC was dropped and dried onto a silicon wafer (Ted Pella) and analyzed on a Nanoscope AFM instrument (Veeco, Santa Barbara, CA) using tapping mode in ambient air.

2.6. Assembly and characterization of Cas9/sgRNA/NC/PEI.

Purified Cas9 and sgRNA at various molar ratios (4:1 – 0.5:1) were mixed in PBS and incubated at room temperature for 5 min, followed by the addition of DNA NC (NC:sgRNA weight ratio of 4:1) and incubated at room temperature for another 5 min. Afterwards, PEI “max” (Polysciences) was coated onto Cas9/sgRNA/NC at PEI:sgRNA weight ratio of 5:1 and equilibrated at room temperature for 5 min. The assemblies were further diluted to the concentration of sgRNA at 100 nM in deionized water for particle characterization or Opti-MEM medium (Life Technologies) for cell study. Size and zeta potential of Cas9/gRNA/NC/PEI were analyzed by a Zetasizer (Nano ZS, Malvern). AFM imaging was performed using a Nanoscope (Veeco, Santa Barbara, CA) on silicon wafer (Ted Pella) as described above. For TEM imaging, the Cas9/sgRNA/NC/PEI was dropped onto a TEM copper grid (300 mesh, Ted Pella) and stained with 2% uranyl acetate (w/v, in

50% ethanol). TEM images were observed on a JEM-2000FX (Hitachi) at 200 kV. The assembly was also visualized with confocal laser scanning microscope (CLSM, LSM 710, Zeiss) to confirm the colocalization of the components. Cas9 was conjugated with Alexa Fluor 647 C2 maleimide (AF647), PEI was conjugated with FITC NHS ester (Life Technologies) and the NC was stained with Hoechst 33342, a nucleic acid dye that stains only DNA but not RNA.

2.7. Cell culture and EGFP gene disruption assay.

The reporter cell line U2OS.EGFP with a single copy of destabilized EGFP gene integrated into the genome was a generous gift from Dr. J Keith Joung at Massachusetts General Hospital. The cells were cultured in a 37 °C incubator under 5% CO₂ and 90% humidity with full serum medium: Dulbecco's Modified Eagle's Medium supplemented with 10% (v/v) FBS, 2 mM GlutaMAX (Life Technologies), penicillin (100 U/mL) and streptomycin (100 µg/mL). U2OS.EGFP cells were seeded into 24-well plates (~25,000 cells per well) one day before the transfection. When the cells reached 70% confluence, the medium was replaced with 0.5 mL Opti-MEM medium (Life Technologies) containing the Cas9/gRNA loaded nanoparticles (gRNA concentration at 100 nM). After incubation for 4h, the Cas9 containing medium was replaced with fresh full serum medium. Two days after the delivery, the cells were analyzed using a fluorescent microscope (IX71, Olympus). For the flow cytometry analysis, the cells were washed with ice cold PBS twice and trypsinized with 0.05 % trypsin (Mediatech) at 37 °C for 1-2 min. Afterwards, the cells were washed and

resuspended in full serum medium and analyzed by a BD Accuri C6 flow cytometer (BD Biosciences).

2.8. SURVEYOR assay to detect genomic modifications.

Genomic DNA of U2OS.EGFP cells was harvested 2 d after the delivery using GeneJET Genomic DNA Purification Kit (Thermo Scientific) according to manufacturer's instructions. The gRNA targeted genomic locus was amplified with Phusion Hot Start II High Fidelity DNA Polymerase (NEB) using primers T7EI-F/T7EI-R (Table 4-1). Touchdown PCR program ((98°C for 10 s; 66-56°C with -1 °C/cycle for 15s, 72°C for 60 s) for 10 cycles and (98°C for 10 s, 56°C for 15 s, 72 °C for 60 s) for 25 cycles) was used to reduce non-specific amplifications. The amplicons were then purified by gel extraction and 200 ng of the purified DNA was added to 20- μ L cleavage reaction containing 1 \times NEBuffer 2. After heating to 95°C for 5 min, the mixture was cooled to form heteroduplex DNA. Afterwards, 1 μ L T7EI (10 U/ μ l, NEB) was added and incubated at 7 °C for 15 min. The digested DNA was analyzed using 2% agarose gel electrophoresis. Indel formation efficiencies were calculated using Image J.

2.9. DNA sequencing to detect genomic mutations.

Purified PCR amplicons of the T7EI assay were cloned into Zero Blunt TOPO DNA sequencing vectors (Life Technologies). The cloned plasmids were purified by GeneJET

Plasmid Miniprep Kit (Thermo Scientific) and sequenced by Eton Bioscience Inc. (RTP, NC, USA) with T7 promoter primer.

2.10. Determination of endocytosis pathways.

Cas9 was fluorescently labeled with AF647 to track its uptake. U2OS.EGFP cells were seeded in 24-well plates (~25000 cells/well) and cultured for 2 d. Then the cells were pre-incubated with several endocytosis inhibitors, such as chlorpromazine (CPZ, 10 μ M) for clathrin-mediated endocytosis, nystatin (NYS, 25 μ g/mL) for caveolin-mediated endocytosis, methyl- β -cyclodextrin (MCD, 3 mM) for lipid raft and amiloride (AMI, 1 mM) for macropinocytosis, for 1h at 37 °C, respectively. Afterwards, the cells were incubated with AF647-Cas9/sgRNA/NC/PEI for another 2 h in the presence of the inhibitors. Cells were then washed, trypsinized and resuspended in full serum medium, intracellular AF647 fluorescence intensities were analyzed by flow cytometry.

2.11. Intracellular distribution of Cas9.

U2OS.EGFP cells were seeded in confocal dishes (MatTek) at a density of 1×10^5 per well and cultured for 24 h. To image the nuclear accumulation of Cas9, the cells were incubated with AF647-Cas9/sgRNA/NC/PEI for 1 h, 2 h, 4h and 6 h. After washing with 4 ° C PBS twice, the cells were stained with Hoechst 33342 (1 μ g/mL) for 10 min. Washed with cold PBS twice again, the cells were observed with CLSM immediately.

2.12. *In vitro* cytotoxicity.

U2OS.EGFP cells delivered with Cas9 were analyzed for cell survival using flow cytometry with TO-PRO-3 live/dead cell stain (Life Technologies).[592] Briefly, the U2OS.EGFP cells were seeded in 24-well plates (~25000 cells/well) and cultured for 24 h. Then the cells were exposed to Cas9/sgRNA/NC-12/PEI and Cas9/sgRNA/PEI at different Cas9 concentrations for 4 h. Afterwards, the cells were washed with PBS and stained with TO-PRO-3 live/dead cell stain (1 μ M) for 15 min. Washed, trypsinized and resuspended, the cells were then analyzed by flow cytometry.

2.13. *In vivo* EGFP disruption.

All animal experiments were conducted according to the Guide for Care and Use of Laboratory Animals approved by the Institutional Animal Care and Use Committee (IACUC) of University of North Carolina at Chapel Hill and North Carolina State University. To set up the U2OS.EGFP tumor model, the female nude mice (6 weeks, J:NU, The Jackson Laboratory) were subcutaneously inoculated with 1×10^7 U2OS.EGFP cells. One mouse was inoculated with one tumor and when the volume of the tumors reached 200 - 400 mm³, the mice were intratumorally injected with 50 μ L of the ~ 56 nm nanoparticles (Cas9/sgRNA/NC-12/PEI or Cas9/cgRNA/NC-12/PEI) in PBS (Cas9 concentration at 5 μ M). At day 10, the mice were euthanized and the tumors were collected, washed by saline thrice and followed by fixation in the 10% neutral buffered formalin. Tumor tissues within 5 mm of distance from the point of injections were sectioned. Cas9-mediated EGFP disruptions were

visualized by staining the tumor sections with FITC conjugated GFP antibody (Thermo Scientific) and the nuclei were counterstained with Hoechst 33342. The stained slides were observed with CLSM.

2.14. Statistics.

All results were presented as Mean \pm SD. Statistical analysis was performed using two-tailed student's t-test. The difference between experimental groups and control groups were considered statistically significant when $p < 0.05$ or highly significant when $p < 0.01$.

3. Results and Discussion

3.1. Preparation of Cas9 protein and sgRNA.

To demonstrate the DNA NC-mediated delivery of CRISPR-Cas9, we first selected the well-characterized and most extensively applied *Streptococcus pyogenes* Cas9.[603] Recombinant Cas9 fused with N-terminal and C-terminal nuclear localization signals[604] was purified following overexpression in *Escherichia coli* (Figure 4-2) and incubated with one of two sgRNAs: one designed to target a sequence within the enhanced green fluorescent protein (EGFP) gene flanked by an NGG PAM, and the other control sgRNA (cgRNA) designed not to appreciably target any DNA sequence in EGFP or the human genome (Figure 4-3a). We confirmed that the resulting Cas9/sgRNA complex was active *in vitro* based on

cleavage of a linearized plasmid encoding the EGFP gene, but only in the presence of Cas9 and the EGFP-targeting sgRNA (Figure 4-3b).

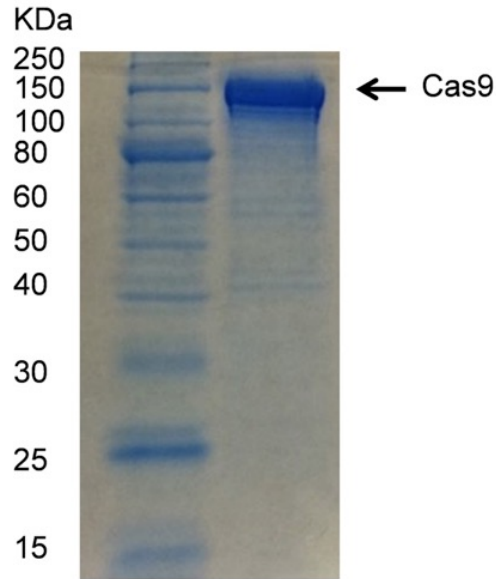


Figure 4-2. SDS-PAGE (12%) of purified Cas9. The purified Cas9 showed molecular weight of ~160 KDa.

Table 4-1. Sequences of DNA oligos

		Sequences	Notes
Cas9 Clone	Cas9-F	5'GCAAATGGGTCGCGGATCCCCAAAGAAGAAGCGG3'	<u>BamH</u>
Primer	Cas9-R	5'CGAGTGCGGCCGCAAGCTTTCACACCTTCCTC3'	<u>HindIII</u>
RNA	sgRNA	5' <u>GTTTTTTTTAATACGACTCACTATA</u> GGGCACGGGCA	<u>T7 Promoter</u>
Transcription Template		GCTTGCCGG GTTTTAGAGCTAGAAATAGCAAGTTAAAAT	GFP Targeting
		AAGGCTAGTCCGTTATCAACTTGAAAAAGTGGCACCGA	Non-Targeting
		GTCGGTGCTTTTTTTT3'	Sequence
	cgRNA	5' <u>GTTTTTTTTAATACGACTCACTATA</u> GGGTAACCGTG CGGTCGTAC GTTTTAGAGCTAGAAATAGCAAGTTAAAAT	

Table 4-1 continued

		AAGGCTAGTCCGTTATCAACTTGAAAAAGTGGCACCGA	
		GTCGGTGCTTTTTTT3'	
RCA	NC-23	5'PO ₄ GGGCACGGGCAGCTTGCCGGTGGAAAGCTAGATGC	gRNA Binding
Template		ATCTAGCAAGCGCCGCCACTGATTCACCGCTTCAAGCT	PAM
		AGATGCATCTAGCAAT3'	Palindromic
	NC-12	5'PO ₄ GCTACCGGGCAGCTTGCAATCAATAAGCTAGATGCA	Sequence
		TCTAGCAAAGCGCCGCCACTGATTCACCGCTTCAAGCT	NC Primer Binding
		AGATGCATCTAGCAAT3'	
	NC-0	5'PO ₄ GAGAAACGAGTGCGGTCACAGCTAAGCTAGATGC	
		ATCTAGCAAGCGCCGCCACTGATTCACCGCTTCAAGCT	
		AGATGCATCTAGCAAT3'	
RCA Primer	NC-F	5'GTGGCGGCGC3'	
SURVEYOR	T7EI-F	5'GGAGTTCCGCGTTACATAACTTACG3'	
assay primer	T7EI-R	5'AACCTCGACTAAACACATGTAAAGCATG3'	

3.2. Characterization of the nanoassembly.

We next generated the DNA NC to bind the Cas9/sgRNA complex. The DNA template for RCA was designed to encode 12 nucleotides complementary to the 5' end of the sgRNA (NC-12) along with the palindromic repeat that drives self-assembly (Table 4-1). The rationale was that the complementary sequence would promote base pairing between the DNA NC and the Cas9/sgRNA complex, thereby forming a strong but reversible interaction. To form the nanoparticle consisting of Cas9, sgRNA, NC-12, and PEI (Cas9/sgRNA/NC-

12/PEI), Cas9 and the sgRNA were incubated together, followed by the addition of the NC-12, and then the addition of PEI. Measuring the zeta potential at each assembly step showed that the positively charged Cas9 ($+19.3 \pm 3.8$ mV) became negatively charged with the addition of sgRNA (-19.4 ± 3.7 mV) and then NC-12 (-28.6 ± 5 mV), which was reverted to positive charge upon the addition of PEI ($+18.6 \pm 4.1$ mV) (Figure 4-4a, 4-5). Dynamic light scattering analysis (Figure 4-4b, 4-5), atomic force microscopy (Figure 4-4c, 4-6) and transmission electron microscopy (Figure 4-4d) revealed that the Cas9/sgRNA/NC-12/PEI nanoparticles were uniformly sized with a hydrodynamic size of ~ 56 nm. Interestingly, the fully assembled particle was more compact and uniformly sized than the NC-12 nanoclew and the Cas9/sgRNA/NC-12 complex, potentially due to offsetting the dispersing charges. To assess the co-localization of each component, we applied confocal laser scanning microscopy (CLSM) to image nanoparticles comprised of Cas9 labeled with Alexa Fluor 647 (AF647), the sgRNA, the NC-12 stained with Hoechst 33342, and PEI conjugated with FITC. Imaging revealed consistent co-localization of all dyes (Figure 4-7), confirming the stable assembly of Cas9/sgRNA/NC-12/PEI.

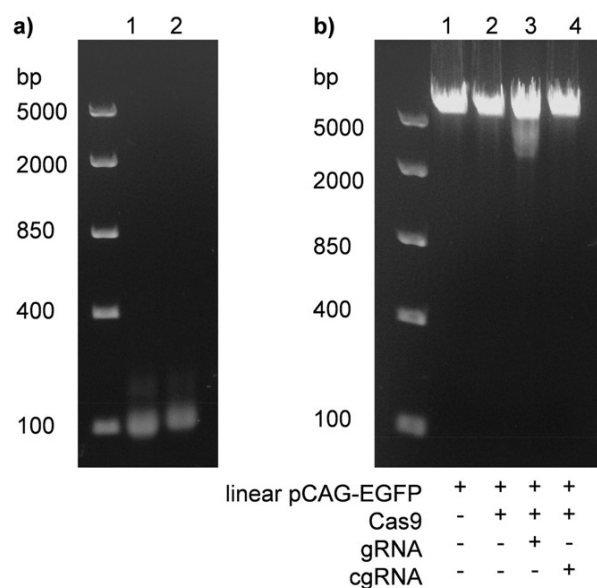


Figure 4-3. a) Agarose gel electrophoresis (0.8%) of purified sgRNA (lane 1) and cgRNA (lane 2). b) Cas9 activity assay using linearized plasmid pCAG-EGFP (5556 bp) as substrate. Only Cas9 complexed with sgRNA can digest the plasmid DNA.

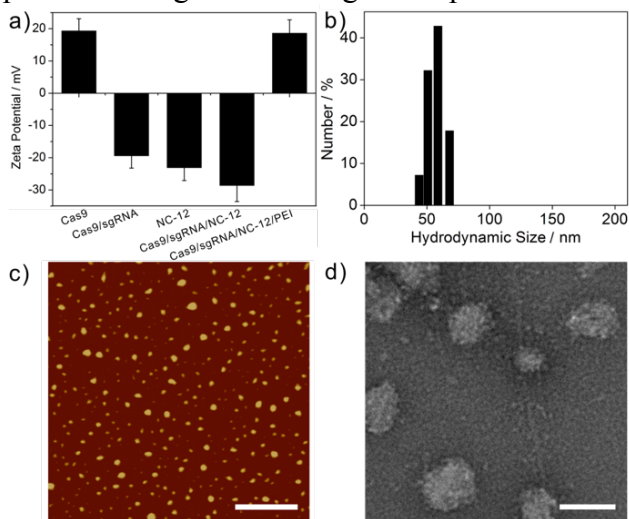


Figure 4-4. Particle characterization of Cas9/sgrNA/NC-12/PEI. (a) Monitoring zeta potential of the Cas9/sgrNA/NC-12/PEI assembly process. Bars represent mean \pm SD (n = 3). (b) Hydrodynamic size distribution of Cas9/sgrNA/NC-12/PEI. (c) AFM image and d) TEM image of Cas9/sgrNA/NC-12/PEI with scale bars of 400 nm and 100 nm, respectively.

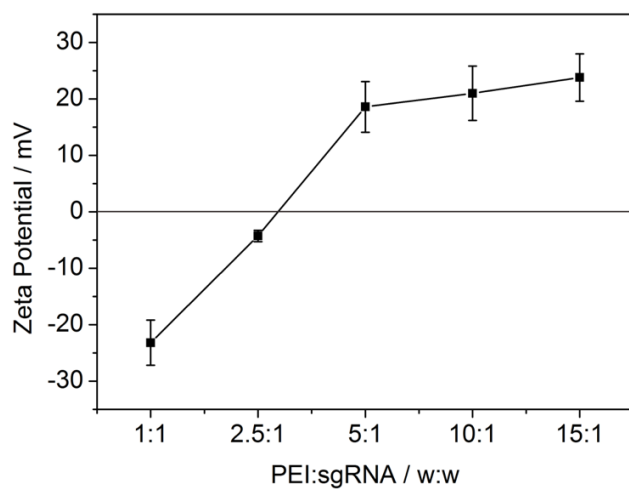


Figure 4-5. Optimization of PEI concentration for coating Cas9/sgRNA/NC-12 by measuring the zeta potential.

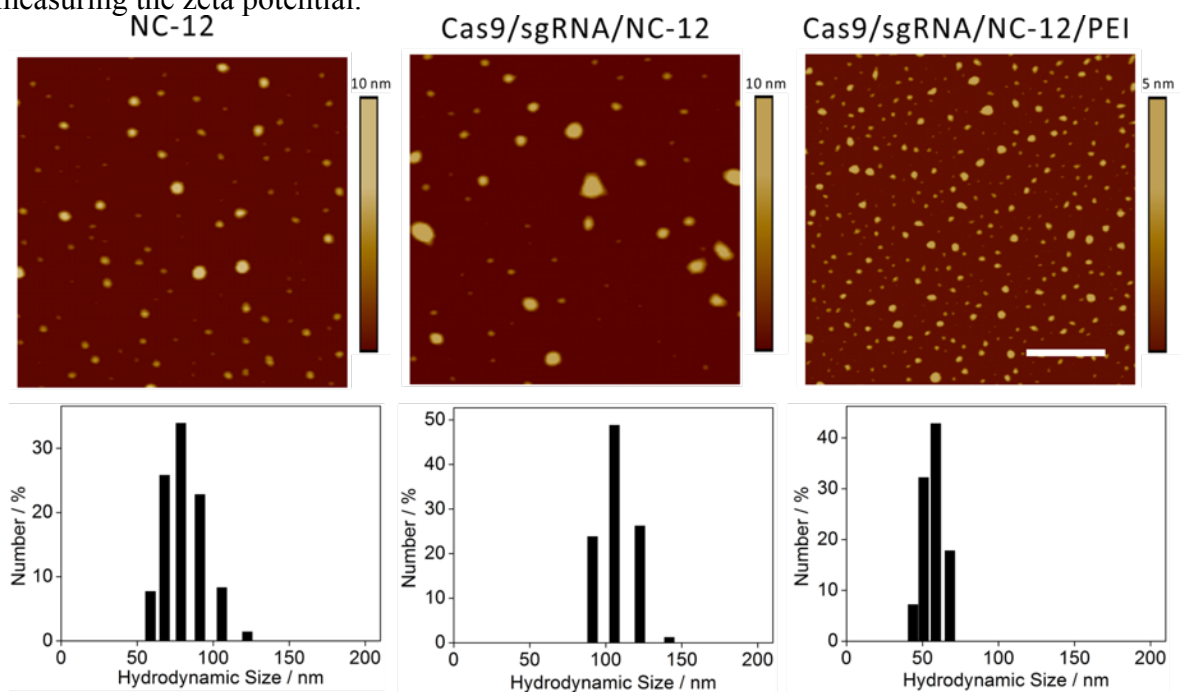


Figure 4-6. Hydrodynamic size distributions and AFM images of NC-12, Cas9/sgRNA/NC-12 and Cas9/sgRNA/NC-12/PEI. Scale bar 400 nm.



Figure 4-7. CLSM images of Cas9/sgRNA/NC-12/PEI assembly. Red for Cas9 stained with AF647, blue for NC-12 stained with Hoechst 33342 and green for PEI labeled with FITC. Scale bar is 20 μm .

3.3. Uptake and intracellular trafficking of delivered Cas9/sgRNA.

We further investigated the ability of the particles to deliver Cas9/sgRNA into cultured cells. As a model, we used an established U2OS cell line that constitutively expresses a destabilized form of EGFP (U2OS.EGFP).[591] CLSM, a technique with depth selectivity for analyzing subcellular location of delivered drugs,[98, 456, 605] was first applied to evaluate the localization of the Cas9/sgRNA/NC-12/PEI nanoparticles containing the AF647-labeled Cas9 (Figure 4-8a, 4-9). Over the course of six hours, the labeled Cas9 first binds to the cell surface, then enters the cytosol, and finally localizes to the nuclei as indicated by the colocalization of the red fluorescence signal from AF647-Cas9 with the blue fluorescent signal of stained nuclei. To elucidate the mechanism of internalization, we applied inhibitors of different endocytosis pathways[456] and measured the relative uptake of the Cas9/sgRNA/NC-12/PEI nanoparticles containing AF647-labeled Cas9. Flow cytometry analysis revealed that the inhibitors methyl- β -cyclodextrin (MCD) and amiloride (AMI)

imparted the greatest reduction in Cas9 uptake (Figure 4-8b), suggesting that the particles were mainly internalized through lipid rafts and macropinocytosis.[456] Furthermore, we evaluated the impact of the nanoparticles on cell viability. TO-PRO-3 live/dead assay[592] demonstrated no measurable impact on viability even at high concentrations (200 nM) of Cas9 (Figure 4-8c).

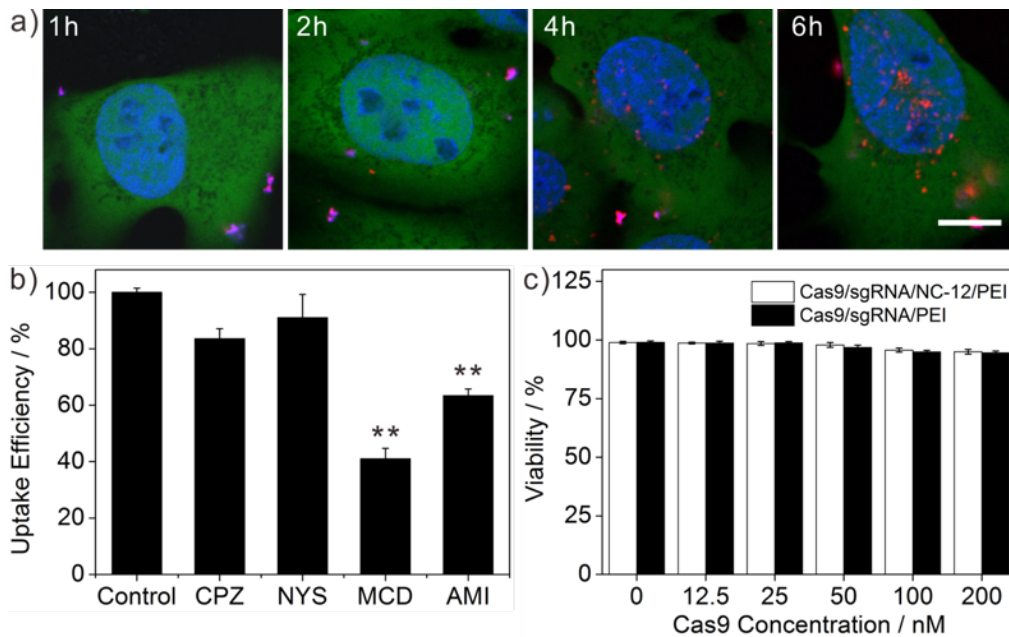


Figure 4-8. a) CLSM images of U2OS.EGFP cells incubated with Cas9/sgRNA/NC-12/PEI for 1 h, 2 h, 4 h and 6 h (Cas9 and sgRNA concentrations at 100 nM). Green for EGFP, red for Cas9 stained with AF647 and blue for nuclei stained with Hoechst 33342. Scale bar is 10 μm. b) Relative Cas9/sgRNA/NC-12/PEI uptake by U2OS.EGFP cells in the presence of different endocytosis inhibitors (Cas9 and sgRNA concentrations at 100 nM). ** $P < 0.01$ as compared to the control group. Bars represent mean \pm SD (n = 3). c) *In vitro* cell viability of U2OS.EGFP cells treated with Cas9/sgRNA/NC-12/PEI and Cas9/sgRNA/PEI by flow cytometry. The cells were stained with TO-PRO-3 live/dead stain after the treatment and analyzed by flow cytometry. Bars represent mean \pm SD (n = 3).

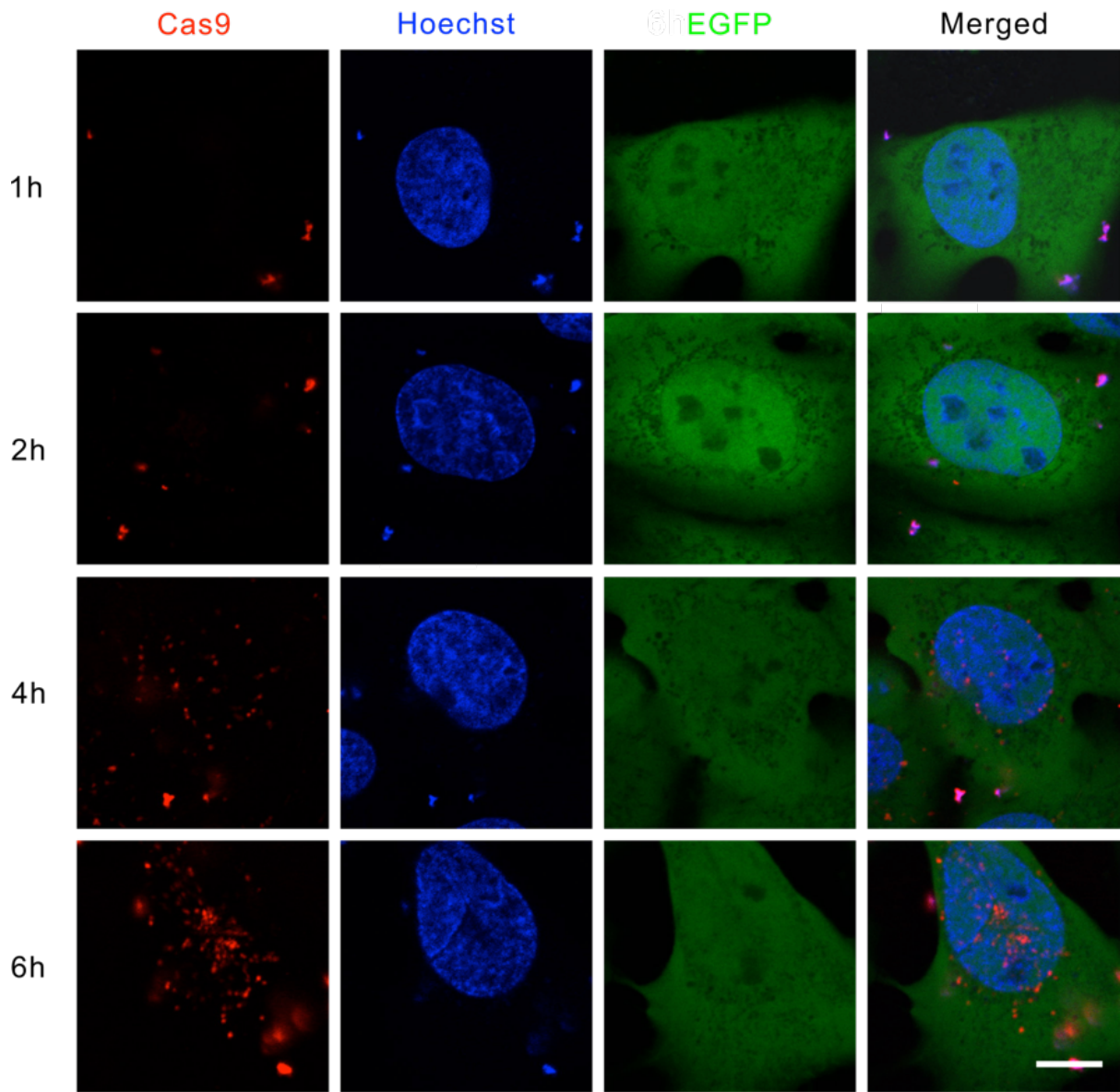


Figure 4-9. Confocal laser scanning microscopy images of U2OS.EGFP cells incubated with Cas9/sgRNA/NC-12/PEI for 1 h, 2 h, 4 h and 6 h (Cas9 and sgRNA concentrations at 100 nM).

3.4. Gene editing in the U2OS-EGFP reporter cell line.

Based on the evidence that the Cas9/sgRNA would reach cell nucleus, we next evaluated the extent to which Cas9/sgRNA could drive the formation of indels through targeted DNA cleavage and repair by the endogenous NHEJ pathway. By targeting the coding region of EGFP, most indels would shift the reading frame, thereby preventing proper EGFP expression. To evaluate the impact on EGFP expression, we incubated cells with the particles containing the EGFP-targeting sgRNA (Cas9/sgRNA/NC-12/PEI, Figure 4-10a) or the non-targeting cgRNA (Cas9/cgRNA/NC-12/PEI, Figure 4-11). Fluorescence microscopy and flow cytometry analysis revealed that the sgRNA reduced fluorescence in ~36% of the cells, whereas the cgRNA had a negligible effect in comparison to untreated cells. We also evaluated particles prepared with only Cas9, sgRNA, and PEI; these particles reduced fluorescence in only 5% of the cells, demonstrating the importance of the DNA NC for effective delivery. To assess whether the reduction in fluorescence was attributed to indel formation, we applied the SURVEYOR assay that quantifies the frequency of mutations within an amplified target region.[585, 586] The assay revealed mutation frequencies of 28% and 1.5% for cells treated with Cas9/sgRNA/NC-12/PEI and Cas9/sgRNA/PEI (Figure 4-10b), respectively, closely paralleling the flow cytometry analysis. We also subcloned the amplified target region of cells incubated with the Cas9/sgRNA/NC-12/PEI nanoparticles. Sanger sequencing of 20 clones revealed 7 clones with typical indels within the PAM or the sequence complementary to the sgRNA guide (Figure 4-12), confirming the genetic disruption of EGFP expression by CRISPR-Cas9.[585, 586] One-time treatment with the

DNA NC mediated Cas9/sgRNA delivery system lead to higher editing efficacy than the cell-penetrating peptides (CPPs) based vector (9.7%) if the variation of cell line and targeted locus were not taken into account.[593] Although the cationic lipid/anionic EGFP based delivery strategy showed higher editing efficacy (80%),[592] lipid-vehicles are often hampered by serum instability, which could be alleviated by polymer-based carriers.[43, 298]

Then we asked how complementarity between the DNA NC and the sgRNA impacted the efficacy of Cas9-driven genome editing. To address this, we generated two additional variants of the DNA NC with 0 or 23 nucleotides complementary to the sgRNA (designated as NC-0 and NC-23, respectively). Agarose gel electrophoresis confirmed that NC-0 and NC-23 yielded similar molecular weight distributions as NC-12 and were resistant to Cas9/sgRNA degradation (Figure 4-13). Subjecting the resulting particles to the U2OS.EGFP cells revealed that NC-12 yielded the highest fraction of EGFP negative cells (Figure 4-10c). This trend was upheld for different molar ratios of Cas9 and the sgRNA, where the 1:1 standard stoichiometry of the Cas9/sgRNA complex yielded the greatest activity. Altogether, these results suggest that partial complementarity between the sgRNA and the NC are important for efficient delivery, which may be attributed to the need for balancing Cas9/sgRNA loading and release.

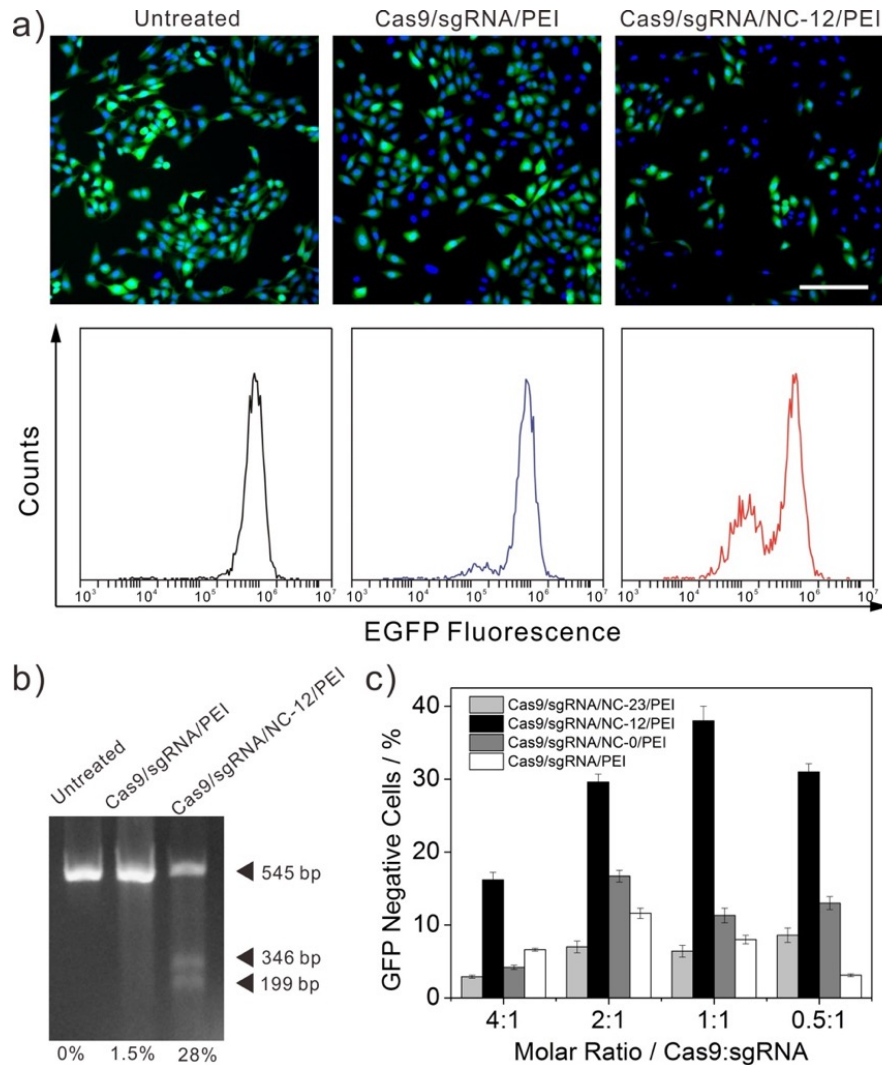


Figure 4-10. Genome editing by Cas9/sgRNA delivered by DNA NC (8 $\mu\text{g}/\text{mL}$) coated with PEI (10 $\mu\text{g}/\text{mL}$). a) Fluorescent microscope images and flow cytometry analysis of U2OS.EGFP cells treated with Cas9/sgRNA/PEI and Cas9/sgRNA/NC-12/PEI (Cas9 and sgRNA concentrations at 100 nM). Green represents EGFP and blue represents nuclei stained with Hoechst 33342. Scale bar is 100 μm . b) T7E1 assay of U2OS.EGFP cells treated with Cas9/sgRNA/NC-12/PEI and Cas9/sgRNA/PEI. c) EGFP disruption assay of Cas9/sgRNA delivered by different DNA NCs. Percentages of EGFP negative cells after treating with Cas9/sgRNA/NC-23/PEI, Cas9/sgRNA/NC-12/PEI, Cas9/sgRNA/NC-0/PEI and Cas9/sgRNA/PEI at different Cas9/sgRNA molar ratios were profiled. Bars represent mean \pm SD (n = 3).

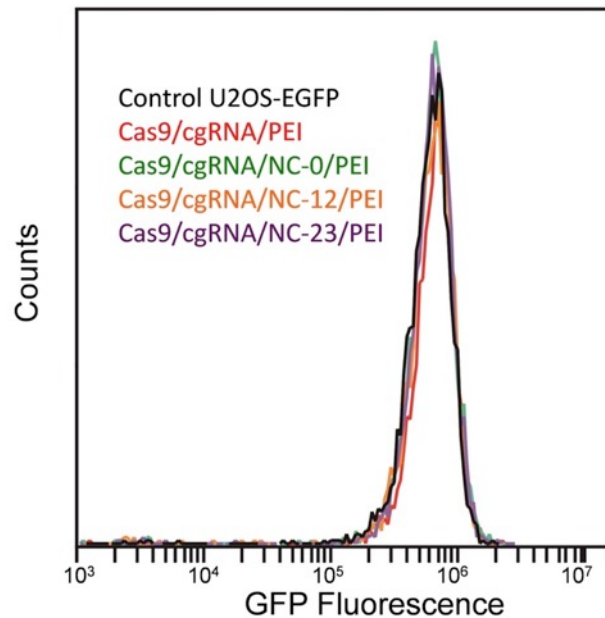


Figure 4-11. Flow cytometry analysis of U2OS.EGFP cells treated with formulations containing cgRNA, which did not show any EGFP disruption efficacy.

GGGTGGGCCAGGGC <u>CAGGGCAGCTTGC</u> ---- CGGTGGT GCAGATGAACTTCAGCTCGATGCGGTTC	WT
GGGTGGGCCAGGGCAGGGCAGCTTGC----CG-----GCTCGATGCGGTTC	-19
GGGTGGGCCAGGGCAGGG-----C---- CGGTGGT GCAGATGAACTTCAGCTCGATGCGGTTC	-8
GGGTGGGCCAGGG-----CAGCTTGC---- CGGTGGT GCAGATGAACTTCAGCTCGATGCGGTTC	-6
GGGTGGGCCAGGGCAGGGC-----GC---- CGGTGGT GCAGATGAACTTCAGCTCGATGCGGTTC	-5
GGGTGGGCCAGGGCAGGGCAGCTT----- CGGTGGT GCAGATGAACTTCAGCTCGATGCGGTTC	-2
GGGTGGGCCAGGGCAGGGCAGCTTGC- TCA CGGTGGT GCAGATGAACTTCAGCTCGATGCGGTTC	+3
GGGTGGGCCAGGGCAGGGCAGCTT GAT -- CCGGTGGT GCAGATGAACTTCAGCTCGATGCGGTTC	+2

Figure 4-12. DNA sequencing of Cas9/sgRNA targeted genomic locus in U2OS.EGFP cells. Target sequence complementary to the sgRNA is underlined and PAM sequence is shown in bold. Mutations were detected in 7 out of 20 sequenced clones. Number of insertion/deletion as compared to the wild type sequence is shown on the right.

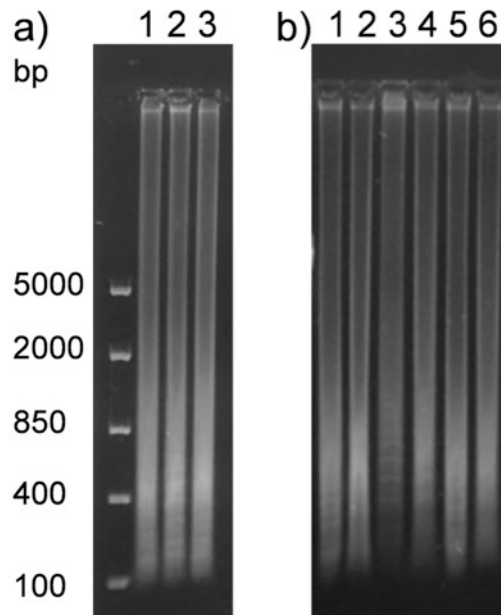


Figure 4-13. a) Agarose gel electrophoresis (0.8%) of synthesized NC-23, NC-12 and NC-0 in lane 1, 2 and 3, respectively. b) Analysis of NC stability after incubating with Cas9/sgRNA for 24 h. Lane 1, 3, 5 were for untreated NC-23, NC-12 and NC-0 and lane 2, 4, 6 showed Cas9/sgRNA treated NC-23, NC-12 and NC-0, respectively.

3.5 Gene editing in U2OS-EGFP xenograft tumor model

We further evaluated the *in vivo* EGFP disruption potency of Cas9/sgRNA delivered by NC-12 using U2OS.EGFP tumor bearing mice as models. 10 days after intratumoral injection, ~25% the U2OS.EGFP cells in the frozen tumor sections near the site of injection lost EGFP expression in the Cas9/sgRNA/NC-12/PEI treated mice, while the tumors in the untreated group or the group treated with Cas9/cgRNA/NC-12/PEI did not show any loss of EGFP signal (Figure 4-14, 4-15).

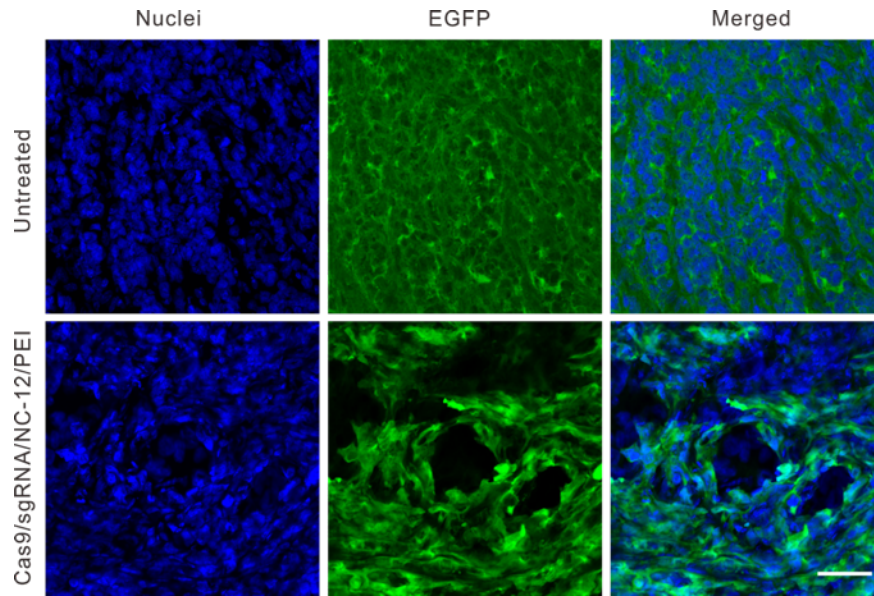


Figure 4-14. *In vivo* delivery of Cas9/sgRNA into U2OS.EGFP xenograft tumors in nude mice. Tumor sections were collected 10 days after intratumoral injection of Cas9/sgRNA/NC-12/PEI. The EGFP was stained by FITC conjugated GFP antibody and nuclei were stained with Hoechst 33342. Scale bar is 50 μ m.

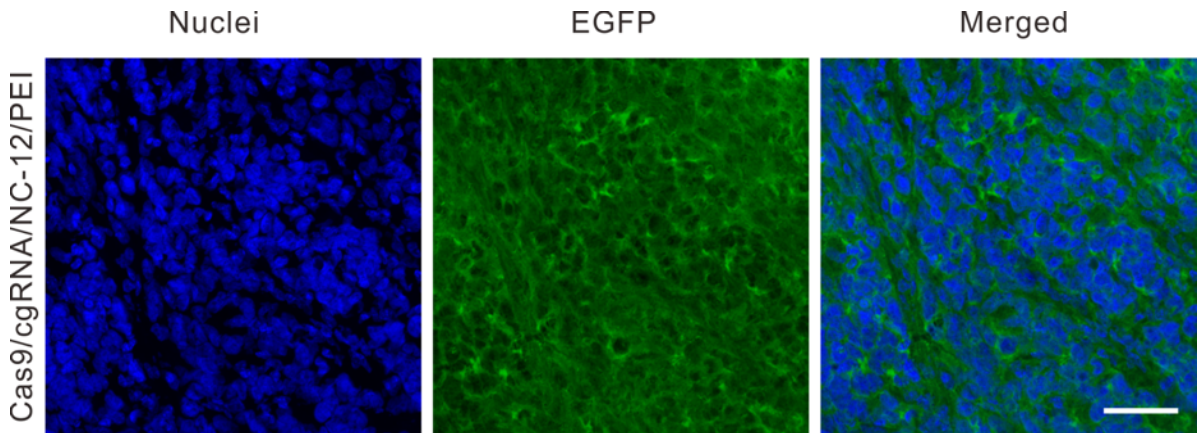


Figure 4-15. Tissue section of tumor treated with Cas9/cgRNA/NC-12/PEI. The EGFP was stained by FITC conjugated GFP antibody and nuclei were stained with Hoechst 33342. The Scale bar is 50 μ m.

4. Summary

In summary, we have demonstrated a novel delivery vehicle to achieve targeted genome editing with CRISPR-Cas9. Our DNA NC-based delivery system represents, to our knowledge, the first example of a polymeric nanoparticle for the delivery of CRISPR-Cas9. The DNA NC pre-organized the Cas9/sgRNA into nanoparticles and increased the charge densities of the core in the core-shell assembly, which may have acted to stabilize the nanoparticle.[592, 606] Partial complementarity between the DNA nanoclew and the sgRNA guide sequence promoted the greatest extent of gene editing, potentially due to balancing binding and release of the Cas9/sgRNA complex by the nanoclew. Future implementation of the delivery vehicles may focus on attaching cell-specific targeting ligands,[62, 163] engineering the environmentally responsive release of the CRISPR-Cas9,[98, 607] modifying the sequence of DNA NC to incorporate multiple sgRNAs for multiplexed editing, or employing the DNA NC or packaged DNA sequences as templates for homology-directed repair. The same NC architecture could also be used to incorporate other functional DNA-binding proteins, such as transcription factors, zinc-finger nucleases, and TALE nucleases, as well as other functional or protein-coding RNAs. The potential immunogenicity associated with DNA NCs should be further investigated for clinical translation.[608, 609]

CHAPTER 5 TRANSFORMABLE DNA NANOCARRIERS FOR PLASMA MEMBRANE TARGETED DELIVERY OF CYTOKINE

1. Introduction

Delivering protein based anticancer therapeutics[43, 69, 506, 610], such as enzymes [412, 611, 612], transcription factors [426, 613, 614], or cytokines [615-617], are gaining increasing interest due to their specific activities in inducing apoptosis in cancer cells, reducing normal cell damage than traditional chemotherapeutics [163, 618]. When compared with delivering nucleic acid based anticancer gene therapies, directly administering protein formulations would enable better control of the dosages as well as ruling out the chance of accidental genetic alterations [619]. While reaching intracellular compartments is a prerequisite for many anticancer proteins, like the caspase-3 that transmits apoptosis signal in the cytosol [577], or apoptin that takes effect in the nucleus [388]; blocking the endocytosis of proteins that target specific receptors on the plasma membrane would enhance their signaling, such as the tumor necrosis factor-related apoptosis-inducing ligand (TRAIL), a cytokine that interacts with death receptors on the plasma membrane and induces tumor specific apoptosis [471, 620]. However, current anticancer protein delivery systems were mostly designed for intracellular delivery by harnessing the size-dependent endocytosis of nanoparticles [356, 621, 622]; strategies for targeted delivery of nanocarriers to plasma membranes while avoiding size-dependent endocytosis remain elusive.

Here, we describe a novel rolling circle amplification (RCA) based strategy for cancer cell membrane targeted delivery of cytokine in a tumor-microenvironment responsive manner [471, 623-625], where the secreted phospholipase A2 (PLA2), an enzyme overexpressed by various tumors, including colon, breast, prostate, and gastric cancers [626], was harnessed as a spatial-temporal trigger for drug release. Compared with conventional DNA structure preparation techniques that require sophisticated DNA oligo design and assembly [285, 532, 600, 609, 627, 628], rolling circle amplification (RCA) is a facile DNA synthesis technique capable of preparing DNA structures spanning the spatial range from nano- [98, 597, 629-631] to micro- [538, 539] and to macroscopic scale [535-537]. One amazing property of DNA is that folded DNA nanostructures are readily internalized by many types of cancer cell lines [310, 513, 632, 633], while free DNA chains are impermeable to cell membranes [134]. In our previous reports, we prepared self-assembled DNA nanoclews (NCs) by RCA for nuclei targeted delivery of DOX as a tumor microenvironment-triggered anticancer therapy [98] or the CRISPR-Cas9 system for targeted genome editing [619]. However, these compact nanocarriers were tailored for intracellular targets. To achieve plasma membrane-targeted cytokine delivery, as shown in Figure 5-1, nanoparticles with a core-shell structure were designed consisting of two functional components: 1) a liposome shell that could be specifically degraded by PLA2 and 2) two DNA NCs encoding complementary sequences as the cores. For convenient designation, one of the complementary DNA NCs was defined as encoding DNA sequence in the forward direction (NCf), while the other was defined as encoding sequence in the reverse direction (NCr). The

model cytokine TRAIL was loaded onto the Ni²⁺ modified DNA NC cores via Ni²⁺-polyhistidine affinity. We hypothesized that the elevated PLA2 level in the tumor microenvironment would promote degradation of the liposome shell, releasing the TRAIL loaded DNA NCs into extracellular environment. In cases when only one of TRAIL-NCf-L or TRAIL-NCr-L was administered, rapid internalization of the TRAIL loaded DNA NC would happen, diminishing the apoptosis signaling induction. However, when both TRAIL-NCf-L and TRAIL-NCr-L were co-administered, hybridization of the complementary DNA NCs could occur extracellularly, transforming the compact DNA nanoparticles into micro-scaled DNA structures that could serve as multivalent scaffolds for presenting TRAIL to death receptors on plasma membrane and reduce its endocytosis to enhance the anticancer efficacy.

2. Materials and Methods

2.1. Materials

All chemicals unless otherwise specified were purchased from Sigma-Aldrich and were used as received. DNA oligos were ordered from Integrated DNA Technologies Inc. (Coralville, IA, USA). Bst 2.0 DNA polymerase was purchased from New England BioLabs Inc. (Ipswich, MA, USA). CircLigase II single-stranded DNA (ssDNA) Ligase was purchased from Epicenter (Madison, WI, USA). Aminoallyl-dUTP and Traut's reagent were

purchased from ThermoFisher Scientific, Inc. (Pittsburgh, PA, USA). Maleimido-C3-NTA was purchased from Dojindo Molecular Technologies Inc. (Kumamoto, Japan).

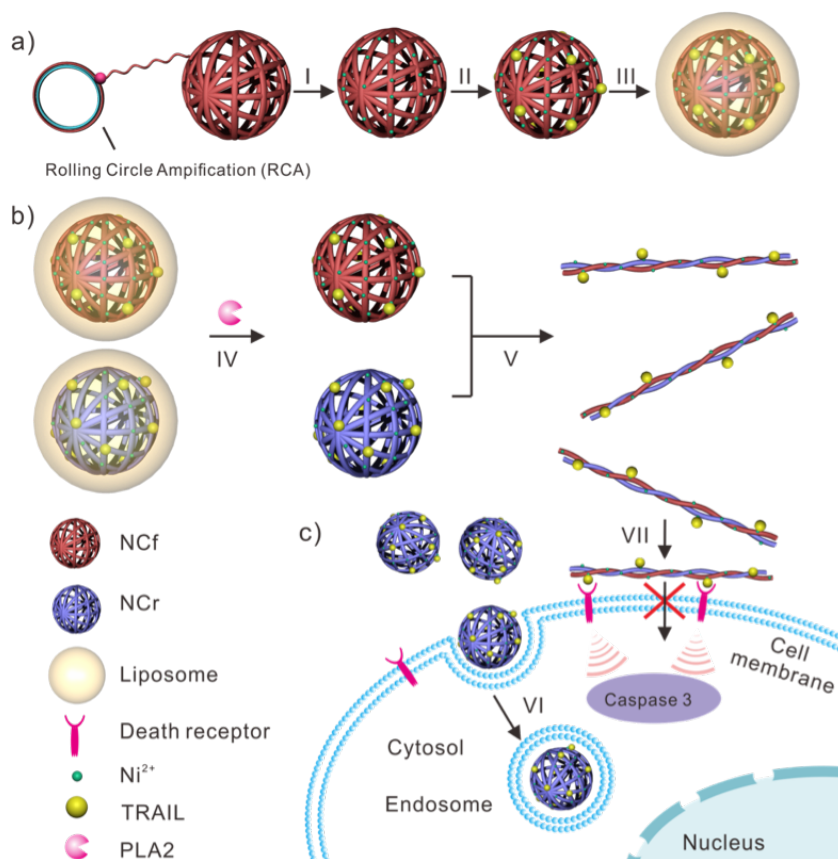


Figure 5-1. Schematic of phospholipase activated membrane targeted cytokine delivery system. (a) Preparation of TRAIL-NC-L. The DNA NC was first prepared by RCA and then (I) modified with Ni²⁺. After (II) loading TRAIL through Ni²⁺-His tag affinity, (III) the TRAIL-NC was encapsulated into a POPC liposome that could be degraded by PLA2. (b) Main components of TRAIL-NC-L and mechanism of PLA2 triggered morphological transformation of the DNA NCs. (IV) Highly expressed PLA2 in the tumor microenvironment degrades the liposome shell to release TRAIL-NC. (V) Complementary DNA NCs hybridize into microscopic fibers. (c) Effect of the morphological change on TRAIL localization. (VI) TRAIL loaded spherical nanoparticle are efficiently internalized. (VII) Hybridized DNA fibers are highly impermeable to cell membrane, facilitating the interaction of TRAIL and death receptors.

2.2. Preparation of TRAIL

Recombinant TRAIL was expressed and purified as described previously [409]. Briefly, *Escherichia coli* harboring the plasmid pET23dw-His-ILZ-hTRAIL that encodes His-ILZ-TRAIL (residues 114-281) was cultured in LB medium until the OD₆₀₀ reached 0.6-0.8. 0.5 mM isopropylthio- β -galactoside (IPTG) was added to induce TRAIL expression at 20 °C for 12 h. The cells were then collected by centrifugation and resuspended in buffer A (20 mM Tris-HCl, pH 8.0, 20 mM imidazole). After lysis by sonication and centrifugation at 20,000 \times g for 20 min, the supernatant of cell lysate was applied to a column containing NTA-Ni²⁺ resin. Followed by washing the column with buffer B (20 mM Tris-HCl, pH 8.0, 60 mM imidazole), TRAIL was eluted by buffer C (20 mM Tris-HCl, pH 8.0, 500 mM imidazole) and dialyzed against PBS at 4 °C overnight. The purified TRAIL was quantified by Bradford assay and analyzed by SDS-PAGE.

2.3. Preparation of Ni²⁺ modified DNA NC

Two complementary DNA NCs modified with NH₂ were prepared by RCA [98] with further modifications to obtain Ni²⁺ modified DNA NCs. The ssDNA templates with 5' phosphorylation (Table 5-1) were cyclized by CircLigase II following manufacturer's instructions and uncyclized ssDNA chains were removed with Exonuclease I (NEB). NCs modified with primary amines were then prepared by applying aminoallyl-dUTP as a building block in the RCA reaction. Briefly, 10 pmol circular ssDNA templates were hybridized with corresponding primers at 95 °C for 5 min in 1 \times isothermal amplification

buffer (NEB) supplemented with 200 μM dUTP and 2 μM aminoallyl-dUTP. After cooling the solution to room temperature, Bst 2.0 DNA polymerase (0.2 U/ μL) was added and the reaction was kept at 60 $^{\circ}\text{C}$ for 17 h. The synthesized NCs were centrifuged at $14,000 \times g$ for 2 min and dialyzed against buffer D (10 mM phosphate buffer, pH 7.4, 2.5 mM EDTA) in a Slide-A-Lyzer dialysis unit (20K MWCO, Thermo Scientific). The primary amines on NCs were then conjugated with thiol groups using 5 μM Traut's reagent at room temperature for 1 h and the thiolation was confirmed by thiol detection kit (Cayman) with an efficiency over 95%. 20 μM maleimido-C3-NTA was then added to conjugate NTA to the thiol groups at room temperature for 3 h.[634] After chelating the NTA with 50 μM NiCl_2 , the Ni^{2+} modified DNA NCs were dialyzed against deionized water for 2-3 days. Concentrations of the prepared DNA NCs were determined using Nanodrop 2000C spectrometer (Thermo Scientific). Zeta potential and particle size were analyzed by Zetasizer (Nano ZS, Malvern). Transmission electron microscopy (TEM) images of the NCs were acquired on a JEOL 2000FX microscope at 200 kV with the samples prepared on a TEM copper grid (300 mesh) (Ted Pella) and stained by phosphotungstic acid (1%, v:v). Elemental mapping of the DNA NCs were performed on an FEI Titan 80-300 aberration corrected STEM with SuperX energy dispersive X-ray spectroscopy (EDS) system.

2.4. Characterization of DNA NCs loaded with TRAIL

The His-tagged TRAIL protein was loaded onto Ni^{2+} modified DNA NCs (1:40, w:w) via the affinity between the His-tag and Ni^{2+} with an excess of Ni^{2+} . The TRAIL loaded NCs,

TRAIL-NCf and TRAIL-NCr, were then visualized by confocal laser scanning microscope (CLSM) with TRAIL labeled by Alexa Fluor 647 (AF 647) and NCs stained with Hoechst 33342. To obtain TEM image of TRAIL loaded DNA NC, TRAIL was pre-stained with mono-sulfo-N-hydroxy-succinimido gold nanoparticle in PBS for 1 h and excessive gold nanoparticle (AuNP) was removed by Seperdex-75 gel filtration. Silver enhancement was applied for better TEM imaging. For atomic force microscope (AFM) imaging, the NCf and NCr were dropped, dried on the silicon wafer and imaged by tapping mode in ambient air using a Nanoscope AFM (Veeco, Santa Barbara, CA). Particle size and zeta potential of TRAIL loaded NCs were characterized by Zetasizer (Nano ZS, Malvern).

Table 5-1. Sequences of DNA oligos.

^aPalindromic sequence underlined for particle assembly.

	Nanocarrier	Sequences
	s	
RCA templates^a	NCf	5'phos- ACAGGCCAACCCCCCATGACAACGTGGGACAGACGCAACCTCTGT AGTGAAAAAAC <u>CATTACGCGTAATG</u> AAAAAAT 3'
	NCr	5'phos- ATTTTTT <u>CATTACGCGTAATG</u> TTTTTTTCACTACAGAGGTTGCGTCTG TCCCACGTTGTCATGGGGGGTTGGCCTGT 3'
Primers	NCf	5' CACTACAGAGG 3'
	NCr	5' CCTCTGTAGTG 3'

2.5. Encapsulation of DNA NC into liposome and PLA2 triggered release

The TRAIL loaded DNA NCs were encapsulated into 1-palmitoyl-2-oleoyl-sn-glycero-3-phosphocholine (POPC) liposome by reverse phase evaporation. Briefly, POPC dissolved in chloroform (1 mg/mL) and water solution containing TRAIL-NC were mixed (3:1, v:v). A nano-emulsion was obtained after sonication and the emulsion was shortly evaporated by a rotary vacuum evaporator (Heidolph). Supplemented with another 1 volume of deionized water, the emulsion was evaporated again to remove excess chloroform from the solution. Unencapsulated TRAIL-NC was removed by dialysis against deionized water in a 1000 KDa dialysis unit (Spectrum) after DNase treatment. Particle size and zeta potential of liposome were characterized by Zetasizer (Nano ZS, Malvern). POPC liposome was lysed with Triton X-100 aqueous solution (1%, v:v) for rapid release of its content. For phospholipase mediated release, 15 U/mL of PLA2 from *Naja mossambica mossambica* (Sigma Aldrich) was incubated with the liposome at room temperature for 10 min [635, 636]. The release of TRAIL-NC from the POPC liposome was analyzed by 0.8% agarose gel electrophoresis with GelRed supplemented as DNA stain and band fluorescence intensity was estimated with Image J. The POPC liposome were also characterized by TEM imaging.

2.6. Cell culture

The human colorectal cancer cell line COLO 205 was cultured in Dulbecco's Modified Eagle's Medium (DMEM) supplemented with 10 % FBS (v:v), 100 U/mL penicillin and 100 µg/mL streptomycin in a 37 °C incubator (Thermal Scientific) under an

atmosphere of 5% CO₂ and 90% humidity. The cells were sub-cultured regularly with a split ratio of 1:3 and the cell densities were quantified using a hemocytometer before each experiment.

2.7. Cellular distribution and endocytosis pathway of delivered TRAIL

Subcellular localization of delivered TRAIL was monitored using CLSM. COLO 205 cells were seeded in confocal microscopy dishes (MatTek) at the density of 1×10^5 cells/well and cultured for 48 h. The cells were then incubated with different formulations containing 50 ng/mL of AF 647 labeled TRAIL at 37 °C for 1 h. After washing the cells with ice-cold PBS twice, the cell membranes were stained with 5 µg/mL Alexa Fluor 488 conjugated Wheat Germ Agglutinin (WGA) at 37 °C for 10 min. The stained cells were then washed with ice-cold PBS again and observed with CLSM immediately. For quantitative analysis of membrane-bound TRAIL, COLO 205 cells were seeded in 6-well plates (1×10^5 cells/well) and cultured for 48 h. The cells were treated with different formulations containing 50 ng/mL of AF 647 labeled TRAIL for 1 h at 37 °C or 4 °C. Afterwards, the cells were collected and analyzed by flow cytometry (Cytoflex, Beckman Coulter) to quantify the total TRAIL contents of the cells, including membrane bound and internalized, by measuring the mean fluorescence intensities of the cells. Samples treated at 37 °C represent the total amount the both membrane-bound and internalized TRAIL while the those treated at 4 °C were referred only as TRAIL bound to the cell membrane due the inhibition of endocytosis at 4 °C [409]. The uptake pathway of delivered TRAIL (stained with AF 647) was also

analyzed. COLO 205 cells in the 6-well plates were pre-incubated with different inhibitors for endocytosis pathways for 1h at 37 °C [chlorpromazine (CPZ, 10 µM) for clathrin-mediated endocytosis; methyl-β-cyclodextrin (MCD, 3 mM) for lipid raft; nystatin (NYS, 25 µg/mL) for cavelolin-mediated endocytosis; and amiloride (AMI, 1 mM) for macropinocytosis]. Then the cells were incubated with PLA2 pretreated TRAIL-NCf-L or TRAIL-NCr-L in the presence of the inhibitors for another 2h. Mean fluorescence intensities of the cells were analyzed by flow cytometry.

2.8. Cell apoptosis assay

The apoptosis inducing capability of TRAIL delivered by different formulations were evaluated with the APO-BrdU based terminal deoxynucleotidyl transferase (TdT) dUTP Nick-End Labeling (TUNEL) assay kit (Life Technologies) and the Annexin V-FITC Apoptosis Detection Kit (BD Biosciences). COLO 205 cells were seeded in 6-well plates and cultured for 48 h. The cells were incubated with different formulations containing 20 ng/mL of TRAIL for 12 h. Afterwards, the cells were stained following the protocol of the manufacturers. For the TUNEL assay, the cells were imaged by fluorescence microscope (IX71, Olympus), while for the Annexin V-FITC Apoptosis assay, the cells were analyzed by flow cytometry (Cytoflex, Beckman Coulter).

2.9. *In vitro* cytotoxicity

COLO 205 cells were seeded in 96 well plates at the density of 1×10^4 cells/well and cultured for 24 h. To evaluate the anticancer efficacy of TRAIL delivered by the NCs, the cells were incubated with TRAIL containing formulations at different TRAIL concentrations for 24 h. To evaluate the biocompatibility of the carrier, nanocarriers without TRAIL were incubated with the cells at the same concentrations used for TRAIL delivery for 24 h. MTT solutions were then added to the cells (final concentration of 0.5 mg/mL) and incubated for 4 h. After removing the medium, the cells were dissolved with 150 μ L DMSO and the absorbances were read on a microplate reader (Infinite M2000 Pro, Tecan) with test wavelength of 570 nm and reference wavelength of 630 nm.

2.10. Statistics

All results were calculated as Mean \pm SD. Two-tailed student's t-test was performed for statistical analysis. The difference between experimental groups and control groups were considered statistically significant when $P < 0.05$ or highly significant when $P < 0.01$.

3. Results and Discussion

3.1. Preparation and characterization of Ni²⁺ modified DNA NC

To validate our delivery strategy, we first synthesized the NH₂-modified DNA NCs by RCA (Figure 5-1a). Two ssDNA oligos with complementary sequences were used as

templates for the RCA (Table 5-1). Aminoallyl-dUTP was supplemented into the RCA reaction for incorporating NH₂ groups into the RCA products. After converting NH₂ into SH with the Traut's reagent, maleimide activated nitrilotriacetic acid (NTA) was conjugated to the DNA NC for chelating Ni²⁺. Both NCf and NCr self-assembled into negatively charged nanoparticles (zeta potential of -21 ± 3 mV) with the mean size of 97 nm as determined by the TEM, AFM and dynamic light scattering (DLS) (Figure 5-2a-c). The Ni²⁺ modification on DNA NC was confirmed by elemental analysis using the EDS mapping on a scanning transmission electron microscope (STEM) (Figure 5-2d). Next, the morphology of the hybridized NCf/NCr was evaluated by TEM and AFM. After incubating at 37 °C for 10 min, the fully complementary NCf and NCr merged into micro-scaled fibers (Figure 5-2b and c). Due to the periodic nature of the DNA strands, strong hybridization of multiple DNA strands generated networked fibers with a width of ~ 40 nm and length spanning a few micrometers.

3.2. Loading TRAIL onto DNA NC

TRAIL with a molecular weight of 24 KDa was purified (Figure 5-3a) and loaded onto the synthesized DNA NCs via the affinity between Ni²⁺ and the fused His-tag on TRAIL. To image the loading of TRAIL onto DNA NC by TEM, TRAIL was labeled with gold nanoparticle. Both NCf and NCr were efficient in loading the His-tagged TRAIL, which caused negligible changes to the zeta potential (-20 ± 4 mV) and sizes as compared with DNA NCs (Figure 5-3b). Binding of the TRAIL protein to DNA NCs was also observed by CLSM with TRAIL labeled by the infrared AF 647 and NCs stained with Hoechst 33342

(Figure 5-3c). Colocalization of the fluorescence signals further confirmed the binding between TRAIL and DNA NCs.

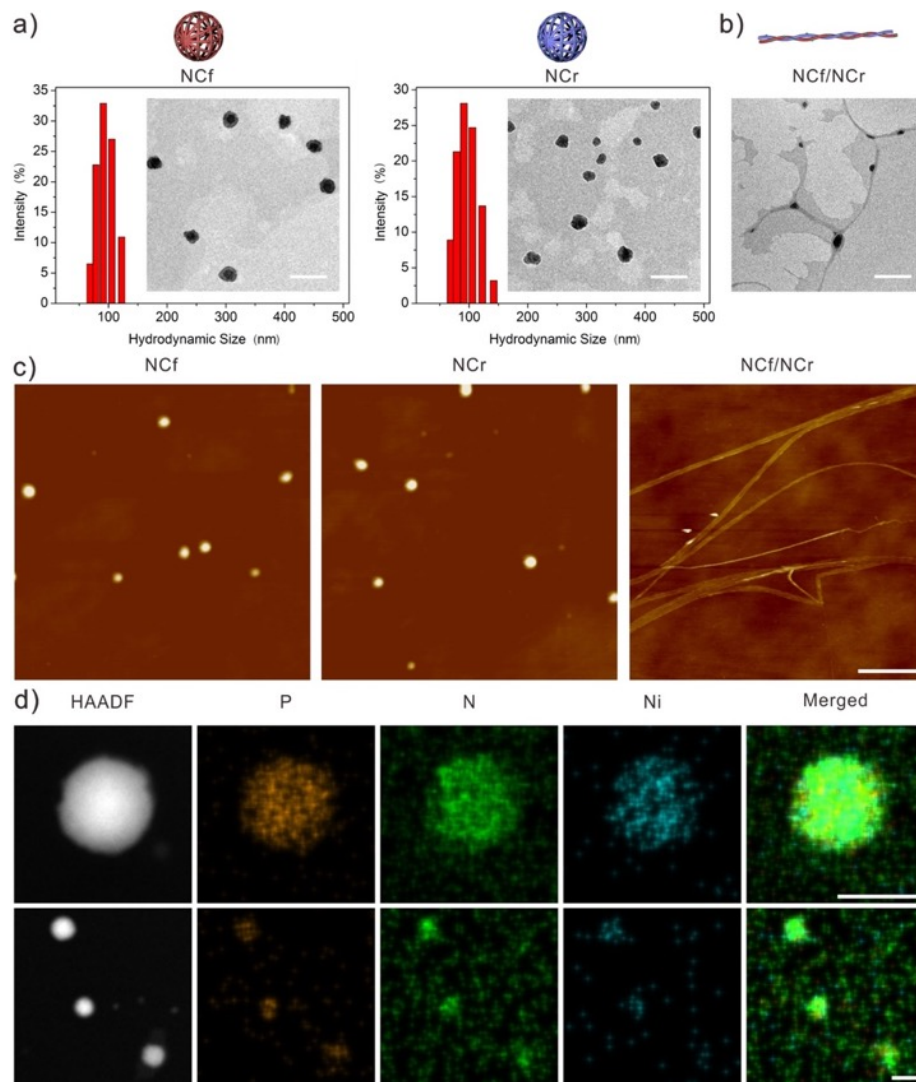


Figure 5-2. (a) Hydrodynamic size distributions and TEM images of the synthesized DNA NCs. scale bars 200 nm (b) TEM image of NCF/NCR mix, scale bar 200 nm. (c) AFM imaging of NCF, NCR, and NCF/NCR mix. Scale bar represents 500 nm. (d) Representative element mapping of Ni²⁺ modified DNA NC. Shown here is Ni²⁺ modified NCF, scale bar represents 100 nm.

3.3. Encapsulation of TRAIL-NC in POPC liposome and PLA2 triggered release

To prevent the TRAIL loaded DNA NCs from premature hybridization, TRAIL-NCf and TRAIL-NCr were encapsulated in liposomes composed of POPC, separately, by the method of reverse evaporation [637]. The sn-2 acyl ester bond in POPC can be rapidly degraded by the surface active enzyme PLA2 [638], making POPC liposome a PLA2-responsive coating for TRAIL delivery. The POPC liposome containing TRAIL-NC showed a mean hydrodynamic size of 215 nm (PDI = 0.29 ± 0.03 , zeta potential -25 ± 4 mV) (Figure 5-4a) and the TRAIL-NC was encapsulated with an encapsulation efficiency of 55 % (Figure 5-4b). Treating the TRAIL-NC-L with PLA2 for 10 min triggered virtually complete release of the encapsulated TRAIL-NC from the liposome (Figure 5-4c). When TRAIL-NC-L was treated with PLA2, the liposome structure was disrupted and nanoparticles with a size of ~ 100 nm were released (Figure 5-4d and e). However, microscaled fibers of hybridized TRAIL-NCf/TRAIL-NCr (1:1 w:w) were observed after PLA2 treatment of the TRAIL-NCf-L/TRAIL-NCr-L mix (Figure 5-4f), reducing the portion of free nanoparticles.

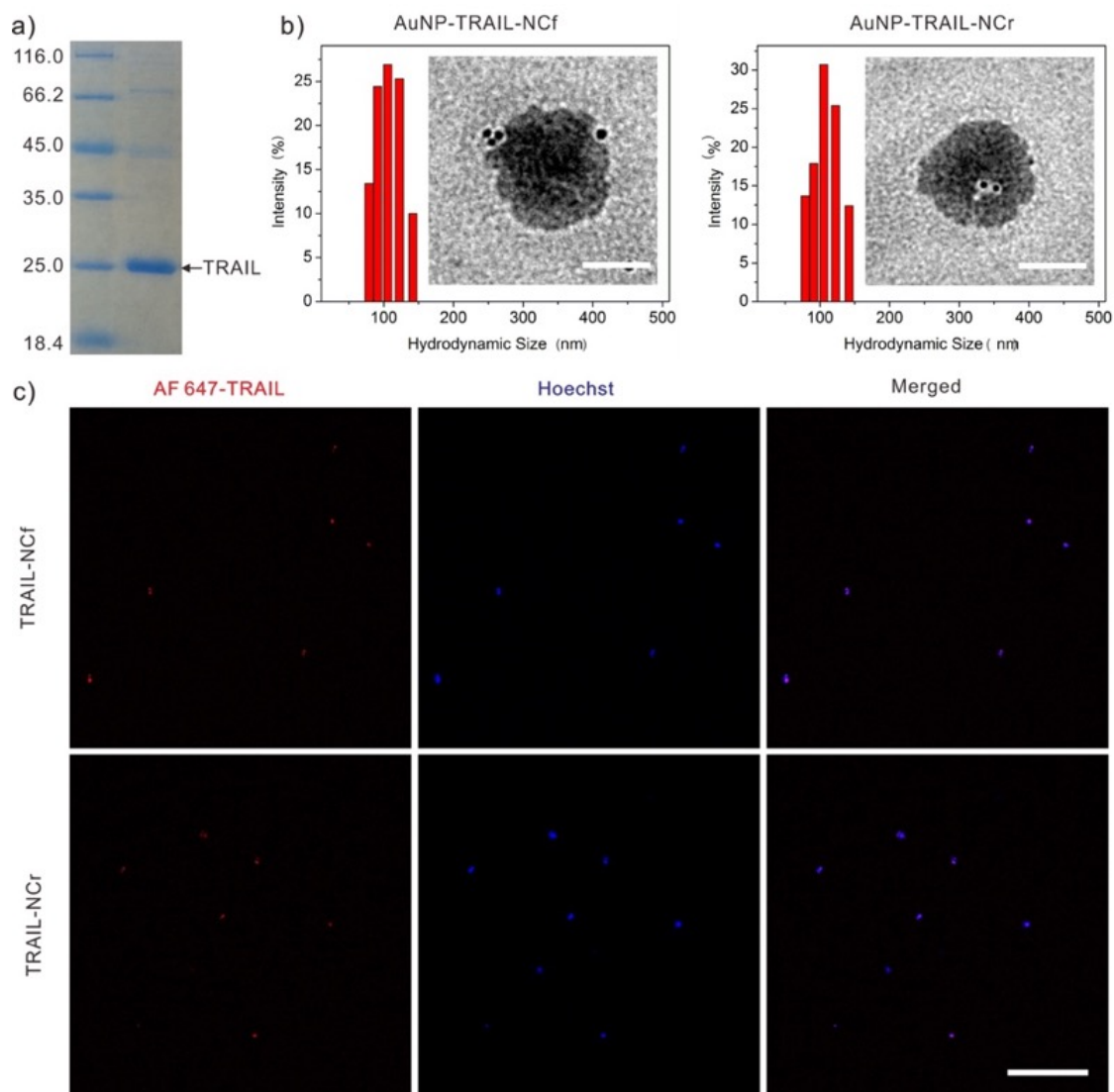


Figure 5-3. (a) SDS-PAGE of purified TRAIL. (b) Hydrodynamic size distributions and TEM imaging of TRAIL loaded DNA NCs. TRAIL-NCf and TRAIL-NCr showed similar size distribution with a mean diameter of ~ 104 nm. TRAIL was stained with AuNP. Scale bars represent 100 nm. (c) CLSM characterization of the colocalization of TRAIL and DNA in TRAIL-NCf and TRAIL-NCr. Red fluorescence indicated AF 647 labeled TRAIL; blue fluorescence showed Hoechst 33342 stained DNA NCs. Scale bar represents 10 μ m.

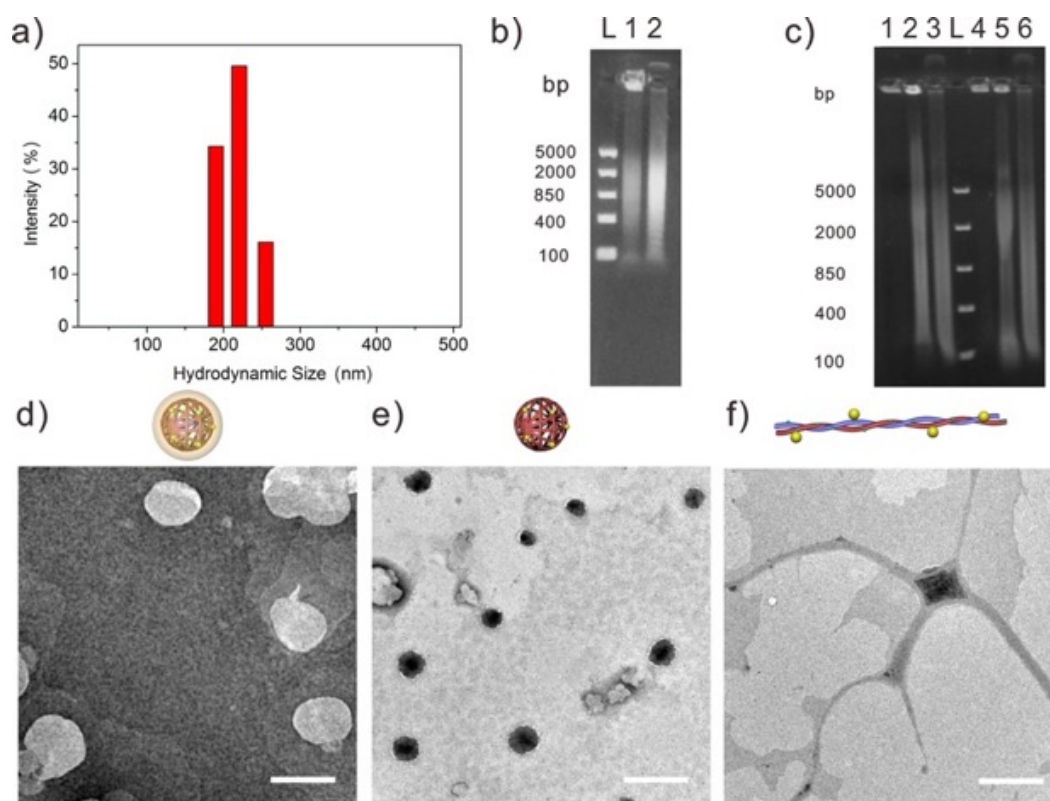


Figure 5-4. (a) Hydrodynamic size distribution of POPC liposome encapsulating TRAIL-NCf. (b) Agarose gel electrophoresis analysis of encapsulating DNA NC into POPC liposome. Lane L showed DNA ladder, Lane 1: Unpurified TRIAL-NCf-L, Lane 2: Unpurified TRIAL-NCf-L treated with 1% Triton X-100. Encapsulation efficiency was estimated from the band intensity by Image J, where the encapsulated amount is the difference between Lane 2 and Lane 1. (c) Release of TRAIL-NC from POPC liposome. Lane L showed DNA ladder; Lane 1 and 4, purified POPC liposome encapsulating TRAIL-NCf and TRAIL-NCr; Lane 2 and 5, TRAIL-NCf-L and TRAIL-NCr-L treated with PLA2; Lane 3 and 6, TRAIL-NCf-L and TRAIL-NCr-L treated with 1% Triton X-100 as 100% release. (d) Representative TEM image of POPC liposome encapsulating TRAIL-NC. Shown is TRAIL-NCf-L. (e) TEM image of TRAIL-NCf-L after PLA2 treatment. (f) TEM image of TRAIL-NCf-L/TRAIL-NCr-L after PLA2 treatment. Scale bars all indicate 200 nm.

3.4. Cell membrane targeted delivery of TRAIL

To evaluate the membrane targeted delivery of TRAIL by TRAIL-NCf-L/TRAIL-NCr-L, the human colorectal carcinoma cell COLO 205 was chosen as a model cell line due

to the significantly elevated expression of PLA2 in its tumor extracellular matrix [639]. To compensate for the inadequate PLA2 secretion caused by the low cell density in the culture, PLA2 pretreatment was applied to release TRAIL-NC from the liposome. Subcellular localization of the delivered TRAIL was studied by incubating COLO 205 cells with TRAIL-NCf-L or TRAIL-NCr-L separately or simultaneously after PLA2 pretreatment of the liposome to mimic the tumor microenvironment. After incubation at 37 °C for 1 h, subcellular localization of AF 647 labeled TRAIL was observed by CLSM. As shown in Figure 5-5a, TRAIL delivered by TRAIL-NCf-L or TRAIL-NCr-L separately was mostly internalized into the cells. However, the internalization was significantly inhibited when TRAIL-NCf-L and TRAIL-NCr-L were co-administered, leaving large part of the administered TRAIL bound on cell membrane. Quantitative analysis also confirmed that co-administration of two nanoparticles significantly enhanced the percentage of membrane-bound TRAIL to ~ 76% from ~42% by separately administered systems (Figure 5-5b). Further analysis of the endocytosis pathways showed that the TRAIL delivered by TRAIL-NCf-L or TRAIL-NCr-L separately was mostly internalized into the COLO 205 cells through clathrin and lipid raft mediated pathways (Figure 5-5c).

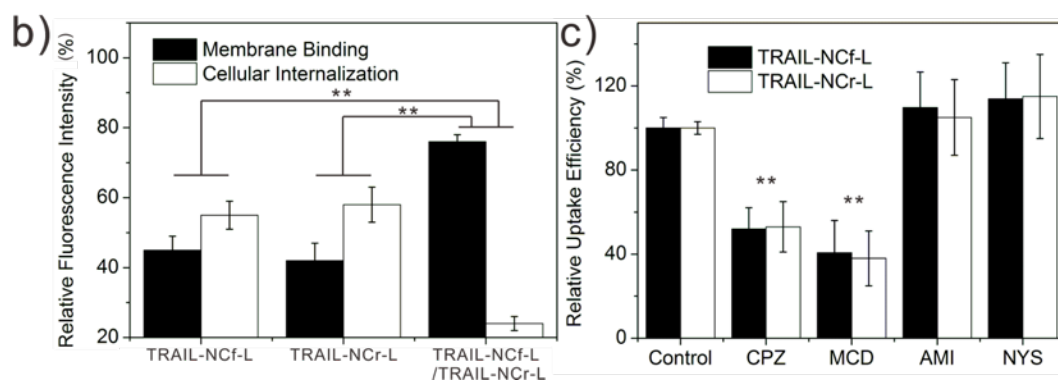
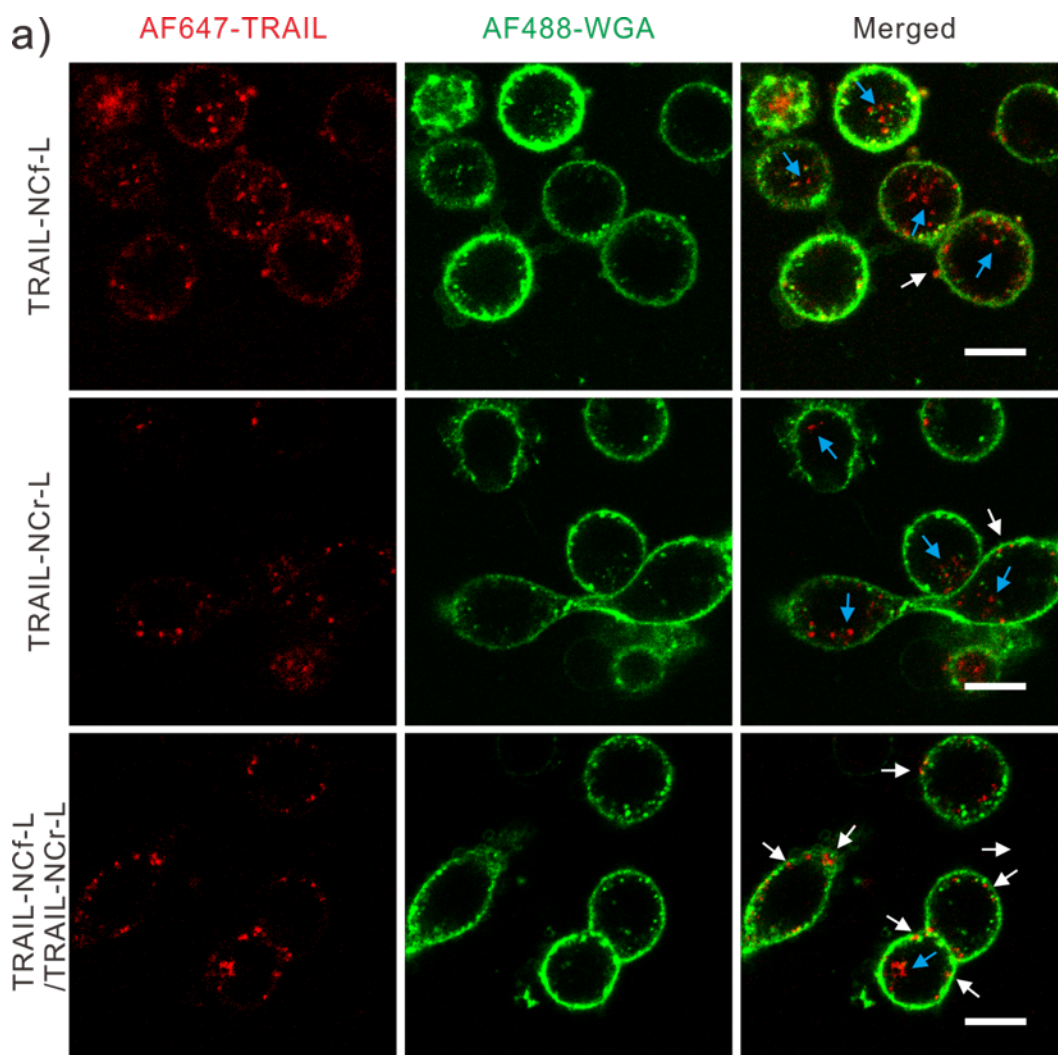


Figure 5-5. (a) CLSM analysis of subcellular localization of delivered TRAIL. COLO 205 cells were incubated with TRAIL-NCf-L and TRAIL-NCr-L separately or simultaneously after PLA2 pretreatment. TRAIL was labeled with AF 647 and membrane of COLO 205 cells was stained with AF488-WGA. White arrows indicate TRAIL on cell membrane and blue arrows indicate internalized TRAIL. Scale bars indicate 20 μm . (b) Quantitative analysis of the amount of TRAIL internalized by COLO 205 cells or bound on cell membrane. (c) Endocytosis pathway analysis of TRAIL delivered by TRAIL-NCf-L and TRAIL-NCr-L. Data was presented as mean \pm SD (n = 3). ** $P < 0.01$.

3.5. *In vitro* cytotoxicity

After confirming the membrane-targeted delivery of TRAIL by TRAIL-NCf-L/TRAIL-NCr-L, the enhanced apoptosis inducing capability of the co-administrated formulation was then evaluated by the TUNEL assay. Cells treated with TRAIL-NCf-L/TRAIL-NCr-L mixture after PLA2 pretreatment exhibited higher level of the apoptotic DNA fragmentation as observed from the green fluorescence signals compared with those incubated with separated formulations (Figure 5-6a). The quantitative analysis of the apoptosis was performed using the Annexin-FITC staining based flow cytometry. As shown in Figure 5-6b, the apoptosis ratios were 31.7% and 29.6% for PLA2 pretreated TRAIL-NCf-L and TRAIL-NCr-L, respectively; while after PLA2 pretreatment, TRAIL-NCf-L/TRAIL-NCr-L co-administration exhibited the highest apoptosis inducing capability with an apoptosis ratio of 43.7% after 12 h of incubation. The enhanced apoptosis of the co-delivered formulation is consistent with the increasing ratio of the membrane bound TRAIL.

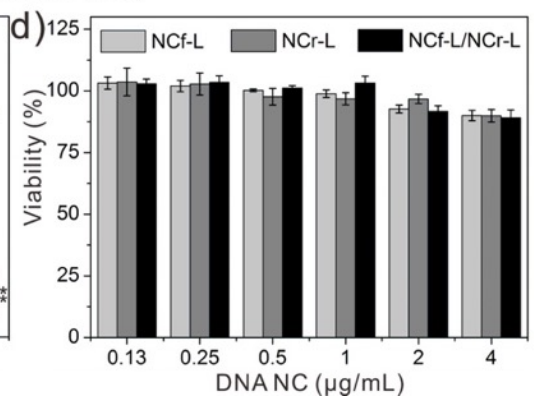
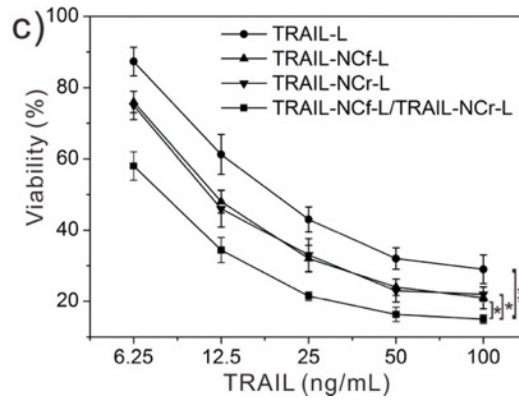
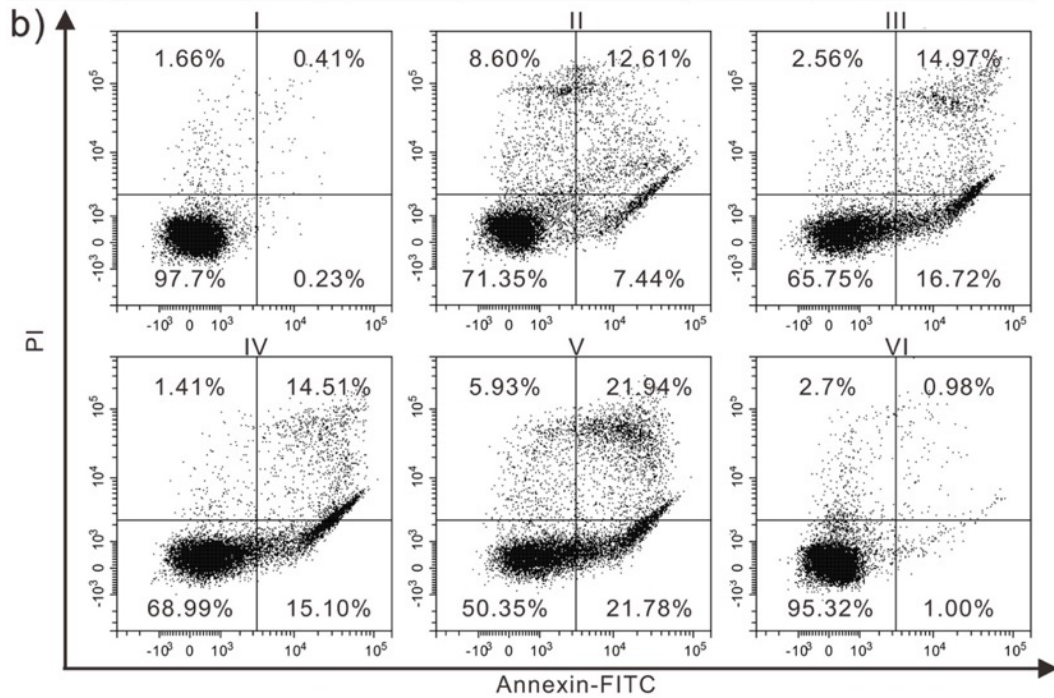
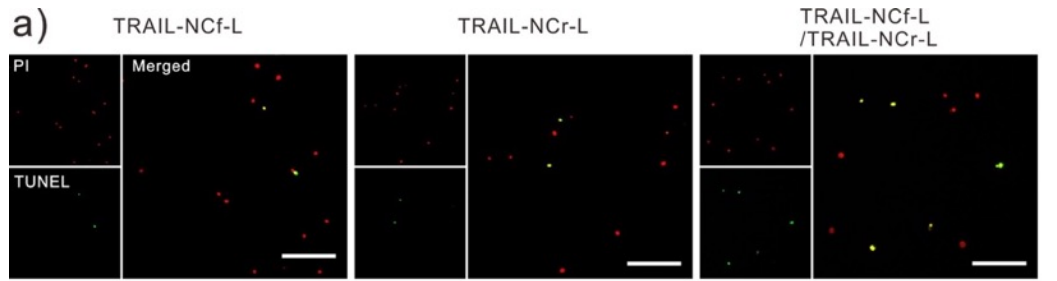


Figure 5-6. (a) APO-BrdU TUNEL assay of COLO 205 apoptosis induced by different TRAIL delivery formulations after PLA2 pretreatment. Scale bar indicates 200 μm . (b) Annexin V-FITC/PI staining based flow cytometry analysis of COLO 205 apoptosis after treating with different TRAIL delivery formulations for 12 h. I, control cell untreated with any formulation; II, TRAIL-L after PLA2 pretreatment; III, TRAIL-NCf-L after PLA2 pretreatment; IV, TRAIL-NCr-L after PLA2 pretreatment; V, TRAIL-NCf-L/TRAIL-NCr-L after PLA2 pretreatment; VI, TRAIL-NCf-L/TRAIL-NCr-L without PLA2 pretreatment. (c) *In vitro* cytotoxicity of TRAIL-L, TRAIL-NCf-L, TRAIL-NCr-L and TRAIL-NCf-L/TRAIL-NCr-L after PLA2 pretreatment. Colo 205 cells were treated with different formulations for 24 h. (d) *In vitro* cytotoxicity of carriers without loaded TRAIL after PLA2 pretreatment. Data were presented as mean \pm SD (n=6). * P <0.05, ** P <0.01.

The absence of PLA2 pretreatment basically abolished apoptosis inducing capability even for the co-administered formulation, indicating that the tumor microenvironment associated PLA2 is a required stimulus for TRAIL release. It is worth noting that, TRAIL bound to the NCs showed higher apoptotic signaling than free TRAIL, possibly due to the nanovectorization enhanced regional clustering of TRAIL [640]. The *in vitro* cytotoxicity of TRAIL against COLO 205 cells was examined by the 3-(4,5-dimethylthiazol-2-yl)-2,5-diphenyltetrazolium bromide (MTT) assay. Separately administered TRAIL-NCf-L and TRAIL-NCr-L after PLA2 pretreatment showed similar cytotoxicity with a half-maximal inhibitory concentration (IC₅₀) of 14 ng/mL, which is significantly lower than that of TRAIL-L (IC₅₀ = 24.2 ng/mL) (Figure 5-6c). TRAIL delivered by TRAIL-NCf-L and TRAIL-NCr-L simultaneously after PLA2 pretreatment showed further enhanced cytotoxicity towards COLO 205 cells (IC₅₀ = 7.8 ng/mL). Meanwhile, the empty vectors without loaded TRAIL did not show any significant cytotoxicity after PLA2 pretreatment (Figure 5-6d), indicating the biocompatibility of the carriers.

4. Conclusion

In conclusion, we have exploited a novel cancer cell membrane targeted drug delivery system using two complementary DNA NCs as a drug loading matrix for regulating protein internalization. An enzyme degradable liposome was utilized for spatial-temporal hybridization of the DNA NCs. Of note, the morphological transformation of the nanoparticles [174, 471] into micro-scaled DNA structures effectively inhibited the endocytosis of TRAIL presenting nanoparticle into cancer cells, increasing its anticancer efficacy. This strategy provides new guidelines for design of cell membrane targeted drug delivery, which can be further expanded to other types of therapeutics.

CHAPTER 6 SUMMARY AND OUTLOOK

In this dissertation, we have reviewed recent progresses in leveraging physiological traits of diseases for tailoring precision nanomedicine as well as the emerging application of the DNA nano-scaffolds for the delivery of therapeutics. Three projects utilizing the DNA NC as carriers were specifically introduced for the delivery of three different types of therapeutic molecules through different drug loading mechanisms. In this chapter, we will summarize the novelty and significance of each project:

1) We have developed a bioinspired “cocoon-like” nano-assembly that could undergo self-degradation upon exposure to acidic environment for the release of the chemotherapeutic drug DOX. DOX has a preference to intercalating into the “GC” pairs of DNA. With the programmability of DNA NC, multiple copies of the “GC” were introduced into the DNA NC, leading to a high DOX loading capacity of 66.7%. Compared with the uncontrolled passive drug release profiles of classic DNA nanocarriers, the adsorption of single protein nanocapsules containing DNase facilitated DOX release process after cellular internalization. The acid degradable nanocapsule was quite stable at physiological pH, caging the activity of DNase; while it would undergo rapid shedding from the surface of DNase to unlock DNase activity in acidic environment. This method of combining a controlled hydrolyzing enzyme with its nanomaterial substrate demonstrated a novel strategy of triggering the disassembly of nanocarriers using an integrated component of the nanocarrier. With high DOX loading

capacity as well as acid triggered drug release, rapid and efficient DOX accumulation in the nucleus of treated cells could be observed within 0.5 h *in vitro*. In addition to loading DOX by intercalation, the DNA NC was also modified with folic acid as targeting ligand through the hybridization of the folic acid containing DNA oligo onto the DNA NC. The facile method of targeting ligand modification endowed the nanococoon with enhanced tumor targeting capability. *In vitro* cytotoxicity analysis revealed a significantly reduced IC₅₀ value (0.9 μM) after incorporation of the caged DNase and the targeting ligand onto the DNA NC compared with 2.3 μM in the bare DNA NC carrier.

2) We have tailored the DNA NC as a customized nanocarrier for the CRISPR–Cas9 system. CRISPR-Cas9 has become a powerful genome editing tool that is promising to treat a large variety of gene associated diseases through precisely manipulating the DNA root of these diseases. However, the need of an efficient delivery system for the CRISPR-Cas9 is the key to the therapeutic translation of the system. Development of a non-viral delivery carrier based on the DNA NC would help bridging the gap between a biotechnology tool and an effective therapy for CRISPR-Cas9. We chose to deliver the CRISPR-Cas9 in the form of purified ribonucleoprotein since it allowed more stringent control over the dosage of Cas9/sgRNA in contrast to the form of plasmid. The controllable dosage alleviated the concern for dosage associated toxicity as well as reduced the possibility of off-target editing. To load the Cas9/sgRNA into the DNA NC, we programmed sequences complementary to the target binding site of the sgRNA. The interaction between the DNA NC and the

ribonucleoprotein was tuned by adjusting the length of the complementary segments. A cationic polymeric layer of PEI was further coated onto the assembly to disrupt the endosomal membrane once the nanoparticle was endocytosed by the treated cells. Using a EGFP expressing reporter cell line, we observed that partial complementation between the DNA NC and the guiding RNA brought about the optimal CRISPR-Cas9 delivery efficacy (36%) in cell culture, possibly due to the balance between loading and release. This observation could provide a guideline for designing nucleic acid based carriers for the delivery of Cas9/sgRNA ribonucleoprotein. Local administration of the DNA NC based Cas9/sgRNA delivery system to the xenograft tumor also demonstrated efficient *in vivo* genome editing efficacy, making this nano-assembly promising for therapeutic translations. The DNA NC based nanocarrier demonstrated the first polymeric system for the CRISPR-Cas9 delivery and it could be readily adapted to deliver many other types of DNA binding proteins, such as zinc finger nuclease or transcription factors.

3) We have developed a shape transformable nanocarrier based on the DNA NC for plasma membrane targeted delivery of a cancer apoptosis inducing cytokine. The property of nanoparticles to enter cells easily through endocytosis pathways has been beneficial to the delivery of cargos that need to reach intracellular compartments. However, in cases where the therapeutic molecule need to stay outside the cells, such as clinging onto the plasma membrane, intracellular uptake could compromise the therapeutic efficacy. We chose the TRAIL as a model therapeutic molecule since it can selectively induce apoptosis signaling in

cancer cells, meanwhile its plasma membrane bound form is more potent in apoptosis signaling than its internalized form. The endocytosis of cells is a very potent process and it has been challenging to design nanoscaled particles that resist being internalized by cancer cells. From the perspective of the subcellular locus targeted delivery, the complementary DNA NC based system is novel since it demonstrated a strategy for constructing nanoparticles that could avoid being internalized when reaching the target cells. To load the His-tagged TRAIL onto the DNA NC, Ni²⁺ was modified onto the DNA NC using an amine group incorporated during the rolling circle amplification as the anchorage point. To control the timing for the contact of the complementary DNA NC, a liposome shell that could be degraded by tumor associated phospholipase A2 was coated onto the TRAIL loaded DNA NC. We observed that the liposome shell could efficiently cage the TRAIL loaded DNA NC for responsive drug release after exposure to phospholipase. Complementary DNA NC released from two separated liposomes were observed to hybridize into micro-scaled fibers, which could avoid the uptake mechanism of cancer cells. Membrane bound form of the administered TRAIL was increased from 42% to 76% after DNA NC hybridization. A significant reduction in IC₅₀ values were also observed correspondingly from 14 ng/mL to 7.8 ng/mL in *in vitro* cytotoxicity study.

In this dissertation, we showed pre-clinical investigations demonstrating the application of DNA NC as a platform for the delivery of multiple types of therapeutic molecules. The aim of the study was to translate the pre-clinical studies into therapeutic

applications. To achieve this goal, we will learn from the lessons gained from FDA approved nanoformulation. We will take actions from the following perspectives:

1) Further understanding the physiology behind diseases [641]. Theoretically, diseases are caused by a combination of perturbances to the complex molecular system of patients. The same disease might be caused through different pathways in different patients and the genetic variations among patients further complicate the outcome of a therapy. In 2015, the federal government announced the Precision Medicine Initiative for optimized therapies based on the genetic and molecular analysis of a patient [642]. In this context, a more rational match between the patient and the tested therapy holds the promise to improve translational rates. Moreover, individual patient-responsive medications can be expected when taking systematic data analysis into account associated with the patient's physiological conditions.

2) Generation of more accurate animal models. Animal models are often used to see drugs or formulations when promising animal study data failed in human tests [643, 644]. Apart from the flaws in design of animal or human study, larger error could be introduced due to the incapability of animal models to accurately reflect the disease in humans [645]. For example, the expressway for tumor-targeted drug delivery – the EPR effect - is not as robust in human subjects as in preclinical animal model [646]; overexpression of receptors could be transient and the fluctuating receptor density would significantly compromise

targeted nanomedicine.

3) Engineering smart but simple formulations. Structurally simplified formulations are more competitive than complicated ones from the perspective of quality control. The pursuit of multifunctional nanomedicine often results in the appendage of extra functional modules. One more component in the nano-formulation not only raises the total cost but also increases the challenge in characterization, scalability and reproducibility.

4) Interdisciplinary collaboration [647]. The field of nanomedicine is multidisciplinary in that it requires knowledge and skills from different areas (life science, material science, chemical engineering, mechanical engineering). It is impossible for any researcher with a single background to realize the process from conception to market. A team composed of experts from different areas is necessary for nanomedicine development. Collaboration between academia and pharmaceutical companies is also an important link for connecting frontier technologies with commercialization channels.

REFERENCES

1. Rosen H, Atribat T. The rise and rise of drug delivery. *Nat. Rev. Drug Discov.* 2005; 4: 381-5.
2. Peluffo H, Unzueta U, Negro-Demontel ML, et al. BBB-targeting, protein-based nanomedicines for drug and nucleic acid delivery to the CNS. *Biotechnol Adv* 2015; 33: 277-87.
3. Nair M, Jayant RD, Kaushik A, et al. Getting into the brain: Potential of nanotechnology in the management of NeuroAIDS. *Adv Drug Deliv Rev* 2016; 103: 202-17.
4. Fox CB, Kim J, Le LV, et al. Micro/nanofabricated platforms for oral drug delivery. *J. Control. Release* 2015; 219: 431-44.
5. Williams AC, Barry BW. Penetration enhancers. *Adv. Drug Del. Rev.* 2012; 64, Supplement: 128-37.
6. Cutler DM, Everett W. Thinking outside the pillbox--medication adherence as a priority for health care reform. *N. Engl. J. Med.* 2010; 362: 1553-5.
7. Truong-Le V, Lovalenti PM, Abdul-Fattah AM. Stabilization challenges and formulation strategies associated with oral biologic drug delivery systems. *Adv Drug Deliv Rev* 2015; 93: 95-108.
8. Martin AR, Finlay WH. Nebulizers for drug delivery to the lungs. *Expert Opin Drug Deliv* 2015; 12: 889-900.
9. Farra R, Sheppard NF, McCabe L, et al. First-in-Human Testing of a Wirelessly Controlled Drug Delivery Microchip. *Sci. Transl. Med.* 2012; 4: 122ra21.

10. Wessely R. New drug-eluting stent concepts. *Nat Rev Cardiol* 2010; 7: 194-203.
11. Park J, Park J, Pei Y, et al. Pharmacokinetics and biodistribution of recently-developed siRNA nanomedicines. *Adv Drug Deliv Rev* 2015; 104: 93-109.
12. Hu Q, Sun W, Wang C, et al. Recent advances of cocktail chemotherapy by combination drug delivery systems. *Adv Drug Deliv Rev* 2016; 98: 19-34.
13. Mukker JK, Singh RSP, Derendorf H. Pharmacokinetic and pharmacodynamic implications in inhalable antimicrobial therapy. *Adv. Drug Del. Rev.* 2015; 85: 57-64.
14. Langer R. Drug delivery and targeting. *Nature* 1998; 392: 5-10.
15. Valencia PM, Farokhzad OC, Karnik R, et al. Microfluidic technologies for accelerating the clinical translation of nanoparticles. *Nat. Nanotechnol.* 2012; 7: 623-9.
16. Santini JJT, Richards AC, Scheidt R, et al. Microchips as Controlled Drug-Delivery Devices. *Angew. Chem. Int. Ed.* 2000; 39: 2396-407.
17. Ranquin A, Versées W, Meier W, et al. Therapeutic Nanoreactors: Combining Chemistry and Biology in a Novel Triblock Copolymer Drug Delivery System. *Nano Lett.* 2005; 5: 2220-4.
18. Siepmann J, Peppas NA. Modeling of drug release from delivery systems based on hydroxypropyl methylcellulose (HPMC). *Adv. Drug Del. Rev.* 2012; 64, Supplement: 163-74.
19. Huebsch N, Kearney CJ, Zhao X, et al. Ultrasound-triggered disruption and self-healing of reversibly cross-linked hydrogels for drug delivery and enhanced chemotherapy. *Proc. Natl. Acad. Sci. U. S. A.* 2014; 111: 9762-7.

20. Danino T, Mondragon-Palomino O, Tsimring L, et al. A synchronized quorum of genetic clocks. *Nature* 2010; 463: 326-30.
21. Fais S, O'Driscoll L, Borrás FE, et al. Evidence-Based Clinical Use of Nanoscale Extracellular Vesicles in Nanomedicine. *ACS Nano* 2016
22. Tibbitt MW, Dahlman JE, Langer R. Emerging Frontiers in Drug Delivery. *J. Am. Chem. Soc.* 2016; 138: 704-17.
23. Banks WA. From blood-brain barrier to blood-brain interface: new opportunities for CNS drug delivery. *Nat. Rev. Drug Discov.* 2016; 15: 275-96.
24. Park K. Facing the Truth about Nanotechnology in Drug Delivery. *ACS Nano* 2013; 7: 7442-7.
25. Peppas NA. Historical perspective on advanced drug delivery: How engineering design and mathematical modeling helped the field mature. *Adv. Drug Del. Rev.* 2013; 65: 5-9.
26. Moroz E, Matorri S, Leroux J-C. Oral delivery of macromolecular drugs: Where we are after almost 100 years of attempts. *Adv. Drug Del. Rev.* 2016; 101: 108-21.
27. Wiedersberg S, Guy RH. Transdermal drug delivery: 30 + years of war and still fighting! *J. Control. Release* 2014; 190: 150-6.
28. Uhrich KE, Cannizzaro SM, Langer RS, et al. Polymeric systems for controlled drug release. *Chem. Rev.* 1999; 99: 3181-98.
29. Park K. Controlled drug delivery systems: Past forward and future back. *J. Control. Release* 2014; 190: 3-8.

30. Santus G, Baker RW. Osmotic drug delivery: a review of the patent literature. *J. Control. Release* 1995; 35: 1-21.
31. Peppas NA, Hilt JZ, Khademhosseini A, et al. Hydrogels in Biology and Medicine: From Molecular Principles to Bionanotechnology. *Adv. Mater.* 2006; 18: 1345-60.
32. Farokhzad OC, Langer R. Impact of Nanotechnology on Drug Delivery. *ACS Nano* 2009; 3: 16-20.
33. Traverso G, Langer R. Engineering precision. *Sci. Transl. Med.* 2015; 7: 289ed6-ed6.
34. Langer R, Weissleder R. Scientific discovery and the future of medicine. *JAMA* 2015; 313: 135-6.
35. Coombes RC. Drug testing in the patient: Toward personalized cancer treatment. *Sci. Transl. Med.* 2015; 7: 284ps10.
36. Collins FS, Varmus H. A New Initiative on Precision Medicine. *N. Engl. J. Med.* 2015; 372: 793-5.
37. Mirnezami R, Nicholson J, Darzi A. Preparing for Precision Medicine. *N. Engl. J. Med.* 2012; 366: 489-91.
38. Davis ME, Zuckerman JE, Choi CHJ, et al. Evidence of RNAi in humans from systemically administered siRNA via targeted nanoparticles. *Nature* 2010; 464: 1067-70.
39. Vogelstein B, Papadopoulos N, Velculescu VE, et al. Cancer Genome Landscapes. *Science* 2013; 339: 1546-58.

40. Mitragotri S, Burke PA, Langer R. Overcoming the challenges in administering biopharmaceuticals: formulation and delivery strategies. *Nat. Rev. Drug Discov.* 2014; 13: 655-72.
41. Hamidi M, Azadi A, Rafiei P, et al. A pharmacokinetic overview of nanotechnology-based drug delivery systems: an ADME-oriented approach. *Crit. Rev. Ther. Drug Carrier Syst.* 2013; 30: 435-67.
42. Zolnik BS, Sadrieh N. Regulatory perspective on the importance of ADME assessment of nanoscale material containing drugs. *Adv. Drug Del. Rev.* 2009; 61: 422-7.
43. Gu Z, Biswas A, Zhao M, et al. Tailoring nanocarriers for intracellular protein delivery. *Chem. Soc. Rev.* 2011; 40: 3638-55.
44. Ernsting MJ, Murakami M, Roy A, et al. Factors controlling the pharmacokinetics, biodistribution and intratumoral penetration of nanoparticles. *J. Control. Release* 2013; 172: 782-94.
45. Hoffman AS. The origins and evolution of “controlled” drug delivery systems. *J. Control. Release* 2008; 132: 153-63.
46. Pillai O, Dhanikula AB, Panchagnula R. Drug delivery: an odyssey of 100 years. *Curr. Opin. Chem. Biol.* 2001; 5: 439-46.
47. Morishita M, Peppas NA. Is the oral route possible for peptide and protein drug delivery? *Drug Discovery Today* 2006; 11: 905-10.

48. Lukyanov AN, Torchilin VP. Micelles from lipid derivatives of water-soluble polymers as delivery systems for poorly soluble drugs. *Adv. Drug Del. Rev.* 2004; 56: 1273-89.
49. Love KT, Mahon KP, Levins CG, et al. Lipid-like materials for low-dose, in vivo gene silencing. *Proc. Natl. Acad. Sci. U. S. A.* 2010; 107: 1864-9.
50. Merisko-Liversidge E, Liversidge GG, Cooper ER. Nanosizing: a formulation approach for poorly-water-soluble compounds. *Eur. J. Pharm. Sci.* 2003; 18: 113-20.
51. Keck CM, Müller RH. Drug nanocrystals of poorly soluble drugs produced by high pressure homogenisation. *Eur. J. Pharm. Biopharm.* 2006; 62: 3-16.
52. Boles MA, Ling D, Hyeon T, et al. The surface science of nanocrystals. *Nat. Mater.* 2016; 15: 141-53.
53. Pouton CW. Formulation of self-emulsifying drug delivery systems. *Adv. Drug Del. Rev.* 1997; 25: 47-58.
54. Kang J, Kumar V, Yang D, et al. Cyclodextrin complexation: influence on the solubility, stability, and cytotoxicity of camptothecin, an antineoplastic agent. *Eur. J. Pharm. Sci.* 2002; 15: 163-70.
55. Palakurthi S. Challenges in SN38 drug delivery: current success and future directions. *Expert Opin Drug Deliv* 2015: 1-11.
56. Davis ME, Brewster ME. Cyclodextrin-based pharmaceuticals: past, present and future. *Nat. Rev. Drug Discov.* 2004; 3: 1023-35.

57. Ruddy K, Mayer E, Partridge A. Patient adherence and persistence with oral anticancer treatment. *CA. Cancer J. Clin.* 2009; 59: 56-66.
58. Yan L, Yang Y, Zhang W, et al. Advanced Materials and Nanotechnology for Drug Delivery. *Adv. Mater.* 2014; 26: 5533-40.
59. Kim Y-C, Park J-H, Prausnitz MR. Microneedles for drug and vaccine delivery. *Adv. Drug Del. Rev.* 2012; 64: 1547-68.
60. Yu J, Zhang Y, Ye Y, et al. Microneedle-array patches loaded with hypoxia-sensitive vesicles provide fast glucose-responsive insulin delivery. *Proc. Natl. Acad. Sci. U. S. A.* 2015; 112: 8260-5.
61. Rösler A, Vandermeulen GWM, Klok H-A. Advanced drug delivery devices via self-assembly of amphiphilic block copolymers. *Adv. Drug Del. Rev.* 2012; 64, Supplement: 270-9.
62. Peer D, Karp JM, Hong S, et al. Nanocarriers as an emerging platform for cancer therapy. *Nat. Nanotechnol.* 2007; 2: 751-60.
63. Allen TM, Cullis PR. Drug Delivery Systems: Entering the Mainstream. *Science* 2004; 303: 1818-22.
64. Zolot RS, Basu S, Million RP. Antibody-drug conjugates. *Nat. Rev. Drug Discov.* 2013; 12: 259-60.
65. Won Y-W, Adhikary PP, Lim KS, et al. Oligopeptide complex for targeted non-viral gene delivery to adipocytes. *Nat. Mater.* 2014; 13: 1157-64.

66. Lee K, Rafi M, Wang X, et al. In vivo delivery of transcription factors with multifunctional oligonucleotides. *Nat. Mater.* 2015; 14: 701-6.
67. Nair JK, Willoughby JLS, Chan A, et al. Multivalent N-Acetylgalactosamine-Conjugated siRNA Localizes in Hepatocytes and Elicits Robust RNAi-Mediated Gene Silencing. *J. Am. Chem. Soc.* 2014; 136: 16958-61.
68. Matsuda S, Keiser K, Nair JK, et al. siRNA Conjugates Carrying Sequentially Assembled Trivalent N-Acetylgalactosamine Linked Through Nucleosides Elicit Robust Gene Silencing In Vivo in Hepatocytes. *ACS chemical biology* 2015; 10: 1181-7.
69. Lu Y, Sun W, Gu Z. Stimuli-responsive nanomaterials for therapeutic protein delivery. *J. Control. Release* 2014; 194: 1-19.
70. Mo R, Jiang T, Di J, et al. Emerging micro- and nanotechnology based synthetic approaches for insulin delivery. *Chem. Soc. Rev.* 2014; 43: 3595-629.
71. Zaykov AN, Mayer JP, DiMarchi RD. Pursuit of a perfect insulin. *Nat. Rev. Drug Discov.* 2016; 15: 425-39.
72. Veisheh O, Tang BC, Whitehead KA, et al. Managing diabetes with nanomedicine: challenges and opportunities. *Nat. Rev. Drug Discov.* 2015; 14: 45-57.
73. Liu J, Huang Y, Kumar A, et al. pH-sensitive nano-systems for drug delivery in cancer therapy. *Biotechnol Adv* 2014; 32: 693-710.
74. Sung HW, Sonaje K, Liao ZX, et al. pH-responsive nanoparticles shelled with chitosan for oral delivery of insulin: from mechanism to therapeutic applications. *Acc Chem Res* 2012; 45: 619-29.

75. Pang X, Jiang Y, Xiao Q, et al. pH-responsive polymer–drug conjugates: Design and progress. *J. Control. Release* 2016; 222: 116-29.
76. Kanamala M, Wilson WR, Yang M, et al. Mechanisms and biomaterials in pH-responsive tumour targeted drug delivery: A review. *Biomaterials* 2016; 85: 152-67.
77. Phillips DJ, Gibson MI. Redox-sensitive materials for drug delivery: targeting the correct intracellular environment, tuning release rates, and appropriate predictive systems. *Antioxid Redox Signal* 2014; 21: 786-803.
78. McCarley RL. Redox-responsive delivery systems. *Annu Rev Anal Chem* 2012; 5: 391-411.
79. Gauthier MA. Redox-responsive drug delivery. *Antioxid Redox Signal* 2014; 21: 705-6.
80. Huo M, Yuan J, Tao L, et al. Redox-responsive polymers for drug delivery: from molecular design to applications. *Polym. Chem.* 2014; 5: 1519-28.
81. Barve A, Jin W, Cheng K. Prostate cancer relevant antigens and enzymes for targeted drug delivery. *J Control Release* 2014; 187: 118-32.
82. Hu Q, Katti PS, Gu Z. Enzyme-responsive nanomaterials for controlled drug delivery. *Nanoscale* 2014; 6: 12273-86.
83. Sun W, Gu Z. ATP-Responsive Drug Delivery Systems. *Expert Opin. Drug Del.* 2016; 13: 311-4.
84. Wang B, He X, Zhang Z, et al. Metabolism of Nanomaterials in Vivo: Blood Circulation and Organ Clearance. *Acc. Chem. Res.* 2013; 46: 761-9.

85. Wachter VJ, Salphati L, Benet LZ. Active secretion and enterocytic drug metabolism barriers to drug absorption. *Adv. Drug Del. Rev.* 2001; 46: 89-102.
86. Wilkinson GR. Drug Metabolism and Variability among Patients in Drug Response. *N. Engl. J. Med.* 2005; 352: 2211-21.
87. Thummel KE, Kunze KL, Shen DD. Enzyme-catalyzed processes of first-pass hepatic and intestinal drug extraction. *Adv. Drug Del. Rev.* 1997; 27: 99-127.
88. Prausnitz MR, Langer R. Transdermal drug delivery. *Nat. Biotechnol.* 2008; 26: 1261-8.
89. Hearnden V, Sankar V, Hull K, et al. New developments and opportunities in oral mucosal drug delivery for local and systemic disease. *Adv. Drug Del. Rev.* 2012; 64: 16-28.
90. Illum L. Nasal drug delivery—possibilities, problems and solutions. *J. Control. Release* 2003; 87: 187-98.
91. Nunes R, Sarmiento B, das Neves J. Formulation and delivery of anti-HIV rectal microbicides: advances and challenges. *J Control Release* 2014; 194: 278-94.
92. Rodriguez-Gascon A, Del Pozo-Rodriguez A, Isla A, et al. Vaginal gene therapy. *Adv Drug Deliv Rev* 2015; 92: 71-83.
93. Ali Khan A, Mudassir J, Mohtar N, et al. Advanced drug delivery to the lymphatic system: lipid-based nanoformulations. *International journal of nanomedicine* 2013; 8: 2733-44.
94. Morrissey KM, Stocker SL, Wittwer MB, et al. Renal Transporters in Drug Development. *Annu. Rev. Pharmacool. Toxicol.* 2013; 53: 503-29.

95. Williams M, Ginhoux F, Jakubzick C, et al. Dendritic cells, monocytes and macrophages: a unified nomenclature based on ontogeny. *Nat. Rev. Immunol.* 2014; 14: 571-8.
96. Yan M, Du J, Gu Z, et al. A novel intracellular protein delivery platform based on single-protein nanocapsules. *Nat. Nanotechnol.* 2010; 5: 48-53.
97. Gu Z, Biswas A, Joo KI, et al. Probing protease activity by single-fluorescent-protein nanocapsules. *Chem. Commun.* 2010; 46: 6467-9.
98. Sun W, Jiang T, Lu Y, et al. Cocoon-Like Self-Degradable DNA Nanoclew for Anticancer Drug Delivery. *J. Am. Chem. Soc.* 2014; 136: 14722-5.
99. Liu C, Wen J, Meng Y, et al. Efficient Delivery of Therapeutic miRNA Nanocapsules for Tumor Suppression. *Adv. Mater.* 2014; 27: 292-7.
100. Roberts MJ, Bentley MD, Harris JM. Chemistry for peptide and protein PEGylation. *Adv. Drug Del. Rev.* 2012; 64, Supplement: 116-27.
101. Gu L, Mooney DJ. Biomaterials and emerging anticancer therapeutics: engineering the microenvironment. *Nat. Rev. Cancer.* 2016; 16: 56-66.
102. Langer R, Folkman J. Polymers for the sustained release of proteins and other macromolecules. *Nature* 1976; 263: 797-800.
103. Hou H, Nieto A, Ma F, et al. Tunable sustained intravitreal drug delivery system for daunorubicin using oxidized porous silicon. *J. Control. Release* 2014; 178: 46-54.
104. Loira-Pastoriza C, Todoroff J, Vanbever R. Delivery strategies for sustained drug release in the lungs. *Adv. Drug Del. Rev.* 2014; 75: 81-91.

105. Fakhari A, Anand Subramony J. Engineered in-situ depot-forming hydrogels for intratumoral drug delivery. *J. Control. Release* 2015; 220, Part A: 465-75.
106. Brudno Y, Mooney DJ. On-demand drug delivery from local depots. *J. Control. Release* 2015; 219: 8-17.
107. Schinkel AH, Jonker JW. Mammalian drug efflux transporters of the ATP binding cassette (ABC) family: an overview. *Adv. Drug Del. Rev.* 2003; 55: 3-29.
108. Kirtane AR, Kalscheuer SM, Panyam J. Exploiting nanotechnology to overcome tumor drug resistance: Challenges and opportunities. *Adv. Drug Del. Rev.* 2013; 65: 1731-47.
109. Brannon-Peppas L, Blanchette JO. Nanoparticle and targeted systems for cancer therapy. *Adv. Drug Del. Rev.* 2012; 64, Supplement: 206-12.
110. Dean M, Fojo T, Bates S. Tumour stem cells and drug resistance. *Nat. Rev. Cancer.* 2005; 5: 275-84.
111. Hubbell JA, Langer R. Translating materials design to the clinic. *Nat. Mater.* 2013; 12: 963-6.
112. Mitragotri S, Lahann J. Materials for Drug Delivery: Innovative Solutions to Address Complex Biological Hurdles. *Adv. Mater.* 2012; 24: 3717-23.
113. Lindsley CW. The Top Prescription Drugs of 2012 Globally: Biologics Dominate, But Small Molecule CNS Drugs Hold on to Top Spots. *ACS Chemical Neuroscience* 2013; 4: 905-7.
114. Imming P, Sinning C, Meyer A. Drugs, their targets and the nature and number of drug targets. *Nat. Rev. Drug Discov.* 2006; 5: 821-34.

115. Nero TL, Morton CJ, Holien JK, et al. Oncogenic protein interfaces: small molecules, big challenges. *Nat. Rev. Cancer*. 2014; 14: 248-62.
116. Mullard A. 2014 FDA drug approvals. *Nat. Rev. Drug Discov*. 2015; 14: 77-81.
117. Radivojac P, Clark WT, Oron TR, et al. A large-scale evaluation of computational protein function prediction. *Nat Meth* 2013; 10: 221-7.
118. Leader B, Baca QJ, Golan DE. Protein therapeutics: a summary and pharmacological classification. *Nat. Rev. Drug Discov*. 2008; 7: 21-39.
119. Vogel FR, Sarver N. Nucleic acid vaccines. *Clin. Microbiol. Rev*. 1995; 8: 406-10.
120. Simonato M, Bennett J, Boulis NM, et al. Progress in gene therapy for neurological disorders. *Nat Rev Neurol* 2013; 9: 277-91.
121. Kershaw MH, Westwood JA, Darcy PK. Gene-engineered T cells for cancer therapy. *Nat. Rev. Cancer*. 2013; 13: 525-41.
122. Askari FK, McDonnell WM. Antisense-Oligonucleotide Therapy. *N. Engl. J. Med*. 1996; 334: 316-8.
123. Zuckerman JE, Davis ME. Clinical experiences with systemically administered siRNA-based therapeutics in cancer. *Nat. Rev. Drug Discov*. 2015; 14: 843-56.
124. Cech Thomas R, Steitz Joan A. The Noncoding RNA Revolution—Trashing Old Rules to Forge New Ones. *Cell* 2014; 157: 77-94.
125. Lam JKW, Chow MYT, Zhang Y, et al. siRNA Versus miRNA as Therapeutics for Gene Silencing. *Mol Ther Nucleic Acids* 2015; 4: e252.

126. Cheng CJ, Bahal R, Babar IA, et al. MicroRNA silencing for cancer therapy targeted to the tumour microenvironment. *Nature* 2015; 518: 107-10.
127. Scholz C, Wagner E. Therapeutic plasmid DNA versus siRNA delivery: Common and different tasks for synthetic carriers. *J. Control. Release* 2012; 161: 554-65.
128. Sahin U, Kariko K, Tureci O. mRNA-based therapeutics [mdash] developing a new class of drugs. *Nat. Rev. Drug Discov.* 2014; 13: 759-80.
129. Zangi L, Lui KO, von Gise A, et al. Modified mRNA directs the fate of heart progenitor cells and induces vascular regeneration after myocardial infarction. *Nat. Biotechnol.* 2013; 31: 898-907.
130. Cox DBT, Platt RJ, Zhang F. Therapeutic genome editing: prospects and challenges. *Nat. Med.* 2015; 21: 121-31.
131. Mali P, Esvelt KM, Church GM. Cas9 as a versatile tool for engineering biology. *Nat Meth* 2013; 10: 957-63.
132. Guo X, Huang L. Recent Advances in Nonviral Vectors for Gene Delivery. *Acc. Chem. Res.* 2012; 45: 971-9.
133. Kanasty R, Dorkin JR, Vegas A, et al. Delivery materials for siRNA therapeutics. *Nat. Mater.* 2013; 12: 967-77.
134. Yin H, Kanasty RL, Eltoukhy AA, et al. Non-viral vectors for gene-based therapy. *Nat. Rev. Genet.* 2014; 15: 541-55.
135. Earl PL, Americo JL, Wyatt LS, et al. Immunogenicity of a highly attenuated MVA smallpox vaccine and protection against monkeypox. *Nature* 2004; 428: 182-5.

136. Greco D, Salmaso S, Mastrantonio P, et al. A Controlled Trial of Two Acellular Vaccines and One Whole-Cell Vaccine against Pertussis. *N. Engl. J. Med.* 1996; 334: 341-9.
137. Lu W, Arraes LC, Ferreira WT, et al. Therapeutic dendritic-cell vaccine for chronic HIV-1 infection. *Nat. Med.* 2004; 10: 1359-65.
138. de Gruijl T, van den Eertwegh AM, Pinedo H, et al. Whole-cell cancer vaccination: from autologous to allogeneic tumor- and dendritic cell-based vaccines. *Cancer Immunol. Immunother.* 2008; 57: 1569-77.
139. Grupp SA, Kalos M, Barrett D, et al. Chimeric Antigen Receptor–Modified T Cells for Acute Lymphoid Leukemia. *N. Engl. J. Med.* 2013; 368: 1509-18.
140. Orive G, Santos E, Pedraz JL, et al. Application of cell encapsulation for controlled delivery of biological therapeutics. *Adv. Drug Del. Rev.* 2014; 67–68: 3-14.
141. Porter CJH, Trevaskis NL, Charman WN. Lipids and lipid-based formulations: optimizing the oral delivery of lipophilic drugs. *Nat. Rev. Drug Discov.* 2007; 6: 231-48.
142. Kearney CJ, Mooney DJ. Macroscale delivery systems for molecular and cellular payloads. *Nat. Mater.* 2013; 12: 1004-17.
143. Ayoob AM, Borenstein JT. The role of intracochlear drug delivery devices in the management of inner ear disease. *Expert Opin Drug Deliv* 2015; 12: 465-79.
144. Kovatchev BP, Renard E, Cobelli C, et al. Safety of outpatient closed-loop control: first randomized crossover trials of a wearable artificial pancreas. *Diabetes Care* 2014; 37: 1789-96.

145. Ugwoke MI, Agu RU, Verbeke N, et al. Nasal mucoadhesive drug delivery: Background, applications, trends and future perspectives. *Adv. Drug Del. Rev.* 2005; 57: 1640-65.
146. Trajkovski B, Petersen A, Strube P, et al. Intra-operatively customized implant coating strategies for local and controlled drug delivery to bone. *Adv. Drug Del. Rev.* 2012; 64: 1142-51.
147. Kleiner LW, Wright JC, Wang Y. Evolution of implantable and insertable drug delivery systems. *J. Control. Release* 2014; 181: 1-10.
148. Webber MJ, Appel EA, Meijer EW, et al. Supramolecular biomaterials. *Nat. Mater.* 2016; 15: 13-26.
149. Delplace V, Nicolas J. Degradable vinyl polymers for biomedical applications. *Nat. Chem.* 2015; 7: 771-84.
150. Folkman J, Long DM. The use of silicone rubber as a carrier for prolonged drug therapy. *J. Surg. Res.* 1964; 4: 139-42.
151. Stevenson CL, Santini Jr JT, Langer R. Reservoir-based drug delivery systems utilizing microtechnology. *Adv. Drug Del. Rev.* 2012; 64: 1590-602.
152. Liechty WB, Kryscio DR, Slaughter BV, et al. Polymers for Drug Delivery Systems. *Annual Review of Chemical and Biomolecular Engineering* 2010; 1: 149-73.
153. Qiu Y, Park K. Environment-sensitive hydrogels for drug delivery. *Adv. Drug Del. Rev.* 2012; 64, Supplement: 49-60.

154. Moon JJ, Huang B, Irvine DJ. Engineering Nano- and Microparticles to Tune Immunity. *Adv. Mater.* 2012; 24: 3724-46.
155. Gu Z, Dang TT, Ma M, et al. Glucose-Responsive Microgels Integrated with Enzyme Nanocapsules for Closed-Loop Insulin Delivery. *ACS Nano* 2013; 7: 6758-66.
156. Maeda H. Toward a full understanding of the EPR effect in primary and metastatic tumors as well as issues related to its heterogeneity. *Adv Drug Deliv Rev* 2015; 91: 3-6.
157. Prabhakar U, Maeda H, Jain RK, et al. Challenges and Key Considerations of the Enhanced Permeability and Retention Effect for Nanomedicine Drug Delivery in Oncology. *Cancer Res.* 2013; 73: 2412-7.
158. Marguet M, Bonduelle C, Lecommandoux S. Multicompartmentalized polymeric systems: towards biomimetic cellular structure and function. *Chem. Soc. Rev.* 2013; 42: 512-29.
159. Azzopardi EA, Ferguson EL, Thomas DW. The enhanced permeability retention effect: a new paradigm for drug targeting in infection. *J. Antimicrob. Chemother.* 2013; 68: 257-74.
160. Marti CN, Gheorghide M, Kalogeropoulos AP, et al. Endothelial dysfunction, arterial stiffness, and heart failure. *J. Am. Coll. Cardiol.* 2012; 60: 1455-69.
161. Zhang L, Gu FX, Chan JM, et al. Nanoparticles in Medicine: Therapeutic Applications and Developments. *Clin. Pharmacol. Ther.* 2008; 83: 761-9.
162. Lamprecht A. Nanomedicines in gastroenterology and hepatology. *Nat Rev Gastroenterol Hepatol* 2015; 12: 195-204.

163. Chow EK-H, Ho D. Cancer Nanomedicine: From Drug Delivery to Imaging. *Sci. Transl. Med.* 2013; 5: 216rv4.
164. Godwin H, Nameth C, Avery D, et al. Nanomaterial categorization for assessing risk potential to facilitate regulatory decision-making. *ACS Nano* 2015; 9: 3409-17.
165. Appel EA, del Barrio J, Loh XJ, et al. Supramolecular polymeric hydrogels. *Chem. Soc. Rev.* 2012; 41: 6195-214.
166. Chacko RT, Ventura J, Zhuang J, et al. Polymer nanogels: A versatile nanoscopic drug delivery platform. *Adv. Drug Del. Rev.* 2012; 64: 836-51.
167. Pattni BS, Chupin VV, Torchilin VP. New Developments in Liposomal Drug Delivery. *Chem. Rev.* 2015; 115: 10938-66.
168. Akinc A, Zumbuehl A, Goldberg M, et al. A combinatorial library of lipid-like materials for delivery of RNAi therapeutics. *Nat. Biotechnol.* 2008; 26: 561-9.
169. Langille MR, Personick ML, Zhang J, et al. Defining Rules for the Shape Evolution of Gold Nanoparticles. *J. Am. Chem. Soc.* 2012; 134: 14542-54.
170. Jans H, Huo Q. Gold nanoparticle-enabled biological and chemical detection and analysis. *Chem. Soc. Rev.* 2012; 41: 2849-66.
171. Mao HY, Laurent S, Chen W, et al. Graphene: Promises, Facts, Opportunities, and Challenges in Nanomedicine. *Chem. Rev.* 2013; 113: 3407-24.
172. Mochalin VN, Shenderova O, Ho D, et al. The properties and applications of nanodiamonds. *Nat. Nanotechnol.* 2012; 7: 11-23.

173. Gao J, Gu H, Xu B. Multifunctional magnetic nanoparticles: design, synthesis, and biomedical applications. *Acc Chem Res* 2009; 42: 1097-107.
174. Lu Y, Hu Q, Lin Y, et al. Transformable liquid-metal nanomedicine. *Nat. Commun.* 2015; 6: 10066.
175. Chen Y-J, Groves B, Muscat RA, et al. DNA nanotechnology from the test tube to the cell. *Nat. Nanotechnol.* 2015; 10: 748-60.
176. Ohta S, Glancy D, Chan WCW. DNA-controlled dynamic colloidal nanoparticle systems for mediating cellular interaction. *Science* 2016; 351: 841-5.
177. Tjong V, Tang L, Zauscher S, et al. "Smart" DNA interfaces. *Chem. Soc. Rev.* 2014; 43: 1612-26.
178. Jones LH. Recent advances in the molecular design of synthetic vaccines. *Nat. Chem.* 2015; 7: 952-60.
179. Jain RK, Stylianopoulos T. Delivering nanomedicine to solid tumors. *Nature reviews. Clinical oncology* 2010; 7: 653-64.
180. Tenzer S, Docter D, Kuharev J, et al. Rapid formation of plasma protein corona critically affects nanoparticle pathophysiology. *Nat. Nanotechnol.* 2013; 8: 772-81.
181. Wan S, Kelly PM, Mahon E, et al. The "Sweet" Side of the Protein Corona: Effects of Glycosylation on Nanoparticle–Cell Interactions. *ACS Nano* 2015; 9: 2157-66.
182. Moghimi SM. Chemical camouflage of nanospheres with a poorly reactive surface: towards development of stealth and target-specific nanocarriers. *Biochim. Biophys. Acta* 2002; 1590: 131-9.

183. Salvati A, Pitek AS, Monopoli MP, et al. Transferrin-functionalized nanoparticles lose their targeting capabilities when a biomolecule corona adsorbs on the surface. *Nat. Nanotechnol.* 2013; 8: 137-43.
184. Inturi S, Wang G, Chen F, et al. Modulatory Role of Surface Coating of Superparamagnetic Iron Oxide Nanoworms in Complement Opsonization and Leukocyte Uptake. *ACS Nano* 2015; 9: 10758-68.
185. Pillai PP, Huda S, Kowalczyk B, et al. Controlled pH Stability and Adjustable Cellular Uptake of Mixed-Charge Nanoparticles. *J. Am. Chem. Soc.* 2013; 135: 6392-5.
186. Harris JM, Chess RB. Effect of pegylation on pharmaceuticals. *Nat. Rev. Drug Discov.* 2003; 2: 214-21.
187. Schottler S, Becker G, Winzen S, et al. Protein adsorption is required for stealth effect of poly(ethylene glycol)- and poly(phosphoester)-coated nanocarriers. *Nat. Nanotechnol.* 2016; 11: 372-7.
188. Klibanov AL, Maruyama K, Torchilin VP, et al. Amphipathic polyethyleneglycols effectively prolong the circulation time of liposomes. *FEBS Lett.* 1990; 268: 235-7.
189. Yang Q, Jones SW, Parker CL, et al. Evading Immune Cell Uptake and Clearance Requires PEG Grafting at Densities Substantially Exceeding the Minimum for Brush Conformation. *Mol. Pharm.* 2014; 11: 1250-8.
190. Li SD, Huang L. Stealth nanoparticles: high density but sheddable PEG is a key for tumor targeting. *J Control Release* 2010; 145: 178-81.

191. Jiang S, Cao Z. Ultralow-Fouling, Functionalizable, and Hydrolyzable Zwitterionic Materials and Their Derivatives for Biological Applications. *Adv. Mater.* 2010; 22: 920-32.
192. Zhang L, Cao Z, Bai T, et al. Zwitterionic hydrogels implanted in mice resist the foreign-body reaction. *Nat. Biotechnol.* 2013; 31: 553-6.
193. Hu C-MJ, Fang RH, Wang K-C, et al. Nanoparticle biointerfacing by platelet membrane cloaking. *Nature* 2015; 526: 118-21.
194. Hu Q, Sun W, Qian C, et al. Anticancer Platelet-Mimicking Nanovehicles. *Adv. Mater.* 2015; 27: 7043-50.
195. Hu Q, Qian C, Sun W, et al. Engineered Nanoplatelets for Enhanced Treatment of Multiple Myeloma and Thrombus. *Adv. Mater.* 2016; doi: 10.1002/adhm.201603463
196. Anselmo AC, Modery-Pawlowski CL, Menegatti S, et al. Platelet-like Nanoparticles: Mimicking Shape, Flexibility, and Surface Biology of Platelets To Target Vascular Injuries. *ACS Nano* 2014; 8: 11243-53.
197. Rodriguez PL, Harada T, Christian DA, et al. Minimal "Self" peptides that inhibit phagocytic clearance and enhance delivery of nanoparticles. *Science* 2013; 339: 971-5.
198. Hamid O, Robert C, Daud A, et al. Safety and Tumor Responses with Lambrolizumab (Anti-PD-1) in Melanoma. *N. Engl. J. Med.* 2013; 369: 134-44.
199. Bachmann MF, Jennings GT. Vaccine delivery: a matter of size, geometry, kinetics and molecular patterns. *Nat. Rev. Immunol.* 2010; 10: 787-96.
200. Hammond PT. Shooting for the Moon: Nanoscale Approaches to Cancer. *ACS Nano* 2016; 10: 1711-3.

201. Seremet T, Brasseur F, Coulie PG. Tumor-specific antigens and immunologic adjuvants in cancer immunotherapy. *Cancer journal (Sudbury, Mass.)* 2011; 17: 325-30.
202. Falo LD, Jr., Kovacsovics-Bankowski M, Thompson K, et al. Targeting antigen into the phagocytic pathway in vivo induces protective tumour immunity. *Nat. Med.* 1995; 1: 649-53.
203. Lynn GM, Laga R, Darrah PA, et al. In vivo characterization of the physicochemical properties of polymer-linked TLR agonists that enhance vaccine immunogenicity. *Nat. Biotechnol.* 2015; 33: 1201-10.
204. Shao K, Singha S, Clemente-Casares X, et al. Nanoparticle-based immunotherapy for cancer. *ACS Nano* 2015; 9: 16-30.
205. Curran MA, Montalvo W, Yagita H, et al. PD-1 and CTLA-4 combination blockade expands infiltrating T cells and reduces regulatory T and myeloid cells within B16 melanoma tumors. *Proc. Natl. Acad. Sci. U. S. A.* 2010; 107: 4275-80.
206. Park J, Wrzesinski SH, Stern E, et al. Combination delivery of TGF- β inhibitor and IL-2 by nanoscale liposomal polymeric gels enhances tumour immunotherapy. *Nat. Mater.* 2012; 11: 895-905.
207. Wang C, Sun W, Wright G, et al. Inflammation-Triggered Cancer Immunotherapy by Programmed Delivery of CpG and Anti-PD1 Antibody. *Adv. Mater.* 2016; 28: 8912–20.
208. Mitchell MJ, Wayne E, Rana K, et al. TRAIL-coated leukocytes that kill cancer cells in the circulation. *Proc. Natl. Acad. Sci. U. S. A.* 2014; 111: 930-5.

209. Dahlman JE, Barnes C, Khan OF, et al. In vivo endothelial siRNA delivery using polymeric nanoparticles with low molecular weight. *Nat. Nanotechnol.* 2014; 9: 648-55.
210. D'Apolito R, Tomaiuolo G, Taraballi F, et al. Red blood cells affect the margination of microparticles in synthetic microcapillaries and intravital microcirculation as a function of their size and shape. *J. Control. Release* 2015; 217: 263-72.
211. Toy R, Hayden E, Shoup C, et al. The effects of particle size, density and shape on margination of nanoparticles in microcirculation. *Nanotechnology* 2011; 22: 115101.
212. Xue W, Dahlman JE, Tammela T, et al. Small RNA combination therapy for lung cancer. *Proc. Natl. Acad. Sci. U. S. A.* 2014; 111: E3553-E61.
213. Blanco E, Shen H, Ferrari M. Principles of nanoparticle design for overcoming biological barriers to drug delivery. *Nat. Biotechnol.* 2015; 33: 941-51.
214. Thompson AJ, Mastria EM, Eniola-Adefeso O. The margination propensity of ellipsoidal micro/nanoparticles to the endothelium in human blood flow. *Biomaterials* 2013; 34: 5863-71.
215. Xu R, Zhang G, Mai J, et al. An injectable nanoparticle generator enhances delivery of cancer therapeutics. *Nat. Biotechnol.* 2016; 34: 414-8.
216. Obermeier B, Daneman R, Ransohoff RM. Development, maintenance and disruption of the blood-brain barrier. *Nat. Med.* 2013; 19: 1584-96.
217. Clapp C, Thebault S, Jeziorski MC, et al. Peptide Hormone Regulation of Angiogenesis. *Physiol. Rev.* 2009; 89: 1177-215.

218. Weis SM, Cheresh DA. Tumor angiogenesis: molecular pathways and therapeutic targets. *Nat. Med.* 2011; 17: 1359-70.
219. Maeda H, Nakamura H, Fang J. The EPR effect for macromolecular drug delivery to solid tumors: Improvement of tumor uptake, lowering of systemic toxicity, and distinct tumor imaging in vivo. *Adv. Drug Del. Rev.* 2013; 65: 71-9.
220. Matsumoto Y, Nichols JW, Toh K, et al. Vascular bursts enhance permeability of tumour blood vessels and improve nanoparticle delivery. *Nat. Nanotechnol.* 2016; 11: 533-8.
221. Barenholz Y. Doxil® — The first FDA-approved nano-drug: Lessons learned. *J. Control. Release* 2012; 160: 117-34.
222. Dosio F, Brusa P, Crosasso P, et al. Preparation, characterization and properties in vitro and in vivo of a paclitaxel–albumin conjugate. *J. Control. Release* 1997; 47: 293-304.
223. Goel S, Duda DG, Xu L, et al. Normalization of the Vasculature for Treatment of Cancer and Other Diseases. *Physiol. Rev.* 2011; 91: 1071-121.
224. Hida K, Maishi N, Sakurai Y, et al. Heterogeneity of tumor endothelial cells and drug delivery. *Adv Drug Deliv Rev* 2016; 99: 140-7.
225. Maas AL, Carter SL, Wileyto EP, et al. Tumor Vascular Microenvironment Determines Responsiveness to Photodynamic Therapy. *Cancer Res.* 2012; 72: 2079-88.
226. Fang J, Nakamura H, Maeda H. The EPR effect: Unique features of tumor blood vessels for drug delivery, factors involved, and limitations and augmentation of the effect. *Adv. Drug Del. Rev.* 2011; 63: 136-51.

227. Carmeliet P, Jain RK. Principles and mechanisms of vessel normalization for cancer and other angiogenic diseases. *Nat. Rev. Drug Discov.* 2011; 10: 417-27.
228. Cabral H, Matsumoto Y, Mizuno K, et al. Accumulation of sub-100 nm polymeric micelles in poorly permeable tumours depends on size. *Nat. Nanotechnol.* 2011; 6: 815-23.
229. Wiig H, Swartz MA. Interstitial Fluid and Lymph Formation and Transport: Physiological Regulation and Roles in Inflammation and Cancer. *Physiol. Rev.* 2012; 92: 1005-60.
230. Trevisan NL, Kaminski LM, Porter CJH. From sewer to saviour [mdash] targeting the lymphatic system to promote drug exposure and activity. *Nat. Rev. Drug Discov.* 2015; 14: 781-803.
231. Swartz MA, Lund AW. Lymphatic and interstitial flow in the tumour microenvironment: linking mechanobiology with immunity. *Nat. Rev. Cancer.* 2012; 12: 210-9.
232. Tong RT, Boucher Y, Kozin SV, et al. Vascular normalization by vascular endothelial growth factor receptor 2 blockade induces a pressure gradient across the vasculature and improves drug penetration in tumors. *Cancer Res.* 2004; 64: 3731-6.
233. Jussila L, Alitalo K. Vascular Growth Factors and Lymphangiogenesis. *Physiol. Rev.* 2002; 82: 673-700.
234. Chauhan VP, Martin JD, Liu H, et al. Angiotensin inhibition enhances drug delivery and potentiates chemotherapy by decompressing tumour blood vessels. *Nat. Commun.* 2013;

235. Stylianopoulos T, Jain RK. Combining two strategies to improve perfusion and drug delivery in solid tumors. *Proc. Natl. Acad. Sci. U. S. A.* 2013; 110: 18632-7.
236. Lu P, Weaver VM, Werb Z. The extracellular matrix: a dynamic niche in cancer progression. *J. Cell Biol.* 2012; 196: 395-406.
237. Mouw JK, Ou G, Weaver VM. Extracellular matrix assembly: a multiscale deconstruction. *Nat. Rev. Mol. Cell. Biol.* 2014; 15: 771-85.
238. Paszek MJ, DuFort CC, Rossier O, et al. The cancer glycocalyx mechanically primes integrin-mediated growth and survival. *Nature* 2014; 511: 319-25.
239. Quail DF, Joyce JA. Microenvironmental regulation of tumor progression and metastasis. *Nat. Med.* 2013; 19: 1423-37.
240. Bonnans C, Chou J, Werb Z. Remodelling the extracellular matrix in development and disease. *Nat. Rev. Mol. Cell. Biol.* 2014; 15: 786-801.
241. Chaudhuri O, Koshy ST, Branco da Cunha C, et al. Extracellular matrix stiffness and composition jointly regulate the induction of malignant phenotypes in mammary epithelium. *Nat. Mater.* 2014; 13: 970-8.
242. Ronnov-Jessen L, Petersen OW, Bissell MJ. Cellular changes involved in conversion of normal to malignant breast: importance of the stromal reaction. *Physiol. Rev.* 1996; 76: 69-125.
243. Arnaoutova I, Kleinman HK. In vitro angiogenesis: endothelial cell tube formation on gelled basement membrane extract. *Nat. Protocols* 2010; 5: 628-35.

244. Albanese A, Lam AK, Sykes EA, et al. Tumour-on-a-chip provides an optical window into nanoparticle tissue transport. *Nat. Commun.* 2013; 4
245. Li C. A targeted approach to cancer imaging and therapy. *Nat. Mater.* 2014; 13: 110-5.
246. Sykes EA, Dai Q, Sarsons CD, et al. Tailoring nanoparticle designs to target cancer based on tumor pathophysiology. *Proc. Natl. Acad. Sci. U. S. A.* 2016; 113: E1142-E51.
247. Vandenbroucke RE, Libert C. Is there new hope for therapeutic matrix metalloproteinase inhibition? *Nat. Rev. Drug Discov.* 2014; 13: 904-27.
248. Orgaz JL, Pandya P, Dalmeida R, et al. Diverse matrix metalloproteinase functions regulate cancer amoeboid migration. *Nat. Commun.* 2014; 5
249. Seo BR, DelNero P, Fischbach C. In vitro models of tumor vessels and matrix: Engineering approaches to investigate transport limitations and drug delivery in cancer. *Adv. Drug Del. Rev.* 2014; 69-70: 205-16.
250. Chauhan Vikash P, Boucher Y, Ferrone Cristina R, et al. Compression of Pancreatic Tumor Blood Vessels by Hyaluronan Is Caused by Solid Stress and Not Interstitial Fluid Pressure. *Cancer Cell* 2014; 26: 14-5.
251. Hallmann R, Zhang X, Di Russo J, et al. The regulation of immune cell trafficking by the extracellular matrix. *Curr. Opin. Cell Biol.* 2015; 36: 54-61.
252. Eikenes L, Tufto I, Schnell EA, et al. Effect of collagenase and hyaluronidase on free and anomalous diffusion in multicellular spheroids and xenografts. *Anticancer Res.* 2010; 30: 359-68.

253. Eikenes L, Tari M, Tufto I, et al. Hyaluronidase induces a transcapillary pressure gradient and improves the distribution and uptake of liposomal doxorubicin (Caelyx) in human osteosarcoma xenografts. *Br. J. Cancer* 2005; 93: 81-8.
254. Zhou H, Fan Z, Deng J, et al. Hyaluronidase Embedded in Nanocarrier PEG Shell for Enhanced Tumor Penetration and Highly Efficient Antitumor Efficacy. *Nano Lett.* 2016
255. Gong H, Chao Y, Xiang J, et al. Hyaluronidase To Enhance Nanoparticle-Based Photodynamic Tumor Therapy. *Nano Lett.* 2016; 16: 2512-21.
256. McGuire S, Yuan F. Improving interstitial transport of macromolecules through reduction in cell volume fraction in tumor tissues. *Nanomedicine* 2012; 8: 1088-95.
257. Magzoub M, Jin S, Verkman AS. Enhanced macromolecule diffusion deep in tumors after enzymatic digestion of extracellular matrix collagen and its associated proteoglycan decorin. *FASEB J.* 2008; 22: 276-84.
258. Lacy P, Stow JL. Cytokine release from innate immune cells: association with diverse membrane trafficking pathways. *Blood* 2011; 118: 9-18.
259. Osborn O, Olefsky JM. The cellular and signaling networks linking the immune system and metabolism in disease. *Nat. Med.* 2012; 18: 363-74.
260. Wei H, Zhuo R-X, Zhang X-Z. Design and development of polymeric micelles with cleavable links for intracellular drug delivery. *Prog. Polym. Sci.* 2013; 38: 503-35.
261. Rajendran L, Knolker H-J, Simons K. Subcellular targeting strategies for drug design and delivery. *Nat. Rev. Drug Discov.* 2010; 9: 29-42.

262. Veber DF, Johnson SR, Cheng H-Y, et al. Molecular Properties That Influence the Oral Bioavailability of Drug Candidates. *J. Med. Chem.* 2002; 45: 2615-23.
263. Panyam J, Labhasetwar V. Biodegradable nanoparticles for drug and gene delivery to cells and tissue. *Adv. Drug Del. Rev.* 2012; 64, Supplement: 61-71.
264. Zhang S, Gao H, Bao G. Physical Principles of Nanoparticle Cellular Endocytosis. *ACS Nano* 2015; 9: 8655-71.
265. Sigismund S, Confalonieri S, Ciliberto A, et al. Endocytosis and Signaling: Cell Logistics Shape the Eukaryotic Cell Plan. *Physiol. Rev.* 2012; 92: 273-366.
266. McMahon HT, Boucrot E. Molecular mechanism and physiological functions of clathrin-mediated endocytosis. *Nat. Rev. Mol. Cell. Biol.* 2011; 12: 517-33.
267. Commisso C, Davidson SM, Soydaner-Azeloglu RG, et al. Macropinocytosis of protein is an amino acid supply route in Ras-transformed cells. *Nature* 2013; 497: 633-7.
268. Agarwal R, Roy K. Intracellular delivery of polymeric nanocarriers: a matter of size, shape, charge, elasticity and surface composition. *Therapeutic delivery* 2013; 4: 705-23.
269. Xu S, Olenyuk BZ, Okamoto CT, et al. Targeting receptor-mediated endocytotic pathways with nanoparticles: Rationale and advances. *Adv. Drug Del. Rev.* 2013; 65: 121-38.
270. Herd H, Daum N, Jones AT, et al. Nanoparticle Geometry and Surface Orientation Influence Mode of Cellular Uptake. *ACS Nano* 2013; 7: 1961-73.
271. Mitragotri S, Lahann J. Physical approaches to biomaterial design. *Nat. Mater.* 2009; 8: 15-23.

272. Perry JL, Herlihy KP, Napier ME, et al. PRINT: A Novel Platform Toward Shape and Size Specific Nanoparticle Theranostics. *Acc. Chem. Res.* 2011; 44: 990-8.
273. Semple SC, Akinc A, Chen J, et al. Rational design of cationic lipids for siRNA delivery. *Nat. Biotechnol.* 2010; 28: 172-6.
274. Ruiz de Almodovar C, Lambrechts D, Mazzone M, et al. Role and Therapeutic Potential of VEGF in the Nervous System. *Physiol. Rev.* 2009; 89: 607-48.
275. van Dam GM, Themelis G, Crane LMA, et al. Intraoperative tumor-specific fluorescence imaging in ovarian cancer by folate receptor-[alpha] targeting: first in-human results. *Nat. Med.* 2011; 17: 1315-9.
276. Yu YJ, Atwal JK, Zhang Y, et al. Therapeutic bispecific antibodies cross the blood-brain barrier in nonhuman primates. *Sci Transl Med* 2014; 6: 261ra154.
277. Pinho SS, Reis CA. Glycosylation in cancer: mechanisms and clinical implications. *Nat. Rev. Cancer.* 2015; 15: 540-55.
278. Lin C-Y, Gustafsson J-A. Targeting liver X receptors in cancer therapeutics. *Nat. Rev. Cancer.* 2015; 15: 216-24.
279. Yang Z, Lee JH, Jeon HM, et al. Folate-Based Near-Infrared Fluorescent Theranostic Gemcitabine Delivery. *J. Am. Chem. Soc.* 2013; 135: 11657-62.
280. Pridgen EM, Alexis F, Kuo TT, et al. Transepithelial Transport of Fc-Targeted Nanoparticles by the Neonatal Fc Receptor for Oral Delivery. *Sci. Transl. Med.* 2013; 5: 213ra167.

281. Sugahara KN, Teesalu T, Karmali PP, et al. Coadministration of a tumor-penetrating peptide enhances the efficacy of cancer drugs. *Science* 2010; 328: 1031-5.
282. Xing H, Wong NY, Xiang Y, et al. DNA aptamer functionalized nanomaterials for intracellular analysis, cancer cell imaging and drug delivery. *Curr. Opin. Chem. Biol.* 2012; 16: 429-35.
283. Srinivasarao M, Galliford CV, Low PS. Principles in the design of ligand-targeted cancer therapeutics and imaging agents. *Nat. Rev. Drug Discov.* 2015; 14: 203-19.
284. Bertrand N, Wu J, Xu X, et al. Cancer nanotechnology: The impact of passive and active targeting in the era of modern cancer biology. *Adv. Drug Del. Rev.* 2014; 66: 2-25.
285. Lee H, Lytton-Jean AKR, Chen Y, et al. Molecularly self-assembled nucleic acid nanoparticles for targeted in vivo siRNA delivery. *Nat. Nanotechnol.* 2012; 7: 389-93.
286. Gilleron J, Querbes W, Zeigerer A, et al. Image-based analysis of lipid nanoparticle-mediated siRNA delivery, intracellular trafficking and endosomal escape. *Nat. Biotechnol.* 2013; 31: 638-46.
287. Wittrup A, Ai A, Liu X, et al. Visualizing lipid-formulated siRNA release from endosomes and target gene knockdown. *Nat. Biotechnol.* 2015; 33: 870-6.
288. Sahay G, Querbes W, Alabi C, et al. Efficiency of siRNA delivery by lipid nanoparticles is limited by endocytic recycling. *Nat. Biotechnol.* 2013; 31: 653-8.
289. Settembre C, Ballabio A. Lysosome: regulator of lipid degradation pathways. *Trends Cell Biol.* 2014; 24: 743-50.

290. Wadia JS, Stan RV, Dowdy SF. Transducible TAT-HA fusogenic peptide enhances escape of TAT-fusion proteins after lipid raft macropinocytosis. *Nat. Med.* 2004; 10: 310-5.
291. Wittrup A, Lieberman J. Knocking down disease: a progress report on siRNA therapeutics. *Nat. Rev. Genet.* 2015; 16: 543-52.
292. Erazo-Oliveras A, Najjar K, Dayani L, et al. Protein delivery into live cells by incubation with an endosomolytic agent. *Nat Methods* 2014; 11: 861-7.
293. Benjaminsen RV, Matthebjerg MA, Henriksen JR, et al. The Possible [ldquo]Proton Sponge [rdquo] Effect of Polyethylenimine (PEI) Does Not Include Change in Lysosomal pH. *Mol. Ther.* 2013; 21: 149-57.
294. Ohya T, Miaczynska M, Coskun U, et al. Reconstitution of Rab- and SNARE-dependent membrane fusion by synthetic endosomes. *Nature* 2009; 459: 1091-7.
295. Xu W, Nathwani B, Lin C, et al. A Programmable DNA Origami Platform to Organize SNAREs for Membrane Fusion. *J. Am. Chem. Soc.* 2016; 138: 4439-47.
296. Kim H, Lee D, Kim J, et al. Photothermally Triggered Cytosolic Drug Delivery via Endosome Disruption Using a Functionalized Reduced Graphene Oxide. *ACS Nano* 2013; 7: 6735-46.
297. Pack DW, Hoffman AS, Pun S, et al. Design and development of polymers for gene delivery. *Nat. Rev. Drug Discov.* 2005; 4: 581-93.
298. Hsu CYM, Uludag H. A simple and rapid nonviral approach to efficiently transfect primary tissue-derived cells using polyethylenimine. *Nat. Protocols* 2012; 7: 935-45.

299. Shim MS, Kwon YJ. Efficient and targeted delivery of siRNA in vivo. *FEBS J.* 2010; 277: 4814-27.
300. Alabi CA, Love KT, Sahay G, et al. Multiparametric approach for the evaluation of lipid nanoparticles for siRNA delivery. *Proc Natl Acad Sci U S A* 2013; 110: 12881-6.
301. Nelson CE, Kintzing JR, Hanna A, et al. Balancing Cationic and Hydrophobic Content of PEGylated siRNA Polyplexes Enhances Endosome Escape, Stability, Blood Circulation Time, and Bioactivity in Vivo. *ACS Nano* 2013; 7: 8870-80.
302. Jayaraman M, Ansell SM, Mui BL, et al. Maximizing the Potency of siRNA Lipid Nanoparticles for Hepatic Gene Silencing In Vivo. *Angew. Chem. Int. Ed.* 2012; 51: 8529-33.
303. Zhou K, Nguyen LH, Miller JB, et al. Modular degradable dendrimers enable small RNAs to extend survival in an aggressive liver cancer model. *Proc. Natl. Acad. Sci. U. S. A.* 2016; 113: 520-5.
304. Hao J, Kos P, Zhou K, et al. Rapid Synthesis of a Lipocationic Polyester Library via Ring-Opening Polymerization of Functional Valerolactones for Efficacious siRNA Delivery. *J. Am. Chem. Soc.* 2015; 137: 9206-9.
305. Pichon C, Gonçalves C, Midoux P. Histidine-rich peptides and polymers for nucleic acids delivery. *Adv. Drug Del. Rev.* 2001; 53: 75-94.
306. Cheng L, Wang C, Feng L, et al. Functional Nanomaterials for Phototherapies of Cancer. *Chem. Rev.* 2014; 114: 10869-939.

307. Park S-j, Park W, Na K. Tumor Intracellular-Environment Responsive Materials Shielded Nano-Complexes for Highly Efficient Light-Triggered Gene Delivery without Cargo Gene Damage. *Adv. Funct. Mater.* 2015; 25: 3472-82.
308. Sahay G, Alakhova DY, Kabanov AV. Endocytosis of nanomedicines. *J Control Release* 2010; 145: 182-95.
309. Rosi NL, Giljohann DA, Thaxton CS, et al. Oligonucleotide-Modified Gold Nanoparticles for Intracellular Gene Regulation. *Science* 2006; 312: 1027-30.
310. Choi CHJ, Hao L, Narayan SP, et al. Mechanism for the endocytosis of spherical nucleic acid nanoparticle conjugates. *Proc. Natl. Acad. Sci. U. S. A.* 2013; 110: 7625-30.
311. Reilly MJ, Larsen JD, Sullivan MO. Polyplexes Traffic through Caveolae to the Golgi and Endoplasmic Reticulum en Route to the Nucleus. *Mol. Pharm.* 2012; 9: 1280-90.
312. Raiborg C, Wenzel EM, Pedersen NM, et al. Repeated ER–endosome contacts promote endosome translocation and neurite outgrowth. *Nature* 2015; 520: 234-8.
313. Huotari J, Helenius A. Endosome maturation. *The EMBO journal* 2011; 30: 3481-500.
314. Wijdeven RH, Jongsma ML, Neefjes J, et al. ER contact sites direct late endosome transport. *Bioessays* 2015; 37: 1298-302.
315. Xiao PJ, Samulski RJ. Cytoplasmic trafficking, endosomal escape, and perinuclear accumulation of adeno-associated virus type 2 particles are facilitated by microtubule network. *J. Virol.* 2012; 86: 10462-73.
316. Tammam SN, Azzazy HM, Lamprecht A. How successful is nuclear targeting by nanocarriers? *J Control Release* 2016

317. Lim RYH, Fahrenkrog B. The nuclear pore complex up close. *Curr. Opin. Cell Biol.* 2006; 18: 342-7.
318. Kowalczyk SW, Kapinos L, Blosser TR, et al. Single-molecule transport across an individual biomimetic nuclear pore complex. *Nat. Nanotechnol.* 2011; 6: 433-8.
319. Davis ME. Non-viral gene delivery systems. *Curr. Opin. Biotechnol.* 2002; 13: 128-31.
320. Konermann S, Brigham MD, Trevino AE, et al. Optical control of mammalian endogenous transcription and epigenetic states. *Nature* 2013; 500: 472-6.
321. Subramanian A, Ranganathan P, Diamond SL. Nuclear targeting peptide scaffolds for lipofection of nondividing mammalian cells. *Nat. Biotechnol.* 1999; 17: 873-7.
322. Pan L, He Q, Liu J, et al. Nuclear-Targeted Drug Delivery of TAT Peptide-Conjugated Monodisperse Mesoporous Silica Nanoparticles. *J. Am. Chem. Soc.* 2012; 134: 5722-5.
323. Wang S, Lu Y, Yin MX, et al. Importin alpha1 Mediates Yorkie Nuclear Import via N-terminal Non-canonical Nuclear Localization Signal. *J. Biol. Chem.* 2016
324. Jäkel S, Gürlich D. Importin β , transportin, RanBP5 and RanBP7 mediate nuclear import of ribosomal proteins in mammalian cells. *The EMBO Journal* 1998; 17: 4491-502.
325. Zanta MA, Belguise-Valladier P, Behr J-P. Gene delivery: A single nuclear localization signal peptide is sufficient to carry DNA to the cell nucleus. *Proc. Natl. Acad. Sci. U. S. A.* 1999; 96: 91-6.

326. Schedlich LJ, Le Page SL, Firth SM, et al. Nuclear Import of Insulin-like Growth Factor-binding Protein-3 and -5 Is Mediated by the Importin β Subunit. *J. Biol. Chem.* 2000; 275: 23462-70.
327. Chan CK, Jans DA. Enhancement of MSH receptor- and GAL4-mediated gene transfer by switching the nuclear import pathway. *Gene Ther.* 2001; 8: 166-71.
328. Hao N, Budnik BA, Gunawardena J, et al. Tunable Signal Processing Through Modular Control of Transcription Factor Translocation. *Science* 2013; 339: 460-4.
329. Lam AP, Dean DA. Progress and prospects: nuclear import of nonviral vectors. *Gene Ther.* 2010; 17: 439-47.
330. Gilbert Luke A, Larson Matthew H, Morsut L, et al. CRISPR-Mediated Modular RNA-Guided Regulation of Transcription in Eukaryotes. *Cell* 2013; 154: 442-51.
331. Takahashi K, Yamanaka S. A decade of transcription factor-mediated reprogramming to pluripotency. *Nat. Rev. Mol. Cell. Biol.* 2016; 17: 183-93.
332. Chaudhary PM, Roninson IB. Induction of Multidrug Resistance in Human Cells by Transient Exposure to Different Chemotherapeutic Drugs. *J. Natl. Cancer Inst.* 1993; 85: 632-9.
333. BREDESEN DE, MEHLEN P, RABIZADEH S. Apoptosis and Dependence Receptors: A Molecular Basis for Cellular Addiction. *Physiol. Rev.* 2004; 84: 411-30.
334. Sarkadi B, Homolya L, Szakács G, et al. Human Multidrug Resistance ABCB and ABCG Transporters: Participation in a Chemoimmunity Defense System. *Physiol. Rev.* 2006; 86: 1179-236.

335. Stein WD. Kinetics of the multidrug transporter (P-glycoprotein) and its reversal. *Physiol. Rev.* 1997; 77: 545-90.
336. Deeley RG, Westlake C, Cole SPC. Transmembrane Transport of Endo- and Xenobiotics by Mammalian ATP-Binding Cassette Multidrug Resistance Proteins. *Physiol. Rev.* 2006; 86: 849-99.
337. Ernst R, Kueppers P, Stindt J, et al. Multidrug efflux pumps: Substrate selection in ATP-binding cassette multidrug efflux pumps – first come, first served? *FEBS J.* 2010; 277: 540-9.
338. Juliano RL, Ling V. A surface glycoprotein modulating drug permeability in Chinese hamster ovary cell mutants. *BBA Biomembranes* 1976; 455: 152-62.
339. Chen YN, Mickley LA, Schwartz AM, et al. Characterization of adriamycin-resistant human breast cancer cells which display overexpression of a novel resistance-related membrane protein. *J. Biol. Chem.* 1990; 265: 10073-80.
340. Cole SP, Bhardwaj G, Gerlach JH, et al. Overexpression of a transporter gene in a multidrug-resistant human lung cancer cell line. *Science* 1992; 258: 1650-4.
341. Kunjachan S, Rychlik B, Storm G, et al. Multidrug resistance: Physiological principles and nanomedical solutions. *Adv Drug Deliv Rev* 2013; 65: 1852-65.
342. Batrakova EV, Kabanov AV. Pluronic block copolymers: evolution of drug delivery concept from inert nanocarriers to biological response modifiers. *J Control Release* 2008; 130: 98-106.

343. Jiang Q, Song C, Nangreave J, et al. DNA Origami as a Carrier for Circumvention of Drug Resistance. *J. Am. Chem. Soc.* 2012; 134: 13396-403.
344. McKinlay CJ, Waymouth RM, Wender PA. Cell-Penetrating, Guanidinium-Rich Oligophosphoesters: Effective and Versatile Molecular Transporters for Drug and Probe Delivery. *J. Am. Chem. Soc.* 2016; 138: 3510-7.
345. Wang J, Goh B, Lu W, et al. In vitro cytotoxicity of Stealth liposomes co-encapsulating doxorubicin and verapamil on doxorubicin-resistant tumor cells. *Biol. Pharm. Bull.* 2005; 28: 822-8.
346. Patel NR, Rathi A, Mongayt D, et al. Reversal of multidrug resistance by co-delivery of tariquidar (XR9576) and paclitaxel using long-circulating liposomes. *Int. J. Pharm.* 2011; 416: 296-9.
347. Wong HL, Bendayan R, Rauth AM, et al. Simultaneous delivery of doxorubicin and GG918 (Elacridar) by new Polymer-Lipid Hybrid Nanoparticles (PLN) for enhanced treatment of multidrug-resistant breast cancer. *J. Control. Release* 2006; 116: 275-84.
348. Meng H, Mai WX, Zhang H, et al. Codelivery of an optimal drug/siRNA combination using mesoporous silica nanoparticles to overcome drug resistance in breast cancer in vitro and in vivo. *ACS Nano* 2013; 7: 994-1005.
349. Myerson JW, Anselmo AC, Liu Y, et al. Non-affinity factors modulating vascular targeting of nano- and microcarriers. *Adv Drug Deliv Rev* 2016; 99: 97-112.
350. Mager MD, LaPointe V, Stevens MM. Exploring and exploiting chemistry at the cell surface. *Nat. Chem.* 2011; 3: 582-9.

351. Albanese A, Tang PS, Chan WCW. The Effect of Nanoparticle Size, Shape, and Surface Chemistry on Biological Systems. *Annu. Rev. Biomed. Eng.* 2012; 14: 1-16.
352. Tenzer S, Docter D, Rosfa S, et al. Nanoparticle Size Is a Critical Physicochemical Determinant of the Human Blood Plasma Corona: A Comprehensive Quantitative Proteomic Analysis. *ACS Nano* 2011; 5: 7155-67.
353. Peppiatt CM, Howarth C, Mobbs P, et al. Bidirectional control of CNS capillary diameter by pericytes. *Nature* 2006; 443: 700-4.
354. Yuan F, Dellian M, Fukumura D, et al. Vascular permeability in a human tumor xenograft: molecular size dependence and cutoff size. *Cancer Res.* 1995; 55: 3752-6.
355. Hobbs SK, Monsky WL, Yuan F, et al. Regulation of transport pathways in tumor vessels: role of tumor type and microenvironment. *Proc Natl Acad Sci U S A* 1998; 95: 4607-12.
356. Tang L, Yang X, Yin Q, et al. Investigating the optimal size of anticancer nanomedicine. *Proc. Natl. Acad. Sci. U. S. A.* 2014; 111: 15344-9.
357. Chauhan VP, Jain RK. Strategies for advancing cancer nanomedicine. *Nat. Mater.* 2013; 12: 958-62.
358. Truong NP, Whittaker MR, Mak CW, et al. The importance of nanoparticle shape in cancer drug delivery. *Expert Opin. Drug Del.* 2015; 12: 129-42.
359. Tao L, Hu W, Liu Y, et al. Shape-specific polymeric nanomedicine: emerging opportunities and challenges. *Exp Biol Med (Maywood)* 2011; 236: 20-9.

360. Hu X, Hu J, Tian J, et al. Polyprodrug amphiphiles: hierarchical assemblies for shape-regulated cellular internalization, trafficking, and drug delivery. *J. Am. Chem. Soc.* 2013; 135: 17617-29.
361. Geng Y, Dalhaimer P, Cai S, et al. Shape effects of filaments versus spherical particles in flow and drug delivery. *Nat. Nanotechnol.* 2007; 2: 249-55.
362. Muro S, Garnacho C, Champion JA, et al. Control of endothelial targeting and intracellular delivery of therapeutic enzymes by modulating the size and shape of ICAM-1-targeted carriers. *Mol. Ther.* 2008; 16: 1450-8.
363. Champion JA, Mitragotri S. Role of target geometry in phagocytosis. *Proc Natl Acad Sci U S A* 2006; 103: 4930-4.
364. Pacardo DB, Neupane B, Rikard SM, et al. A dual wavelength-activatable gold nanorod complex for synergistic cancer treatment. *Nanoscale* 2015; 7: 12096-103.
365. Lock LL, Reyes CD, Zhang P, et al. Tuning Cellular Uptake of Molecular Probes by Rational Design of Their Assembly into Supramolecular Nanoprobes. *J. Am. Chem. Soc.* 2016; 138: 3533-40.
366. Sun W, Ji W, Hu Q, et al. Transformable DNA nanocarriers for plasma membrane targeted delivery of cytokine. *Biomaterials* 2016; 96: 1-10.
367. Yoo J-W, Mitragotri S. Polymer particles that switch shape in response to a stimulus. *Proc. Natl. Acad. Sci. U. S. A.* 2010; 107: 11205-10.
368. Yeung T, Gilbert GE, Shi J, et al. Membrane Phosphatidylserine Regulates Surface Charge and Protein Localization. *Science* 2008; 319: 210-3.

369. He C, Hu Y, Yin L, et al. Effects of particle size and surface charge on cellular uptake and biodistribution of polymeric nanoparticles. *Biomaterials* 2010; 31: 3657-66.
370. Kim B, Han G, Toley BJ, et al. Tuning payload delivery in tumour cylindroids using gold nanoparticles. *Nat. Nanotechnol.* 2010; 5: 465-72.
371. Verma A, Stellacci F. Effect of surface properties on nanoparticle-cell interactions. *Small* 2010; 6: 12-21.
372. Harush-Frenkel O, Rozentur E, Benita S, et al. Surface charge of nanoparticles determines their endocytic and transcytotic pathway in polarized MDCK cells. *Biomacromolecules* 2008; 9: 435-43.
373. Yu T, Malugin A, Ghandehari H. Impact of Silica Nanoparticle Design on Cellular Toxicity and Hemolytic Activity. *ACS Nano* 2011; 5: 5717-28.
374. Arvizo RR, Miranda OR, Thompson MA, et al. Effect of Nanoparticle Surface Charge at the Plasma Membrane and Beyond. *Nano Lett.* 2010; 10: 2543-8.
375. Xu P, Van Kirk EA, Zhan Y, et al. Targeted Charge-Reversal Nanoparticles for Nuclear Drug Delivery. *Angew. Chem. Int. Ed.* 2007; 46: 4999-5002.
376. Han SS, Li ZY, Zhu JY, et al. Dual-pH Sensitive Charge-Reversal Polypeptide Micelles for Tumor-Triggered Targeting Uptake and Nuclear Drug Delivery. *Small* 2015; 11: 2543-54.
377. Huang Y, Tang Z, Zhang X, et al. pH-Triggered charge-reversal polypeptide nanoparticles for cisplatin delivery: preparation and in vitro evaluation. *Biomacromolecules* 2013; 14: 2023-32.

378. Nel AE, Madler L, Velegol D, et al. Understanding biophysicochemical interactions at the nano-bio interface. *Nat. Mater.* 2009; 8: 543-57.
379. Medzhitov R, Janeway CA. Decoding the Patterns of Self and Nonself by the Innate Immune System. *Science* 2002; 296: 298-300.
380. Takahashi Y, Kitadai Y, Bucana CD, et al. Expression of vascular endothelial growth factor and its receptor, KDR, correlates with vascularity, metastasis, and proliferation of human colon cancer. *Cancer Res.* 1995; 55: 3964-8.
381. Lu Y, Low PS. Folate-mediated delivery of macromolecular anticancer therapeutic agents. *Adv. Drug Del. Rev.* 2012; 64, Supplement: 342-52.
382. Demoulin J-B, Essaghir A. PDGF receptor signaling networks in normal and cancer cells. *Cytokine Growth F. R.* 2014; 25: 273-83.
383. Anselmo AC, Mitragotri S. Impact of particle elasticity on particle-based drug delivery systems. *Adv. Drug Del. Rev.* 2016; doi: 10.1016/j.addr.2016.01.007
384. Discher DE, Janmey P, Wang Y-l. Tissue Cells Feel and Respond to the Stiffness of Their Substrate. *Science* 2005; 310: 1139-43.
385. Yi X, Shi X, Gao H. Cellular Uptake of Elastic Nanoparticles. *Phys. Rev. Lett.* 2011; 107: 098101.
386. Cui J, Bjornmalm M, Liang K, et al. Super-soft hydrogel particles with tunable elasticity in a microfluidic blood capillary model. *Advanced materials (Deerfield Beach, Fla.)* 2014; 26: 7295-9.

387. Wong PT, Choi SK. Mechanisms of Drug Release in Nanotherapeutic Delivery Systems. *Chem. Rev.* 2015; 115: 3388-432.
388. Zhao M, Hu B, Gu Z, et al. Degradable polymeric nanocapsule for efficient intracellular delivery of a high molecular weight tumor-selective protein complex. *Nano Today* 2013; 8: 11-20.
389. Yu M, Zheng J. Clearance Pathways and Tumor Targeting of Imaging Nanoparticles. *ACS Nano* 2015; 9: 6655-74.
390. Chou LYT, Zagorovsky K, Chan WCW. DNA assembly of nanoparticle superstructures for controlled biological delivery and elimination. *Nat. Nanotechnol.* 2014; 9: 148-55.
391. Estrella V, Chen T, Lloyd M, et al. Acidity Generated by the Tumor Microenvironment Drives Local Invasion. *Cancer Res.* 2013; 73: 1524-35.
392. Fleige E, Quadir MA, Haag R. Stimuli-responsive polymeric nanocarriers for the controlled transport of active compounds: Concepts and applications. *Adv. Drug Del. Rev.* 2012; 64: 866-84.
393. Poon Z, Chang D, Zhao X, et al. Layer-by-Layer Nanoparticles with a pH-Sheddable Layer for in Vivo Targeting of Tumor Hypoxia. *ACS Nano* 2011; 5: 4284-92.
394. Tseng SJ, Liao Z-X, Kao S-H, et al. Highly specific in vivo gene delivery for p53-mediated apoptosis and genetic photodynamic therapies of tumour. *Nat. Commun.* 2015; 6

395. Clark AJ, Davis ME. Increased brain uptake of targeted nanoparticles by adding an acid-cleavable linkage between transferrin and the nanoparticle core. *Proc. Natl. Acad. Sci. U. S. A.* 2015; 112: 12486-91.
396. Cui L, Cohen JL, Chu CK, et al. Conjugation Chemistry through Acetals toward a Dextran-Based Delivery System for Controlled Release of siRNA. *J. Am. Chem. Soc.* 2012; 134: 15840-8.
397. Mignatti P, Rifkin DB. Biology and biochemistry of proteinases in tumor invasion. *Physiol. Rev.* 1993; 73: 161-95.
398. Greenlee KJ, Werb Z, Kheradmand F. Matrix Metalloproteinases in Lung: Multiple, Multifarious, and Multifaceted. *Physiol. Rev.* 2007; 87: 69-98.
399. Ferrari M, Onuoha SC, Pitzalis C. Trojan horses and guided missiles: targeted therapies in the war on arthritis. *Nat Rev Rheumatol* 2015; 11: 328-37.
400. Malumbres M. Physiological Relevance of Cell Cycle Kinases. *Physiol. Rev.* 2011; 91: 973-1007.
401. Vandooren J, Opdenakker G, Loadman PM, et al. Proteases in cancer drug delivery. *Adv. Drug Del. Rev.* 2016; 97: 144-55.
402. Jiang T, Olson ES, Nguyen QT, et al. Tumor imaging by means of proteolytic activation of cell-penetrating peptides. *Proc. Natl. Acad. Sci. U. S. A.* 2004; 101: 17867-72.
403. Huang S, Shao K, Liu Y, et al. Tumor-Targeting and Microenvironment-Responsive Smart Nanoparticles for Combination Therapy of Antiangiogenesis and Apoptosis. *ACS Nano* 2013; 7: 2860-71.

404. Zhu L, Wang T, Perche F, et al. Enhanced anticancer activity of nanopreparation containing an MMP2-sensitive PEG-drug conjugate and cell-penetrating moiety. *Proc. Natl. Acad. Sci. U. S. A.* 2013; 110: 17047-52.
405. van Rijt SH, Bölükbas DA, Argyo C, et al. Protease-Mediated Release of Chemotherapeutics from Mesoporous Silica Nanoparticles to ex Vivo Human and Mouse Lung Tumors. *ACS Nano* 2015; 9: 2377-89.
406. Seidah NG, Day R, Marcinkiewicz M, et al. Precursor convertases: an evolutionary ancient, cell-specific, combinatorial mechanism yielding diverse bioactive peptides and proteins. *Ann. N. Y. Acad. Sci.* 1998; 839: 9-24.
407. Thomas G. Furin at the cutting edge: From protein traffic to embryogenesis and disease. *Nat. Rev. Mol. Cell. Biol.* 2002; 3: 753-66.
408. Jiang T, Sun W, Zhu Q, et al. Furin-Mediated Sequential Delivery of Anticancer Cytokine and Small-Molecule Drug Shuttled by Graphene. *Adv. Mater.* 2015; 27: 1021-8.
409. Jiang T, Mo R, Bellotti A, et al. Gel-Liposome-Mediated Co-Delivery of Anticancer Membrane-Associated Proteins and Small-Molecule Drugs for Enhanced Therapeutic Efficacy. *Adv. Funct. Mater.* 2013; 24: 2259-304.
410. Dall E, Brandstetter H. Mechanistic and structural studies on legumain explain its zymogenicity, distinct activation pathways, and regulation. *Proc Natl Acad Sci U S A* 2013; 110: 10940-5.
411. Liu Z, Xiong M, Gong J, et al. Legumain protease-activated TAT-liposome cargo for targeting tumours and their microenvironment. *Nat. Commun.* 2014; 5

412. Biswas A, Joo K-I, Liu J, et al. Endoprotease-Mediated Intracellular Protein Delivery Using Nanocapsules. *ACS Nano* 2011; 5: 1385-94.
413. Kang J-H, Asai D, Kim J-H, et al. Design of Polymeric Carriers for Cancer-Specific Gene Targeting: Utilization of Abnormal Protein Kinase $C\alpha$ Activation in Cancer Cells. *J. Am. Chem. Soc.* 2008; 130: 14906-7.
414. Ong W, Yang Y, Cruciano AC, et al. Redox-Triggered Contents Release from Liposomes. *J. Am. Chem. Soc.* 2008; 130: 14739-44.
415. de la Torre C, Mondragon L, Coll C, et al. Caspase 3 Targeted Cargo Delivery in Apoptotic Cells Using Capped Mesoporous Silica Nanoparticles. *Chemistry* 2015; 21: 15506-10.
416. Bernardos A, Mondragón L, Aznar E, et al. Enzyme-Responsive Intracellular Controlled Release Using Nanometric Silica Mesoporous Supports Capped with “Saccharides”. *ACS Nano* 2010; 4: 6353-68.
417. de la Torre C, Mondragon L, Coll C, et al. Cathepsin-B induced controlled release from peptide-capped mesoporous silica nanoparticles. *Chemistry* 2014; 20: 15309-14.
418. Lei XG, Zhu J-H, Cheng W-H, et al. Paradoxical Roles of Antioxidant Enzymes: Basic Mechanisms and Health Implications. *Physiol. Rev.* 2016; 96: 307-64.
419. Schafer FQ, Buettner GR. Redox environment of the cell as viewed through the redox state of the glutathione disulfide/glutathione couple. *Free Radical Biol. Med.* 2001; 30: 1191-212.

420. Estrela JM, Ortega A, Obrador E. Glutathione in cancer biology and therapy. *Crit. Rev. Clin. Lab. Sci.* 2006; 43: 143-81.
421. Kuppusamy P, Li H, Ilangovan G, et al. Noninvasive imaging of tumor redox status and its modification by tissue glutathione levels. *Cancer Res.* 2002; 62: 307-12.
422. Luo Z, Ding X, Hu Y, et al. Engineering a hollow nanocontainer platform with multifunctional molecular machines for tumor-targeted therapy in vitro and in vivo. *ACS Nano* 2013; 7: 10271-84.
423. Wang K, Hu Q, Zhu W, et al. Structure-Invertible Nanoparticles for Triggered Co-Delivery of Nucleic Acids and Hydrophobic Drugs for Combination Cancer Therapy. *Adv. Funct. Mater.* 2015; 25: 3380-92.
424. Dunn SS, Tian S, Blake S, et al. Reductively Responsive siRNA-Conjugated Hydrogel Nanoparticles for Gene Silencing. *J. Am. Chem. Soc.* 2012; 134: 7423-30.
425. Zhao M, Biswas A, Hu B, et al. Redox-responsive nanocapsules for intracellular protein delivery. *Biomaterials* 2011; 32: 5223-30.
426. Zhao M, Liu Y, Hsieh RS, et al. Clickable Protein Nanocapsules for Targeted Delivery of Recombinant p53 Protein. *J. Am. Chem. Soc.* 2014; 136: 15319-25.
427. He Y, Nie Y, Cheng G, et al. Viral Mimicking Ternary Polyplexes: A Reduction-Controlled Hierarchical Unpacking Vector for Gene Delivery. *Adv. Mater.* 2014; 26: 1534-40.

428. Chang Y, Yang K, Wei P, et al. Cationic Vesicles Based on Amphiphilic Pillar[5]arene Capped with Ferrocenium: A Redox-Responsive System for Drug/siRNA Co-Delivery. *Angew. Chem. Int. Ed.* 2014; 53: 13126-30.
429. Zorov DB, Juhaszova M, Sollott SJ. Mitochondrial Reactive Oxygen Species (ROS) and ROS-Induced ROS Release. *Physiol. Rev.* 2014; 94: 909-50.
430. Waris G, Ahsan H. Reactive oxygen species: role in the development of cancer and various chronic conditions. *Journal of carcinogenesis* 2006; 5: 14.
431. Bhattacharyya A, Chattopadhyay R, Mitra S, et al. Oxidative Stress: An Essential Factor in the Pathogenesis of Gastrointestinal Mucosal Diseases. *Physiol. Rev.* 2014; 94: 329-54.
432. Fang J, Seki T, Maeda H. Therapeutic strategies by modulating oxygen stress in cancer and inflammation. *Adv Drug Deliv Rev* 2009; 61: 290-302.
433. Barnham KJ, Masters CL, Bush AI. Neurodegenerative diseases and oxidative stress. *Nat. Rev. Drug Discov.* 2004; 3: 205-14.
434. Houstis N, Rosen ED, Lander ES. Reactive oxygen species have a causal role in multiple forms of insulin resistance. *Nature* 2006; 440: 944-8.
435. Gallagher EJ, LeRoith D. Obesity and Diabetes: The Increased Risk of Cancer and Cancer-Related Mortality. *Physiol. Rev.* 2015; 95: 727-48.
436. Cai H. Hydrogen peroxide regulation of endothelial function: origins, mechanisms, and consequences. *Cardiovasc. Res.* 2005; 68: 26-36.

437. Wilson DS, Dalmaso G, Wang L, et al. Orally delivered thioketal nanoparticles loaded with TNF- α -siRNA target inflammation and inhibit gene expression in the intestines. *Nat. Mater.* 2010; 9: 923-8.
438. Yuan Y, Liu J, Liu B. Conjugated-Polyelectrolyte-Based Polyprodrug: Targeted and Image-Guided Photodynamic and Chemotherapy with On-Demand Drug Release upon Irradiation with a Single Light Source. *Angew. Chem. Int. Ed.* 2014; 53: 7163-8.
439. Wang M, Sun S, Neufeld CI, et al. Reactive Oxygen Species-Responsive Protein Modification and Its Intracellular Delivery for Targeted Cancer Therapy. *Angew. Chem. Int. Ed.* 2014; 53: 13444-8.
440. Liu X, Xiang J, Zhu D, et al. Fusogenic Reactive Oxygen Species Triggered Charge-Reversal Vector for Effective Gene Delivery. *Adv. Mater.* 2015; 28: 1743-52.
441. Yu SS, Koblin RL, Zachman AL, et al. Physiologically relevant oxidative degradation of oligo(proline) cross-linked polymeric scaffolds. *Biomacromolecules* 2011; 12: 4357-66.
442. Fuhrmann K, Polomska A, Aeberli C, et al. Modular design of redox-responsive stabilizers for nanocrystals. *ACS Nano* 2013; 7: 8243-50.
443. Allen BL, Johnson JD, Walker JP. Encapsulation and Enzyme-Mediated Release of Molecular Cargo in Polysulfide Nanoparticles. *ACS Nano* 2011; 5: 5263-72.
444. Staff RH, Gallei M, Mazurowski M, et al. Patchy nanocapsules of poly(vinylferrocene)-based block copolymers for redox-responsive release. *ACS Nano* 2012; 6: 9042-9.

445. Krall N, da Cruz FP, Boutureira O, et al. Site-selective protein-modification chemistry for basic biology and drug development. *Nat. Chem.* 2016; 8: 103-13.
446. Weinstain R, Savariar EN, Felsen CN, et al. In Vivo Targeting of Hydrogen Peroxide by Activatable Cell-Penetrating Peptides. *J. Am. Chem. Soc.* 2014; 136: 874-7.
447. LaGory EL, Giaccia AJ. The ever-expanding role of HIF in tumour and stromal biology. *Nat Cell Biol* 2016; 18: 356-65.
448. Wilson WR, Hay MP. Targeting hypoxia in cancer therapy. *Nat. Rev. Cancer.* 2011; 11: 393-410.
449. Sun JD, Liu Q, Wang J, et al. Selective Tumor Hypoxia Targeting by Hypoxia-Activated Prodrug TH-302 Inhibits Tumor Growth in Preclinical Models of Cancer. *Clin. Cancer Res.* 2012; 18: 758-70.
450. Yu B, Yang M, Shi L, et al. Explicit hypoxia targeting with tumor suppression by creating an "obligate" anaerobic *Salmonella Typhimurium* strain. *Scientific reports* 2012; 2: 436.
451. Du J, Lane LA, Nie S. Stimuli-responsive nanoparticles for targeting the tumor microenvironment. *J. Control. Release* 2015; 219: 205-14.
452. Zheng X, Wang X, Mao H, et al. Hypoxia-specific ultrasensitive detection of tumours and cancer cells in vivo. *Nat. Commun.* 2015; 6
453. Perche F, Biswas S, Wang T, et al. Hypoxia-Targeted siRNA Delivery. *Angew. Chem. Int. Ed.* 2014; 53: 3362-6.

454. Thambi T, Deepagan VG, Yoon HY, et al. Hypoxia-responsive polymeric nanoparticles for tumor-targeted drug delivery. *Biomaterials* 2014; 35: 1735-43.
455. Zhou Y, Tozzi F, Chen J, et al. Intracellular ATP levels are a pivotal determinant of chemoresistance in colon cancer cells. *Cancer Res.* 2012; 72: 304-14.
456. Mo R, Jiang T, DiSanto R, et al. ATP-triggered anticancer drug delivery. *Nat. Commun.* 2014; 5: 3364.
457. He X, Zhao Y, He D, et al. ATP-Responsive Controlled Release System Using Aptamer-Functionalized Mesoporous Silica Nanoparticles. *Langmuir* 2012; 28: 12909-15.
458. Liao W-C, Lu C-H, Hartmann R, et al. Adenosine Triphosphate-Triggered Release of Macromolecular and Nanoparticle Loads from Aptamer/DNA-Cross-Linked Microcapsules. *ACS Nano* 2015; 9: 9078-86.
459. Mo R, Jiang T, Sun W, et al. ATP-Responsive DNA-Graphene Hybrid Nanoaggregates for Anticancer Drug Delivery. *Biomaterials* 2015; 50: 67-74.
460. Lai J, Shah BP, Zhang Y, et al. Real-Time Monitoring of ATP-Responsive Drug Release Using Mesoporous-Silica-Coated Multicolor Upconversion Nanoparticles. *ACS Nano* 2015; 9: 5234-45.
461. Naito M, Ishii T, Matsumoto A, et al. A Phenylboronate-Functionalized Polyion Complex Micelle for ATP-Triggered Release of siRNA. *Angew. Chem. Int. Ed.* 2012; 51: 10751-5.
462. Biswas S, Kinbara K, Niwa T, et al. Biomolecular robotics for chemomechanically driven guest delivery fuelled by intracellular ATP. *Nat. Chem.* 2013; 5: 613-20.

463. Pacardo DB, Ligler FS, Gu Z. Programmable nanomedicine: synergistic and sequential drug delivery systems. *Nanoscale* 2015; 7: 3381-91.
464. Lu Y, Mo R, Tai W, et al. Self-folded redox/acid dual-responsive nanocarriers for anticancer drug delivery. *Chem. Commun.* 2014; 50: 15105-8.
465. Pathak RK, Dhar S. A Nanoparticle Cocktail: Temporal Release of Predefined Drug Combinations. *J. Am. Chem. Soc.* 2015; 137: 8324-7.
466. Pu H-L, Chiang W-L, Maiti B, et al. Nanoparticles with Dual Responses to Oxidative Stress and Reduced pH for Drug Release and Anti-inflammatory Applications. *ACS Nano* 2014; 8: 1213-21.
467. Wang J, Sun X, Mao W, et al. Tumor redox heterogeneity-responsive prodrug nanocapsules for cancer chemotherapy. *Advanced materials (Deerfield Beach, Fla.)* 2013; 25: 3670-6.
468. Zhang J, Yuan Z-F, Wang Y, et al. Multifunctional Envelope-Type Mesoporous Silica Nanoparticles for Tumor-Triggered Targeting Drug Delivery. *J. Am. Chem. Soc.* 2013; 135: 5068-73.
469. Choi KY, Silvestre OF, Huang X, et al. Versatile RNA Interference Nanoplatfom for Systemic Delivery of RNAs. *ACS Nano* 2014; 8: 4559-70.
470. Mo R, Jiang T, Gu Z. Enhanced Anticancer Efficacy by ATP-Mediated Liposomal Drug Delivery. *Angew. Chem. Int. Ed.* 2014; 53: 5815-20.
471. Hu Q, Sun W, Lu Y, et al. Tumor Microenvironment-Mediated Construction and Deconstruction of Extracellular Drug-Delivery Depots. *Nano Lett.* 2016; 16: 1118-26.

472. Eckert RL, Kaartinen MT, Nurminskaya M, et al. Transglutaminase Regulation of Cell Function. *Physiol. Rev.* 2014; 94: 383-417.
473. Ye Y, Yu J, Wang C, et al. Microneedles Integrated with Pancreatic Cells and Synthetic Glucose-Signal Amplifiers for Smart Insulin Delivery. *Adv. Mater.* 2016; 28: 3115-21.
474. Díez P, Sánchez A, Gamella M, et al. Toward the Design of Smart Delivery Systems Controlled by Integrated Enzyme-Based Biocomputing Ensembles. *J. Am. Chem. Soc.* 2014; 136: 9116-23.
475. Etheridge ML, Campbell SA, Erdman AG, et al. The big picture on nanomedicine: the state of investigational and approved nanomedicine products. *Nanomed. Nanotechnol. Biol. Med.* 2013; 9: 1-14.
476. Chudasama V, Maruani A, Caddick S. Recent advances in the construction of antibody-drug conjugates. *Nat. Chem.* 2016; 8: 114-9.
477. Duncan R. Polymer conjugates as anticancer nanomedicines. *Nat. Rev. Cancer.* 2006; 6: 688-701.
478. Landesman-Milo D, Peer D. Transforming Nanomedicines From Lab Scale Production to Novel Clinical Modality. *Bioconjug. Chem.* 2016; 27: 855-62.
479. Gabizon A, Catane R, Uziely B, et al. Prolonged circulation time and enhanced accumulation in malignant exudates of doxorubicin encapsulated in polyethylene-glycol coated liposomes. *Cancer Res.* 1994; 54: 987-92.

480. Allen TM, Cullis PR. Liposomal drug delivery systems: From concept to clinical applications. *Adv. Drug Del. Rev.* 2013; 65: 36-48.
481. Irvine DJ, Swartz MA, Szeto GL. Engineering synthetic vaccines using cues from natural immunity. *Nat. Mater.* 2013; 12: 978-90.
482. Miele E, Spinelli GP, Miele E, et al. Albumin-bound formulation of paclitaxel (Abraxane ABI-007) in the treatment of breast cancer. *International journal of nanomedicine* 2009; 4: 99-105.
483. Rowinsky EK, Donehower RC. Paclitaxel (taxol). *N. Engl. J. Med.* 1995; 332: 1004-14.
484. Cirstea D, Hideshima T, Rodig S, et al. Dual inhibition of akt/mammalian target of rapamycin pathway by nanoparticle albumin-bound-rapamycin and perifosine induces antitumor activity in multiple myeloma. *Mol Cancer Ther* 2010; 9: 963-75.
485. Mullard A. Maturing antibody-drug conjugate pipeline hits 30. *Nat. Rev. Drug Discov.* 2013; 12: 329-32.
486. Foss FM. DAB389IL-2 (ONTAK): A Novel Fusion Toxin Therapy for Lymphoma. *Clinical lymphoma* 2000; 1: 110-6.
487. Verma S, Miles D, Gianni L, et al. Trastuzumab Emtansine for HER2-Positive Advanced Breast Cancer. *N. Engl. J. Med.* 2012; 367: 1783-91.
488. Seymour LW, Ferry DR, Anderson D, et al. Hepatic drug targeting: phase I evaluation of polymer-bound doxorubicin. *J. Clin. Oncol.* 2002; 20: 1668-76.

489. Kim SC, Kim DW, Shim YH, et al. In vivo evaluation of polymeric micellar paclitaxel formulation: toxicity and efficacy. *J Control Release* 2001; 72: 191-202.
490. Hamaguchi T, Doi T, Eguchi-Nakajima T, et al. Phase I study of NK012, a novel SN-38-incorporating micellar nanoparticle, in adult patients with solid tumors. *Clin. Cancer Res.* 2010; 16: 5058-66.
491. Danson S, Ferry D, Alakhov V, et al. Phase I dose escalation and pharmacokinetic study of pluronic polymer-bound doxorubicin (SP1049C) in patients with advanced cancer. *Br. J. Cancer* 2004; 90: 2085-91.
492. Hrkach J, Von Hoff D, Mukkaram Ali M, et al. Preclinical development and clinical translation of a PSMA-targeted docetaxel nanoparticle with a differentiated pharmacological profile. *Sci Transl Med* 2012; 4: 128ra39.
493. Plummer R, Wilson RH, Calvert H, et al. A Phase I clinical study of cisplatin-incorporated polymeric micelles (NC-6004) in patients with solid tumours. *Br. J. Cancer* 2011; 104: 593-8.
494. Yamamoto Y, Hyodo I, Takigahira M, et al. Effect of combined treatment with the epirubicin-incorporating micelles (NC-6300) and 1,2-diaminocyclohexane platinum (II)-incorporating micelles (NC-4016) on a human gastric cancer model. *Int. J. Cancer* 2014; 135: 214-23.
495. Matsumura Y, Hamaguchi T, Ura T, et al. Phase I clinical trial and pharmacokinetic evaluation of NK911, a micelle-encapsulated doxorubicin. *Br. J. Cancer* 2004; 91: 1775-81.

496. McLachlan SJ, Morris MR, Lucas MA, et al. Phase I clinical evaluation of a new iron oxide MR contrast agent. *J. Magn. Reson. Imaging* 1994; 4: 301-7.
497. Haldemann Heusler RC, Wight E, Marincek B. Oral superparamagnetic contrast agent (ferumoxsil): tolerance and efficacy in MR imaging of gynecologic diseases. *J. Magn. Reson. Imaging* 1995; 5: 385-91.
498. Maier-Hauff K, Ulrich F, Nestler D, et al. Efficacy and safety of intratumoral thermotherapy using magnetic iron-oxide nanoparticles combined with external beam radiotherapy on patients with recurrent glioblastoma multiforme. *J. Neurooncol.* 2011; 103: 317-24.
499. Kharlamov AN, Gabinsky JL. Plasmonic photothermic and stem cell therapy of atherosclerotic plaque as a novel nanotool for angioplasty and artery remodeling. *Rejuvenation research* 2012; 15: 222-30.
500. Libutti SK, Paciotti GF, Byrnes AA, et al. Phase I and pharmacokinetic studies of CYT-6091, a novel PEGylated colloidal gold-rhTNF nanomedicine. *Clin. Cancer Res.* 2010; 16: 6139-49.
501. Bradley AM, Devine M, DeRemer D. Brentuximab vedotin: an anti-CD30 antibody-drug conjugate. *Am. J. Health. Syst. Pharm.* 2013; 70: 589-97.
502. Li C, Yu DF, Newman RA, et al. Complete regression of well-established tumors using a novel water-soluble poly(L-glutamic acid)-paclitaxel conjugate. *Cancer Res.* 1998; 58: 2404-9.

503. Singer JW. Paclitaxel poliglumex (XYOTAX™, CT-2103): A macromolecular taxane. *J. Control. Release* 2005; 109: 120-6.
504. Seymour LW, Ferry DR, Kerr DJ, et al. Phase II studies of polymer-doxorubicin (PK1, FCE28068) in the treatment of breast, lung and colorectal cancer. *Int. J. Oncol.* 2009; 34: 1629-36.
505. Ulbrich K, Etrych T, Chytil P, et al. HEMA copolymers with pH-controlled release of doxorubicin: In vitro cytotoxicity and in vivo antitumor activity. *J. Control. Release* 2003; 87: 33-47.
506. Sun W, Lu Y, Gu Z. Advances in Anticancer Protein Delivery using Micro-/Nanoparticles. *Part. Part. Syst. Charact.* 2014; 31: 1204-22.
507. Yoo J-W, Irvine DJ, Discher DE, et al. Bio-inspired, bioengineered and biomimetic drug delivery carriers. *Nat. Rev. Drug Discov.* 2011; 10: 521-35.
508. Zhang Y, Chan HF, Leong KW. Advanced materials and processing for drug delivery: The past and the future. *Adv. Drug Del. Rev.* 2013; 65: 104-20.
509. Venditto VJ, Szoka Jr FC. Cancer nanomedicines: So many papers and so few drugs! *Adv. Drug Del. Rev.* 2013; 65: 80-8.
510. Zhang F, Nangreave J, Liu Y, et al. Structural DNA Nanotechnology: State of the Art and Future Perspective. *J. Am. Chem. Soc.* 2014; 136: 11198-211.
511. Rothmund PWK. Folding DNA to create nanoscale shapes and patterns. *Nature* 2006; 440: 297-302.

512. Tan SJ, Campolongo MJ, Luo D, et al. Building plasmonic nanostructures with DNA. *Nat. Nanotechnol.* 2011; 6: 268-76.
513. Li J, Fan C, Pei H, et al. Smart Drug Delivery Nanocarriers with Self-Assembled DNA Nanostructures. *Adv. Mater.* 2013; 25: 4386-96.
514. Lu CH, Willner B, Willner I. DNA nanotechnology: from sensing and DNA machines to drug-delivery systems. *ACS Nano* 2013; 7: 8320-32.
515. Samejima K, Earnshaw WC. Trashing the genome: the role of nucleases during apoptosis. *Nat. Rev. Mol. Cell. Biol.* 2005; 6: 677-88.
516. Liang L, Li J, Li Q, et al. Single-Particle Tracking and Modulation of Cell Entry Pathways of a Tetrahedral DNA Nanostructure in Live Cells. *Angew. Chem. Int. Ed.* 2014; 53: 7745-50.
517. Chang M, Yang C-S, Huang D-M. Aptamer-Conjugated DNA Icosahedral Nanoparticles As a Carrier of Doxorubicin for Cancer Therapy. *ACS Nano* 2011; 5: 6156-63.
518. Keefe AD, Pai S, Ellington A. Aptamers as therapeutics. *Nat. Rev. Drug Discov.* 2010; 9: 537-50.
519. Mo R, Jiang T, Gu Z. Enhanced Anticancer Efficacy by ATP-Mediated Liposomal Drug Delivery. *Angew. Chem. Int. Ed.* 2014; 126: 5925-30.
520. Song L, Ho VHB, Chen C, et al. Efficient, pH-Triggered Drug Delivery Using a pH-Responsive DNA-Conjugated Gold Nanoparticle. *Adv. Healthcare Mater.* 2013; 2: 275-80.
521. Kotula JW, Pratico ED, Ming X, et al. Aptamer-mediated delivery of splice-switching oligonucleotides to the nuclei of cancer cells. *Nucleic Acid Ther.* 2012; 22: 187-95.

522. Pan W, Yang H, Zhang T, et al. Dual-targeted nanocarrier based on cell surface receptor and intracellular mRNA: an effective strategy for cancer cell imaging and therapy. *Anal. Chem.* 2013; 85: 6930-5.
523. Kallenbach NR, Ma R-I, Seeman NC. An immobile nucleic acid junction constructed from oligonucleotides. *Nature* 1983; 305: 829-31.
524. de Vries JW, Zhang F, Herrmann A. Drug delivery systems based on nucleic acid nanostructures. *J. Control. Release* 2013; 172: 467-83.
525. Chen J, Seeman NC. Synthesis from DNA of a molecule with the connectivity of a cube. *Nature* 1991; 350: 631-3.
526. Wang Y, Mueller JE, Kemper B, et al. Assembly and characterization of five-arm and six-arm DNA branched junctions. *Biochemistry* 1991; 30: 5667-74.
527. Zheng J, Constantinou PE, Micheel C, et al. Two-Dimensional Nanoparticle Arrays Show the Organizational Power of Robust DNA Motifs. *Nano Lett.* 2006; 6: 1502-4.
528. Wei B, Dai M, Yin P. Complex shapes self-assembled from single-stranded DNA tiles. *Nature* 2012; 485: 623-6.
529. Douglas SM, Bachelet I, Church GM. A Logic-Gated Nanorobot for Targeted Transport of Molecular Payloads. *Science* 2012; 335: 831-4.
530. Andersen ES, Dong M, Nielsen MM, et al. Self-assembly of a nanoscale DNA box with a controllable lid. *Nature* 2009; 459: 73-6.
531. Andersen ES, Dong M, Nielsen MM, et al. DNA Origami Design of Dolphin-Shaped Structures with Flexible Tails. *ACS Nano* 2008; 2: 1213-8.

532. Douglas SM, Marblestone AH, Teerapittayanon S, et al. Rapid prototyping of 3D DNA-origami shapes with caDNAno. *Nucleic Acids Res.* 2009; 37: 5001-6.
533. Kim D-N, Kilchherr F, Dietz H, et al. Quantitative prediction of 3D solution shape and flexibility of nucleic acid nanostructures. *Nucleic Acids Res.* 2012; 40: 2862-8.
534. Rajendran A, Endo M, Sugiyama H. Single-Molecule Analysis Using DNA Origami. *Angew. Chem. Int. Ed.* 2012; 51: 874-90.
535. Qi H, Ghodousi M, Du Y, et al. DNA-directed self-assembly of shape-controlled hydrogels. *Nat. Commun.* 2013; 4: 2275.
536. Lee JB, Peng S, Yang D, et al. A mechanical metamaterial made from a DNA hydrogel. *Nat. Nanotechnol.* 2012; 7: 816-20.
537. Ali MM, Li F, Zhang Z, et al. Rolling circle amplification: a versatile tool for chemical biology, materials science and medicine. *Chem. Soc. Rev.* 2014; 43: 3324-41.
538. Lee JB, Hong J, Bonner DK, et al. Self-assembled RNA interference microsponges for efficient siRNA delivery. *Nat. Mater.* 2012; 11: 316-22.
539. Roh YH, Lee JB, Shopsowitz KE, et al. Layer-by-Layer Assembled Anti-Sense DNA Microsponge Particles for Efficient Delivery of Cancer Therapeutics. *ACS Nano* 2014; 8: 9767-80.
540. Hu R, Zhang X, Zhao Z, et al. DNA Nanoflowers for Multiplexed Cellular Imaging and Traceable Targeted Drug Delivery. *Angew. Chem. Int. Ed.* 2014; 53: 5821-6.

541. Hamblin GD, Carneiro KMM, Fakhoury JF, et al. Rolling Circle Amplification-Templated DNA Nanotubes Show Increased Stability and Cell Penetration Ability. *J. Am. Chem. Soc.* 2012; 134: 2888-91.
542. Lo PK, Karam P, Aldaye FA, et al. Loading and selective release of cargo in DNA nanotubes with longitudinal variation. *Nat. Chem.* 2010; 2: 319-28.
543. Li J, Pei H, Zhu B, et al. Self-Assembled Multivalent DNA Nanostructures for Noninvasive Intracellular Delivery of Immunostimulatory CpG Oligonucleotides. *ACS Nano* 2011; 5: 8783-9.
544. Sheng W, Chen T, Tan W, et al. Multivalent DNA nanospheres for enhanced capture of cancer cells in microfluidic devices. *ACS Nano* 2013; 7: 7067-76.
545. Mohri K, Nishikawa M, Takahashi N, et al. Design and Development of Nanosized DNA Assemblies in Polypod-like Structures as Efficient Vehicles for Immunostimulatory CpG Motifs to Immune Cells. *ACS Nano* 2012; 6: 5931-40.
546. Zhang Z, Eckert MA, Ali MM, et al. DNA-Scaffolded Multivalent Ligands to Modulate Cell Function. *ChemBioChem* 2014; 15: 1268-73.
547. Zhao Y-X, Shaw A, Zeng X, et al. DNA Origami Delivery System for Cancer Therapy with Tunable Release Properties. *ACS Nano* 2012; 6: 8684-91.
548. Zhang Q, Jiang Q, Li N, et al. DNA Origami as an In Vivo Drug Delivery Vehicle for Cancer Therapy. *ACS Nano* 2014; 8: 6633-43.
549. Wang K, You M, Chen Y, et al. Self-Assembly of a Bifunctional DNA Carrier for Drug Delivery. *Angew. Chem. Int. Ed.* 2011; 50: 6098-101.

550. Chen C, Zhou L, Geng J, et al. Photosensitizer-incorporated quadruplex DNA-gated nanovehicles for light-triggered, targeted dual drug delivery to cancer cells. *Small* 2013; 9: 2793-800, 653.
551. Lipps HJ, Rhodes D. G-quadruplex structures: in vivo evidence and function. *Trends Cell Biol.* 2009; 19: 414-22.
552. Klinman DM. Immunotherapeutic uses of CpG oligodeoxynucleotides. *Nat. Rev. Immunol.* 2004; 4: 249-59.
553. Whitehead KA, Langer R, Anderson DG. Knocking down barriers: advances in siRNA delivery. *Nat. Rev. Drug Discov.* 2009; 8: 129-38.
554. Dias N, Stein CA. Antisense Oligonucleotides: Basic Concepts and Mechanisms. *Mol. Cancer Ther.* 2002; 1: 347-55.
555. Dean NM, Bennett CF. Antisense oligonucleotide-based therapeutics for cancer. *Oncogene* 2003; 22: 9087-96.
556. Keum J-W, Ahn J-H, Bermudez H. Design, Assembly, and Activity of Antisense DNA Nanostructures. *Small* 2011; 7: 3529-35.
557. Mohri K, Nishikawa M, Takahashi Y, et al. DNA nanotechnology-based development of delivery systems for bioactive compounds. *Eur. J. Pharm. Sci.* 2014; 58: 26-33.
558. Uno S, Nishikawa M, Mohri K, et al. Efficient delivery of immunostimulatory DNA to mouse and human immune cells through the construction of polypod-like structured DNA. *Nanomed. Nanotechnol. Biol. Med.* 2014; 10: 765-74.

559. Schüller VJ, Heidegger S, Sandholzer N, et al. Cellular Immunostimulation by CpG-Sequence-Coated DNA Origami Structures. *ACS Nano* 2011; 5: 9696-702.
560. Ouyang X, Li J, Liu H, et al. Rolling Circle Amplification-Based DNA Origami Nanostructures for Intracellular Delivery of Immunostimulatory Drugs. *Small* 2013; 9: 3082-7.
561. Scott AM, Wolchok JD, Old LJ. Antibody therapy of cancer. *Nat. Rev. Cancer*. 2012; 12: 278-87.
562. Rosenberg SA, Yang JC, Restifo NP. Cancer immunotherapy: moving beyond current vaccines. *Nat. Med.* 2004; 10: 909-15.
563. Liu X, Xu Y, Yu T, et al. A DNA Nanostructure Platform for Directed Assembly of Synthetic Vaccines. *Nano Lett.* 2012; 12: 4254-9.
564. Zhu C-L, Lu C-H, Song X-Y, et al. Bioresponsive Controlled Release Using Mesoporous Silica Nanoparticles Capped with Aptamer-Based Molecular Gate. *J. Am. Chem. Soc.* 2011; 133: 1278-81.
565. Liu Y, Du J, Yan M, et al. Biomimetic enzyme nanocomplexes and their use as antidotes and preventive measures for alcohol intoxication. *Nat. Nanotechnol.* 2013; 8: 187-92.
566. Donnelly JJ, Wahren B, Liu MA. DNA vaccines: progress and challenges. *J. Immunol.* 2005; 175: 633-9.
567. Brown DA, Kang SH, Gryaznov SM, et al. Effect of phosphorothioate modification of oligodeoxynucleotides on specific protein binding. *J. Biol. Chem.* 1994; 269: 26801-5.

568. McConkey SJ, Reece WHH, Moorthy VS, et al. Enhanced T-cell immunogenicity of plasmid DNA vaccines boosted by recombinant modified vaccinia virus Ankara in humans. *Nat. Med.* 2003; 9: 729-35.
569. Bugl H, Danner JP, Molinari RJ, et al. DNA synthesis and biological security. *Nat. Biotechnol.* 2007; 25: 627-9.
570. Lin C, Rinker S, Wang X, et al. In vivo cloning of artificial DNA nanostructures. *Proc. Natl. Acad. Sci. U. S. A.* 2008; 105: 17626-31.
571. Zhang Z, Ali MM, Eckert MA, et al. A polyvalent aptamer system for targeted drug delivery. *Biomaterials* 2013; 34: 9728-35.
572. Zhu G, Hu R, Zhao Z, et al. Noncanonical Self-Assembly of Multifunctional DNA Nanoflowers for Biomedical Applications. *J. Am. Chem. Soc.* 2013; 135: 16438-45.
573. Kim K-R, Kim D-R, Lee T, et al. Drug delivery by a self-assembled DNA tetrahedron for overcoming drug resistance in breast cancer cells. *Chem. Commun.* 2013; 49: 2010-2.
574. Xiao Z, Ji C, Shi J, et al. DNA Self-Assembly of Targeted Near-Infrared-Responsive Gold Nanoparticles for Cancer Thermo-Chemotherapy. *Angew. Chem. Int. Ed.* 2012; 51: 11853-7.
575. Zhang Z, Che Y, Smaldone RA, et al. Reversible Dispersion and Release of Carbon Nanotubes Using Foldable Oligomers. *J. Am. Chem. Soc.* 2010; 132: 14113-7.
576. Shi J, Votruba AR, Farokhzad OC, et al. Nanotechnology in drug delivery and tissue engineering: from discovery to applications. *Nano Lett* 2010; 10: 3223-30.

577. Gu Z, Yan M, Hu B, et al. Protein Nanocapsule Weaved with Enzymatically Degradable Polymeric Network. *Nano Lett.* 2009; 9: 4533-8.
578. Murthy N, Thng YX, Schuck S, et al. A Novel Strategy for Encapsulation and Release of Proteins: Hydrogels and Microgels with Acid-Labile Acetal Cross-Linkers. *J. Am. Chem. Soc.* 2002; 124: 12398-9.
579. Murthy N, Xu M, Schuck S, et al. A macromolecular delivery vehicle for protein-based vaccines: acid-degradable protein-loaded microgels. *Proc Natl Acad Sci U S A* 2003; 100: 4995-5000.
580. Bachelder EM, Beaudette TT, Broaders KE, et al. Acetal-derivatized dextran: an acid-responsive biodegradable material for therapeutic applications. *J. Am. Chem. Soc.* 2008; 130: 10494-5.
581. Li K, Jiang Y, Ding D, et al. Folic acid-functionalized two-photon absorbing nanoparticles for targeted MCF-7 cancer cell imaging. *Chem. Commun.* 2011; 47: 7323-5.
582. Alcazar-Leyva S, Ceron E, Masso F, et al. Incubation with DNase I inhibits tumor cell proliferation. *Med. Sci. Monit.* 2009; 15: CR51-5.
583. Hsu Patrick D, Lander Eric S, Zhang F. Development and Applications of CRISPR-Cas9 for Genome Engineering. *Cell* 2014; 157: 1262-78.
584. Jinek M, Chylinski K, Fonfara I, et al. A programmable dual-RNA-guided DNA endonuclease in adaptive bacterial immunity. *Science* 2012; 337: 816-21.
585. Cong L, Ran FA, Cox D, et al. Multiplex Genome Engineering Using CRISPR/Cas Systems. *Science* 2013; 339: 819-23.

586. Mali P, Yang L, Esvelt KM, et al. RNA-Guided Human Genome Engineering via Cas9. *Science* 2013; 339: 823-6.
587. Ran FA, Cong L, Yan WX, et al. In vivo genome editing using *Staphylococcus aureus* Cas9. *Nature* 2015; 520: 186-91.
588. Platt Randall J, Chen S, Zhou Y, et al. CRISPR-Cas9 Knockin Mice for Genome Editing and Cancer Modeling. *Cell* 2014; 159: 440-55.
589. Kotterman MA, Schaffer DV. Engineering adeno-associated viruses for clinical gene therapy. *Nat. Rev. Genet.* 2014; 15: 445-51.
590. Pattanayak V, Lin S, Guilinger JP, et al. High-throughput profiling of off-target DNA cleavage reveals RNA-programmed Cas9 nuclease specificity. *Nat. Biotechnol.* 2013; 31: 839-43.
591. Fu Y, Foden JA, Khayter C, et al. High-frequency off-target mutagenesis induced by CRISPR-Cas nucleases in human cells. *Nat. Biotechnol.* 2013; 31: 822-6.
592. Zuris JA, Thompson DB, Shu Y, et al. Cationic lipid-mediated delivery of proteins enables efficient protein-based genome editing in vitro and in vivo. *Nat. Biotechnol.* 2015; 33: 73-80.
593. Ramakrishna S, Kwaku Dad AB, Beloor J, et al. Gene disruption by cell-penetrating peptide-mediated delivery of Cas9 protein and guide RNA. *Genome Res.* 2014; 24: 1020-7.
594. Gerngross TU. Advances in the production of human therapeutic proteins in yeasts and filamentous fungi. *Nat. Biotechnol.* 2004; 22: 1409-14.

595. Sliwkowski MX, Mellman I. Antibody Therapeutics in Cancer. *Science* 2013; 341: 1192-8.
596. Wade M, Li Y-C, Wahl GM. MDM2, MDMX and p53 in oncogenesis and cancer therapy. *Nat. Rev. Cancer.* 2013; 13: 83-96.
597. Hu R, Zhang X, Zhao Z, et al. DNA Nanoflowers for Multiplexed Cellular Imaging and Traceable Targeted Drug Delivery. *Angew. Chem. Int. Ed.* 2014; 126: 5931-6.
598. Lee HY, Jeong H, Jung IY, et al. DhITACT: DNA Hydrogel Formation by Isothermal Amplification of Complementary Target in Fluidic Channels. *Adv. Mater.* 2015; 27: 3513-7.
599. Macfarlane RJ, Thaner RV, Brown KA, et al. Importance of the DNA “bond” in programmable nanoparticle crystallization. *Proc. Natl. Acad. Sci. U. S. A.* 2014; 111: 14995-5000.
600. Jones MR, Seeman NC, Mirkin CA. Programmable materials and the nature of the DNA bond. *Science* 2015; 347
601. Gasiunas G, Barrangou R, Horvath P, et al. Cas9–crRNA ribonucleoprotein complex mediates specific DNA cleavage for adaptive immunity in bacteria. *Proc. Natl. Acad. Sci. U. S. A.* 2012; 109: E2579–E86.
602. Varkouhi AK, Scholte M, Storm G, et al. Endosomal escape pathways for delivery of biologicals. *J. Control. Release* 2011; 151: 220-8.
603. Doudna JA, Charpentier E. The new frontier of genome engineering with CRISPR-Cas9. *Science* 2014; 346: 1258096.

604. Fujii W, Kawasaki K, Sugiura K, et al. Efficient generation of large-scale genome-modified mice using gRNA and CAS9 endonuclease. *Nucleic Acids Res.* 2013; 41: e187.
605. Bolte S, CordeliÈRes FP. A guided tour into subcellular colocalization analysis in light microscopy. *J. Microsc.* 2006; 224: 213-32.
606. Hong CA, Eltoukhy AA, Lee H, et al. Dendrimeric siRNA for Efficient Gene Silencing. *Angew. Chem. Int. Ed. Engl.* 2015; 54: 6740-4.
607. Zetsche B, Volz SE, Zhang F. A split-Cas9 architecture for inducible genome editing and transcription modulation. *Nat. Biotechnol.* 2015; 33: 139-42.
608. Tian J, Avalos AM, Mao S-Y, et al. Toll-like receptor 9-dependent activation by DNA-containing immune complexes is mediated by HMGB1 and RAGE. *Nat Immunol* 2007; 8: 487-96.
609. Sun W, Gu Z. Engineering DNA scaffolds for delivery of anticancer therapeutics. *Biomater. Sci.* 2015; 3: 1018-24.
610. Ghosh P, Han G, De M, et al. Gold nanoparticles in delivery applications. *Adv. Drug Del. Rev.* 2008; 60: 1307-15.
611. Tang R, Kim CS, Solfiell DJ, et al. Direct Delivery of Functional Proteins and Enzymes to the Cytosol Using Nanoparticle-Stabilized Nanocapsules. *ACS Nano* 2013; 7: 6667-73.
612. Anraku Y, Kishimura A, Kamiya M, et al. Systemically Injectable Enzyme-Loaded Polyion Complex Vesicles as In Vivo Nanoreactors Functioning in Tumors. *Angew. Chem. Int. Ed.* 2016; 128: 570-5.

613. Vegran F, Berger H, Boidot R, et al. The transcription factor IRF1 dictates the IL-21-dependent anticancer functions of TH9 cells. *Nat Immunol* 2014; 15: 758-66.
614. Liu Y, Du J, Choi J-s, et al. A High-Throughput Platform for Formulating and Screening Multifunctional Nanoparticles Capable of Simultaneous Delivery of Genes and Transcription Factors. *Angew. Chem. Int. Ed.* 2015; 128: 177-81.
615. Zitvogel L, Galluzzi L, Kepp O, et al. Type I interferons in anticancer immunity. *Nat. Rev. Immunol.* 2015; 15: 405-14.
616. Li J, Ai Y, Wang L, et al. Targeted drug delivery to circulating tumor cells via platelet membrane-functionalized particles. *Biomaterials* 2016; 76: 52-65.
617. Spiller KL, Nassiri S, Witherel CE, et al. Sequential delivery of immunomodulatory cytokines to facilitate the M1-to-M2 transition of macrophages and enhance vascularization of bone scaffolds. *Biomaterials* 2015; 37: 194-207.
618. Mitragotri S, Anderson DG, Chen X, et al. Accelerating the Translation of Nanomaterials in Biomedicine. *ACS Nano* 2015; 9: 6644–54.
619. Sun W, Ji W, Hall JM, et al. Self-Assembled DNA Nanoclews for the Efficient Delivery of CRISPR–Cas9 for Genome Editing. *Angew. Chem. Int. Ed.* 2015; 54: 12029-33.
620. Kohlhaas SL, Craxton A, Sun XM, et al. Receptor-mediated endocytosis is not required for tumor necrosis factor-related apoptosis-inducing ligand (TRAIL)-induced apoptosis. *J. Biol. Chem.* 2007; 282: 12831-41.
621. Gratton SEA, Ropp PA, Pohlhaus PD, et al. The effect of particle design on cellular internalization pathways. *Proc. Natl. Acad. Sci. U. S. A.* 2008; 105: 11613-8.

622. Gao H, Shi W, Freund LB. Mechanics of receptor-mediated endocytosis. *Proc. Natl. Acad. Sci. U. S. A.* 2005; 102: 9469-74.
623. Mo R, Gu Z. Tumor microenvironment and intracellular signal-activated nanomaterials for anticancer drug delivery. *Mater. Today* 2015; doi:10.1016/j.mattod.2015.11.025
624. Wang H, Agarwal P, Zhao S, et al. Hyaluronic acid-decorated dual responsive nanoparticles of Pluronic F127, PLGA, and chitosan for targeted co-delivery of doxorubicin and irinotecan to eliminate cancer stem-like cells. *Biomaterials* 2015; 72: 74-89.
625. Zhong J, Li L, Zhu X, et al. A smart polymeric platform for multistage nucleus-targeted anticancer drug delivery. *Biomaterials* 2015; 65: 43-55.
626. Brglez V, Lambeau G, Petan T. Secreted phospholipases A2 in cancer: Diverse mechanisms of action. *Biochimie* 2014; 107, Part A: 114-23.
627. Pei H, Zuo X, Zhu D, et al. Functional DNA Nanostructures for Theranostic Applications. *Acc. Chem. Res.* 2013; 47: 550-9.
628. Tian C, Li X, Liu Z, et al. Directed Self-Assembly of DNA Tiles into Complex Nanocages. *Angew. Chem. Int. Ed.* 2014; 53: 8041-4.
629. Kim M-G, Park JY, Miao W, et al. Polyaptamer DNA nanothread-anchored, reduced graphene oxide nanosheets for targeted delivery. *Biomaterials* 2015; 48: 129-36.
630. Kim M-G, Park JY, Shim G, et al. Biomimetic DNA nanoballs for oligonucleotide delivery. *Biomaterials* 2015; 62: 155-63.

631. Hong CA, Jang B, Jeong EH, et al. Self-assembled DNA nanostructures prepared by rolling circle amplification for the delivery of siRNA conjugates. *Chem. Commun.* 2014; 50: 13049-51.
632. Brodin JD, Sprangers AJ, McMillan JR, et al. DNA-Mediated Cellular Delivery of Functional Enzymes. *J. Am. Chem. Soc.* 2015; 137: 14838-41.
633. Sellner S, Kocabey S, Nekolla K, et al. DNA nanotubes as intracellular delivery vehicles in vivo. *Biomaterials* 2015; 53: 453-63.
634. Shen W, Zhong H, Neff D, et al. NTA Directed Protein Nanopatterning on DNA Origami Nanoconstructs. *J. Am. Chem. Soc.* 2009; 131: 6660-1.
635. Jin Y, Yang F, Du L. Nanoassemblies containing a fluorouracil/zidovudine glyceryl prodrug with phospholipase A2-triggered drug release for cancer treatment. *Colloids Surf. B. Biointerfaces* 2013; 112: 421-8.
636. Kundu GC, Mukherjee AB. Evidence that porcine pancreatic phospholipase A2 via its high affinity receptor stimulates extracellular matrix invasion by normal and cancer cells. *J. Biol. Chem.* 1997; 272: 2346-53.
637. Szoka F, Papahadjopoulos D. Procedure for preparation of liposomes with large internal aqueous space and high capture by reverse-phase evaporation. *Proc. Natl. Acad. Sci. U. S. A.* 1978; 75: 4194-8.
638. Aili D, Mager M, Roche D, et al. Hybrid Nanoparticle–Liposome Detection of Phospholipase Activity. *Nano Lett.* 2010; 11: 1401-5.

639. Jensen SS, Andresen TL, Davidsen J, et al. Secretory phospholipase A2 as a tumor-specific trigger for targeted delivery of a novel class of liposomal prodrug anticancer etherlipids. *Mol Cancer Ther* 2004; 3: 1451-8.
640. Zakaria AB, Picaud F, Rattier T, et al. Nanovectorization of TRAIL with Single Wall Carbon Nanotubes Enhances Tumor Cell Killing. *Nano Lett.* 2015; 15: 891-5.
641. Biankin AV, Piantadosi S, Hollingsworth SJ. Patient-centric trials for therapeutic development in precision oncology. *Nature* 2015; 526: 361-70.
642. Ashley EA. The precision medicine initiative: A new national effort. *JAMA* 2015; 313: 2119-20.
643. van der Worp HB, van Gijn J. Clinical practice. Acute ischemic stroke. *N. Engl. J. Med.* 2007; 357: 572-9.
644. Besselink MG, van Santvoort HC, Buskens E, et al. Probiotic prophylaxis in predicted severe acute pancreatitis: a randomised, double-blind, placebo-controlled trial. *Lancet* 2008; 371: 651-9.
645. Van Der Worp HB, Howells DW, Sena ES, et al. Can Animal Models of Disease Reliably Inform Human Studies? *PLoS Med* 2010; 7: e1000245.
646. Lammers T, Kiessling F, Hennink WE, et al. Drug targeting to tumors: Principles, pitfalls and (pre-) clinical progress. *J. Control. Release* 2012; 161: 175-87.
647. Moses H, Iii, Matheson DM, et al. The anatomy of medical research: Us and international comparisons. *JAMA* 2015; 313: 174-89.

648. Drmanac R, Sparks AB, Callow MJ, et al. Human Genome Sequencing Using Unchained Base Reads on Self-Assembling DNA Nanoarrays. *Science* 2010; 327: 78-81.